Inaugural dissertation
for
obtaining the doctoral degree
of the
Combined Faculty of Mathematics, Engineering and Natural Sciences
of the
Ruprecht - Karls - University
Heidelberg

Presented by
M.Sc. Lena Bohaumilitzky
born in: Linz, Austria

Oral examination: 11.10.2022

Comprehensive characterization of local and systemic neoantigen-specific immune responses and biomarkers in Lynch syndrome

Referees: Prof. Dr. med. Magnus von Knebel Doeberitz
Prof. Dr. Hans-Reimer Rodewald

And I knew exactly what to do.
But in a much more real sense, I had no idea what to do.

- Michael Scott -

The presented Dissertation was started in May 2019 and completed in May 2022 under the supervision of Prof. Dr. med. Magnus von Knebel Doeberitz at the department of Applied Tumor Biology at the Institute for Pathology, University of Heidelberg (Germany) and the Clinical Cooperation Unit Applied Tumor Biology of the German Cancer Research Center (DKFZ), Heidelberg (Germany).

Affidavit according to §8 of the doctoral degree regulations of the Combined Faculty of Mathematics, Engineering and Natural Sciences

1. The thesis I have submitted entitled 'Comprehensive characterization of local and systemic neoantigen-specific immune responses and biomarkers in Lynch syndrome' is my own work.

2. I have only used the sources indicated and have not made unauthorized use of services of a third party. Where the work of others has been quoted or reproduced, the source is always given.

3. I have not yet presented this thesis or parts thereof to a university as part of an examination or degree.

4. I confirm that the declarations made above are correct.

5. I am aware of the importance of a sworn affidavit and the criminal prosecution in case of a false or incomplete affidavit.

I affirm that the above is the absolute truth to the best of my knowledge and that I have not concealed anything.

Heidelberg, _____

(Lena Bohaumilitzky)

Contents

List of Figures

List of Tables

Abbreviations

5-FU	5-Fluorouracil
ACVR2A	Activin type 2 receptor
AIM2	Absent in melanoma 2
ALP	Alkaline phosphatase
APC	Adenomatous polyposis coli
APCs	Antigen-presenting cells
APM	Antigen processing machinery
B2M	β2-microglobulin
BAX	BCL2-associated X protein
BCIP/NBT	5-Bromo-4-chloro-3'-indolyphosphate/nitro-blue tetrazolium
bp	Base pairs
BSA	Bovine serum albumin
CAPP2	Cancer Prevention Program 2
CCL2	Chemokine C-C motif ligand 2
CD	Cluster of differentiation
cDNA	Complementary DNA
CEF	Cytomegalovirus, Epstein-Barr and influenza virus
CI	Confidence interval
CIITA	Class II transactivator
CIMP	CpG island methylator phenotype
CIN	Chromosomal instability
cMS	Coding microsatellites
CMV	Cytomegalovirus
ConA	Concanavalin A
CRC	Colorectal cancer
CTLA-4	Cytotoxic T lymphocyte-associated antigen 4
DAB	3,3'-Diaminobenzidine
DCC	Netrin 1 receptor
DMP	Dimethyl pimelimidate
DMSO	Dimethyl sulfoxide
EC	Endometrial cancer
ECL	Enhanced chemiluminescence
EDTA	Ethylenediamine tetraacetic acid
EGFR	Epidermal growth factor receptor
ELISA	Enzyme-linked immunosorbent assay
ELISpot	Enzyme-linked immuno spot assay
ER	Endoplasmic reticulum

ESCRT	Endosomal sorting complex required for transport
EVs	Extracellular vesicles
FACS	Fluorescence activated cell sorting
FAP	Familial adenomatous polyposis
FBS	Fetal bovine serum
FC	Fold change
FDA	U.S. Food and Drug Administration
FDR	False discovery rate
FFPE	Formalin-fixed paraffin-embedded
FOXP3	Forkhead box P3
FSPs	Frameshift peptides
FVS	Fixable viability stain
G-CSF	Granulocyte-colony stimulating factor
GUCY2C	Guanylyl cyclase C
HDI	Human Development Index
HE	Hematoxylin and eosin
HEPES	4-(2-Hydroxyethyl)-1-piperazineethanesulfonic acid
HEV	High endothelial venules
HLA	Human leukocyte antigen
HNPCC	Hereditary nonpolyposis colorectal cancer
hpf	High power field
HPV	Human papillomavirus
HRP	Horseradish peroxidase
HT001	Asteroid homolog
ICB	Immune checkpoint blockade
IDLs	Insertion/deletion loops
IDO	Indoleamine 2’3’-dioxygenase
IFNγ	Interferon-γ
IgA	Immunoglobulin class A
IgG	Immunoglobulin class G
IHC	Immunohistochemistry
IL	Interleukin
ILVs	Intraluminal vesicles
Indel	Insertion/deletion
InSiGHT	International Society for Gastrointestinal and Hereditary Tumors
IP	Immunoprecipitation
ITS	Insulin-Transferrin-Selenium
kDa	Kilodalton
KRAS	Kirsten rat sarcoma viral oncogene

kV	Kilovolt
LDS	Lithiumdodecylsulfat
LOH	Loss of heterozygosity
LS	Lynch syndrome
MDSCs	Myeloid-derived suppressor cells
MHC	Major histocompatibility complex
MIF	Macrophage migration inhibitory factor
miRNAs	MicroRNAs
MMR	Mismatch repair
MMR-D	MMR-deficient
MMR-DCF	MMR-deficient crypt foci
MMR-P	MMR-proficient
MR	Mixed response
MSI	Microsatellite instability
MSS	Microsatellite stability
MVBs	Multivesicular bodies
n.a.	Not available
NGS	Next generation sequencing
NHS	N-Hydroxysulfosuccinimid
NK cells	Natural killer cells
NSAIDs	Non-steroidal anti-inflammatory drugs
NTA	Nanoparticle tracking analysis
OR	Odds ratio
P/S	Penicillin/Streptomycin
PBMCs	Peripheral blood mononuclear cells
PBS	Phosphate-buffered saline
PBS-T	PBS with 0.1 % Tween 20
PCA	Principle component analysis
PCNA	Proliferating cell nuclear antigen
PD	Progressive disease
PD-1	Programmed cell death protein 1
PD-L1	Programmed cell death 1 ligand 1
PEG	Polyethylene glycol
PFA	Paraformaldehyde
PGE2	Prostaglandin E_2
PLSD	Prospective Lynch Syndrome Database
PR	Partial response
PRISMA	Preferred Reporting Items for Systematic Reviews and Meta-Analyses
PVDF	Polyvinylidene difluoride

RFX5	Regulatory factor 5
rhIL	Recombinant human interleukin
ROIs	Region of interest
rpm	Revolutions per minute
RT-qPCR	Reverse transcription-quantitative PCR
SB	Strong binder
SD	Stable disease
SDS	Sodium dodecyl sulfate
SMAD4	Mothers against decapentaplegic homolog 4
SNHG14	Small nucleolar RNA host gene 14
STR	Short tandem repeat
TAF1B	TATA box-binding protein-associated RNA polymerase I B
TAMs	Tumor-associated macrophages
TAP	Transporter associated with antigen processing
TAPBP	TAP binding protein
TCR	T cell receptor
TEM	Transmission electron microscopy
TGFBR2	Transforming growth factor beta receptor 2
TILs	Tumor-infiltrating lymphocytes
TMB	3,3,5,5'-Tetramethylbenzidine
TME	Tumor microenvironment
TRIS	Trishydroxymethylaminomethane
VEGF	Vascular endothelial growth factor
VUS	Variants of uncertain significance
WB	Weak binder
Wb	Western blot
WT	Wild type

Summary

Colorectal cancer (CRC) is the third most common cancer worldwide and the number of early onset CRCs in individuals younger than 50 years is rising. A genetic predisposition for cancer is identified in 20 % of young onset CRC patients. The most common inherited CRC syndrome, estimated to affect around 25 million people worldwide, is Lynch syndrome (LS). LS carriers present with a germline variant in a DNA mismatch repair (MMR) gene and an elevated risk of developing cancer in different organ systems, most commonly in the colorectum and endometrium. Thus, timely diagnosis of LS is paramount for the initiation of preventive screening programs and reduction of cancer risk. However, current diagnostic strategies are mainly based on molecular screening of an already manifest cancer, rendering the identification of healthy LS carriers challenging. LS-associated cancers are characterized by MMR deficiency leading to the accumulation of numerous mutations in the entire genome, particularly at microsatellite regions and resulting in microsatellite instability (MSI). The MSI phenotype is associated with high immunogenicity due to the generation of immunogenic peptides, termed frameshift peptides (FSPs), upon mutations in coding microsatellites (cMS). Systemic FSP-specific immune responses have been identified in MSI cancer patients and healthy LS carriers. The presence of FSP-specific immune responses prior to cancer manifestation is thought to be attributable to LS-specific, MMR-deficient premalignant lesions in the colonic mucosa. The proposed immune activation in LS carriers may possess potential to be used diagnostically and to enable the identification of healthy LS carriers. The present thesis undertook the comprehensive characterization of local and systemic immune responses in LS individuals and the evaluation of their clinical potential. In addition, the suitability of plasma-derived extracellular vesicles (EVs) for tumor tissue-independent MSI testing was explored.

First, the systematic analysis of local immune responses in LS-associated tumors and the normal colorectal mucosa formed the basis of the project. The qualitative and quantitative review of existing literature on immune infiltration and immune evasion indicated that the hereditary origin shapes the immune phenotype of MSI tumors. LS-associated tumors presented with a more pronounced immune infiltration and a higher frequency of *B2M* mutations, compared to sporadic cases. The observed immunological differences between hereditary and sporadic MSI tumors possibly reflect differences in their pathogenesis and point towards a life-long immune surveillance in LS carriers. As a consequence, the normal colorectal mucosa of LS carriers might already carry traces of the tumor-independent immune activation. Thus, the present thesis, for the first time, characterized the mucosal immune milieu of LS carriers. The quantification of different T cell subpopulations and gene expression analysis revealed distinct immune profiles in the normal colonic mucosa of LS carriers with and without cancer manifestation. Moreover, a positive correlation between T cell density in the rectal mucosa and time to tumor manifestation in LS was observed for the first time, pointing at a possible role of the mucosal immune status as a temporary or permanent cancer risk modifier in LS.

Second and underpinned by the described local immunological alterations in LS carriers, systemic FSP-specific immune responses were characterized in LS carriers and MSI cancer patients. The analysis of FSP-specific T cell and antibody responses in healthy LS carriers enabled the identification of seven FSPs which were associated with significantly stronger immune responses in LS individuals, compared to healthy non-LS controls. The respective candidates may be suited for the immune-based identification of LS carriers prior to cancer development and establish the basis for prospective validation studies in larger cohorts. The analysis of FSP-specific immune responses in MSI cancer patients did not yield a clear picture and was possibly influenced by cancer- and therapy-mediated effects. The potential of FSP-specific T cell responses as immune checkpoint blockade (ICB) therapy response markers was descriptively assessed in MSI cancer patients. Therefore, the present thesis contributed to expanding available data on FSP-specific T cell responses under ICB therapy which are currently scarce. However, no substantial correlation between FSP-specific T cell responses and a patient's clinical course was observed, underscoring the need for larger clinically defined cohorts and a stringent patient follow-up. In addition, systemic FSP-specific T cell responses in MSI cancer patients were correlated with the tumor's cMS mutation pattern, providing evidence for strong peripheral T cell responses against cMS mutation-derived FSPs and the potential counterselection of highly immunogenic FSPs during tumor evolution. An additional aspect of the present project accounted for an individual's HLA type as a factor possibly influencing the immune response. The analysis of HLA-FSP epitope binding predictions generally supported the suitability of the used FSP panel.

Third, the potential of plasma-derived vesicular DNA as a minimally invasive MSI diagnostic approach was explored. The present thesis, for the first time, demonstrated MSI in vesicular DNA from MSI cancer patients, implying that plasma EVs sustain the MSI phenotype of their parental cancer cell. Moreover, the vesicular MSI status was found to change with advancing ICB therapy, suggesting its suitability as therapy response marker and a possible link between MSI detectability in vesicular DNA and tumor burden. This correlation not only supported the clinical potential of EVs as cancer DNA carriers, but also underlined the dependence of successful sampling on the quantity of cancer-specific EVs in the plasma, thereby calling for the enrichment of specific EV populations. Respective enrichment strategies for colon-specific EVs were successfully established using an MSI CRC cell line and preliminary results indicate their feasibility for the application in plasma-derived EVs. The detection of MSI in plasma EVs opens doors for their versatile diagnostic and predictive application in the context of MSI cancers and LS.

In summary, the present thesis demonstrated the significance of local and systemic immune responses in LS carriers and outlined novel approaches for using such in tumor-independent LS diagnostics. Moreover, the presented work provides an incentive for further research on EVs as MSI-specific biomarkers.

Zusammenfassung

Darmkrebs ist weltweit die dritthäufigste Krebserkrankung und die Zahl der früh auftretenden Fälle bei Personen unter 50 Jahren steigt. Bei 20 % der jungen Darmkrebspatienten wird eine genetische Veranlagung festgestellt. Das häufigste vererbte Darmkrebssyndrom, von dem schätzungsweise 25 Millionen Menschen weltweit betroffen sind, ist das Lynch-Syndrom (LS). LS-Anlageträger weisen eine Keimbahnvariante in einem DNA-Mismatch-Repair (MMR)-Gen auf und haben ein erhöhtes Risiko in verschiedenen Organsystemen Krebs zu entwickeln, am häufigsten im Kolorektum und Endometrium. Daher ist die frühzeitige Diagnose von LS von entscheidender Bedeutung für die Einleitung von Präventionsmaßnahmen und die Verringerung des Krebsrisikos. Die derzeitigen Diagnosestrategien basieren jedoch hauptsächlich auf der molekularen Analyse eines bereits manifesten Tumors, was die Identifizierung von krebsfreien LS-Anlageträgern erschwert. LS-assoziierte Tumoren sind durch einen Ausfall des MMR-Systems gekennzeichnet. Dieser resultiert in der Anhäufung zahlreicher Mutationen im gesamten Genom, insbesondere in Mikrosatellitenregionen, was zu dem molekularen Phänotyp der Mikrosatelliten-Instabilität (MSI) führt. MSI ist mit einer hohen Immunogenität verbunden, da bei Mutationen in kodierenden Mikrosatelliten (cMS) immunogene Peptide, so genannte Frameshift-Peptide (FSPs), entstehen. Systemische FSP-spezifische Immunantworten wurden nicht nur bei MSI-Krebspatienten, sondern auch bei gesunden LS-Anlageträgern festgestellt. Das Vorhandensein von FSP-spezifischen Immunantworten vor der Krebsmanifestation wird auf LS-spezifische, MMR-defiziente prämaligne Läsionen in der Darmschleimhaut zurückgeführt. Die beschriebene Immunaktivierung vor der Tumorentstehung könnte das Potenzial haben diagnostisch genutzt zu werden und die Identifikation von krebsfreien LS-Anlageträgern zu ermöglichen. In der vorliegenden Arbeit wurden die lokalen und systemischen Immunantworten bei LS-Anlageträgern umfassend charakterisiert und ihr klinisches Potenzial evaluiert. Ergänzend dazu wurde die Eignung von aus Plasma gewonnenen extrazellulären Vesikeln (EVs) für Tumorgewebe-unabhängige MSI-Analyse im Zusammenhang mit MSI-Tumoren und LS untersucht.

Die Grundlage des Projekts bildete zunächst die systematische Analyse lokaler Immunantworten in LS-assoziierten Tumoren und in der normalen Darmschleimhaut. Die qualitative und quantitative Auswertung der vorhandenen Literatur zur Immuninfiltration und -evasion zeigte, dass ein erblicher Hintergrund den Immunphänotyp von MSI-Tumoren prägt. Insgesamt zeigten LS-assoziierte Tumore eine ausgeprägtere Immuninfiltration und eine höhere Häufigkeit von *B2M*-Mutationen im Vergleich zu sporadischen Fällen. Die beobachteten immunologischen Unterschiede zwischen erblichen und sporadischen MSI-Tumoren spiegeln möglicherweise Unterschiede in ihrer Pathogenese wider und weisen auf eine lebenslange Immunüberwachung bei LS-Anlageträgern hin. Infolgedessen könnte die normale Darmschleimhaut von LS-Anlageträgern bereits Spuren der tumorunabhängigen Immunaktivierung zeigen. In der vorliegenden Arbeit wurde daher erstmalig das mukosale Immunmilieu von LS-Anlageträgern charakterisiert. Die Quantifizierung verschiedener T-Zell-Subpopulationen und eine umfassende

Genexpressionsanalyse ergaben unterschiedliche Immunprofile in der normalen Darmschleimhaut von LS-Anlageträgern mit und ohne Krebsmanifestation. Darüber hinaus konnte erstmals eine positive Korrelation zwischen der T-Zell-Dichte in der Rektumschleimhaut und der Zeit bis zur Tumormanifestation bei LS beobachtet werden. Dies deutet auf eine mögliche Rolle des mukosalen Immunmilieus als vorübergehender oder dauerhafter Modifikator des Krebsrisikos bei LS hin.

Zweitens wurden, gestützt auf die beschriebenen immunologischen Veränderungen bei LS-Anlageträgern auf lokaler Ebene, systemische FSP-spezifische Immunantworten und ihr klinisches Potenzial bei LS-Anlageträgern und MSI-Krebspatienten charakterisiert. Die Analyse der FSP-spezifischen T-Zell- und Antikörperantworten bei gesunden LS-Anlageträgern ermöglichte die Identifizierung von sieben FSPs, die bei LS-Anlageträgern im Vergleich zu gesunden Kontrollen mit signifikant stärkeren Immunantworten verbunden waren. Die entsprechenden Kandidaten könnten für die immunbasierte Identifizierung von LS-Anlageträgern vor der Krebsentstehung geeignet sein und bilden die Grundlage für prospektive Validierungsstudien in größeren Kohorten. Die Analyse der FSP-spezifischen Immunantworten bei MSI-Krebspatienten ergab kein klares Bild und wurde möglicherweise durch krebs- und therapiebedingte Effekte beeinflusst. Das Potenzial von FSP-spezifischen T-Zell-Reaktionen als Marker für das Ansprechen auf Immuntherapie wurde in MSI-Krebspatienten deskriptiv untersucht. Somit trug die vorliegende Arbeit dazu bei die bisher spärlichen Daten über FSP-spezifische Immunantworten unter ICB-Therapie zu erweitern. Es wurde jedoch keine wesentliche Korrelation zwischen FSP-spezifischen T-Zell-Reaktionen und dem klinischen Verlauf eines Patienten beobachtet, was die Notwendigkeit größerer, klinisch definierter Kohorten und einer strengen Nachbeobachtung der Patienten unterstreicht. Darüber hinaus wurden die systemischen FSP-spezifischen T-Zell-Antworten bei MSI-Krebspatienten mit dem cMS-Mutationsmuster des Tumors korrelierten. Diese Analyse lieferte Evidenz für starke periphere T-Zell-Antworten gegen die von cMS-Mutationen hervorgehenden FSPs, sowie für eine potenzielle Gegenselektion von hoch immunogenen FSPs während der Tumorevolution. Ein weiterer Aspekt dieser Arbeit war die Berücksichtigung des HLA-Typs eines Individuums als Faktor, der möglicherweise die Immunantwort beeinflusst. Die Analyse der HLA-FSP-Epitop-Bindungsvorhersagen bestätigte im Allgemeinen die Eignung des verwendeten FSP-Panels.

Drittens wurde das Potenzial der molekularen Analyse von aus Plasma gewonnenen EVs als minimalinvasives MSI-Diagnoseinstrument erforscht. In der vorliegenden Arbeit wurde erstmals MSI in aus Plasma gewonnener vesikulärer DNA von MSI-Krebspatienten nachgewiesen. Dies deutet darauf hin, dass Plasma-EVs den MSI Phänotyp ihrer elterlichen Krebszelle erhalten. Darüber hinaus wurde festgestellt, dass sich der vesikuläre MSI-Status mit fortschreitender ICB-Therapie verändert, was auf seine Eignung als Marker für das Ansprechen auf die Therapie und einen möglichen Zusammenhang zwischen der MSI-Nachweisbarkeit in der vesikulären DNA und der Tumorlast hindeutet. Diese Korrelation untermauert nicht nur das diagnostische

Potenzial von EVs als Tumor-DNA-Träger, sondern unterstreicht auch die Abhängigkeit einer erfolgreichen Probenahme von der Menge krebsspezifischer EVs im Plasma, was die Anreicherung spezifischer EV-Populationen erforderlich macht. Entsprechende Anreicherungsstrategien für kolonspezifische EVs wurden unter Verwendung einer MSI-Krebszelllinie erfolgreich etabliert, und vorläufige Ergebnisse deuten darauf hin, dass sie auch für die Anwendung bei aus Plasma gewonnenen EVs geeignet sind. Insgesamt öffnet der Nachweis von MSI in Plasma-EVs die Türen für ihre vielseitigen diagnostischen und prädiktiven Anwendung im Zusammenhang mit MSI-Tumoren und LS.

Zusammenfassend wurde in der vorliegenden Arbeit die Bedeutung von lokalen und systemischen Immunantworten bei LS-Anlageträgern demonstriert und die Basis für grundlegend neue Ansätze in der LS-Diagnostik gelegt. Darüber hinaus bietet die Arbeit einen Anreiz für die weitere Erforschung von EVs als MSI-spezifische Biomarker.

1 Introduction

1.1 Colorectal cancer

Worldwide, cancer is among the leading causes of death and cases are rapidly rising with 19.3 million new cases in the year 2020 [1]. Cancer burden is especially increasing in developed countries, even surpassing cardiovascular disease in 57 countries [2].

Colorectal cancer (CRC) is the third most common cancer, after female breast and lung cancer, and over 1.9 million new cases were registered in 2020. After lung cancer, CRC overall presents with the second highest mortality and in 2020 one in ten cancer deaths was CRC-related (9.4 %). The highest incidence of CRC is found in Northern America, Europe and Australia/New Zealand, whereas most African and South Central Asian regions present with low rates [1]. CRC is associated with socioeconomic factors and incidence rates are correlated with the Human Development Index (HDI), reflected in rising CRC cases in economically transitioning countries with increasing HDI [1, 3]. The rise of CRC cases in various regions can be ascribed to lifestyle and dietary changes, including a higher intake of red/processed meat, decreased physical activity and obesity [4, 5]. Cigarette smoking and alcohol consumption further increase the risk of CRC [6, 7]. Accordingly, a healthier lifestyle and diet can help to reduce CRC risk in individuals and the effect of population-wide changes can be observed in several high incidence, highly developed countries with stabilizing or decreasing CRC rates [4]. Since the early 2000s, CRC incidence could be reduced by implementing colonoscopy screening programs with the removal of precursor lesions [8, 9]. Measures for early detection also contribute to reducing CRC-related mortality [4].
CRC survival greatly depends on the disease stage at diagnosis and can vary from a 90 % 5-year survival rate for local disease to a 10 % 5-year survival rate for metastasized disease [10, 11]. The 5-year relative survival rate steadily increased since the mid-1970s (50 %) to around 64 % in 2015. This is not only attributable to the aforementioned screening programs but also to improved treatment (e.g. immune checkpoint blockade therapy (ICB)) and advanced imaging techniques (e.g chromoendoscopy). However, disparities in survival exist geographically as well as racially [5, 12, 13].

CRC treatment comprises surgery, chemotherapy, radiotherapy (for rectal cancer), various targeted therapy approaches and most recently ICB [13]. Surgical intervention is the typical curative treatment for non-metastatic CRC patients. Some cases might require chemo- or radiotherapy in the neoadjuvant or adjuvant setting to reduce tumor size and the risk of recurrence [14]. However, almost 25 % of CRCs are diagnosed at an advanced stage presenting metastases and systemic chemotherapy is considered the primary treatment for those patients. If the primary CRC and metastases are resectable, surgical intervention is possible but only achieves a long-term cure for 20 % of patients. In general, metastatic CRC is mostly incurable and exhibits a poor 5-year survival of around 14 % [15].

The majority of CRCs occur sporadically in individuals older than 50 years and are influenced by environmental, mostly lifestyle-related factors. However, it is estimated that 20–30 % of CRC cases, particularly those in young patients, have a heritable cause even though the responsible genes are often not fully characterized. Although increased screening led to an overall decline in CRC incidence, numbers are rising in individuals younger than 50 years and 20 % of young onset CRC patients present with a germline mutation associated with cancer predisposition [16, 17]. Familial clustering studies found that having a first-degree relative diagnosed with CRC is associated with a 2-fold increased risk of also developing CRC, compared to the general population [18]. In 3–5 % of CRC cases a defined genetic background can be identified. Lynch syndrome, also called hereditary nonpolyposis colorectal cancer (HNPCC), is the most common inherited CRC syndrome (see 1.3), followed by familial adenomatous polyposis (FAP), which is characterized by a mutation in the adenomatous polyposis coli (*APC*) gene [18, 19]. Due to a significantly increased CRC risk, young age of onset and predisposition to multiple tumors, patients with inherited CRC syndromes require special clinical care including intensified cancer surveillance and prevention programs [20].

1.1.1 Genomic instability in CRC

Mechanistically, CRCs arise through a multi-step accumulation of genetic alterations in the context of one or a combination of three molecular pathways: chromosomal instability (CIN), CpG island methylator phenotype (CIMP) and microsatellite instability (MSI) [21, 22].

The majority of sporadic CRCs (around 65–70 %) display CIN, which describes accelerated chromosomal changes leading to imbalanced chromosome numbers, subchromosomal genomic amplifications and loss of heterozygosity (LOH). The CIN phenotype can be caused by defects in pathways associated with chromosomal segregation, telomere regulation and DNA damage repair [23]. Accurate chromosome segregation can be impaired by mutations in genes that control the mitotic checkpoint, e.g. *hBUB1* and *hBUBR1*, resulting in CIN [22, 24]. Telomere dysfunction, which can lead to telomere crisis, is another driving force for CIN and shortened telomeres, compared to adjacent normal tissue, were observed in 77–90 % of CRCs [23]. As a consequence of telomere crisis, telomere-telomere fusion events occur, creating dicentric chromosomes which initiate CIN via breakage-fusion-bridge cycles [25]. Lastly, defects in DNA damage pathways can also lead to CIN and mutations in involved genes, such as *ATM*, *TP53*, *BRCA1* and *BRCA2*, are strongly associated with tumorigenesis [26]. Besides the structural and/or numerical chromosomal abnormalities in CIN tumors, mutations in a specific set of oncogenes and tumor suppressor genes are relevant for CRC pathogenesis [23]. As of yet, it is still not fully understood if CIN initiates tumorigenesis or if it is acquired as a result of the malignant process. Additionally, the stage of CRC tumorigenesis in which CIN occurs has not been defined yet [23]. However, several studies indicate that chromosomal aberrations hap-

pen early during colorectal tumorigenesis and over 90 % of colorectal adenomas display allelic imbalance [27]. CRCs that arise via the CIN pathway typically display microsatellite stability (MSS). However, around 12 % of CIN-positive CRCs also exhibit MSI, as the three named pathways are not mutually exclusive [28].

According to the widely accepted adenoma-carcinoma model for sporadic CRC (Figure 1) by Fearon and Vogelstein [29], mutations in *APC*, activating the Wnt signaling pathway, are early events in CRC tumorigenesis and initiate transformation of normal colonic epithelial cells [30]. Interestingly, several studies indicate that mutated *APC* or Wnt signaling might act as initiators of CIN [31–34]. 70–80 % of sporadic colorectal adenomas present *APC* mutations which matches the mutation frequency in sporadic CRCs. Further, *APC* mutations could be identified in the earliest microscopic adenomas, supporting the initiating character of this mutation [35, 36]. Following the initiation stage, around 30–50 % of CRCs acquire a mutation in the *KRAS* gene in the adenomatous stage [37]. The progression to a carcinoma is then characterized by deletion of chromosome 18q (in around 65 % of MSS CRCs [38]), including tumor suppressor genes such as *DCC* and *SMAD4*, and the inactivation of *TP53* on chromosome 17p (55–60 % of MSS CRCs [39, 40]).

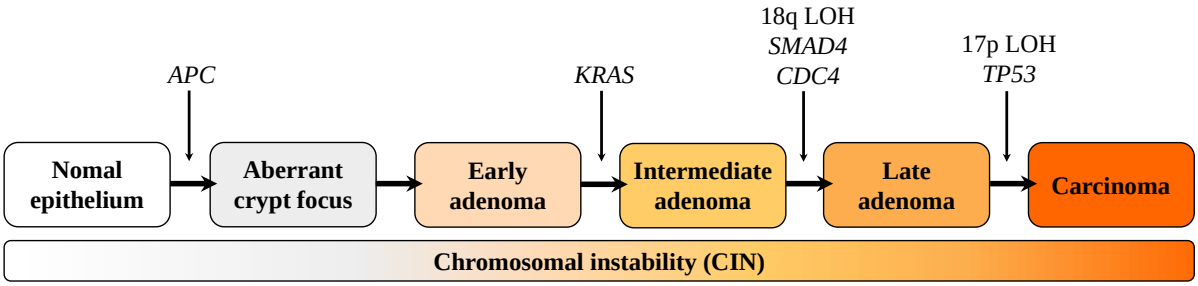

Figure 1: The adenoma-carcinoma model by Fearon and Vogelstein describing colorectal tumorigenesis. The sequential transformation from normal colorectal epithelium is initiated by mutations in *APC*. Progression to larger adenomas and ultimately carcinomas requires mutations in *KRAS* and *TP53*. Reproduced from: [29, 41].

A subset of CRCs develop through the CIMP pathway, which is characterized by epigenetic instability and global DNA hypermethylation [42, 43]. Around 50 % of human genes present with short CpG dinucleotide-rich sequences in the 5' region, so-called CpG islands. CpG islands are the favored substrate of DNA methyltransferases and are mainly found in promoter regions. Methlyation of such a CpG island results in transcriptional silencing of the respective gene [44]. Aberrant hypermethylation and subsequent inactivation of tumor suppressor genes is strongly associated with different cancer types [45]. Around 20 % of CRCs are thought to be CIMP-positive and present with several distinct features. CIMP CRCs are associated with female sex, often located in the proximal colon, show a high frequency of *BRAF* mutations and low *TP53* mutation rates [46]. Further, CIMP CRCs present with mucinous histology, poor dif-

ferentiation and mostly arise though the serrated pathway [43]. Importantly, CIMP is strongly associated with MSI, another major mechanism of genomic instability outlined below, and hypermethylation of *MLH1* is responsible for the majority of sporadic MSI CRCs (see 1.2) [47]. However, due to the defined histology, precursor lesions and molecular features, CIMP is considered a CRC subtype independent of the MSI status [43, 46].

1.2 Microsatellite instability

1.2.1 DNA mismatch repair

Around 15 % of CRCs exhibit MSI, which is caused by impairment of the DNA mismatch repair (MMR) system due to genetic and/or epigenetic mechanisms [36, 48].

The MMR system is a replication-coupled DNA repair mechanism that maintains genomic stability by correcting base mismatches and removing insertion/deletion loops (IDLs) from newly replicated DNA. Errors during DNA synthesis occur constantly and can escape the proofreading function of the DNA polymerase. MMR increases the replication fidelity by approximately 100–1,000-fold [49, 50]. Successful MMR requires the discrimination between normal base pairs and various kinds of mismatches as well as the distinction between the newly synthesized daughter strand containing mismatches and the parental template strand [51]. The strand-specific MMR is best characterized in *Escherichia coli* and mainly relies on three proteins: MutS, MutL and MutH [49, 52]. Briefly, the MutS homodimer recognizes DNA mismatches. Next, MutL acts as a mediator and recruits MutH, a sequence- and methylation-specific endonuclease, to MutS and the mismatch site. Crucially, MutH only targets the unmethylated, newly synthesized daughter strand, enabling strand discrimination. After nicking the daughter strand, excision is carried out by DNA helicases and DNA exonucleases. Lastly, re-synthesis is conducted by DNA polymerase III and a DNA ligase seals the newly synthesized strand [52, 53].
The MMR system is highly conserved across species, from bacteria to mammals, and MutS/MutL homologues have been identified in almost all organisms [54, 55]. Multiple human MMR proteins could be identified due to their homology to *Escherichia coli* MMR components. Mismatch recognition is executed by the human MutS homologues MSH2, MSH6 and MSH3 which form the heterodimers MutSα (MSH2-MSH6) and MutSβ (MSH2-MSH3). MutSα preferentially recognizes single base mismatches and small IDLs, whereas MutSβ mainly detects large IDLs up to 16 nucleotides [49, 56]. Similarly, four different human MutL homologues (MLH1, MLH3, PMS1, PMS2) exist that form functionally different heterodimers. MutLα (MLH1-PMS2), an endonuclease, is involved in MMR and introduces DNA nicks into the daughter strand. The role of MutLγ (MLH1-MLH3) is less well characterized, but it is though to play a minor role in MMR [49]. The function of MutLβ (MLH1-PMS1) is poorly understood.

More recent findings have demonstrated that MutLβ seems to be a unique endonuclease which potentially initiates triplet repeat DNA expansion, a mechanism that is involved in various inherited disorders, e.g. Huntington's disease [57]. The MutH protein has only been observed in *Escherichia coli* and closely related Gram-negative bacteria, and no homologues have been identified in eukaryotes [58]. Additionally to the described MMR protein homologues, several accessory proteins are known to be crucial for MMR in eukaryotes. Among others, proliferating cell nuclear antigen (PCNA), replication protein A, and exonuclease I assist the main MMR proteins in the repair process. PCNA is thought to mediate the strand-specific incision of the daughter strand by the MutLα endonuclease [59, 60].

A defective MMR system leads to a 100–1,000-fold increase in replication errors, which particularly occur at repetitive sequences such as microsatellites [61, 62]. The repetitive nature of these DNA stretches renders them especially prone to DNA polymerase slippage during DNA replication. Slippage events lead to the formation of IDLs, which are normally recognized and repaired by the MMR machinery. In a MMR-deficient setting, IDLs are not corrected, which results in the accumulation of insertion/deletion (indel) mutations and ultimately genomic instability (Figure 2). MMR deficiency and subsequent MSI are strongly associated with different types of cancer [48, 59].

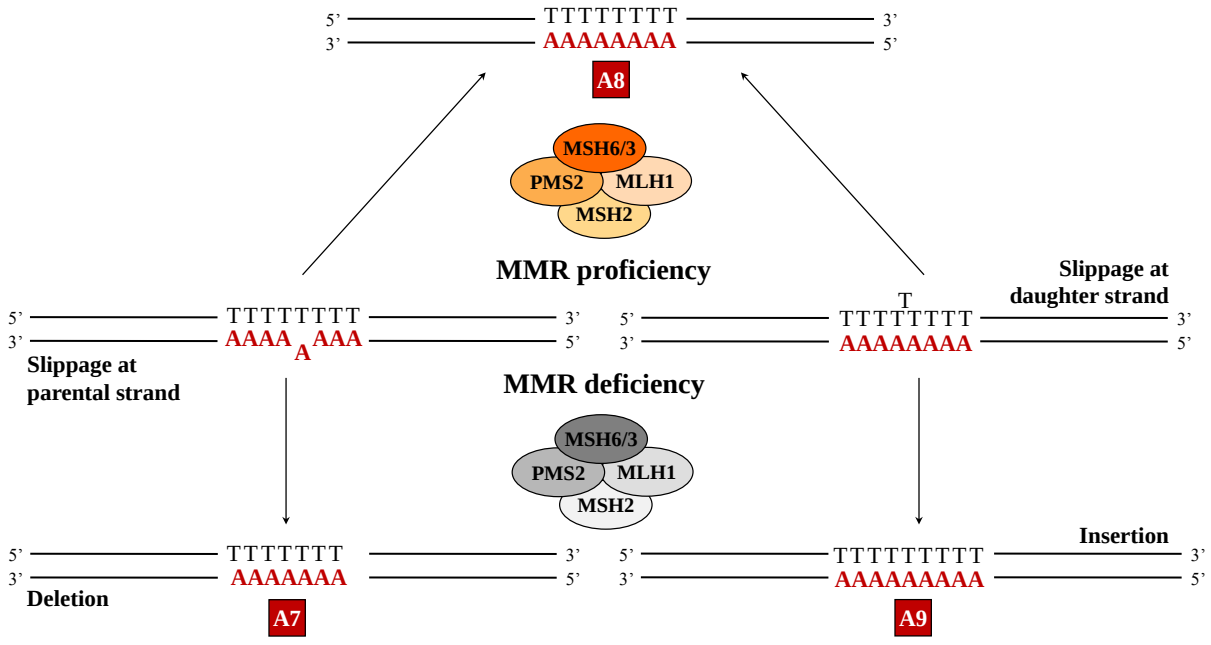

Figure 2: DNA polymerase slippage event in a MMR-proficient and -deficient setting. Repetitive microsatellite regions (here polyadenine: A8) are prone to DNA polymerase slippage during DNA replication. This type of replication error is typically corrected by the MMR system. Impairment of the MMR system leads to the addition (A9) or deletion (A7) of a nucleotide.

1.2.2 MSI CRC tumorigenesis

Microsatellites, or short tandem repeats (STR), are iterations of short nucleotide sequences that are highly abundant in eukaryotic genomes. Microsatellites mainly present as short mono-, di-, tri- and tetranucleotide repeats but can consist of up to six nucleotides [63]. Microsatellites are estimated to account for 3 % of the human genome. The majority of microsatellite sequences are located in non-coding intergenic and intronic regions and, due to their high degree of variability, are used as genetic markers, e.g. in forensic science [63, 64]. Non-coding microsatellites are assumed to evolve neutrally and are thought to play no role in malignant transformation. In contrast, microsatellites located in protein-encoding DNA, so-called coding microsatellites (cMS), play a crucial role in MSI tumorigenesis (Figure 3) [48, 65].

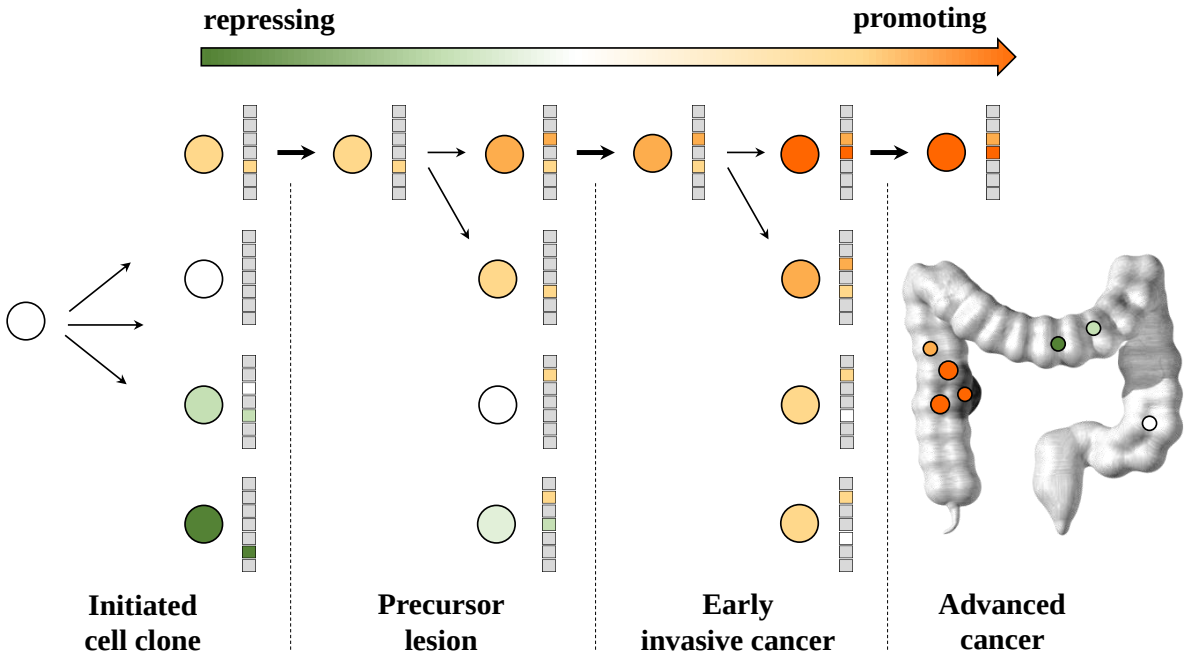

Figure 3: Evolutionary concept of MSI CRC development. The development of MSI CRCs is characterized by the accumulation of microsatellite mutations. Mutations in cMS are key events in MSI tumorigenesis and underlie an evolutionary process. Mutations promoting cell proliferation and tumor outgrowth are positively selected against neutral or growth-repressing mutations. The manifest CRC consequently presents with an overrepresentation of growth-promoting cMS mutations. Circles represent MMR-deficient cells and their cMS mutation pattern is visualized by the array of boxes. Green illustrates the growth-repressing nature of a cMS mutation/cell clone and orange indicates growth-promoting qualities. Modified from: [65].

The MSI phenotype was first discovered in CRC and is most commonly observed in CRC and endometrial cancer (EC) [66]. The majority of MSI CRCs arise sporadically and in around 80 % of cases the hypermethylation and subsequent silencing of *MLH1* is responsible for MMR deficiency and the resulting MSI phenotype. Around 20 % of MSI CRCs can be attributed to LS, which is characterized by a germline variant in one of the MMR genes (see 1.3) [65].

In the hereditary as well as sporadic setting, MMR-deficient cells accumulate large numbers of mutations in microsatellite regions (see 1.2.1). cMS mutations are considered drivers of malignant transformation and multiple cMS-containing genes have been identified to be frequently mutated in MSI CRCs, e.g. transforming growth factor beta receptor 2 (*TGFBR2*), BCL2-associated X protein (*BAX*) and activin type 2 receptor (*ACVR2A*) [67, 68]. One of the first described cancer-related cMS is the A10 microsatellite in exon 3 of the *TGFBR2* gene, which is mutated in around 80 % of MSI CRCs [69, 70]. *BAX*, a regulator of apoptosis, contains a G8 repeat and is also commonly mutated in MSI CRCs (around 50 %) [71]. Crucially, the introduction of cMS mutations, due to a defective MMR system, occurs randomly but is followed by a non-random, evolutionary persistence of mutations. In a Darwinian selection process mutations that favor tumor progression and outgrowth, e.g. due to the inactivation of a tumor suppressor gene, are positively selected against neutral or growth-repressing mutations. Consequently, recurrent cMS mutation patterns and an overrepresentation of growth-promoting mutations can be observed in manifest MSI CRCs (Figure 3) [48, 65].

1.2.3 Immunogenicity of frameshift peptide neoantigens

Mutations in cMS cannot only inactivate genes that are involved in various tumor-suppressive pathways, they can also lead to the production of altered and/or truncated protein products, so-called frameshift peptides (FSPs) [65]. If an insertion/deletion mutation in a cMS is not corrected by the MMR system, the addition or loss of a nucleotide manifests as shift in the translational reading frame. As a consequence, the transcription and translation of the affected gene leads to the generation of non-functional proteins with a novel FSP sequence at their C terminus (Figure 4) [65]. FSPs are considered true tumor-specific antigens as they are only present in emerging cancer cell clones. Importantly, MSI-induced FSPs are foreign to the host's immune system and their immunological potential was recognized early on [72]. The neopeptide stretches encompass multiple potential epitopes which render FSPs highly immunogenic and their immunogenicity was extensively demonstrated by multiple studies [73]. Initial observations by Linnebacher et al. and Saeterdal et al. identified frameshift mutation-derived FSPs that were capable of inducing T cell expansion. The produced cytotoxic T cells could successfully lyse CRC cells loaded with the respective peptide [74]. Further studies confirmed the proposed immunogenicity of FSPs and more cMS mutation-derived epitopes presenting with T cell reactivity could be identified [75–78]. Interestingly, Ballhausen et al. found that the cMS mutation frequency in a tumor is negatively correlated with the predicted immunogenicity of the respective FSP, indicating that highly immunogenic FSPs are counterselected during MSI tumor evolution [79].

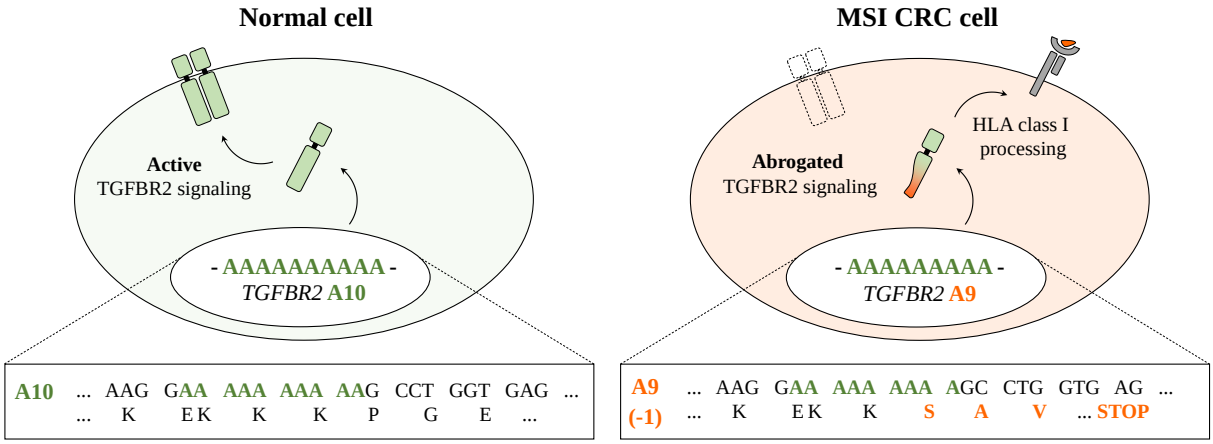

Figure 4: Generation of a FSP in a MSI CRC cell. The generation of a FSP starts with a polymerase slippage event at a microsatellite sequence (here A10 in *TGFBR2*), resulting in an insertion/deletion mutation (here -1). As the error is not corrected by the MMR system, the translational reading frame shifts producing an altered peptide. After translation, the FSP is processed by the human leukocyte antigen (HLA) machinery (here HLA class I) and presented on the cell surface. HLA-bound FSP neoantigens are able to trigger FSP-specific immune responses. In a normal cell the slippage of the polymerase does not lead to an indel mutation due to repair by the MMR system. Consequently, a TGFBR2 wild type protein is translated and active TGFBR2-mediated signaling is maintained.

FSP-specific T cell responses are commonly observed in tumor tissue and peripheral blood of MSI CRC patients. Moreover, it was shown that FSP-specific tumor-infiltrating lymphocytes (TILs) are able to effectively kill MSI CRC cells *in vitro* [80]. Consequently, vaccination with FSP neoantigens might represent a mechanism to control MSI CRCs and improve the patients' outcome [73]. FSP sequences can be predicted *in silico* using human genome sequence data and, due to the described clonal selection process (see 1.2.2), common tumor-specific FSPs that are shared among MSI CRCs can be identified [48]. In a phase I/IIa clinical trial, MSI CRC patients were vaccinated with three commonly mutated MSI-induced FSP antigens (derived from *HT001*, *TAF1B*, *AIM2*). This first-in-man study demonstrated low toxicity and rare adverse side effects of the vaccine as well as the induction of humoral and T cell-based immune responses [81].

1.2.3.1 Human leukocyte antigen system

The recognition of FSP neoantigens by the immune system requires processing through the cellular antigen processing machinery and presentation via human leukocyte antigen (HLA) molecules. The HLA system, referring to the human version of the major histocompatibility complex (MHC), is located on the short arm of chromosome 6 and encompasses more than 200 genes [82, 83]. The HLA genetic complex contains immune as well as non-immune genes and can be divided into three main regions: class I, II and III [84]. HLA surface molecules, responsible for the presentation of short peptides to T cells and therefore essential regulators of adaptive

immune responses, are encoded in class I and II genes. The class I region, consisting of approximately 20 genes, encodes for the α-chains of class I molecules. HLA-A, -B and -C are classic HLA I molecules and play a central role in antigen presentation. Non-classical HLA I subtypes are less polymorphic and their functions are less well studied [82, 85]. Notably, the class I β-chain is encoded by the β2-microglobulin (*B2M*) gene, which is not located in the HLA genetic complex but on chromosome 15 [82]. HLA class I proteins are ubiquitously expressed on the surface of all nucleated cells [86]. The HLA class II region comprises the subregions HLA-DM, -DO, -DP, -DQ and -DR, each containing genes (*A* and *B*) encoding for the α- and β-chains. An HLA class II molecule is formed by the non-covalent association of the α- and β-chain and its expression is restricted to immune cells such as B cells and other antigen-presenting cells (APCs) [82]. Lastly, genes in the class III region encode, e.g, components of the complement system [87]. The determination of an individual's HLA genotype is of immense importance for various medical treatments, e.g. transplantation of organs or hematopoietic stem cells [88].

The peptides that are presented by class I and II molecules differ in nature and source. Class I-associated peptides are predominantly generated from intracellular proteins via proteasomal degradation. The produced peptides are transported into the endoplasmic reticulum (ER) by the transporter associated with antigen processing (TAP) protein complex. Next, peptides (8–10 amino acid residues) are loaded onto HLA class I molecules, which are physically associated with TAP, and the assembled complexes translocate to the cell surface where the HLA-peptide complex is recognized by CD8-positive T cells. Importantly, the successful assembly of HLA class I molecules and their translocation to the surface require the association of the B2M light chain. Under normal physiological conditions class I peptides are the result of the continual turnover of proteins to which the immune system is not reactive. However, infection or malignant transformation of a cell results in the generation of foreign peptides, which are displayed on the cell surface and initiate immune responses [82, 89–91]. Class II peptides are exogenously derived and are internalized via endocytosis or phagocytosis by the HLA class II molecule-bearing cell, thereby entering the endocytic pathway. In contrast to class I, class II molecules are not assembled in the ER but are transported to the endocytic system and peptide loading occurs in late endosomes or MHC class II containing compartments. The trimming of peptides to 10–15 amino acid residues is thought to happen after binding to class II molecules via lysosomal proteases. Assembled class II complexes are transported to the cell surface where they interact with CD4-positive T cells [92–94]. Noteworthy, non-classical antigen presentation pathways exist, in which intracellular antigens are presented by class II molecules and exogenous peptides gain access to class I molecules [94, 95]. The presentation of exogenous, internalized antigens on HLA class I molecules is termed cross-presentation and mainly performed by dendritic cells. The cross-presenting mechanism is essential for the initiation of cytotoxic T cell responses if APCs are not directly affected by infection or malignant transformation [96, 97].

HLA class I and II molecules are integral for the T cell selection in the thymus. Upon entering the thymic cortex, T cell precursors differentiate into CD4- and CD8-double-positive T cells, which require recognition of HLA-peptide complexes on thymic epithelial cells via their T cell receptor (TCR) to survive and further differentiate into CD4- and CD8-single-positive T cells. During this so-called positive selection, T cells acquire MHC restriction [98], which refers to the ability of T cells to only recognize antigens bound by self-MHC molecules [99]. Positively selected T cells migrate further into the thymic medulla and undergo negative selection. Doing so, T cells interact with APCs displaying numerous HLA-peptide complexes. High affinity interactions between the TCR and HLA-peptide ligands initiate apoptosis of the T cell and ultimately results in the elimination of most self-reactive T cells. Eventually, T cells that express a functional TCR without major reactivity to self-antigens and therefore survived the positive and negative selection processes enter the periphery [82, 99]. Importantly, the diversity of HLA-bound peptides during thymic maturation shapes the mature T cell repertoire [100, 101]. Thus, the variability of HLA molecules correlates with the diversity of TCR which in turn affects disease resistance of an individual. Different HLA alleles increase the number of potential epitopes and therefore facilitate broader immune responses as well as a more versatile protection. The immense diversity of HLA alleles is thought to has evolved under a strong selection pressure and the constant encounter of new infections [102, 103].

The HLA system also plays a crucial role in cancer development and therapy response as the HLA type determines the repertoire of presented tumor-derived antigens, impacting anti-tumor immunity [104]. Interestingly, HLA polymorphism was also found to be an influential factor in response to ICB therapy as cancer patients with maximal HLA class I heterozygosity presented with improved overall survival upon treatment, compared to patients displaying homozygosity for at least one HLA class I locus [105]. In the context of MSI cancers, Ballhausen et al. observed evidence for HLA type-dependent immunoediting as the patient's HLA-A*02:01 status was related to the cMS mutation pattern. MSI CRCs from HLA-A*02:01-positive patients presented significantly less cMS mutations that would give rise to predicted HLA-A*02:01 FSP neoepitopes [79]. However, the systematic characterization of HLA-dependent FSP neoantigen-specific immune responses in MSI cancers is lacking. Further, little is known about the impact of the HLA type on cancer risk of LS carriers.

1.2.3.2 Immune evasion mechanisms in MSI CRC

Despite the constant immune surveillance and their strong immunogenicity, MMR-deficient cell clones still manage to grow out and progress to manifest MSI CRCs. For this to be possible, outgrowing tumor cells need to defy the anti-tumoral environment and circumvent the immune system. Different mechanisms enable successful immune evasion, such as defective antigen presentation and processing [106, 107].

About 70 % of MSI CRCs present with the loss of HLA class I antigen presentation via various mechanisms. This prevents CD8-positive T cell recognition and killing, enabling immune evasion [107]. The most frequent and best characterized mechanism thereof is mutations in the *B2M* gene [108, 109]. *B2M* encodes the B2M β-chain which is crucial for the assembly of the HLA class I complex, further consisting of the class I α-chain and a peptide fragment (see 1.2.3.1) [110]. Importantly, the *B2M* gene harbors four microsatellite stretches in its coding region, rendering *B2M* particularly susceptible to mutations in a MMR-deficient scenario [106, 111]. Around 30 % of all MSI CRCs display *B2M* mutations and a subsequent loss of HLA class I-based antigen presentation. LS-associated MSI CRCs seem to present with a higher frequency of *B2M* mutations (36 %), compared to sporadic MSI CRCs (15 %), which is possibly attributable to the immunoselective pressure during the development of hereditary MSI CRCs [111]. In line, *B2M* mutations are often associated with a highly activated immune microenvironment and predominantly occur under strong immune surveillance [112, 113]. The immunoselective pressure seems to build up early as *B2M* mutations can occur at a precancerous stage of MSI CRC tumorigenesis and around 15 % of MSI adenomas present with such a mutation. The *B2M* mutation frequency further increases with tumor progression [111].
Alongside *B2M* mutations, other mechanisms, such as mutations in antigen processing machinery (APM) component genes, e.g. *TAP1*, *TAP2* and TAP binding protein (*TAPBP*), are involved in the abrogation of HLA class I-mediated antigen presentation in MSI CRCs [107, 114].

Another, less well characterized, immune evasion mechanism reported for MSI CRCs is the aberration of HLA class II antigen presentation and subsequent loss of CD4-positive T cell-mediated immune responses [106]. The presentation of HLA class II antigens in the colonic epithelium is not constitutive but inducible by immunostimulatory factors, e.g. interferon-γ (IFNγ). Further, several regulatory proteins, such as class II transactivator (*CIITA*) and regulatory factor 5 (*RFX5*), control the expression of class II antigens [115]. Around one third of MSI CRCs lack HLA class II antigen expression and various alterations, e.g. in the regulator genes *CIITA* and *RFX5*, have been identified [116, 117]. *CIITA* and *RFX5* both harbor microsatellite sequences in their coding region and frameshift mutations in both genes were observed in MSI CRCs. *RFX5* cMS mutations are found in around 30 % of HLA class II antigen-negative MSI CRCs. The underlying mechanism appears to be similar to the previously described MMR deficiency-induced inactivation of *B2M* [117, 118]. Mutations in HLA class II regulatory genes were predominantly observed in CRCs with a high number of CD4-positive TILs, indicating that a dense infiltration with CD4-positive T cells favors the outgrowth of HLA class II antigen-negative tumor cell clones [118].

The loss of antigen presentation has prognostic implications for MSI CRC patients. *B2M* mutations and a subsequent loss of HLA class I antigen expression are associated with a favorable clinical course as well as lack of disease relapse and distant metastases [111, 119, 120]. Further-

more, *B2M*-mutated metastatic MSI gastrointestinal cancers present with a distinct metastatic pattern, compared to *B2M*-wild type (WT) cancers. Concretely, *B2M* mutations were found to be associated with peritoneal metastases which generally have a more favorable outcome, compared to hematogenous metastases [121]. Additionally, it was observed that a partial downregulation of HLA class I antigen presentation correlates with a worse prognosis, compared to a complete loss of HLA class I. It has been suggested that a complete lack of HLA class I antigens might render cells susceptible towards natural killer (NK) cell-mediated killing. Therefore, a downregulation of class I antigens, retaining HLA class I expression, could prevent effective T cell recognition and at the same time avoid NK cell activation [122].

1.2.4 Clinicopathological characteristics of MSI CRC

CRCs that arise through the MSI pathway display certain clinical and pathological features which distinguish them from MSS CRCs. MSI CRCs are predominantly located in the proximal colon where they display an expansive and cohesive invasion pattern. Further, MSI tumors are less prone to form distant metastases but often occur with syn- or metachronous additional tumors [65]. Histopathologically, MSI CRCs are characterized by poor or mixed differentiation, often presenting with mucinous or signet cell areas [123]. Importantly, a reliable characteristic for MSI CRCs is the high number of TILs [124–126]. The majority of TILs have been found to be activated cytotoxic lymphocytes and exhibit expression of granzyme B [127, 128]. Moreover, MSI CRC-associated TILs display an upregulation of multiple immune checkpoints, such as programmed cell death protein 1 (PD-1), cytotoxic T lymphocyte-associated antigen 4 (CTLA-4) and indoleamine 2'3'-dioxygenase (IDO). MSI tumor cells and tumor-associated myeloid cell populations frequently express programmed cell death 1 ligand 1 (PD-L1). The increased expression of immune checkpoints is not only a direct consequence of the immunologically active milieu, it also counterbalances the tumor's vigorous immune microenvironment and renders MSI CRCs susceptible to ICB therapy (see 1.2.4.1) [129, 130]. The strong T cell infiltration is often accompanied by lymphocyte aggregations, so-called Crohn's-like reactions [131]. The pronounced local immune responses are thought to be associated with the production of immunogenic FSP neoantigens following MMR deficiency and MSI (see 1.2.3) [65].

Compared to MSS CRCs, MSI CRCs are associated with a more favorable prognosis and present with longer disease-free and overall survival [132–134]. Importantly, the MSI phenotype can also affect therapy response. The 5-fluorouracil (5-FU) agent is an integral component of the standard chemotherapeutic treatment for CRC and often applied in combination with levamisole or leucovorin [135]. The tumor's MSI status was found to be a determining factor for 5-FU-based therapy response. While stage II/III MSS CRC patients benefit from 5-FU-based chemotherapy, overall survival of MSI CRC patients is not prolonged under this treatment and detrimental effects have been observed [136, 137]. Mechanistically, a functioning MMR sys-

tem seems to be a prerequisite for cell death induction upon 5-FU integration, which explains the poor response of MMR-deficient cancers to this therapy. However, MSI CRCs respond well to irinotecan-based therapies, which seem to be independent of the DNA MMR system [138]. MSI is an important predictor for ICB treatment response (see 1.2.4.1) [139].

1.2.4.1 Immune Checkpoint Blockade Therapy

In general, the immune system is capable of recognizing and killing tumor cells, which is mainly orchestrated by T cells. However, tumor cells can escape tumor-reactive immune responses and hence destruction via various mechanisms, e.g. loss of antigen presentation (see 1.2.3.2) and dysregulation of immune checkpoints. As surface molecules immune checkpoints can be easily targeted by antibodies that block ligand-receptor engagement and thereby enable reactivation of anti-tumor immunity [140]. Within the last decade, immunotherapy with immune checkpoint modulators achieved unprecedented clinical success [141].

Besides the interaction between the TCR and HLA-bound peptides on the surface of APCs, productive T cell activation requires the engagement with antigen-independent co-stimulatory receptors, also known as immune checkpoints. Under normal physiological conditions immune checkpoints maintain self-tolerance, prevent unwanted auto-immunity and act as gatekeepers of immune responses. They provide co-stimulatory or co-inhibitory signals and thereby tightly control T cell activation. Interaction with co-stimulatory receptors, e.g. CD28, completes T cell activation and allows T cells to proliferate. On the contrary, engagement with co-inhibitory receptors, such as CTLA-4, leads to suppression of T cell activation. Importantly, tumors can co-opt immune checkpoint pathways, enabling immune resistance and evasion [141–143]. In the context of ICB the two inhibitory receptors CTLA-4 and PD-1 are the best characterized ones and have been successfully targeted in the clinical setting [141].

CTLA-4 is a CD28 homolog and while presenting structural and biochemical similarities, these receptors have opposite immunoregulatory functions. CTLA-4 is predominantly but not constitutively expressed on T cells and is rapidly upregulated upon antigen recognition. CTLA-4 dampens T cell responses and therefore counteracts the activity of CD28, which is constitutively expressed on T cells and strongly induces T cell activation. Both receptors share and compete for the same ligands, namely CD80 (also called B7.1) and CD86 (B7.2), which are expressed on APCs [144, 145]. CTLA-4 has a 100–1,000-fold greater affinity to the B7 proteins than CD28 and is capable of a process called trans-endocytosis [146]. Trans-endocytosis leads to the removal of B7 ligands from the cell surface and lysosomal degradation of such in the CTLA-4 expressing cell. Consequently, CTLA-4 deprives the T cell of CD28-mediated signaling and limits T cell activation [147]. The attenuation of T cell activity due to CTLA-4 primarily occurs during the T cell priming phase at an early stage of T cell activation and within lymphoid organs [141,

148]. The importance of CTLA-4 in negatively regulating T cell activation becomes apparent in CTLA-4-deficient mice, which die within three to four weeks of age due to massive lymphocytic tissue infiltration and organ destruction [149]. CTLA-4 was not only the first negative regulator of T cell activation to be identified, it was also the first clinically targeted immune checkpoint [141]. Allison et al. first observed that blocking CTLA-4 using antibodies enhances anti-tumor immunity and can lead to tumor rejection in mice [150]. In the year 2000, clinical testing of CTLA-4 antibodies was initiated and finally led to the FDA-approval of ipilimumab for the treatment of advanced melanoma [141, 151].

PD-1 is another co-inhibitory receptor and also functions as a negative regulator of T cell activation. In contrast to CTLA-4, PD-1 acts at later phases of T cell activation and regulates continued T cell activation and proliferation, predominantly in peripheral tissues. The PD-1 pathway plays a major role in maintaining self-tolerance [141, 148]. PD-1 is expressed on activated immune cells, including T, B and NK cells as well as macrophages and dendritic cells [152]. PD-1 exerts its inhibitory function by binding to its two ligands PD-L1 (also known as CD273) and PD-L2 (B7-DC), which are both members of the B7 protein family. While PD-L1 is widely expressed on various hematopoietic and non-hematopoietic cells, the expression of PD-L2 is mainly restricted to APCs [153]. Engagement of PD-1 with its ligands leads to the phosphorylation of PD-1 at cytoplasmic tyrosine residues, which enables the binding of protein tyrosine phosphatases, inducing inhibitory intracellular signaling. Functionally, PD-1 signaling leads to decreased T cell activation, proliferation, survival and cytokine production [148, 154]. Tumors can hijack the PD-1 pathway and overexpression of PD-1 ligands, especially PD-L1, was observed in several cancer types, e.g. ovarian, breast and lung cancer as well as melanoma [141, 155]. Moreover, PD-1 was found to be highly expressed on TILs from different tumor types and binding to PD-L1 promotes immune evasion by inhibiting anti-tumor immune responses, enabling tumor progression [156]. Accordingly, several preclinical studies demonstrated that blocking the PD-1/PD-L1 axis can enhance anti-tumor T cell reactivity [157, 158]. In 2014, the first PD-1 antibody for the treatment of advanced melanoma was approved by the FDA [159]. Up to now, five antibody-based PD-1/PD-L1 inhibitors have been approved by the FDA for the treatment of various cancers, e.g. melanoma, non-small cell lung cancer, renal cell carcinoma, bladder cancer and Hodgkin lymphoma [148]. Importantly, in 2017 the PD-1 inhibitor pembrolizumab was approved for the use in advanced solid tumors presenting the MSI phenotype, making it the first FDA approval for a treatment based on a molecular tumor biomarker, independent of the tissue of origin [160]. A phase II clinical trial by Le at al. demonstrated an enhanced effectiveness of pembrolizumab therapy in MSI CRC, compared to MSS CRC, patients [161]. Further, Le et al. could show that treatment with pembrolizumab induced the expansion of FSP neoantigen-specific T cell clones *in vivo*. The responsiveness of MSI tumors to ICB therapy is possibly attributable to the large proportion of MSI-induced neoantigens (see 1.2.3) [139]. The pronounced T cell infiltration, which is characteristic for

MSI tumors, seems to be one prerequisite of ICB-induced anti-tumor immune responses [162]. In addition to the immune status of the tumor microenvironment, the tumor mutational burden and neoantigen load, the microbiome and the host's immunity seem to play a role in determining the efficacy of ICB treatment. Exploration of the key factors influencing ICB response is necessary for the identification of reliable, predictive biomarkers and the subsequent improvement of the currently restricted response rates [162, 163].

1.3 Lynch syndrome

1.3.1 Molecular and clinical characteristics of Lynch syndrome

Lynch syndrome (LS) is caused by a monoallelic germline variant in one of the MMR genes which inactivates the respective MMR gene allele. A second somatic hit (Knudson's two-hit hypothesis), inactivating the remaining functioning allele, leads to MMR deficiency and ultimately induces MSI tumor formation [164, 165]. LS is characterized by an autosomal dominant inheritance and classical LS families present with 50 % carriers in consecutive generations [166]. Interestingly, disease expression, e.g. age of cancer onset and prognosis, are variable between and within LS families with the same MMR variant, which is probably attributable to genetic and environmental factors [167, 168]. Overall, LS is a highly variable disease and displays genetic as well as phenotypic heterogeneity, which is reflected by alterations in different signaling pathways as well as great variation in disease penetrance [168, 169]. LS carriers are predisposed to the development of cancer in different organ systems, most commonly in the colorectum and endometrium. Approximately 20–30 % of MSI CRCs and 2–3 % of all CRCs are associated with LS [19, 66]. However, a wide spectrum of cancers in, e.g. ovary, stomach, kidney, bladder, pancreas and brain, has been reported in the context of LS [19, 170]. The pattern and incidence rates of cancer types vary geographically, indicating that environmental and lifestyle factors also play a role in LS-associated tumorigenesis [171]. The lifetime tumor risk in affected individuals varies according to the tumor type and ranges between 30–80 % for CRC (see 1.3.3) [19, 172].

LS-associated MSI CRCs generally share the clinicopathological features described for MSI CRCs (see 1.2.4). However, LS MSI CRCs also present characteristics that distinguish them from sporadic MSI CRCs. First, they are characterized by an early age of cancer onset. LS carriers typically develop CRC under 50 years of age, which is decades earlier compared to the general population [166]. Sporadic MSI CRCs commonly arise in patients older than 60 years of age [173]. Second, LS-related CRCs arise through distinct pathogenic mechanisms. Sporadic MSI CRCs predominantly occur due to the CIMP-associated methylation of *MLH1*, which is strongly associated with the serrated pathway and *BRAF* mutations (see 1.1.1). Around 64 % of sporadic MSI CRCs present with a *BRAF* V600E mutation, contrary to LS-associated

MSI CRCs which are rarely *BRAF*-mutated (1.4 %) [174]. LS-associated CRCs do not develop through a single pathway but can arise through three distinct molecular pathways outlined below.

1.3.2 Pathogenesis of Lynch syndrome

A subset of CRCs in LS carriers arise through conventional adenomas after secondary inactivation of the affected MMR gene [175]. In general, the incidence of colorectal adenomas is slightly higher in LS carriers, compared to the general population [176, 177]. Adenomas in LS carriers, compared to the ones in non-LS individuals, have been reported to be larger and more frequently present with high-grade dysplasia as well as extensive villous architecture, which are associated with a high risk of malignant transformation [176, 178]. In LS carriers the progression from adenoma to invasive carcinoma is accelerated and was reported to occur within three to five years [179]. In the context of sporadic CRCs the progression through the adenoma-carcinoma sequence is estimated to happen over approximately ten years [180]. The rapid malignant transformation of LS-associated adenomas is thought to be induced by the inactivation of the MMR system and the subsequent accumulation of mutations [168]. In line, MMR deficiency in LS adenomas is associated with larger size and higher grade [181, 182]. The observation that LS carriers frequently present with CRCs within surveillance intervals and after a colonoscopy without pathological findings further supports an accelerated adenoma-carcinoma sequence [166, 183]. However, the occurrence of LS-associated CRCs even under regular colonoscopic surveillance and despite the removal of adenomas indicates that a substantial proportion of colorectal lesions might not be detectable by conventional colonoscopy [175, 184].

In addition to the described pathway in which MMR deficiency is not an initiating event but acts as an accelerator of tumorigenesis, Ahadova et al. propose two additional pathways which are both initiated by nonpolypous and MMR-deficient precursor lesions, so-called MMR-deficient crypt foci (MMR-DCF) [175]. MMR-DCF are a type of LS-specific premalignant lesion and thousands of MMR-DCF (about one per 1 cm^2) are found in the intestinal mucosa of LS carriers. MMR-DCF are morphologically mostly indistinguishable from normal colonic crypts, even though fission, nuclear enlargement and altered branching of the affected crypts have been reported. On the molecular level MMR-DCF are characterized by a loss of MMR protein expression (Figure 5) [185, 186]. The detection of MSI (in around 89 %) and FSP-associated cMS mutations (e.g. in *TGFBR2*, *BAX*, *HT001*, *AIM2*) in MMR-DCF supports the precancerous nature of these lesions [185, 187]. The development of CRC through MMR-DCF is characterized by the preceding role of MMR deficiency and can follow two different pathways. First, the MMR-DCF can progress into a MMR-deficient adenoma and ultimately into a carcinoma. Second, MMR-DCF can immediately progress into an invasive carcinoma without the formation of adenomatous polyps.

Incorporation of three distinct pathways into one integrative model of LS-associated CRC tumorigenesis (Figure 6) allows resolution of the conflicting observations concerning the onset and timing of MMR deficiency. The relative distribution of each of the pathways will have to be assessed in future studies and presumably varies between populations. However, it is thought that only a small subset of LS-associated CRCs develops through the conventional adenoma-carcinoma sequence and the larger proportion of CRCs arise from MMR-deficient, nonpolypous lesions [175].

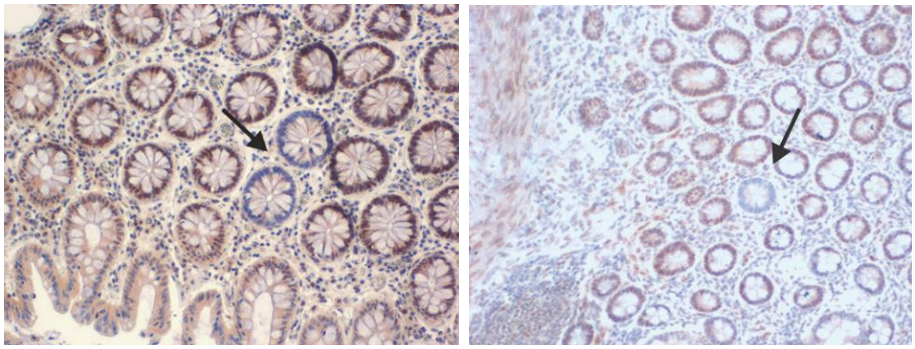

Figure 5: Representative example of two MMR-DCF in the normal colonic mucosa of a LS carrier. Staining for the respective MMR protein corresponding to the germline mutation of the given LS carrier reveals the selective absence of MMR protein expression. Adapted from: [187].

Importantly, the different molecular pathways seem to be associated with the underlying MMR germline variant as well as the affected signaling pathways which are involved in tumorigenesis [169]. The majority of CRCs (ca. 90 %) present with mutations within the Wnt/β-catenin pathway and Wnt signaling-activating mutations in *APC* and *CTNNB1* are frequently observed in LS-associated CRCs [188, 189]. Interestingly, LS-associated CRCs more frequently present with frameshift mutations in repetitive regions of *APC*, which are rare in MSS CRCs, indicating that MMR deficiency often precedes *APC* mutations [175, 190]. In a scenario in which MMR deficiency acts as an initial event, a secondary *APC* mutation in a MMR-DCF might induce adenoma formation with subsequent progression to a carcinoma. Ahadova et al. estimate that approximately 60 % of *APC* mutations occur after inactivation of the MMR system [175]. In contrast, *CTNNB1* mutations seem to be associated with nonpolypous LS CRC development and the MMR-DCF-carcinoma pathway as CRCs harboring such a mutation present with a growth pattern indicative of immediate invasive growth [191]. *CTNNB1* mutations are commonly found in *MLH1* carriers (ca. 50 %), rarely observed in *MSH2* carriers (7 %) and not reported for *PMS2* carriers [169, 192, 193]. Intriguingly, *MLH1* and *MSH2* carriers have a similar incident CRC risk but possibly display differences in their carcinogenesis. *MSH2* carriers present a substantially higher adenoma incidence and a higher frequency of somatic *APC* mutations, indicating a potentially accelerated adenoma-carcinoma sequence. On the contrary, a lower adenoma incidence and more frequent *CTNNB1* mutations are reported for *MLH1* carriers, pointing towards

CRC manifestation via the MMR-DCF-carcinoma pathway. In line, *PMS2* carries, who present with a high efficacy of colonoscopic surveillance and no incident CRCs, do not present with *CTNNB1* mutations [193–195].

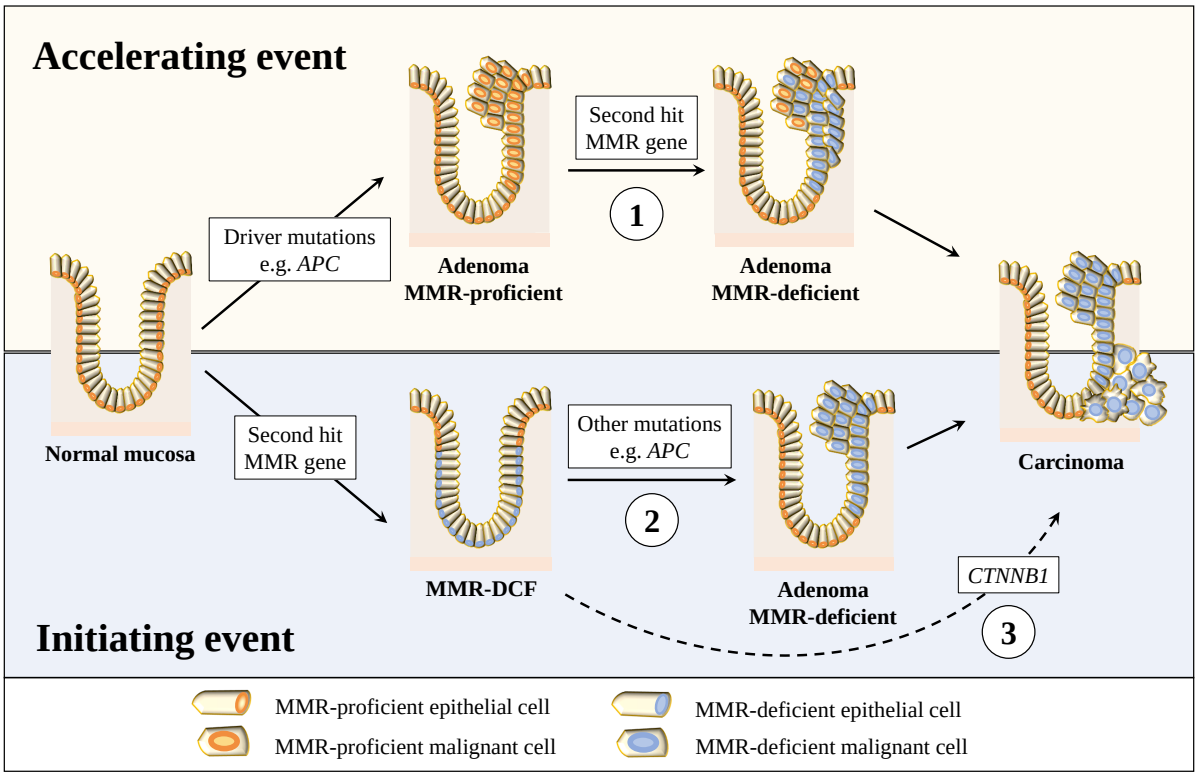

Figure 6: Three distinct pathways of LS-associated CRC development with MMR deficiency as an accelerating or initiating event. (1) LS CRC development begins with the formation of a MMR-proficient adenoma, e.g. due to an *APC* mutation, and MMR deficiency is a potentially accelerating event. (2) CRCs arise from MMR-DCF and undergo an adenomatous phase before progressing into an invasive carcinoma. (3) MMR-DCF immediately give rise to an invasive carcinoma without the formation of macroscopically visible adenomatous polyps. The MMR-DCF-carcinoma pathways is thought to be associated with somatic *CTNNB1* mutations.

1.3.3 Prevalence and cancer risk

LS is the most common inherited CRC syndrome with an estimated allele frequency of 1:280 or higher, affecting approximately 25 million people worldwide [196]. Over 500 pathogenic LS-associated MMR variants have been identified, predominantly in *MLH1*, *MSH2*, *MSH6* and *PMS2* (Figure 7) [197]. Germline alterations in *MLH1* and *MSH2* account for ca. 90 % of all LS-associated cancers with *MLH1* variants found in around 50 % and *MSH2* variants in 30–40 % of LS cancers [198, 199]. Among the general population variants in *MSH6* (1 in 758) and *PMS2* (1 in 714) were found to be more prevalent, compared to the more pathogenic *MLH1* (1 in 1,946) and *MSH2* (1 in 2,841) gene variants [196]. In 1–3 % of LS cases germline deletions

in 3' exons of the *EPCAM* gene lead to an inactivation of *MSH2*. Disruption of the 3' region of *EPCAM,* removing the transcriptional termination sequence, causes continued transcription into the adjacent *MSH2* gene inducing hypermethylation of the *MSH2* promoter and ultimately leading to an epigenetic silencing of *MSH2* [200, 201].

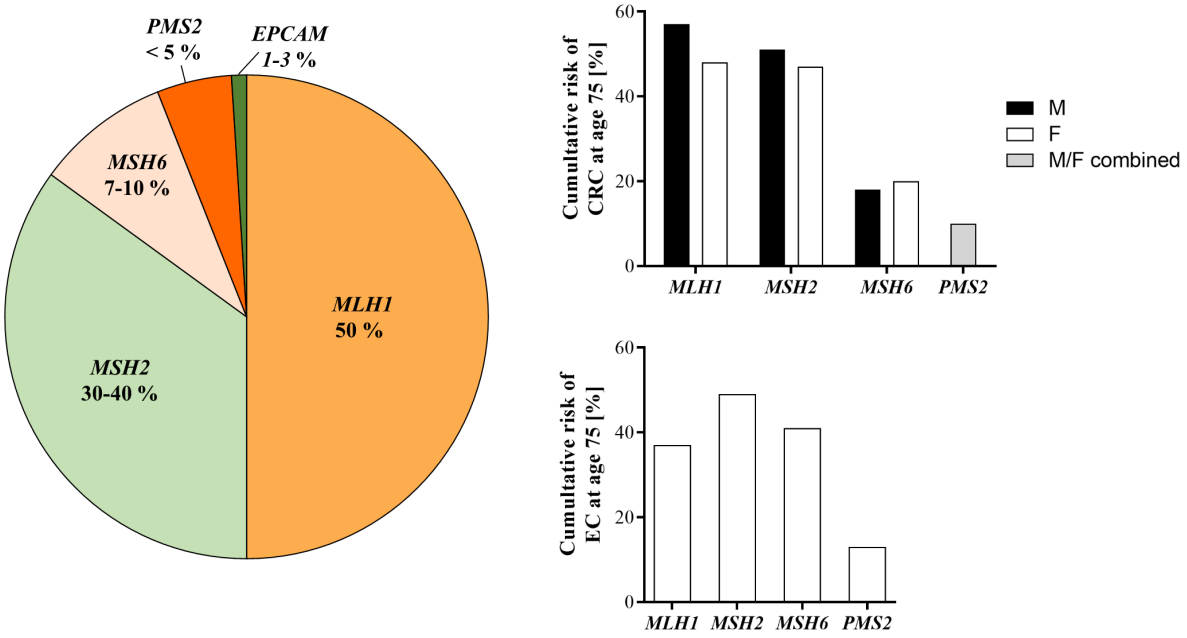

Figure 7: Frequency and associated cancer risk for MMR gene variants. *MLH1* and *MSH2* germline variants account for more than 90 % of LS-associated cancers. Alterations in *MSH6*, *PMS2* and *EPCAM* occur to a lesser extent. The highest lifetime risk for CRC has been reported for *MLH1* and *MSH2*. Compared to *MLH1* and *MSH2*, *MSH6* is associated with a lower CRC risk in both genders and an increased risk for EC in females. *PMS2* carriers have a low risk for CRC and EC. Cumulative cancer risks at age 75 were calculated using the Prospective Lynch Syndrome Database (PLSD): `http://www.plsd.eu/`.

The overall tumor risk is dependent on the MMR gene affected in the germline (Figure 7). The highest cumulative risk for CRC (50–80 %) was observed in *MLH1* and *MSH2* carriers [184, 202]. While *MSH2* carriers of both genders have a similarly high risk of CRC, male *MLH1* carriers are at higher risk to develop CRC, compared to females [202]. Carriers of an *EPCAM* deletion have a similar CRC risk as *MSH2* carriers [203]. Compared to *MLH1* and *MSH2* carriers, the lifetime cancer risk for *MSH6* and *PMS2* carriers is lower, ranging from 10–20 % for *MSH6* and amounting to around 10 % for *PMS2* [202, 204–206]. *MSH6*, while being associated with a moderately increased risk for CRC in both genders, displays a sex-limited trait as female carriers are at high risk of EC [202]. Further, the carrier's sex impacts CRC risk in *PMS2* carriers and males have an increased risk of developing CRC (20 %), compared to females (10 %) [205]. Additionally, *MSH6* and *PMS2* germline variants have been associated with a later CRC onset (around 10 years later), compared to *MLH1* and *MSH2* [204, 205, 207].

The generally low penetrance of *MSH6* and *PMS2* variants may be attributable to the formation of alternative MMR heterodimers. In the case of MSH6 deficiency heterodimerization between MSH2 and MSH3 occurs. In the absence of PMS2 MLH1 forms a heterodimer with MLH3 or PMS1 [208].

1.3.4 FSP-specific immune responses in Lynch syndrome and their clinical potential

The immunogenicity of LS-associated cancers is the result of the disease-defining germline variant affecting one of the MMR genes and the loss of MMR function upon a second somatic hit. Tumors arising from MMR-deficient cells accumulate frameshift mutations, present with a high mutational load and the MSI phenotype. cMS mutations lead to the production of neopeptides and a high antigen load (see 1.2.3) [65]. Consequently, LS-associated CRCs and extracolonic cancers display dense immune infiltration, which is characteristic for the MSI phenotype (see 1.2.4). MSI CRCs of hereditary origin seem to be associated with elevated T cell infiltration and local immune responses, compared to sporadic MSI CRCs [113, 118, 209–211]. One possible explanation for the potential immunological differences might be the proposed life-long stimulation of the immune system via FSP neoantigens in LS carriers. Interestingly, FSP-specific T cell responses have been detected in the peripheral blood of LS carriers without a history of cancer, indicating early interaction between the immune system and arising MSI lesions. Notably, such responses were not identified in healthy, non-LS individuals [80]. In addition, antibody responses against multiple FSPs were not only observed in LS-associated MSI CRC patients but also in the serum of healthy LS carriers [212].

MMR-DCF in the normal colonic mucosa of LS carriers (see 1.3.2) could represent a possible and cancer-independent source of FSP neoantigens and might induce an auto-immunization mechanism in LS individuals. Such a mechanism might also explain the comparatively low and incomplete penetrance of LS as the FSP neoantigen-mediated immune surveillance would prevent the outgrowth of many early lesions into invasive carcinomas, exemplifying the ‘elimination phase’ of cancer immunoediting [65, 185, 186, 213]. Based on these observations a FSP neoantigen-based vaccination strategy might be able to boost immune surveillance and therefore prevent cancer development in LS individuals. A recent study by Gebert et al. demonstrated the effectiveness of such an immunopreventive approach in a *VCMsh2* LS mouse model. This model is characterized by a conditional knockout of *MSH2* in the intestine, leading to the development of intestinal tumors. The recurrent vaccination of *VCMsh2* mice with four different FSPs greatly increased FSP-specific immunity, delayed intestinal tumor formation and prolonged overall survival. Furthermore, FSP vaccination in combination with non-steroidal anti-inflammatory drugs (NSAIDs) resulted in prolonged survival and reduced tumor burden, compared to FSP vaccination alone. This points towards potentiated FSP-specific immune responses and a synergistic effect between NSAIDs and FSP vaccination [214].

The presence of immune responses against MSI-induced FSP antigens in LS carriers prior to cancer development might also harbor diagnostic potential. The identification of LS carriers, e.g. on an immunological basis, without the requirement of an already manifest tumor could aid to overcome current shortcomings of LS diagnostics (see 1.3.5).

1.3.5 Diagnosis and management of Lynch syndrome

Early diagnosis of LS is of the essence in order to initiate preventive screening programs and therefore reduce the cancer risk of affected individuals. Two different diagnostic strategies are applied: screening of a tumor for MSI and MMR deficiency as LS indicators or direct genetic testing of individuals with a strong personal or family history indicating LS [215]. In general, at-risk individuals are offered molecular genetic testing to detect a potential pathogenic germline variant in one of the MMR genes. LS-related pathogenic variants are distributed throughout the MMR genes and more than 3,000 different germline MMR sequence variants have been archived in the International Society for Gastrointestinal and Hereditary Tumors (InSiGHT) database. The most frequently observed genetic variants represent point mutations but large rearrangements have also been reported [208]. Importantly, 20–30 % of detected MMR variants are classified as so-called variants of uncertain significance (VUS) and are characterized by an unknown pathogenicity [216]. In recent years, targeted next generation sequencing (NGS) has increasingly replaced Sanger sequencing in the genetic diagnostics of LS due to its cost-effectiveness, high throughput and multiple gene (panel) testing [217].

Currently, LS diagnostics relies on the molecular screening, including PCR-based MSI and immunohistochemical (IHC) analysis, of an already manifest tumor. MSI is considered as a hallmark of LS and is observed in around 90 % of LS-related tumors [218]. MSI tumor analysis is recommended for all CRC patients under 70 years of age and selection of tumors can further be guided by the Bethesda and revised Bethesda guidelines [219–221]. Previously, the more restrictive Amsterdam Criteria and updated Amsterdam II Criteria, which were defined by the International Collaborative Group on HNPCC, have also been used as clinicopathological selection criteria for LS families [222, 223]. However, different MSI testing strategies are pursued, e.g. the UK National Institute of Health and Care Excellence (NICE) guidelines recommend general MSI testing of all CRCs independent of age and family history [224]. Similarly, general MSI testing for CRC and EC is recommended by the guidelines of the US National Comprehensive Cancer Network (NCCN) [225]. The described screening of all newly diagnosed CRCs is termed ‘universal screening’ and can facilitate the identification of LS carriers who do not meet diagnostic criteria, e.g. revised Bethesda guidelines [226, 227].

Various panels of microsatellite markers for MSI diagnosis are available, one of the most commonly used ones is the Bethesda panel which comprises two mononucleotide repeats (BAT25, BAT26) and three dinucleotide repeats (D2S123, D5S346, D17S250) [228]. Additionally, more sensitive mononucleotide markers, such as CAT25 and BAT40, have been incorporated into standard MSI testing [229, 230]. The MSI status is typically determined by PCR-based fragment analysis. More recently, NGS approaches have been described which allow the analysis of significantly more markers and streamlining of MSI testing with additional mutational analysis [231, 232].
IHC analysis of MMR protein expression in tumor tissue is also commonly used in LS screening. The concordance between IHC and MSI testing is high, for CRC it ranges between 92–99 %. IHC analysis further allows the identification of the affected MMR gene [233]. Additional evaluation of the tumor can comprise *BRAF* V600E mutation and *MLH1* promoter methylation analyses to exclude sporadic MSI CRCs [174, 233, 234]. Ultimately, identified at-risk individuals are offered germline sequencing and the confirmative LS diagnosis is typically made by genetic testing [219].

Right now, direct genetic testing is subsidiary in LS diagnostics and mainly applied in the research setting. However, with the broad availability of NGS methods upfront genetic screening for LS becomes a viable alternative to the MSI pre-screening of tumors. Additionally, multiple prediction tools, e.g. MMRpredict, PREMM, MMRpro, have been developed which determine the risk of a MMR germline variant in an individual with given personal and familial information [235–237]. Further, so-called cascade testing entails genetic testing for MMR gene germline variants in all first degree relatives of a diagnosed LS carrier. Crucially, such a testing approach enables the timely application of cancer surveillance and prevention strategies in identified individuals [238].

Although LS diagnostics has improved in regard to availability for patients, healthy LS carriers in families without a tumor are missed by current approaches as these are heavily based on tumoral testing and the assessment of family history [215]. The heterogeneity and incomplete penetrance of LS further complicate the identification of carriers [239]. The genetic diagnosis is hampered by VUS, which subsequently aggravate clinical management of the affected individuals [216]. As a consequence, LS is largely underdiagnosed and it is estimated that only around 5 % of carriers are identified, which prohibits the application of necessary screening programs and preventive measures [240].

Appropriate surveillance of LS carriers is paramount to reduce cancer risk and enable early tumor detection [219]. However, the only surveillance protocol that has been proven to be effective is regular colonoscopy. Colonoscopic screening in 3-year intervals was shown to decrease the CRC risk in LS carriers by ca. 50 % and the overall mortality of LS families by

around 65 % [241, 242]. LS carriers are recommended to undergo colonoscopy every 1–2 years beginning at the age of 20–25 years. *MSH6* and *PMS2* carriers present with a lower CRC risk and colonoscopic surveillance may be initiated later (25–30 years) [219, 243]. However, Engel et al. has demonstrated no difference in CRC incidence between 1-, 2- or 3-yearly colonoscopy strategies. Moreover, no association between cancer stage at detection and the surveillance interval was observed [244, 245]. Consequently and contrary to expectations, more frequent colonoscopy is not associated with a lower CRC incidence and estimations indicate higher incidences for shorter screening intervals. These findings point towards over-diagnosis caused by intense monitoring and resulting in the detection of tumors that might not have progressed to be clinically relevant. The spontaneous regression of LS-associated tumors, potentially mediated by the host's immune system, might offer a conceivable explanation for these observations [245]. In addition to regular colonoscopy, the daily intake of acetylsalicylic acid is recommended to reduce the CRC risk in LS carriers. Kune et al. first reported a preventive effect of acetylsalicylic acid and other NSAIDs [246], and recently the CAPP2 (Cancer Prevention Program 2) study has demonstrated a significant reduction of CRCs in LS carriers receiving 600 mg acetylsalicylic acid daily [247].
The value of surveillance for EC and ovarian cancer in female LS carriers is still unknown and lacks sufficient evidence. However, several studies indicate that endometrial surveillance, beginning at the age of 35–40 years, may enable the detection of premalignant lesions and early cancers [219]. Moreover, prophylactic hysterectomy and bilateral salpingo-oophorectomy after finalized family planning are an effective strategy for preventing endometrial and ovarian cancer in female LS carriers [248]. Screening benefits for other extracolonic LS-related cancers have not been reported [215].

1.4 Extracellular vesicles

1.4.1 Classification and biogenesis of extracellular vesicles

The MSI phenotype has prognostic and therapeutic impact and is typically assessed by PCR-based fragment and/or IHC analysis using tumor tissue (see 1.2, 1.3.5). MSI detection via liquid biopsies would potentially aid to overcome certain limitations of tumor tissue-based MSI testing, e.g. intratumoral heterogeneity, and enable longitudinal monitoring. Liquid biopsies refer to the collection and analysis of components found in different bodily fluids, e.g. blood, urine and cerebrospinal fluid. Respective analytes include plasma cell-free DNA, circulating tumor cells, cell-free RNAs, tumor-educated platelets and extracellular vesicles [249, 250].

The term extracellular vesicles (EVs) encompasses a heterogeneous group of membrane-enclosed particles which are involved in various cellular processes and are crucial players in cell–cell communication [251]. The secretion of membranous structures into the extracellular

space is conserved across species and has been reported for pro- as well as eukaryotes [252]. Initially, EVs were thought to serve the elimination of unnecessary cellular compounds and their role in intercellular communication was proposed in the late 1990s [253]. EVs facilitate functional communication by transporting various cargo molecules, including nucleic acids, proteins, lipids, carbohydrates and metabolites, between donor and recipient cells. Enclosed by a stable lipid-bilayer membrane, EVs are released from the producing cell. Upon uptake EVs can impact diverse cellular functions and initiate phenotypic changes in the recipient cell. Further, EVs can elicit functional responses without delivering their cargo but by binding and activating membrane receptors. The EVs' cargo composition greatly varies between cells and cellular conditions, and reflects the physiological/pathological state of the parental cell [253, 254]. Hence, EVs are involved in numerous physiological and pathological processes, e.g. blood coagulation, immune responses, neuronal communication as well as cardiovascular diseases and cancer [251, 253].

Based on their different biogenesis three main EV subtypes have been defined: exosomes, microvesicles and apoptotic bodies (Figure 8) [255]. EVs can originate from endocytic pathways, which are responsible for the internalization of proteins and other cellular components, and subsequent recycling or degradation of those, or be formed by budding of the plasma membrane. Importantly, the different subcellular origin of EVs is thought to be accompanied by differing cargos and functions [256]. However, the distinction between those subtypes remains challenging and no reliable subcellular markers to distinguish different EV types have been identified. Thus, the designation 'EVs' is used as a generic term, as in the present thesis, for lipid-bilayer-enclosed particles without the ability to replicate, which are naturally released by cells [257].

Exosomes, with a diameter of 50–150 nm, present one of the three EV subtypes and originate from the endocytic route. During the maturation of early to late endosomes, the inward budding of the endosomal membrane can lead to the formation of intraluminal vesicles (ILVs). Endosomes containing ILVs are referred to as multivesicular bodies (MVBs) and can either undergo degradation in lysosomes or fuse with the plasma membrane, releasing ILVs as exosomes [253, 258]. Different mechanisms have been described for ILVs formation and associated exosome biogenesis. The best described mechanism is based on the endosomal sorting complex required for transport (ESCRT) machinery, which comprises around 30 proteins forming four ESCRT complexes. Briefly, ESCRT complexes, along with accessory proteins (Alix, VPS4, VTA1), recognize and bind future exosomal cargo proteins in an ubiquitin-dependent manner and initiate the invagination of the endosomal membrane enabling ILVs assembly [258, 259]. However, ESCRT-independent mechanisms have been identified as well, involving the sphingolipid ceramide which induces membrane budding [260].

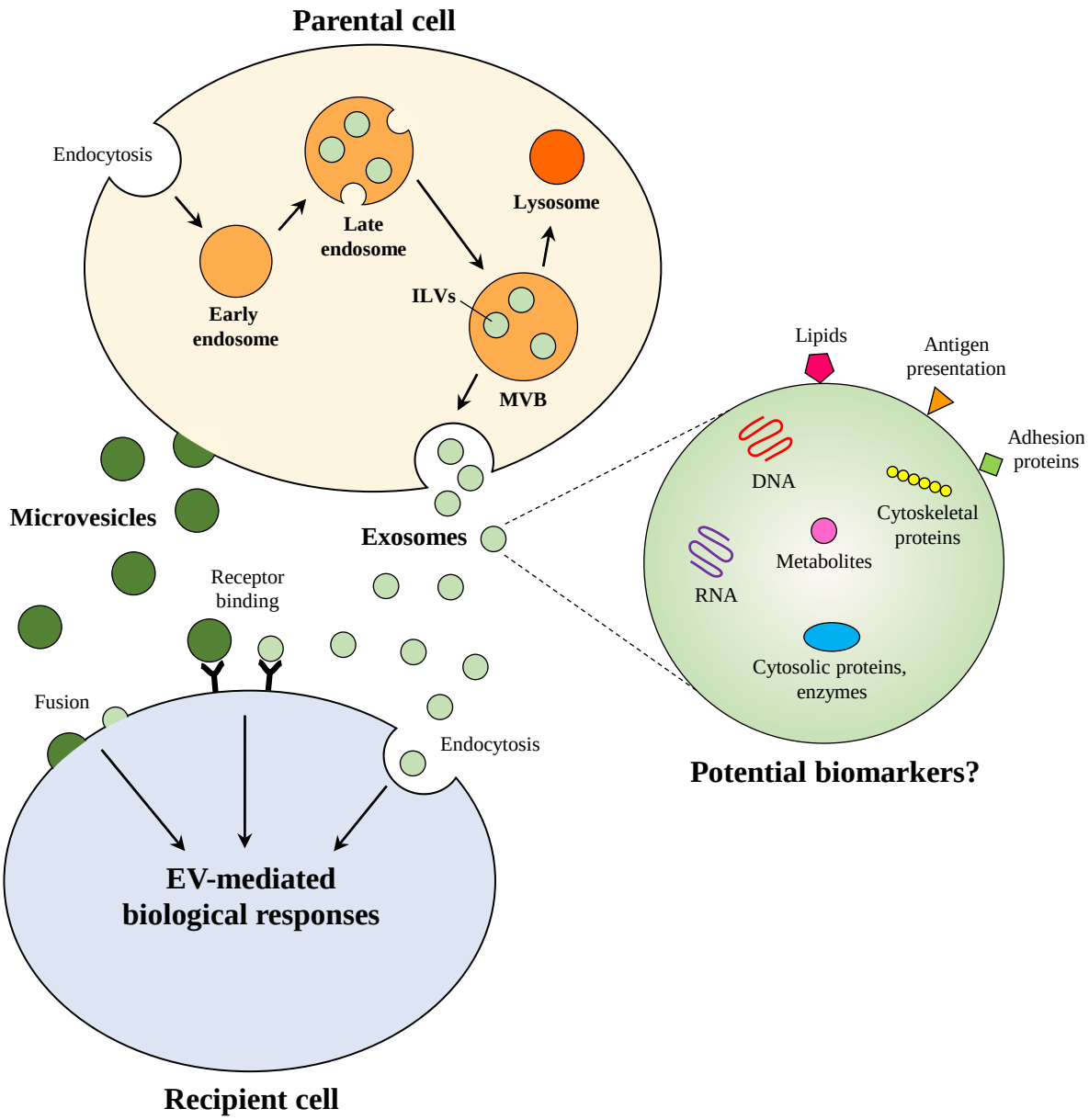

Figure 8: Biogenesis and uptake of EVs. Based on their biogenesis EVs are distinguished into three main subtypes. EVs can derive from the endocytic pathway involving an inward budding of the endosomal membrane and the subsequent generation of MVBs, which can fuse with the plasma membrane releasing ILVs as exosomes into the extracellular space. EVs that are shed directly from the plasma membrane are termed microvesicles. Apoptotic bodies, released from a cell undergoing apoptosis present the third EV subgroup (not depicted). Once released, EVs serve as crucial vehicles for intercellular communication, transporting various cargo molecules, such as DNA, RNA, proteins and lipids. The uptake of EVs by a cell can occur via fusion, receptor binding or endocytosis. Ultimately, EVs impact a variety of physiological and pathological processes in the recipient cell. As EVs and their diverse cargo can be isolated from different bodily fluids they show potential to be used as novel biomarkers in liquid biopsy-based approaches.

Microvesicles, also known as ectosomes, represent the second main EV subtype and are formed by direct budding and fission of the plasma membrane. Microvesicles are larger particles and range between 200–500 nm of diameter [254]. The microvesicle biogenesis mechanism is less well characterized and not fully understood yet. Generally, formation of these vesicles involves a regulated outward budding of plasma membrane domains, which in turn requires cytoskeletal reformation and the increase of the intracellular Ca^{2+} level. The enhanced Ca^{2+} level can disturb the protein and lipid composition of the plasma membrane, eventually resulting in phosphatidylserine externalization and changes in the membrane's curvature and rigidity [261]. Furthermore, the ESCRT machinery and its associated proteins are involved in the formation of microvesicles and small GTPase proteins (e.g. ARF1, ARF6, RhoA) are assumed to regulate the process [261–263].

Lastly, apoptotic bodies are considered the third EV subtype and are released by dying cells. The fragmentation and release of cellular components into apoptotic bodies is termed apoptotic cell disassembly. Even though the formation of this EV subtype is not well studied, three key morphological steps have been identified: blebbing of the plasma membrane, formation of apoptotic membrane protrusions and fragmentation into separate apoptotic bodies [261, 264, 265]. Compared to exosomes and microvesicles, apoptotic bodies are large particles and range between 800–5,000 nm of diameter [261, 266].

1.4.2 Extracellular vesicles in cancer and their clinical potential

EVs and EV-associated intercellular communication have diverse roles in different phases of tumorigenesis and contribute to several hallmarks of cancer as defined by Hanahan and Weinberg [267, 268]. Multiple studies have demonstrated that tumor-derived EVs impact various oncogenic processes, e.g. angiogenesis, metastasis and immune suppression, and further play an integral role in establishing and maintaining the tumor microenvironment (TME) [269–271]. Malignant transformation of a cell does not only alter the biomolecular cargo composition of EVs, it further impacts EV emission rate, size and subtype. Cancer cells are known to release an increased amount of EVs and overexpression of ESCRT components has been identified in different tumors. The deregulation of EV release can be induced by cell-intrinsic and microenvironmental factors [272]. For instance, expression of oncogenic HRAS and hypoxia facilitate shedding of EVs [273, 274].
Activated oncogenic signaling and environmental changes are also associated with a changed cargo in tumor-derived EVs, compared to their non-malignant counterparts [272]. Exemplary, Al-Nedawi et al. identified an EV-mediated intercellular transfer of the oncogenic epidermal growth factor receptor (EGFR) variant III (EGFRvIII) between glioma cells [275]. Moreover, it was found that *KRAS* mutations in CRC cells affect the EVs' proteome and the respective EVs transport several tumor-promoting proteins, including KRAS and EGFR [276].

In general, cancer cells both release and receive EVs, enabling communication between tumor cells as well as crosstalk with surrounding stromal cells, e.g. endothelial cells and fibroblasts. Tumor-to-tumor communication for example allows the transmission of oncogenic activity among cancer cell subsets [275]. Interactions between tumors and cells in the TME via tumor-derived EVs can foster a tumor-promoting environment [277, 278]. For instance, tumor-derived EVs can induce the transformation from normal stromal fibroblasts to cancer-associated fibroblasts which remodel the extracellular matrix and greatly influence the TME by establishing a tumor-promoting milieu [279, 280].

Tumor-derived EVs carry a plethora of cargos that drive cancer development and progression, such as oncoproteins, oncogenic microRNAs (miRNA), genomic DNA and oncogenes, growth factors as well as immunomodulatory molecules [272, 279]. Mediated by their cargo, EVs can impact various aspects of tumorigenesis. Tumor-derived EVs can facilitate angiogenesis by carrying high levels of pro-angiogenic vascular endothelial growth factor A (VEGF-A) or miRNAs [281, 282]. EVs also present with immunomodulatory activities in the TME, e.g. Lundholm et al. could demonstrate that EVs released by prostate cancer cells express ligands of the NKG2D receptor, which is an activating cytotoxicity receptor expressed on different immune cells. The NKG2D ligand-expressing EVs exert an immunosuppressive effect on NK and CD8-positive T cells [283]. In addition to primary tumor growth and outside of the TME, tumor-secreted EVs also play a major role in distant metastasis and are crucial drivers of pre-metastatic niche formation, requiring vascular permeability, angiogenesis, immunosuppression and fibroblast reprogramming [272, 277, 284]. Clinically, EVs have been shown to impact the resistance to various therapeutic agents [285]. For example, the EV-mediated transmission of the SNHG14 long non-coding RNA in breast cancer patients is involved in the resistance to trastuzumab, a human epidermal growth factor receptor 2 inhibitor [286].

Due to their broad involvement in tumorigenesis, EVs might serve as a novel source of cancer biomarkers as they reflect the status of the donor cell and carry cancer-associated cargo. EVs comprise a great spectrum of different molecules (e.g. proteins and nucleic acids) they could therefore provide complex information on the state of the tumor. Importantly, EVs can be isolated from various bodily fluids, e.g. blood, saliva and urine, using non- or minimally invasive procedures and are eligible for liquid biopsy-based approaches [277, 287]. EVs might show potential to be used for cancer diagnosis and disease monitoring and their easy accessibility would allow longitudinal monitoring of patients.

Multiple studies have examined the diagnostic potential of EVs using various types of bodily fluids and different cargo molecules [277, 288, 289]. Yoshioka et al. developed an assay for the analysis of circulating EVs in blood samples without the need of any purification steps. Application of this technique revealed an enrichment of CD147, a member of the immunoglobulin

superfamily, on EVs derived from the serum of CRC patients. CD147-positive EVs could be detected in serum samples from early stage CRC patients demonstrating the potential of EVs for early CRC detection [290]. Logozzi et al. identified caveolin-1 as a potential EV-based tumor marker as it was found to be significantly increased on plasma-derived EVs from melanoma patients, compared to healthy individuals [291]. In addition, several EV-associated miRNAs have shown diagnostic potential for various cancer types. For instance, Bhagirath et al. demonstrated that the serum level of the exosomal miRNA-1246 could be used for the discrimination between prostate cancer patients and healthy individuals [292]. Moreover, the analysis of EVs might have prognostic value and provide information on tumor progression and metastasis. Exemplary, a high frequency of exosomal *KRAS* mutations could be correlated with decreased disease-free survival in pancreatic ductal adenocarcinoma patients [293]. More recently, Lucchetti et al. applied the exosomal *KRAS* mutational status to predict the disease outcome in CRC patients and observed a lower overall survival in patients with a high abundance of exosomal *KRAS* mutations [294]. Further, expression of the macrophage migration inhibitory factor (MIF) on EVs derived from pancreatic ductal adenocarcinoma patients could be associated with liver metastasis [295]. Several studies have also demonstrated that EVs might be suitable for therapeutic response monitoring [296, 297]. Noteworthy, EVs may also be used therapeutically, e.g. as drug delivery vehicles or EV-based vaccines [287, 298]. Despite their promising potential, no EV-associated biomarker has been approved by national or international agencies responsible for the approval of novel biomedical tests and devices [299].

In the MSI setting, Fricke et al. demonstrated that MSI-associated frameshift mutation patterns in CRC cell lines are reflected in the cargo of the respective EVs and frameshift mutations in different MSI target genes, e.g. *TGFBR2*, have been identified in vesicular DNA. Moreover, MSI-associated driver mutations in *TGFBR2* altered the protein and miRNA composition in EVs derived from MSI CRC cells. The described MSI- and *TGFBR2*-dependent changes in the EV's proteome might qualify EVs to be used as MSI-specific diagnostic markers [300, 301].

1.5 Aims

Lynch syndrome (LS), the most common inherited cancer syndrome, is still largely underdiagnosed. Importantly, current diagnostic strategies fail to identify LS carriers in families without tumor history as they rely on assessing family history and evaluating an already manifest tumor for MSI and MMR deficiency. Furthermore, unclassified MMR gene variants (VUS) with an unclear pathogenicity can complicate interpretation of the germline sequencing results. Immune responses against FSPs can already be detected in the peripheral blood of LS carriers prior to tumor manifestation. These systemic, specific T cell responses are potentially caused by a life-long interaction of immune cells with MMR-DCF in the normal colonic mucosa of LS individuals and might have diagnostic potential. The assessment of local and systemic immune responses and tumor-independent biomarkers in the setting of MSI CRC and LS is the overarching aim of the present thesis.

First, the immune surveillance during the initial steps of colonic tumorigenesis in the context of LS shall be analyzed. For that, a systematic literature analysis of existing data on immune responses in hereditary and sporadic MSI tumor patients shall be performed. Furthermore, local T cell responses in the normal colonic mucosa shall be characterized. For that purpose, normal colonic mucosa from healthy LS carriers and CRC patients will undergo comprehensive immune profiling.

Second, to assess the potential of tumor-independent immune responses for LS diagnostics, systemic FSP-specific immune responses shall be characterized in healthy LS carriers and cancer patients. The characterization shall be performed on the cellular and humoral level using peripheral blood and serum/plasma samples. Different methodologies shall be applied, working towards an immunological distinction between LS carriers and healthy non-LS individuals. Furthermore, the potential of FSP-specific responses as therapy response markers for ICB treatment shall be explored.

Lastly, the use of plasma-derived vesicular DNA for MSI detection shall be investigated. This includes the optimization of EV isolation from human plasma and subsequent mutational analysis of obtained vesicular DNA, including MSI-specific and canonical driver mutations.

The present thesis will realize the following aims: (I) characterization of local, mucosal T cell responses with particular focus on the immune profile in the normal colorectal mucosa of LS carriers; (II) evaluation of systemic cellular and humoral FSP-specific T cell responses, working towards an immune-based diagnostic approach for LS and (III) the exploration of plasma-derived EVs for tumor tissue-independent MSI testing.

2 Material

2.1 Chemicals and reagents

Table 1: List of used chemicals and reagents.

Chemical/Reagent	Supplier (City, Country)
β-Mercaptoethanol	Thermo Fisher Scientific (Waltham, USA)
β-Mercaptoethanol	Sigma-Aldrich (St. Louis, USA)
3,3´,5,5´-Tetramethylbenzidine (TMB) substrate solution	Sigma-Aldrich (St. Louis, USA)
5-Bromo-4-chloro-3'-indolyl-phosphate/nitro-blue tetrazolium (BCIP/NBT) substrate	Thermo Fisher Scientific (Waltham, USA)
Acridine orange/propidium iodide stain	Logos Biosystems (Anyang, South Korea)
Agarose	Biozym (Hessisch Oldendorf, Germany)
Aquatex	Merck (Darmstadt, Germany)
Bi-distilled water (MilliQ)	Merck Millipore (Darmstadt, Germany)
Boric acid	neoFroxx GmbH (Einhausen, Germany)
Bovine serum albumin (BSA), fraction V	Sigma-Aldrich (St. Louis, USA)
Bovine serum albumin (BSA), fraction V, biotin-free	Carl Roth (Karlsruhe, Germany)
Bradford reagent (Protein Dye Reagent Concentrate)	Bio-Rad Laboratories GmbH (Munich, Germany)
Bromophenol blue	Chroma-Gesellschaft Schmid (Stuttgart, Germany)
Calcium chloride ($CaCl_2$)	Merck (Darmstadt, Germany)
CEF peptide pool	Mabtech (Nacka Strand, Sweden)
Citric acid monohydrate	Merck (Darmstadt, Germany)
Concanavalin A (ConA)	Sigma-Aldrich (St. Louis, USA)
Dimethyl pimelimidate (DMP)	Thermo Fisher Scientific (Waltham, USA)
Dimethyl sulfoxide (DMSO)	Serva Electrophoresis GmbH (Heidelberg, Germany)
Disodium hydrogen phosphate dihydrate ($Na_2HPO_4 \cdot 2\,H_2O$)	Carl Roth (Karlsruhe, Germany)

Chemical/Reagent	**Supplier (City, Country)**
DNA ladder (100 bp)	Thermo Fisher Scientific (Waltham, USA)
dNTP mix (100 mM)	Thermo Fisher Scientific (Waltham, USA)
Dulbecco's PBS (without Ca & Mg)	Thermo Fisher Scientific (Waltham, USA)
Dynabead™ MyOne™ Streptavidin T1	Thermo Fisher Scientific (Waltham, USA)
Dynabeads™ Protein G	Thermo Fisher Scientific (Waltham, USA)
EDTA	Sigma-Aldrich (St. Louis, USA)
Eosin	Waldeck (Münster, Germany)
Ethanol ($\geq$ 99.8 %)	VWR International S.A.S. (Fontenay-sous-Bois, France)
Ethanol (96 %)	Zentrallager INF 367 (Heidelberg, Germany)
Ethanol (99 %)	Zentrallager INF 367 (Heidelberg, Germany)
ExtrAvidin®-peroxidase	Sigma-Aldrich (St. Louis, USA)
Fetal bovine serum (FBS)	Thermo Fisher Scientific (Waltham, USA)
Fixable viability stain (FVS780)	Becton, Dickinson and Company (Franklin Lakes, USA)
FSPs	Genaxxon bioscience (Ulm, Germany)
FSPs (Micoryx)	Bachem (Bubendorf, Switzerland)
FSP epitopes	DKFZ (Heidelberg, Germany)
Glacial acetic acid AnalaR® NORMAPUR® (100 %)	VWR International S.A.S. (Fontenay-sous-Bois, France)
Glycerol	Carl Roth (Karlsruhe, Germany)
HEPES buffer solution (1 M)	Thermo Fisher Scientific (Waltham, USA)
HiDi™ formamide	Thermo Fisher Scientific (Waltham, USA)
HiSep™ lymphocyte separation medium	HIMEDIA (Mumbai, India)
Histofluid	Paul Marienfeld (Lauda-Königshofen, Germany)
Human serum (from human male AB plasma, sterile-filtered)	Sigma-Aldrich (St. Louis, USA)
Hydrochloric acid (HCl) ($\geq$ 37 %)	Honeywell International Inc. (Charlotte, USA)

Chemical/Reagent	**Supplier (City, Country)**
Hydrocortisone	Sigma-Aldrich (St. Louis, USA)
Hydrogen peroxide solution (30 % (w/w))	Sigma-Aldrich (St. Louis, USA)
Hyrophobic pen	Dako (Carpinteria, USA)
Insulin	Sigma-Aldrich (St. Louis, USA)
Insulin-Transferrin-Selenium (ITS) (100 x)	Thermo Fisher Scientific (Waltham, USA)
Isopropanol	Zentrallager INF 367 (Heidelberg, Germany)
L-Glutamine (200 mM)	PAA Laboratories GmbH (Pasching, Austria)
Magnesium chloride ($MgCl_2$)	Merck (Darmstadt, Germany)
Mayer's hematoxylin	PanReac AppliChem ITW Reagents (Darmstadt, Germany)
Methanol	VWR International S.A.S. (Fontenay-sous-Bois, France)
Midori Green	Biozym (Hessisch Oldendorf, Germany)
Milk, powdered	Carl Roth (Karlsruhe, Germany)
Monopotassium phosphate (KH_2PO_4)	GERBU Biotechnik GmbH (Gaiberg, Germany)
Normal horse serum	Vector Laboratories (Burlingame, USA)
NuPage™ Antioxidant	Thermo Fisher Scientific (Waltham, USA)
NuPage™ LDS Sample Buffer (4 x)	Thermo Fisher Scientific (Waltham, USA)
NuPage™ MES SDS Running Buffer (20 x)	Thermo Fisher Scientific (Waltham, USA)
NuPage™ MOPS SDS Running Buffer (20 x)	Thermo Fisher Scientific (Waltham, USA)
NuPage™ reducing agent (10 x)	Thermo Fisher Scientific (Waltham, USA)
NuPage™ Transfer Buffer (20 x)	Thermo Fisher Scientific (Waltham, USA)
Oligo(dT) 12–18 primer	Thermo Fisher Scientific (Waltham, USA)
Paraformaldehyde (PFA)	Carl Roth (Karlsruhe, Germany)
PBMC qualified freezing medium	Cell Applications (San Diego, USA)
Penicillin/streptomycin (10,000 U/ml; 10,000 µg/ml)	Thermo Fisher Scientific (Waltham, USA)

Chemical/Reagent	**Supplier (City, Country)**
Ponceau S	Serva Electrophoresis (Heidelberg, Germany)
Potassium chloride (KCl)	Merck (Darmstadt, Germany)
Primer	Integrated DNA Technologies (Coralville, USA)
Primer (Sequencing)	Microsynth (Balgach, Switzerland)
Protease Inhibitor Cocktail Tablets (cOmplete, Mini, EDTA-free)	Roche (Basel, Switzerland)
Proteinase K	Qiagen (Hilden, Germany)
Random hexamer primer	Bioron (Römerberg, Germany)
Recombinant human interleukin 2 (rhIL-2)	PeproTech (London, UK)
Recombinant human interleukin 7 (rhIL-7)	R&D Systems (Minneapolis, USA)
ROX Reference Dye	Thermo Fisher Scientific (Waltham, USA)
RPMI 1640 Medium	Thermo Fisher Scientific (Waltham, USA)
SeeBlue Plus2 pre-stained standard	Thermo Fisher Scientific (Waltham, USA)
Sodium acetate trihydrate	Merck (Darmstadt, Germany)
Sodium chloride (NaCl)	Fisher Scientific (Loughborough, UK)
Sodium dodecyl sulfate (SDS)	Carl Roth (Karlsruhe, Germany)
Sodium hydroxide (NaOH)	Sigma-Aldrich (St. Louis, USA)
NaOH pellets	Thermo Fisher Scientific (Waltham, USA)
Sodium phosphate dibasic dihydrate ($Na_2HPO_4 \cdot 2\,H_2O$)	Labochem (Athens, Greece)
Strepatvidin-coated polystyrene particles (6.0–8.0 µm)	Spherotech (Lake Forest, USA)
Streptavidin-alkaline phosphatase (ALP)	Mabtech (Nacka Strand, Sweden)
Streptavidin-PE (0.5 mg/ml)	Becton, Dickinson and Company (Franklin Lakes, USA)
Thioglycerol	Sigma-Aldrich (St. Louis, USA)
Triethanolamine	Sigma-Aldrich (St. Louis, USA)
TRIS	Carl Roth (Karlsruhe, Germany)
TRIS-HCl	AppliChem (Darmstadt, Germany)
Triton X-100	Merck (Darmstadt, Germany)

Chemical/Reagent	Supplier (City, Country)
Trypsin EDTA (0.05 %)	Thermo Fisher Scientific (Waltham, USA)
Tween 20	Carl Roth (Karlsruhe, Germany)
Uranylacetat dihydrat	Ted Pella (Redding, USA)
Water, DNase-/RNase-free	MP Biomedicals (Solon, USA)
Western Lightning Plus ECL	Perkin Elmer (Boston, USA)
Xylene	Fisher Scientific (Loughborough, UK)

2.2 Consumables

Table 2: List of used consumables.

Consumables	Supplier (City, Country)
Ahlstrom folded filter (3 hw)	Munktell (Falun, Sweden)
Amersham™ Hybond™ P 0.45 PVDF blotting membrane	GE Healthcare Life Sciences (Chicago, USA)
Amicon®Ultra-0.5 centrifugal filter units (10,000 NMWL)	Merck (Darmstadt, Germany)
Cell culture flasks (CELLSTAR: 25 cm^2; 75 cm^2; 175 cm^2)	Greiner Bio-One (Frickenhausen, Germany)
Cell culture plate (CELLSTAR: 24-well, F-bottom)	Greiner Bio-One (Frickenhausen, Germany)
Cell scraper	Greiner Bio-One (Frickenhausen, Germany)
Cell suspension plate (96-well, U-bottom)	Greiner Bio-One (Frickenhausen, Germany)
Centrifugal concentrators (Vivaspin 20, 10,000 MWCO PES)	Sartorius (Göttingen, Germany)
Combitips advanced (5 ml)	Eppendorf (Hamburg, Germany)
Cooper grids (100 Mesh)	Plano (Wetzlar, Germany)
Cryo tubes (Cyro.S™)	Greiner Bio-One (Frickenhausen, Germany)
Disposable cuvettes made of PS, semi-micro (E-1642)	neoLab Migge (Heidelberg, Germany)
Electronic multichannel pipettes E1-ClipTip™ tips (1–30 µl; 2–125 µl)	Thermo Fisher Scientific (Waltham, USA)

Consumables	**Supplier (City, Country)**
Falcon tubes (15 ml; 50 ml)	Greiner Bio-One (Frickenhausen, Germany)
Luna™ cell counting slides	Logos Biosystems (Anyang, South Korea)
MaxiSorp™ ELISA plate	Thermo Fisher Scientific (Waltham, USA)
Micolance™ 3 needle (20Gx1/2"-Nr. 1)	Becton, Dickinson and Company (Franklin Lakes, USA)
Microscope cover slips	Paul Marienfeld (Lauda-Königshofen, Germany)
Microscope slides	Paul Marienfeld (Lauda-Königshofen, Germany)
Microscope slides (Superfrost®Plus)	Gerhard Menzel (Braunschweig, Germany)
Microtome blade	PFM Medical (Cologne, Germany)
MultiScreen™ 96-Well assay plate (ELISpot)	Thermo Fisher Scientific (Waltham, USA)
Nitrocellulose membrane	Thermo Fisher Scientific (Waltham, USA)
Nunc™ sealing tape	Thermo Fisher Scientific (Waltham, USA)
NuPage™ 4–12 % Bis-Tris gradient gels	Thermo Fisher Scientific (Waltham, USA)
Parafilm M laboratory film	Bemis Corporate (Neenah, USA)
PCR plate ABI Sequencer 3100/30, 96-well	Biozym (Hessisch Oldendorf, Germany)
PCR plate primaPLATE, 96-well	Steinbrenner Laborsysteme (Wiesenbach, Germany)
PCR reaction tubes (0.2 ml)	Greiner Bio-One (Frickenhausen, Germany)
Pipette filter tips (DeckWorks: 10 µl; 20 µl; 200 µl; 1000 µl)	Corning Incorporated (Corning, USA)
Pipette tips (10 µl; 200 µl; 1000 µl)	Greiner Bio-One (Frickenhausen, Germany)
Pipette tips MµltiFlex®(1–200 µl)	Carl Roth (Karlsruhe, Germany)
qPCR seal primaSEAL	Steinbrenner Laborsysteme (Wiesenbach, Germany)
Reaction tubes (1.5 ml; 2.0 ml; 5 ml)	Eppendorf (Hamburg, Germany)
Reinraumtuch Bemcot M3-II (M3 Scaffold)	Reinraum-Produkte GmbH (Braunschweig, Germany)
Round bottom polystyrene tubes (5 ml) with cell strainer cap (35 µm)	Greiner Bio-One (Frickenhausen, Germany)

Consumables	Supplier (City, Country)
Serological pipettes (2 ml)	Corning Incorporated (Corning, USA)
Serological pipettes (5 ml; 10 ml; 25 ml; 50 ml)	Sarstedt (Nümbrecht, Germany)
S-Monovette®(K2E-Gel, 9 ml)	Sarstedt (Nümbrecht, Germany)
Sterile filter (0.22 µm)	Merck (Darmstadt, Germany)
Syringe (5 ml; 10 ml; 20 ml; 50 ml)	Becton, Dickinson and Company (Franklin Lakes, USA)
Syringe Injekt®-F (1 ml)	B.Braun Melsungen (Melsungen, Germany)
Tissue embedding cassettes	Kartell Spa (Noviglio, Italy)
Whatman®filter paper	Whatman International (Maidstone, UK)

2.3 Instruments

Table 3: List of used instruments.

Instrument	Supplier (City, Country)
Analytic scale (SBC 32)	Sartorius (Göttingen, Germany)
BioWizard Silver Line safety cabinet	Kojair (Mänttä-Vilppula, Finland)
Centrifuge (5417 R)	Eppendorf (Hamburg, Germany)
Centrifuge (5424)	Eppendorf (Hamburg, Germany)
Centrifuge (5810 R)	Eppendorf (Hamburg, Germany)
Centrifuge (Biofuge fresco)	Heraeus Holding (Hanau, Germany)
Centrifuge (Heraeus Fresco 21)	Thermo Fisher Scientific (Waltham, USA)
ChemiDoc imaging system	Bio-Rad Laboratories (Munich, Germany)
Electronic multichannel pipettes E1-ClipTip™ (1–30 µl; 2–125 µl)	Thermo Fisher Scientific (Waltham, USA)
Electrophoresis chamber SubCell GT	Bio-Rad Laboratories GmbH (Munich, Germany)
Electrophoresis power supply	Consort bvba (Turnhout, Belgium)
FACSCanto II	Becton, Dickinson and Company (Franklin Lakes, USA)

Instrument	Supplier (City, Country)
Genetic analyzer ABI 3130xl	Applied Biosystems (Darmstadt, Germany)
Heating plate (MR HeiTec)	Heidolph Instruments (Schwabach, Germany)
Homogenizer (Sonopuls HD 2070)	Bandelin Electronics (Berlin, Germany)
Hot plate stirrer (AREX Digital)	VELP Scientifica (Usmate Velate, Italy)
Humidity chamber	Steinbrenner Laborsysteme (Wiesenbach, Germany)
ImmunoSpot®analyzer (automated ELISpot plate reader)	Cellular Technology Limited (Cleveland, USA)
Incubator (no CO_2)	Heraeus Holding (Hanau, Germany)
Incubator (with CO_2)	Memmert (Schwabach, Germany)
Incubator (with CO_2)	Binder GmbH (Tuttlingen, Germany)
LSRFortessa with high throughput sampler	Becton, Dickinson and Company (Franklin Lakes, USA)
LUNA™-fl dual fluorescence cell counter	Logos Biosystems (Anyang, South Korea)
Magnetic separation rack	New England Biolabs (Ipswich, USA)
Magnetic stirrer (MR 2002)	Heidolph Instruments (Schwabach, Germany)
Maxwell®16 research extraction system	Promega (Madison, USA)
Microscope Fluorescence Olympus AX70	Olympus (Tokyo, Japan)
Microscope Olympus BX43	Olympus (Tokyo, Japan)
Microscope Olympus CK40	Olympus (Tokyo, Japan)
Microscope Olympus IX70	Olympus (Tokyo, Japan)
Microtome (RM2245)	Leica Biosystems (Nußloch, Germany)
Microwave	Siemens (Munich, Germany)
Multipette plus	Eppendorf (Hamburg, Germany)
Multipipette Finnpipette F1 (5–50 µl; 30–300 µl)	Thermo Fisher Scientific (Waltham, USA)
Nalgene™ Mr. Frosty®Cryo 1 °C freezing container	Thermo Fisher Scientific (Waltham, USA)
NanoDrop 1000 spectrophotometer	Thermo Fisher Scientific (Waltham, USA)
NanoSight LM10	Malvern Panalytical (Malvern, UK)

Instrument	Supplier (City, Country)
NanoString nCounter®gene expression platform	NanoString Technologies (Seattle, WA)
Orbital shaker MixMate 5353 PCR96	Eppendorf (Hamburg, Germany)
pH meter (PB-11)	Sartorius (Göttingen, Germany)
Pipette aid (accu-jet®pro)	BRAND (Wertheim, Germany)
Pipettes (P10; P20; P200; P1000)	Gilson (Limburg-Offheim, Germany)
Pipettes (P10; P20; P200; P1000)	Thermo Fisher Scientific (Waltham, USA)
Qubit™ 2.0 fluorometer	Thermo Fisher Scientific (Waltham, USA)
Real-Time PCR system (StepOnePlus)	Applied Biosystems (Darmstadt, Germany)
Rotator (2-1175)	neoLab Migge (Heidelberg, Germany)
Rotator (Loopster digital)	IKA-Works (Wilmington, USA)
Rotor (100.2)	Beckman Coulter (Brea, USA)
Rotor (SW 28)	Beckman Coulter (Brea, USA)
Rotor (SW28.1)	Beckman Coulter (Brea, USA)
Scale (BP 310 S)	Sartorius (Göttingen, Germany)
Scale (HT-500)	A&D Company (San Jose, USA)
Scale (Mettler PM4800 DeltaRange)	Mettler-Toledo (Gießen, Germany)
Shaker (RS-OS 5)	Phoenix Instruments (Garbsen, Germany)
Shaker (Unimax 2010)	Heidolph Instruments (Schwabach, Germany)
Slide scanner NanoZoomer S210	Hamamatsu Photonics K.K. (Hamamatsu, Japan)
Spectrophotometer (Ultrospec 7000)	GE Healthcare Life Sciences (Chicago, USA)
Tecan GENios plate reader	Tecan Group AG (Männedorf, Switzerland)
Thermocycler peqlab peqstar 2 x gradient	PEQLAB Biotechnologie (Erlangen, Germany)
Thermomixer (5320)	Eppendorf (Hamburg, Germany)
Thermomixer (5436)	Eppendorf (Hamburg, Germany)
Thermomixer comfort	Eppendorf (Hamburg, Germany)
Transmission electron microscope (JEM-1400)	JEOL (Freising, Germany)

Instrument	**Supplier (City, Country)**
Tube roller (SU1400)	SunLab Instruments (Mannheim, Germany)
Ultracentrifuge (TLA-100.2)	Beckman Coulter (Brea, USA)
Ultracentrifuge (XL-70)	Beckman Coulter (Brea, USA)
Ultrasonic bath (Sonorex Super)	Bandelin Electronics (Berlin, Germany)
Vacuum centrifuge (Speedvac concentrator, Savant SPD111V)	Thermo Fisher Scientific (Waltham, USA)
Vacuum pump (WOB-L Pump 2511)	Welch-Ilmvac (Niles, USA)
Vortex (REAX 2000)	Heidolph Instruments (Schwabach, Germany)
Vortex (VF2)	IKA-Works (Wilmington, USA)
Waterbath (HI1201)	Leica Biosystems (Nußloch, Germany)
Waterbath (SUB6)	Grant Instruments (Cambridge, UK)
Waterbath (SW20)	Julabo Labortechnik (Seelbach, Germany)
Waterbath (WBT22)	Carl Roth (Karlsruhe, Germany)
XCell II™ blot module	Thermo Fisher Scientific (Waltham, USA)

2.4 Kits

Table 4: List of used kits.

Kit	Supplier (City, Country)
BigDye Terminator v2.2 Cycle Sequencing Kit	Thermo Fisher Scientific (Waltham, USA)
DNase I Amplification Grade Kit	Thermo Fisher Scientific (Waltham, USA)
DNeasy Blood & Tissue Kit	Qiagen (Hilden, Germany)
EZ-Link™ Sulfo-NHS-Biotin Kit	Thermo Fisher Scientific (Waltham, USA)
FFPE Plus LEV RNA Purification Kit	Promega (Madison, USA)
FlexiGene DNA Kit	Qiagen (Hilden, Germany)
HLA-A*02:01 easYmer®Kit	ImmunAware (Hørsholm, Denkmark)
Liquid DAB+ Substrate Chromogen System	Dako (Carpinteria, USA)
Platinum Taq DNA polymerase Kit	Thermo Fisher Scientific (Waltham, USA)
QIAamp DNA FFPE Tissue Kit	Qiagen (Hilden, Germany)
QIAamp DNA Mini Kit	Qiagen (Hilden, Germany)
QIAquick PCR Purification Kit	Qiagen (Hilden, Germany)
QuBit™ 2.0 RNA high sensitivity Kit	Thermo Fisher Scientific (Waltham, USA)
RNeasy Mini Kit	Qiagen (Hilden, Germany)
Standard Taq DNA polymerase Kit	Thermo Fisher Scientific (Waltham, USA)
SuperScript™ II Kit	Thermo Fisher Scientific (Waltham, USA)
Total Exosome Isolation Reagent (from cell culture media)	Thermo Fisher Scientific (Waltham, USA)
Total Exosome Isolation Reagent (from plasma)	Thermo Fisher Scientific (Waltham, USA)
TURBO DNA-free™ Kit	Thermo Fisher Scientific (Waltham, USA)
Vectastain®Elite®ABC Kit, peroxidase	Vector Laboratories (Burlingame, USA)
Venor®GeM Classic	Minerva Biolabs (Berlin, Germany)

2.5 Antibodies

Table 5: List of used primary antibodies.

Antibody	Supplier (City, Country)	Additional information	Source	Dilution
Primary Antibodies				
B2M-PE	Santa Cruz (Dallas, USA)	monoclonal, BBM.1	mouse	1:200 (FACS)
A33	Abcam (Cambridge, UK)	monoclonal, ERP4240	rabbit	1:300 (IHC) 1:1,000 (Wb)
A33	A.M. Scott, Ludwig Institute for Cancer Research, Melbourne, Australia	monoclonal	mouse	10 µg (IP) 4 µg/ml (ELISA)
Alix	Abcam (Cambridge, UK)	monoclonal, EPR15314	rabbit	1:1,000 (Wb)
CD3	Abcam (Cambridge, UK)	monoclonal, SP7	rabbit	1:200 (IHC)
CD63	System Biosciences (Palo Alto, USA)	polyclonal	rabbit	1:1,000 (Wb)
CD8	Thermo Fisher Scientific (Waltham, USA)	monoclonal, SP16	rabbit	1:100 (IHC)
CD8a-APC	Thermo Fisher Scientific (Waltham, USA)	monoclonal, RPA-T8	mouse	1:100 (FACS)
CD81	System Biosciences (Palo Alto, USA)	polyclonal	rabbit	1:1,000 (Wb)
FOXP3	Thermo Fisher Scientific (Waltham, USA)	monoclonal, 236A/E7	mouse	1:50 (IHC)
IFNγ	Mabtech (Nacka Strand, Sweden)	monoclonal, 1-D1K	mouse	1:133.33 (ELISpot)
MLH1	Becton, Dickinson and Company (Franklin Lakes, USA)	monoclonal, G168-15	mouse	1:50 (IHC)

Antibody	Supplier (City, Country)	Additional information	Source	Dilution
MSH2	Calbiochem (San Diego, USA)	monoclonal, FE11	mouse	1:200 (IHC)
MSH6	Epitomics (Burlingame, USA)	monoclonal, EP49	rabbit	1:200 (IHC)
PMS2	Bio SB (Santa Barbara, USA)	monoclonal, EP51	rabbit	1:100 (IHC)

Table 6: List of used secondary antibodies.

Antibody	Supplier (City, Country)	Source	Dilution
Secondary Antibodies			
Anti-human IFNγ, biotinylated	Mabtech (Nacka Strand, Sweden)	mouse	1:1,000 (ELISpot)
Anti-mouse IgG, biotinylated	Vector Laboratories (Burlingame, USA)	goat	1:50 (IHC)
Anti-mouse/anti-rabbit IgG, biotinylated	Vector Laboratories (Burlingame, USA)	horse	1:50 (IHC)
Anti-mouse IgG, HRP-linked	Cytiva (Marlborough, USA)	sheep	1:5,000 (Wb, ELISA)
Anti-rabbit IgG, HRP-linked	Cell Signaling (Danvers, USA)	goat	1:2,000 (Wb)

2.6 Peptides

Table 7: List of used FSPs. Peptides are derived from -1 frameshifts in the cMS of the respective gene.

Peptide	Sequence	Supplier (City, Country)
AIM2 (-1)	HSTIKVIKAKKKHREVKRTNSS QLV	Bachem (Bubendorf, Switzerland)
CASP5 (9–34) (-1)	KQLRCWNTWAKMFFMVFLIIW QNTMF	Genaxxon bioscience (Ulm, Germany)
HT001 (-1)	EIFLPKGRSNSKKKGRRNRIPAV LRTEGEPLHTPSVGMRETTGLGC	Bachem (Bubendorf, Switzerland)
MARCKS (-1)	SNETPKKKRSAFPSRSLSS	Genaxxon bioscience (Ulm, Germany)
MYH11.1 (16–48) (-1)	APGEETRPLSFLLEGLEDVELL KMQMVLRRKRT	Genaxxon bioscience (Ulm, Germany)
MYH11.2 (41–72) (-1)	MVLRRKRTLETQTSMEPRPVN KQLSTVLHHGK	Genaxxon bioscience (Ulm, Germany)
SLC22A9.1 (23–52) (-1)	VKGSPSCPLRDLQTLWPILALIS MSSIWGT	Genaxxon bioscience (Ulm, Germany)
SLC22A9.2 (45–74) (-1)	SMSSIWGTMFSCCRLSLVQSSS WPTVLHLG	Genaxxon bioscience (Ulm, Germany)
SLC35F5 (-1)	VAKISFFFALCGFWQICHIKKHF QTHKLL	Genaxxon bioscience (Ulm, Germany)
TAF1B (-1)	NTQIKALNRGLKKKTILKKAGI GMCVKVSSIFFINKQKP	Bachem (Bubendorf, Switzerland)
TCF7L2 (-1)	CGPCRRKKSAFATYKVKAAAS AHPLQMEAY	Genaxxon bioscience (Ulm, Germany)
TGFBR2 (-1)	KCIMKEKKSLVRLSSCVPVALM SAMTTSSSQKNITPAILTCC	Genaxxon bioscience (Ulm, Germany)
TTK (-1)	DLQLFVMSDTTYKIYWTVILLN PCGNLHLKTTSL	Genaxxon bioscience (Ulm, Germany)

Table 8: List of FSPs analyzed as part of the PEPperPRINT peptide microarray. Peptides are derived from -1 or -2 frameshifts in the cMS of the respective gene.

Peptide	Sequence
FLJ32202 (-1)	KKKKKEKKSLLISFFLISTEQGSKI
FLJ32202 (-2)	KKKKKRNPS
DAMS (-1)	PPPPPKAPAGQETLSLQSR
DAMS (-2)	PPPPPKLQLVRKHCLYNQDKHLAQGVQPFLTYRLA
BANP (-1)	FFPFFCSVGA
BANP (-2)	PCFFFSLFSAL
HT001 (ASTE) (-1)	NSKKKGRRNRIPAVLRTEGEPLHTPSVGMRETTGLGC
HT001 (ASTE) (-2)	NSKKKAEETEYQLF
TAF1B (-1)	GLKKKTILKKAGIGMCVKVSSIFFINKQKP
TAF1B (-2)	GLKKKQY
FLJ25378 (-1)	SFFFFKQPSPKTQDHLRQQRASAR
FLJ25378 (-2)_A	PSFFFSSSPVPRRKTTCASSVHQQDSKSRTRAARKTSTWP
FLJ25378 (-2)_B	ARKTSTWPEDTYPGRKTCTPEDRERGHRVLRSSHVRLGHF
FLJ25378 (-2)_C	SHVRLGHFLFTEDYKTPVLSSLGADAILGLSPPAARRSLKQ
FLJ25378 (-2)_D	AARRSLKQHVAPHRLVLFVGPTLWARTNTSTFQAVYSSVS
PTHL3 (PTHLH) (-1)	GLKKKRKTTEEHIICN
PTHL3 (PTHLH) (-2)	GLKKKGKQQKNTSYATNDLII
ZNF294 (-1)	SSKKKMVRLDLLMRYLKAIKRMKNVYLQKERRLKAGN
ZNF294 (-2)	SSKKKW
TGFBR2 (-1)	KCIMKEKKSLVRLSSCVPVALMSAMTTSSSQKNITPA
TGFBR2 (-2)	MKEKKAW
MARCKS (-1)	SNETPKKKRSAFPSRSLSS
MARCKS (-2)	TPKKKEALFLQEVFQAERLLLQEEQEGGWRRR
Q96PS6 (-1)	IFFFFKDGVLLSHLG
Q96PS6 (-2)	PIFFFSKMESYSLT
SLC22A9 (UST3) (-1)_A	AAQKKNLLCVKCSTCPTYVKGSPSCPLRDLQTLWPILA
SLC22A9 (UST3) (-1)_B	QTLWPILALISMSSIWGTMFSCCRLSLVQSSSWPTVLHLGH
SLC22A9 (UST3) (-2)	AAQKKTFSV
ACVR2 (-1)	VVHKKRGLF

Peptide	Sequence
ACVR2 (-2)	VHKKEACFKRLLAETCWNGNAL
ADAMTSL1 (C9orf94) (-1)	FCFFFSS
ADAMTSL1 (C9orf94) (-2)	FCFFFLPRSA
CASP5 (9–34) (-1)	KQLRCWNTWAKMFFMVFLIIWQNTMF
SLC35F5 (-1)	VAKISFFFALCGFWQICHIKKHFQTHKLL
TCF7L2 (-1)	CGPCRRKKSAFATYKVKAAASAHPLQMEAY
MYH11.1 (16–48) (-1)	APGEETRPLSFLLEGLEDVELLKMQMVLRRKRT
MYH11.2 (41–72) (-1)	MVLRRKRTLETQTSMEPRPVNKQLSTVLHHGK
LTN (6–36) (-1)	KKKMVRLDLLMRYLKAIKRMKNVYLQKERRL
ATRX (-1)	CCESVKKNKEISRFRMHSCPLYGPW
NKTR (-1)	EKKVSENNALNHKR
AIM2 (-1)	KAKKKHREVKRTNSSQLV

Table 9: List of used FSP epitopes.

FSP epitope	Sequence	Supplier (City, Country)
hSLC35F5_E1	FALCGFWQI	DKFZ (Heidelberg, Germany)
hTGFBR2_E1	SLVRLSSCVPV	DKFZ (Heidelberg, Germany)
hTGFBR2_E2	RLSSCVPVAL	DKFZ (Heidelberg, Germany)
hTGFBR2_E3	RLSSCVPVA	DKFZ (Heidelberg, Germany)
hTGFBR2_E4	LVRLSSCVPV	DKFZ (Heidelberg, Germany)
hTGFBR2_E5	SLVRLSSCV	DKFZ (Heidelberg, Germany)
hTGFBR2_E6	ALMSAMTTS	DKFZ (Heidelberg, Germany)
hTGFBR2_E7	RLSSCVPV	DKFZ (Heidelberg, Germany)
hTGFBR2_E8	SQKNITPAI	DKFZ (Heidelberg, Germany)
hSLC22A9.2 (45–74)_E1	TMFSCCRLSL	DKFZ (Heidelberg, Germany)
hSLC22A9.2 (45–74)_E2	TMFSCCRLSLV	DKFZ (Heidelberg, Germany)
hSLC22A9.2 (45–74)_E3	SSWPTVLHL	DKFZ (Heidelberg, Germany)
hTTK(13–46)_E1	FVMSDTTYKIYWTV	DKFZ (Heidelberg, Germany)
hTTK(13–46)_E2	FVMSDTTYKI	DKFZ (Heidelberg, Germany)

FSP epitope	Sequence	Supplier (City, Country)
hTTK(13–46)_E3	VMSDTTYKI	DKFZ (Heidelberg, Germany)
hTTK(13–46)_E4	VMSDTTYKIYWTV	DKFZ (Heidelberg, Germany)
hTTK(13–46)_E5	TTYKIYWTV	DKFZ (Heidelberg, Germany)
hTTK(13–46)_E6	ILLNPCGNLHL	DKFZ (Heidelberg, Germany)
hTTK(13–46)_E7	LLNPCGNLHL	DKFZ (Heidelberg, Germany)
hTTK(13–46)_E8	KIYWTVILL	DKFZ (Heidelberg, Germany)
hMYH11.1 (16–48)_E1	FLLEGLEDV	DKFZ (Heidelberg, Germany)
hMYH11.1 (16–48)_E2	FLLEGLEDVEL	DKFZ (Heidelberg, Germany)
hMYH11.1 (16–48)_E3	FLLEGLEDVELL	DKFZ (Heidelberg, Germany)
hMYH11.1 (16–48)_E4	SFLLEGLEDV	DKFZ (Heidelberg, Germany)
hMYH11.1 (16–48)_E5	SFLLEGLEDVEL	DKFZ (Heidelberg, Germany)
hMYH11.1 (16–48)_E6	FLLEGLEDVE	DKFZ (Heidelberg, Germany)
hMYH11.1 (16–48)_E7	LLEGLEDVELL	DKFZ (Heidelberg, Germany)
hCASP5(9–34)_E1	KMFFMVFLI	DKFZ (Heidelberg, Germany)
hCASP5(9–34)_E2	KMFFMVFLII	DKFZ (Heidelberg, Germany)
hCASP5(9–34)_E3	FLIIWQNTM	DKFZ (Heidelberg, Germany)
hSLC22A9.1 (23–52)_E1	TLWPILALI	DKFZ (Heidelberg, Germany)
hSLC22A9.1 (23–52)_E2	QTLWPILALI	DKFZ (Heidelberg, Germany)
hSLC22A9.1 (23–52)_E3	ALISMSSIWGT	DKFZ (Heidelberg, Germany)
hSLC22A9.1 (23–52)_E4	TLWPILAL	DKFZ (Heidelberg, Germany)
hSLC22A9.1 (23–52)_E5	TLWPILALISM	DKFZ (Heidelberg, Germany)

2.7 Primers

Table 10: List of used primers. T_m indicates the annealing temperature for the primer pair.

Gene	Forward primer [5' > 3']	Reverse primer [5' > 3']	T_m
Non-coding microsatellite loci			
BAT25	TCGCCTCCAAGAATGTAAGT	TATGGCTCTAAAATGCTCTGTTC	55 °C
BAT26	TGACTACTTTTGACTTCAGCC	AACCATTCAACATTTTTAACCC	55 °C
BAT40	AGTCCATTTTATATCCTCAAGC	GTAGAGCAAGACCACCTTG	55 °C
CAT25	CCTAGAAACCTTTATCCTGCTT	GAGCTTGCAGTGAGCTGAGA	55 °C
Coding microsatellite loci			
AIM2	TTCTCCATCCAGGTTATTAAGGC	TTAGACCAGTTGGCTTGAATTG	58 °C
HT001	ATATGCCCCCGCTGAAATA	TTGGTGTGTGCAGTGGTTCT	58 °C
MARCKS	GACTTCTTCGCCCAAGGC	GCCGCTCAGCTTGAAAGA	58 °C
MYH11	CGGGGATTCTCTCTCTGTTTC	CTGAAGGCATGATACCTGGTG	58 °C
SLC22A9	GCGCCTACAGTGCCTACTCT	GCATGTGGAGCATTTCACAC	58 °C
SLC35F5	TGTGGGGAAACTTACTGCAA	TCAAGTTTCAAACATCAATGCAA	58 °C
TAF1B	ACCCAAATAAAAGCCCTCAAC	CTACTTAAAATTCCATTCCATGTCC	58 °C
TGFBR2	GCTGCTTCTCCAAAGTGCAT	CAGATCTCAGGTCCCACACC	58 °C
TTK	TTCTTCATCCTCCAAGACTTTT	GATTTCCACAGGGATTCAAGA	58 °C
Sanger sequencing			
HLA-A*02	TCTCAGCCACTCCTCGTC	TGTCGAACCGCACGAACTG	60 °C
B2M exon 1	GGCATTCCTGAAGCTGACA	AGAGCGGGAGAGGAAGGAC	59 °C
B2M exon 2A	TTTTCCCGATATTCCTCAGGTA	AATTCAGTGTAGTACAAGAG	57 °C
B2M exon 2B	CATTCAGACTTGTCTTTCAG	TTTCAGCAGCTTACAA	64 °C
BRAF	TCATAATGCTTGCTCTGATAGGA	GGCCAAAAATTTAATCAGTGGA	58 °C
KRAS	AAGGCCTGCTGAAAATGACTG	AGAATGGTCCTGCACCAGTAA	58 °C

Gene	Forward primer [5' > 3']	Reverse primer [5' > 3']	T_m
	RT-qPCR		
β-actin	ATGTGGCCGAGGACTTTGATT	AGTGGGGTGGCTTTTAGGATG	56 °C
IFNγ	CTGTTACTGCCAGGACCCAT	TTTCTGTCACTCTCCTCTTTCCA	56 °C

2.8 Buffers and solutions

Table 11: List of used buffers and solutions.

Buffer	Composition
Eosin solution	water 0.5 % eosin 0.2 % glacial acetic acid
Citrate buffer (10 x) (IHC)	100 mM citric acid monohydrate adjust pH to 6.0
Citrate-phosphate buffer (1 x) (crosslinking)	water 50 mM $Na_2HPO_4 \cdot 2\,H_2O$ 20 mM citric acid monohydrate adjust pH to 5
Crosslinking buffer	water 0.2 M triethanolamine adjust pH to 8.2
Dilution buffer (tetramer staining)	PBS 5 % glycerol
DMP solution (crosslinking)	crosslinking buffer 20 mM DMP
DNA sample buffer (1 x)	water 25 mM TRIS 0.042 % bromophenol blue 10 % glycerol adjust pH to 7.6
ELISA blocking solution	PBS (1 x) 0.5 % BSA

Buffer	**Composition**
ELISA (biotinylation) blocking solution	PBS (1 x) 0.1 % biotin-free BSA
FACS buffer	PBS 1 % BSA
Hydrochloric acid solution (2 M)	water 2 M HCl
5 % milk (Wb)	TBS-T (1 x) 5 % skim milk
PBS (10 x) (IHC)	water 1.37 M NaCl 27 mM KCl 18 mM KH_2PO_4 100 mM $Na_2HPO_4 \cdot 2\,H_2O$ adjust pH to 7.2
PBS-T (1 x) (IHC)	dilute PBS for IHC (10 x) 1:10 with water 0.1 % Tween 20
Peroxidase block (IHC)	methanol 30 % hydrogen peroxide solution
Ponceau solution	water 0.1 % Ponceau S 5 % acetic acid
RIPA buffer (1 x)	water 50 mM TRIS-HCl 150 mM NaCl 1 % Triton X-100 1 % sodium deoxycholate 0.1 % SDS 0.1 mM $CaCl_2$ 0.01 mM $MgCl_2$ adjust pH to 7.4
Sodium acetate solution (3 M)	water 3 M NaOAc adjust pH to 5

Buffer	**Composition**
Sodium hydroxide solution (1 M)	water 1 M NaOH
TBE (1 x)	water 0.1 M TRIS 83 mM boric acid 1 mM EDTA adjust pH to 8
TBS (1 x) (Wb)	water 50 mM TRIS-HCl 150 mM NaCl adjust pH to 7.5
TBS-T (1 x) (Wb)	water 50 mM TRIS-HCl 150 mM NaCl 0.1 % Tween 20 adjust pH to 7.5
Transfer buffer (1 x)	1x NuPage Transfer buffer 0.1 % NuPage Antioxidant 10 % methanol
TRIS solution (crosslinking)	water 50 mM TRIS adjust pH to 7.5
Wash buffer (crosslinking)	PBS (1 x) 0.05 % Tween 20
Wash buffer (ELISA)	PBS (1 x) 0.05 % Tween 20
Wash buffer (IP)	TBS (1 x) 0.05 % Tween 20

2.9 Cell lines

Table 12: List of used cell lines.

Cell line	Medium	Source (city, country)
LIM1215	RPMI 1640, 10 % FBS, 1 % P/S, 10 µM thioglycerol, 0.6 µg/ml insulin, 1 µg/ml hydrocortisone	Dr. R.H. Whitehead, Ludwig Institute of Cancer Research (Melbourne, Australia)

2.10 Special cell culture media

Table 13: List of used special cell culture media.

Medium	Composition
T cell medium	500 ml RPMI 1640 10 % human serum 1 % L-Glutamine 1 % P/S 12.5 mM HEPES 0.05 mM β-Mercaptoethanol
ELISpot medium	500 ml RPMI 1640 5 % FBS 1 % L-Glutamine 12.5 mM HEPES 0.05 mM β-Mercaptoethanol

2.11 Software

Table 14: List of used software.

Software	Version	Supplier (City, Country)
Cell Imaging Software for Life Science Microscopy	2.8	Olympus Soft Imaging Solutions (Tokyo, Japan)
FlowJo	10.7.1	Becton, Dickinson and Company (Franklin Lakes, USA)
GeneMarker software	1.5	SoftGenetics (State College, USA)
GraphPad Prism	6.07	GraphPad Software Inc. (La Jolla, USA)
ImmunoSpot®software	7.0.24.1	Cellular Technology Limited (Cleveland, USA)
Magellan Software	7.1	Tecan Group AG (Männedorf, Switzerland)
NanoDrop 1000	3.8.1	Thermo Fisher Scientific (Waltham, USA)
NDP.view2	2.7.25	Hamamatsu Photonics K.K. (Hamamatsu, Japan)
NTA software	3.0	Malvern Panalytical (Malvern, UK)
QuPath	0.2.0-m2	University of Edinburgh (Edinburgh, UK) [302]
R	3.4.3	Bioconductor, Vienna University of Economics and Business (Vienna, Austria) [303]
R Studio	1.2.5033	R Studio (Boston, USA)
Sequencing Analysis Software	6.0	Thermo Fisher Scientific (Waltham, USA)
StepOnePlus	2.1	Thermo Fisher Scientific (Waltham, USA)
TEM Center	1.4.4.3222	JEOL (Freising, Germany)

2.12 Patient samples

Formalin-fixed paraffin-embedded (FFPE) specimens, normal mucosa and cancer tissue, were retrieved from the archive of the Institute of Pathology, University Hospital Heidelberg and the Department of Surgery, University Hospital Heidelberg, Germany. Additional tissue samples could be acquired from the Department of Internal Medicine I, University Hospital Bonn, Germany and the National LS registry of Finland at the Central Finland Central Hospital, Jyväskylä, Finland. Tumor-distant normal mucosa from CRC patients (LS and non-LS) was collected from tumor-free resection margins synchronous with CRC resection (Figure S1). Normal colonic mucosa biopsies from healthy LS carriers were obtained during surveillance colonoscopy examinations (Figure S1).
Furthermore, samples collected within the CAPP2 clinical trial [247], following trial protocols, were analyzed. The trial is registered with the ISRCTN registry (ISRCTN59521990).

Blood samples from healthy LS carriers and cancer patients were collected at the National Center for Tumor Diseases, Heidelberg, Germany. In addition, blood from healthy volunteers was collected at the Department of Applied Tumor Biology, Institute of Pathology, University Hospital Heidelberg, Germany.

Written informed consent was obtained from all participants and studies were approved by the institutional ethics committees (V5.1 S-207/2005, S-583/2016, S-375/2021, S-735/2021).

3 Methods

3.1 Systematic literature search

A systematic literature search on differences between hereditary and sporadic MSI tumors regarding immune infiltration and immune evasion was conducted. Inclusion and exclusion criteria were defined prior to the search as follows: a direct comparison between hereditary and sporadic MSI tumors was required for inclusion, a lack thereof and no clear definition of the analyzed groups qualified for exclusion. An online MEDLINE search (http://www.pubmed.com) was conducted between February 29th and March 10th, 2020 using the following keywords: {Lynch} OR {Lynch syndrome} OR {HNPCC} OR {MSI} OR {microsatellite instability} OR {MMR-deficient} OR {MMR deficiency} OR {hereditary MSI} OR {sporadic MSI} OR {microsatellite instable} OR {RER +} OR {mutator phenotype} AND {immune infiltration} OR {immune microenvironment} OR {T cell infiltration} OR {TIL} OR {tumor infiltration} OR {immune evasion} OR {T cell density} OR {B2M} OR {RFX5} OR {CIITA} OR {HLA} OR {TAP} OR {NLRC5} [304].

The results of the search were screened manually and Preferred Reporting Items for Systematic Reviews and Meta-Analyses (PRISMA) recommendations (updated PRISMA statement: [305, 306]) were followed. Briefly, eligibility of publications was checked by screening in the following order: title, abstract and full text. A subset of the total search results was screened by a second, independent observer and the inter-rater reliability was determined by the Cohen's κ coefficient. All selected papers were analyzed qualitatively and included data on immune evasion was assessed quantitatively whenever possible. Quantitative analysis of immune infiltration data was not conducted due to different antibodies, counting methods and analyzed cell categories (e.g. stromal vs. epithelial). In addition, several suited publications were added independently of the systematic search [304].

3.2 Processing and analysis of tissue samples

3.2.1 Preparation of tissue slides

FFPE tissue blocks, to be used for staining and microdissection, were placed at -20 °C for at least 2 h prior to sectioning with a microtome. Sections, between 2 µm (for immunohistochemical staining) and 6 µm (for microdissection), were mounted onto glass slides and dried at 37 °C. For subsequent analysis slides underwent deparaffinization and re-hydration by incubation in xylene (3 x 5 min) and a graded ethanol series (2 x 5 min in 100 %, 5 min in 96 %, 5 min in 70 %). Finally, slides were washed in deionized water (1 x 5 min).

3.2.2 Hematoxylin and eosin staining

Deparaffinized slides (see 3.2.1) were stained in filtered hematoxylin for 3 min and bluing was performed in tap water for 2 min. Slides were counterstained with an eosin solution for 45 sec. After several wash steps with deionized water, slides were either dried and used for manual microdissection or mounted with histofluid. For mounting, slides were shortly dipped into water with glacial acetic acid, passed through a graded ethanol series (3 sec in 70 %, 3 sec in 96 %, 3 sec in 100 %) and incubated in xylene (2 x 3 min). Lastly, coverslips were mounted onto the tissue using histofluid and slides were dried at room temperature. As needed, hematoxylin and eosin (HE)-stained slides were scanned at 40 x magnification using the NanoZoomer 2.0 HT scan system.

3.2.3 Immunohistochemical staining

After deparaffinization (see 3.2.1), tissue slides underwent heat-induced epitope retrieval which was performed in 10 mM citrate buffer (pH 6). Slides were heated in a microwave (3 x 5 min, 550 W) and subsequently cooled for around 30 min at room temperature. Afterwards, slides were washed (3 x 30 sec) in deionized water and endogenous peroxidase activity was blocked by incubating slides in methanol with 2 % hydrogen peroxide for 20 min. Next, slides were washed in deionized water and placed in phosphate-buffered saline (PBS) with 0.1 % Tween 20 (PBS-T) for at least 2 min. The tissues were encircled with a hydrophobic pen and transferred to a humidified chamber in which all following steps were conducted. Reduction of unspecific antibody binding was achieved by blocking with 10 % horse serum diluted in PBS for 30 min. Staining with the primary antibody, diluted in PBS with 1 % horse serum (Table 5), was conducted overnight at 4 °C.

After incubation, slides were washed in PBS-T (2 x 5 min) and the biotinylated secondary IgG antibody, diluted in PBS with 1 % horse serum (Table 6), was applied for 30 min at room temperature. After two wash steps in PBS-T, samples were incubated with avidin-biotin complexes coupled to horseradish peroxidase (HRP) for 30 min at room temperature, which enabled signal amplification during antigen visualization. After two wash steps with PBS-T, visualization was performed with 3,3' Diaminobenzidine (DAB) substrate, which was applied for 1–10 min depending on the used primary antibody. The detectable brown staining is a result of the reaction between the DAB chromogen and the peroxidase. Lastly, samples were counterstained with filtered hematoxylin for 10–30 sec, blued for 5 min in tap water and mounted with Aquatex.

3.2.3.1 Quantification of stainings

Sufficient staining quality was confirmed microscopically before the stained sections (see 3.2.3) were scanned at 40 x magnification using the NanoZoomer 2.0 HT scan system. For quantification, four regions of interest (ROIs), each 0.1 mm^2, were randomly placed within the normal colonic mucosa and tumor tissue, respectively. For the FOXP3 staining eight ROIs were used to overcome the overall low density of FOXP3-positive T cells and increase the counting accuracy. When placing the ROIs in the colonic mucosa lymph follicles and stromal regions outside of the mucosa were avoided. Quantification of the positive cells within the ROIs was performed manually using the open-source software QuPath (version: 0.2.0-m2) [302].

3.2.4 Manual microdissection

Isolation of DNA and RNA from tissue required microdissection of the respective areas, which was performed manually with a cannula under the microscope. The obtained tissue was directly transferred into lysis buffer (for DNA isolation, see 3.6.1) or mineral oil (for RNA isolation, see 3.7.1).

3.3 Processing and analysis of blood samples

3.3.1 Isolation of peripheral blood mononuclear cells

Blood samples were collected in K2 EDTA gel collection tubes and stored at room temperature upon processing for which all steps were conducted in a laminar flow hood. Notably, 1 ml of whole blood was collected and stored at -20°C for subsequent DNA isolation. Following, the blood was transferred to a cell culture flask and diluted 1:2 with RPMI medium without any supplements. Up to 35 ml of the blood-medium mixture were carefully layered onto 15 ml of lymphocyte separation medium in a 50 ml falcon tube. Centrifugation at 2,500 rpm (1,200 x g) for 15 min without brake resulted in phase separation. The interphase, containing peripheral blood mononuclear cells (PBMCs) between the plasma phase and pelleted erythrocytes, was collected and transferred to a new tube. Additionally, 6–12 ml of plasma were collected for further analysis and stored at -20 °C. RPMI, up to 50 ml, was added to the isolated PBMCs and cells were centrifuged at 1,800 rpm (630 x g) for 15 min. After removal of the supernatant, the cell pellet was resuspended in 50 ml RPMI and centrifuged at 1,500 rpm (435 x g) for 15 min. The cell pellet was resuspended in 20 ml RPMI and viable cells were counted using an automated fluorescence cell counter and an acridine orange/propidium iodide dye. Lastly, cells were centrifuged again at 1,500 rpm for 15 min and up to $40*10^6$ cells were resuspended in 1 ml of serum-free PBMC freezing medium, transferred into a cryo vial and frozen at -80 °C using a Mr. Frosty® freezing container. After 24–48 h, cells were transferred to liquid nitrogen for long-term storage.

3.3.2 *In vitro* expansion of antigen-specific T cells

Frozen PBMCs (see 3.3.1) were thawed by briefly placing the cryo vial in a 37 °C water bath. Cells were immediately transferred to a falcon tube containing 10 ml of PBS, centrifuged at 1,200 rpm (280 x g) for 10 min and resuspended in 10 ml of RPMI medium without supplements. Viable cells were quantified by using an automated fluorescence cell counter and an acridine orange/propidium iodide dye. Subsequently, cells were centrifuged again at 1,200 rpm for 10 min. Next, cells were resuspended in T cell medium containing 10 ng/ml recombinant human interleukin 7 (rhIL-7) resulting in $1*10^6$ cells/ml. 1 ml of this cell suspension, corresponding to $1*10^6$ PBMCs, was added to each well of a 24-well plate.
In parallel, FSPs (Table 7) and controls were prepared. Synthesized FSPs were dissolved in sterile dimethyl sulfoxide (DMSO) resulting in a 5,000 mg/ml stock solution. Peptides were further diluted 1:10 with PBS (500 mg/ml) and aliquoted, avoiding repeated freeze-thaw cycles. FSPs were supplemented to T cell medium and 1 ml was added to the plated cells in a final concentration of 10 µg/ml. Further, two positive controls were applied: concanavalin A (ConA), a T cell mitogen, and a cytomegalovirus, Epstein-Barr and influenza virus (CEF) peptide pool containing 23 MHC class I-restricted viral peptides [307]. Both positive controls were diluted in T cell medium and 1 ml was added to the cells in a final concentration of 2 µg/ml ConA and 1 µg/ml CEF, respectively. 0.4 % DMSO in T cell medium, the equivalent amount as present in the FSP preparations, was used as a negative control and 1 ml of this solution was added to the cells. For each stimuli one well with $1*10^6$ cells was prepared. Following, incubation was conducted at 37 °C in a 5 % CO_2 atmosphere and 85–95 % humidity.
Cultures were examined daily during the twelve days of expansion and half-medium changes were performed whenever needed. For the medium change the cell culture plate was centrifuged at 1,400 rpm (380 x g), 1 ml of medium was carefully removed and 1 ml of fresh T cell medium (without FSPs) was added. Furthermore, recombinant human interleukin 2 (rhIL-2), in a final concentration of 20 U/ml, was supplemented on days three and seven to promote further T cell proliferation (Figure 9). On day twelve cells were ready to be used for IFNγ ELISpot (Enzyme-linked immuno spot) assay (see 3.3.3). If not enough isolated PBMCs were available, the expansion was still conducted with $1*10^6$ cells per FSP but only selected FSPs could be analyzed in such case.

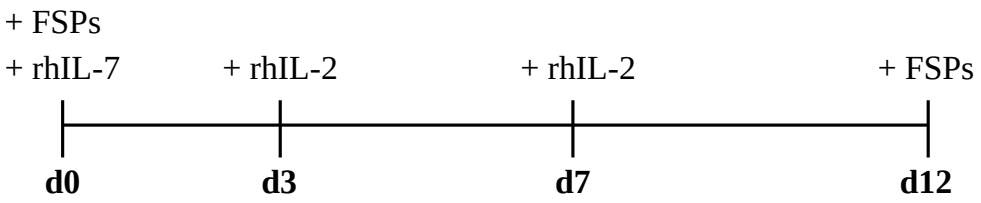

Figure 9: FSP-specific T cell expansion. Timeline for the *in vitro* expansion of antigen-specific T cells over 12 days (d) with supplementation of selected FSPs, rhIL-7 and rhIL-2.

3.3.3 IFNγ ELISpot assay

FSP-specific responses of expanded PBMCs (see 3.3.2) were assessed applying an IFNγ ELISpot assay [308]. The 96-well ELISpot plate was prepared one day in advance. First, the polyvinylidene difluoride (PVDF) membrane was activated by adding 50 µl of 70 % ethanol to each well for 5 min at room temperature. Second, ethanol was removed and the membrane was washed five times using 200 µl PBS for each well. Third, the activated membrane was coated with 100 µl/well anti-human IFNγ antibody, diluted 1:133 in sterile PBS. The plate was incubated at 4 °C overnight.

On the next day, the antibody was removed from the plate and after five wash steps with 200 µl PBS, the membrane was blocked to reduce unspecific binding using 200 µl ELISpot medium per well. Further, all PBMCs samples (see 3.3.2) were harvested to be re-plated in the prepared ELISpot plate. For that, cells were transferred to falcon tubes, centrifuged for 10 min at 1,200 rpm (280 x g) and resuspended in 2 ml ELISpot medium. Viable cells were counted using the automated fluorescence cell counter with an acridine orange/propidium iodide dye and centrifuged again at 1,200 rpm for 10 min. Cells were resuspended in ELISpot medium resulting in 100,000 cells/50 µl. For the re-stimulation of the cells FSPs and controls were prepared in the same concentrations as described in 3.3.2, all dilutions were conducted in ELISpot medium. 50 µl of peptides and controls were added to the ELISpot plate in triplicates. Finally, 50 µl cell suspension, equaling 100,000 cells, were added and the plate was incubated for 24 h at 37 °C.

After incubation, cells were removed from the plate and the membrane was washed five times with 200 µl PBS/well. Next, 100 µl of biotinylated IFNγ antibody, diluted 1:1,000 in PBS containing 0.5 % fetal bovine serum (FBS), were added to the membrane and incubated for 2 h at room temperature. The antibody was filtered using a 0.22 µm sterile filter to limit background staining. The membrane was washed again as described above and 100 µl of a streptavidin-coupled alkaline phosphatase, diluted 1:1,000 in PBS with 0.5 % FBS, were added for 1.5 h at room temperature. The final step, spot visualization, was induced by adding 100 µl of filtered (0.45 µm) 5-bromo-4-chloro-3'-indolyl-phosphate/nitro-blue tetrazolium (BCIP/NBT) substrate to each well. The reaction was conducted at room temperature for ca. 20 min until it was stopped by rinsing the membrane from both sides with tap water. The membrane was dried overnight and spots were quantified using an automated ELISpot reader.

Remaining, expanded PBMCs that were not required for the ELISpot assay were used for IFNγ reverse transcription-quantitative PCR (RT-qPCR) and processed accordingly. Cells were re-stimulated with the respective FSPs in a final concentration of 10 µg/ml and a total volume of 1 ml. During re-stimulation, cells were incubated at 37 °C for 4 h. Following, cells were centrifuged at 280 x g for 10 min at 4 °C and resuspended in 1 ml of PBS. This was repeated once more and the obtained cell pellet was frozen at -80 °C until RNA was isolated (see 3.7.2).

3.3.4 Tetramer staining

In order to detect FSP-specific T cell populations, PBMCs underwent *in vitro* expansion (see 3.3.2) before being used for tetramer staining, applying the HLA class I easYmer®system. For that purpose, all HLA-A*02:01 restricted epitopes from the used FSPs (Table 7) were selected using the NetMHCpan-4.1 prediction tool [309] and subsequently synthesized (Table 9). Following, the efficiency of the epitope-HLA-A interaction was assessed by a flow cytometry-based complex formation assay. The purchased HLA-A complexes contain a biotin-tagged heavy chain which could be captured by streptavidin-coated beads. Subsequently, a PE-conjugated, anti-human B2M antibody was applied and the respective bead-associated fluorescence signal could be measured by flow cytometric analysis. As the epitope-HLA-A interaction is solely dependent on the respective peptide, a strong fluorescent signal is only detectable if stable complexes are formed and the used FSP epitope supports the folding of the HLA-A monomer. Further, negative (no peptide) and positive (cytomegalovirus (CMV) protein pp65) controls were applied.

HLA-epitope complexes were prepared as follows (all steps were performed on ice): peptides were diluted to a final concentration of 75 µM in water and combined with folding buffer as well as easYmer®molecules (Table 15).

Table 15: Setup for the production of HLA class I monomers.

Reagents	
Water	45 µl
Peptide (75 µM)	3 µl
Folding buffer (6 x)	12 µl
easYmer®	12 µl
Total volume	72 µl

After thorough mixing, the reactions were incubated at 18 °C for 48 h on a shaker. Assuming optimal binding epitopes, 500 nM folded HLA monomers were obtained. Positive and negative controls were equally generated and water was added instead of the diluted peptides in case of the negative control. For the described complex formation assay, produced HLA monomers and controls were diluted with a dilution buffer containing glycerol and analyzed in three serial dilutions (13.3 nM, 4.4 nM and 1.5 nM). 40 µl of each dilution were transferred to a U-bottom shape 96-well plate and 20 µl of streptavidin-coated beads (diluted 1:45 in dilution buffer) were added to each well. The plate was sealed and incubated at 37°C for 1 h on a shaker. Next, 160 µl FACS buffer were added to each sample and the plate was centrifuged at 700 x g for 3 min. The supernatant was removed by flipping the plate and beads were resuspended in 200 µl FACS

buffer, this washing step was repeated two more times. After washing, 50 µl/well of PE-labeled anti-B2M antibody, diluted 1:200 in FACS buffer, were added to the beads and incubated for 30 min at 4 °C. Following, beads were washed three times using FACS buffer. Lastly, beads were resuspended in 200 µl FACS buffer and analyzed on the BD LSRFortessa flow cytometer with a high throughput sampler. The obtained flow cytometry data were analyzed using the FlowJo (version 10.7.1) software.

The produced monomers with confirmed complex formation were combined with a streptavidin-coupled fluorophore in order to form fluorescent tetramers which could be used for the analysis of FSP-specific CD8-positive T cells. For that, $1*10^6$ expanded PBMCs were transferred to a 96-well U-bottom plate, centrifuged 3 min at 700 x g and resuspended in 200 µl PBS. After another centrifugation step, cells were resuspended in a fixable viability stain (FVS780), diluted 1:1,000 in PBS, and incubated for 15 min in the dark at room temperature. Next, cells were washed two times using FACS buffer and stained for 20 min at room temperature with 40 µl (20 nM) of the respective tetramer. After incubation, cells were again washed with FACS buffer and stained for 30 min at 4 °C with an anti-CD8 antibody, diluted 1:100 in FACS buffer. Lastly and after two more washing steps, cells were fixed in 200 µl PBS containing 1 % paraformaldehyde (PFA) for at least 30 min at 4 °C. Before cells could be analyzed, they were washed twice in FACS buffer and filtered through a 35 µm strainer. Flow cytometric analysis was conducted with the BD FACSCanto II. Analysis of the obtained flow cytometry data was conducted with the FlowJo (version 10.7.1) software.

3.4 Cell culture

3.4.1 Maintenance of cell lines

All cell culture experiments were conducted under sterile conditions and a laminar flow hood. Cells were cultured in the respective medium (Table 12) at 37 °C in a 5 % CO_2 atmosphere and 85–95 % humidity. Cells were typically passaged two times a week depending on their proliferation rate. For passaging adherent cell lines, the culture medium was removed and cells were washed with PBS. Cells were detached by adding 0.05 % trypsin EDTA and incubation at 37 °C. After adding cell culture medium, cells were split by adding a proportion of cells back into the same flask, which was re-used up to ten times. Lastly, the split cells were supplied with fresh medium. Cells in culture were regularly checked for mycoplasma contamination using PCR and the Venor® GeM Classic Kit according to the manufacturer's protocol.
Primary PBMCs were cultured and expanded as described in 3.3.2.

3.4.2 Freezing and thawing of cells

For cryopreservation of cell lines, cells were expanded in T175 cell culture flasks until they reached 90 % confluence. Following, cells were trypsinized and centrifuged 10 min at 1,200 rpm (280 x g). After removal of the supernatant, cells were resuspended in cold FBS containing 10 % DMSO and transferred into a cryo vial. Up to 1/2 of the cells in a T175 flask were used for one cryo vial. Vials were placed at -80 °C using a Mr. Frosty® freezing container and transferred to liquid nitrogen after 24–48 h.
For thawing, the cryo vial was placed into a 37 °C water bath and cells were immediately transferred to 10 ml of warm PBS. After 10 min of centrifugation at 1,200 rpm, cells were resuspended in the respective medium, transferred to a new cell culture flask and placed into an incubator (see 3.4.1).
PBMCs were frozen and thawed as described previously (see 3.3.1, 3.3.2).

3.5 Extracellular vesicles

3.5.1 Polyethylene glycol-based precipitation

3.5.1.1 Human plasma

Human plasma samples were obtained as described in 3.3.1 and stored at -20 °C. For EV isolations, samples were thawed at 25 °C using a thermal block and centrifuged two times (2,500 x g, 10,000 x g) for 10 min each at 4 °C. The cleared supernatant was transferred to a new tube. The Total Exosome Isolation reagent (from plasma) was applied according to the manufacturer's recommendations and 0.5 volumes of PBS as well as 0.2 volumes (i.e. volume of plasma and PBS) of the reagent were added to the plasma sample. After 30 min of incubation at room temperature on a rotator, samples were centrifuged at 20,000 x g for 1 h at 4 °C. The resulting pellet, containing the EVs, was resuspended according to downstream analyses. EVs were resuspended in PBS for isolation of exosomal DNA, nanoparticle tracking analysis (NTA), transmission electron microscopy (TEM) and immunoprecipitation (IP). RIPA buffer, supplemented with a protease inhibitor cocktail, was used for exosomal protein extraction. EV preparations were stored at -20 °C.

For a subset of samples, a DNase I treatment was applied to remove all surface-bound DNA from isolated EVs. Briefly, 0.15 U/µl DNase I were added to EV preparations and incubated for 30 min at 30 °C. The digestion was stopped by adding 0.5 M EDTA and incubation for 5 min at 70 °C. EVs were centrifuged at 100,000 x g for 70 min and resuspended in PBS for the subsequent isolation of intravesicular DNA.

3.5.1.2 Cell culture medium

In preparation for EV isolation, adherent cells (Table 12) were grown to 80–90 % confluence in T175 cell culture flasks. Following, the respective culture medium was removed and cells were washed two times with PBS. For the purpose of EV isolation, the use of FBS had to be avoided due to the presence of bovine-derived EVs. Consequently, 17 ml of medium supplemented with 1 x Insulin-Transferrin-Selenium (ITS) were added to each flask and cells were incubated under normal conditions (see 3.4.1) for 18 h. The cell culture medium, containing released EVs, was collected and stored on ice. Floating cells were removed by 5 min centrifugation at 480 x g and 4 °C. The supernatant was transferred to a new tube and centrifuged at 2,000 x g for 10 min at 4 °C to remove cellular debris. The cleared medium was filtered through a sterile filter (0.22 µm) and ultrafiltration was performed. The volume of the medium was reduced by concentrating EVs (40-fold) via Vivaspin-20 tubes according to the manufacturer's specifications. The remaining concentrate was processed using the Total Exosome Isolation reagent (from cell culture media) as recommended: 0.5 volumes of the reagent were added to the concentrated EV suspension and incubated overnight on a rotator at 4 °C. On the next day, EVs were pelleted by a 1 h centrifugation step at 20,000 x g and 4 °C. The pellet was resuspended in PBS for DNA extraction, NTA, TEM, IP and enzyme-linked immunosorbent assay (ELISA). RIPA buffer, including a protease inhibitor cocktail, was used in preparation for protein extraction. Isolated EVs were stored at -20 °C.

3.5.2 Differential ultracentrifugation-based sedimentation

3.5.2.1 Human plasma

Plasma samples were thawed at 25 °C in a thermal block and prepared by 15 min centrifugation at 10,000 x g and 4 °C. The obtained supernatant was filtered (0.22 µm) and transferred to ultracentrifugation tubes. The tubes were filled up to 38 ml using PBS and their weight was equalized. Ultracentrifugation was performed with the XL-70 ultracentrifuge (rotor: SW28.1) at 140,000 x g for 2 h at 4 °C. The supernatant was removed until around 1 ml of suspension remained which was used for resuspending the pellet. The resuspended samples were transferred to smaller ultracentrifugation tubes, filled up to ca. 1.5 ml and centrifuged with the TLA-100.2 ultracentrifuge (rotor: 100.2) at 120,000 x g for 2 h at 4 °C. The pellets, containing EVs, were resuspended in PBS or RIPA buffer and stored at -20 °C.

3.5.2.2 Cell culture medium

Cells (Table 12) were ready for EV isolation when they reached 80–90 % confluence. Prior to isolation, cells were washed two times with PBS and the respective culture medium without FBS was added for 18 h (see 3.5.1.2). Following, the culture medium was collected and pre-cleared with two centrifugation steps (480 x g, 5 min, 4 °C; 2000 x g, 10 min, 4 °C). The cleared medium was filtered (0.22 µm), transferred to ultracentrifugation tubes and PBS was added to a total volume of 38 ml. The tubes' weight was equalized using PBS. Ultracentrifugation was conducted with the XL-70 centrifuge (rotor: SW28.1) at 140,000 x g for 2 h at 4 °C. After removal of most of the supernatant, the obtained pellets were resuspended in around 1 ml of remaining suspension and samples were transferred to smaller ultracentrifugation tubes. The second round of ultracentrifugation was conducted with the TLA-100.2 centrifuge (rotor: 100.2) at 120,000 x g for 2 h at 4 °C. EV pellets were resuspended in PBS or RIPA buffer and stored at -20 °C until further use.

3.5.3 Transmission electron microscopy

After isolation, EV morphology was assessed with a JEM-1400 transmission microscope equipped with a Tietz 2 K digital camera at 80 kV. Depending on amount and source, isolated EVs were diluted 1:5 to 1:75 in PBS. 5 µl of the EV suspension were incubated on 100 mesh formvar-coated copper grids and negatively stained with 2 % aqueous uranyl acetate, enhancing the contrast between particles and background. Lastly, samples were air-dried and visualized.

3.5.4 Nanoparticle tracking analysis

Size and concentration of the isolated EVs were analyzed by NTA using the NanoSight LM10 system equipped with a 405 nm laser and NTA software (version: 3.0). Isolated EVs were typically diluted 1:100 with cold, particle-free PBS. If necessary, the dilution was adjusted accordingly. After preparing the system following the manufacturer's instructions, 300 µl of the sample were injected into the sample chamber and particles were recorded at five different positions for 60 sec each. Temperature of the chamber was measured throughout the recordings and considered during analysis.

3.6 DNA techniques

3.6.1 DNA isolation from tissue

DNA was isolated from microdissected tissue (see 3.2.4) using the DNeasy Blood & Tissue Kit. Typically, eight to twelve 6 µm tissue sections were used and lysed with supplementation of proteinase K overnight at 56 °C on a shaker. After lysis, the manufacturer's protocol was followed and DNA was eluted from the spin column in 30–100 µl elution buffer depending on the expected amount of DNA. Lastly, DNA concentration was determined photospectrometically. DNA was stored at 4 °C and transferred to -20 °C for long-term storage.

If little tissue was available, the DNA FFPE tissue Kit was applied to effectively obtain sufficient DNA concentrations. For that purpose, tissue was again lysed overnight and the manufacturer's protocol was followed. The volume of elution buffer was adjusted to the expected DNA yield and 30–100 µl were added to the spin column. DNA concentration was measured and samples were stored at 4 °C till use or at -20 °C for long-term storage.

3.6.2 DNA isolation from whole blood

If possible, 1 ml of whole blood was collected from each patient sample (see 3.3.1) and DNA was isolated using the FlexiGene DNA Kit. The manufacturer's protocol for the respective volume of blood was followed and DNA was eluted in 200 µl elution buffer. Concentration of the eluted DNA was measured and samples were transferred to long-term storage at -20 °C.
For some samples, DNA was extracted from isolated PBMCs following the provided protocol of the DNeasy Blood & Tissue Kit. DNA was eluted in 50 µl elution buffer and the concentration was measured. Samples were stored -20 °C.

3.6.3 DNA isolation from cells and extracellular vesicles

Isolated cell culture and plasma-derived EVs (see 3.5.1, 3.5.2) were resuspended in 200 µl PBS and exosomal DNA was isolated using the QIAamp DNA Kit according to the manufacturer's protocol. DNA elution was conducted twice with the same 50 µl nuclease-free water and DNA concentration was determined by a spectrophotometer.
In addition, cell lines (Table 12) that were used for EV production and isolation were harvested for DNA extraction. Briefly, cells were washed once using PBS and harvested using a cell scraper and 1–2 ml cold PBS per flask. Detached cells were transferred to a falcon tube and centrifuged at 280 x g for 5 min at 4 °C. The resulting cell pellet was resuspended in 200 µl PBS and DNA was isolated using the QIAamp DNA Kit as described above.

3.6.4 Sanger sequencing

The presence of point or small deletion mutations was assessed by Sanger sequencing. After isolation of the respective DNA from tumor tissue (see 3.6.1) and EVs (see 3.6.3), the DNA region of interest was amplified by PCR. PCR was performed in a total volume of 25 µl and the respective reactions were set up with 3 µl DNA and 22 µl master mix (Table 16). A negative control, containing DNase-/RNase-free water, was added to each run to rule out DNA contamination. The annealing temperature (Table 16) was adjusted according to the respective primer pair (Table 10).

Table 16: Composition of the PCR reaction (left) and the respective PCR conditions (right) for Sanger sequencing. Final concentrations of reagents are provided in the square brackets.

PCR mixture		PCR program		
Template DNA [150 ng]	3 µl	94 °C	5 min	
DNase-/RNase-free water	13.55 µl	94 °C	30 sec	
dNTPs [0.2 mM]	4 µl	T_m °C*	30 sec	40 x
PCR buffer [1 x]	2.5 µl	72 °C	1 min	
$MgCl_2$ [1.5 mM]	0.75 µl	72 °C	6 min	
Primer reverse [0.3 µM]	0.5 µl	4 °C	hold	
Primer forward [0.3 µM]	0.5 µl			
Taq polymerase [0.04 U/µl]	0.2 µl			
		*T_m value of the primer		

Successful PCR amplification of the region of interest was confirmed by agarose gel electrophoresis. Briefly, a 2 % (w/v) agarose gel was prepared by heating agarose in 1 x TBE buffer using a microwave (800 W). Once the agarose was completely dissolved, it was allowed to cool down to 60 °C before 4 µl of Midori Green DNA stain were added per 100 ml. The solution was poured into a gel chamber and could be used after around 30 min of polymerization. Next, the gel was placed into an electrophoresis chamber filled with 1x TBE buffer. 5 µl of the PCR product were mixed with 1 µl of DNA sample buffer and loaded into the gel pockets. 5 µl of DNA ladder were loaded for determination of the fragment size. Electrophoresis was conducted at a constant voltage of 120 V for 45 min and DNA bands were visualized with UV light. If an amplicon at the right size was present and no contamination was detected in the negative control, PCR products were processed further.

A silica membrane-based purification kit (QIAquick PCR Purification) was used to remove primers, nucleotides and other reagents from PCR products. Samples were loaded onto QIAquick columns and the manufacturer's protocol was followed. DNA was eluted in 30 µl DNase-/RNase-free water.

Sequencing reactions with a total volume of 15 µl were set up with the BigDye Terminator v2.2 Cycle Sequencing Kit, the respective sequencing primer and the purified PCR products (Table 17). Cycle sequencing was performed in a thermal cycler (Table 17).

Table 17: Sanger sequencing reaction setup (left) and cycler program (right). Final concentrations of reagents are provided in the square brackets.

PCR mixture		PCR program		
Purified PCR product	6 µl	96 °C	10 sec	
BigDye Terminator ready reaction mix	6 µl	60 °C	10 sec	36 x
Sequencing primer [2 µM]	3 µl	60 °C	4 min	

The sequencing reactions were purified using ethanol precipitation. 85 µl DNase-/RNase-free water were added to 15 µl sequencing sample resulting in a total volume of 100 µl. Following, 250 µl 100 % ethanol and 10 µl 3 M sodium acetate were added to the sample and the solution was inverted 30 x. After centrifugation at 18,000 x g for 16 min at 4 °C, the supernatant was carefully removed and 250 µl 75 % ethanol were added without resuspending or inverting. Samples were centrifuged a second time at 18,000 x g for 6 min at 4 °C and the supernatant was discarded. The remaining liquid was removed by using a vacuum concentrator at medium drying rate for 10 min. Lastly, 12 µl HiDi™ formamide were added to the dried pellet and incubated for 30 min at room temperature. Samples were transferred into a 96-well reaction plate and capillary electrophoresis was performed on the ABI3130xl genetic analyzer. Obtained sequencing data were processed using the Sequencing Analysis software (version: 6.0).

The described protocol was also applied for determining the HLA-A*02 status of individuals. For that purpose, whole blood DNA (see 3.6.2) was used and a region spanning the 5' end of exon 2 and an upstream intronic region of the HLA-A locus was amplified. Sanger sequencing enabled the distinction between HLA-A*02 and non-HLA-A*02 via the nucleotide at position 78 of the HLA-A gene locus, a T indicating HLA-A*02 alleles [79, 310]. The described identification of HLA-A*02 alleles was validated by an NGS-approach with high sensitivity and specificity [311].

3.6.5 PCR-based fragment analysis

3.6.5.1 MSI analysis

The MSI status of tumors and EVs was determined by analyzing four standard, non-coding MSI markers (BAT25, BAT26, CAT25 and BAT40) (Table 10). Three markers, BAT25, BAT26 and CAT25, could be amplified simultaneously in a multiplex PCR reaction (Table 18). A separate reaction was setup for BAT40 (Table 19). All reactions were conducted in a total volume of 25 µl and with inclusion of a negative water control.

Table 18: Multiplex PCR setup (left) and applied PCR conditions (right). Final concentrations of reagents are provided in the square brackets.

Multiplex PCR mixture		**PCR program**		
Template DNA [1–2 ng]	3 µl	94 °C	5 min	
DNase-/RNase-free water	1.75 µl	94 °C	30 sec	
dNTPs [0.25 mM]	0.25 µl	55 °C	30 sec	38x
PCR buffer [1 x]	1 µl	72 °C	1 min	
$MgCl_2$ [1.5 mM]	0.3 µl	72 °C	5 min	
BAT25/BAT26/CAT25 primer reverse [0.3 µM]	each 0.6 µl	4 °C	hold	
BAT25/BAT26/CAT25 primer forward [0.3 µM]	each 0.6 µl			
Platinum Taq polymerase [0.2 U/µl]	0.1 µl			

Table 19: BAT40 PCR mixture (left) and applied cycler program (right). Final concentrations of reagents are provided in the square brackets.

PCR mixture		**PCR program**		
Template DNA [1–2 ng]	3 µl	94 °C	5 min	
DNase-/RNase-free water	3.35 µl	94 °C	30 sec	
dNTPs [0.25 mM]	0.25 µl	55 °C	30 sec	38 x
PCR buffer [1 x]	1 µl	72 °C	1 min	
$MgCl_2$ [1.5 mM]	0.3 µl	72 °C	5 min	
BAT40 primer reverse [0.5 µM]	1 µl	4 °C	hold	
BAT40 primer forward [0.5 µM]	1 µl			
Platinum Taq polymerase [0.2 U/µl]	0.2 µl			

Following, 1 µl of amplified PCR product was added to 12 µl HiDi™ formamide supplemented with a ROX size standard and analyzed on the ABI3130xl genetic analyzer. The GeneMarker software (version: 1.5) was applied for data analysis. Instability of all markers was always assessed using matched normal tissue or blood samples.

3.6.5.2 Analysis of cMS mutations

Frameshift mutations in selected cMS were also analyzed in tumor and exosomal DNA applying PCR-based fragment analysis. PCR was performed in a total volume of 5 µl (Table 20) and with the respective primer pairs (Table 10).

Table 20: PCR composition for cMS analysis (left) and respective PCR conditions (right). Final concentrations of reagents are provided in the square brackets.

PCR mixture		PCR program		
Template DNA [2 ng]	2 µl	94 °C	5 min	
DNase-/RNase-free water	0.25 µl	94 °C	30 sec	
dNTPs [0.20 mM]	0.8 µl	58 °C	45 sec	36 x
PCR buffer [1 x]	0.5 µl	72 °C	1 min	
$MgCl_2$ [1.5 mM]	0.15 µl	72 °C	7 min	
Primer reverse [0.3 µM]	0.6 µl	4 °C	hold	
Primer forward [0.3 µM]	0.6 µl			
Taq polymerase [0.1 U/µl]	0.1 µl			

Fragment analysis was conducted on the ABI3130xl genetic analyzer by adding 1 µl of the PCR product to 12 µl HiDi™ formamide supplemented with ROX. The obtained raw data were processed using the GeneMarker software (version: 1.5) and peak height profiles were extracted for further analysis. The frequency of mutations in analyzed cMS was quantified applying the R (version 3.4.3)-based ReFrame algorithm [79].

3.6.6 HLA typing

DNA was isolated as described in 3.6.2 and submitted to the Institute for Clinical Transfusion Medicine and Immunogenetics (Institut für Klinische Transfusionsmedizin und Immungenetik, IKT) in Ulm, Germany. The commissioned high resolution HLA typing was conducted for HLA-A, -B and -C covering exon 2 and 3 as well as for HLA-DRB1, -DQB1 and -DPB1 with a complete coverage of exon 2.

Identified HLA class I alleles were attributed to the respective HLA supertype according to the classification by Sidney et al. [312]. Allele frequency data from the general population were obtained from `http://allelefrequencies.net/` choosing the 'Germany pop 8' population [313]. All HLA class I alleles with a frequency of over 0.1 % were included in the analysis and supertypes were classified as described above.

The prediction of candidate epitopes, binding to the respective HLA molecules, was conducted for HLA-A, -B (class I) and -DR (class II). The NetMHCpan-4.1 prediction tool [309] was applied for HLA class I predictions covering 8–11mer peptides. As recommended, strong and weak binders were determined using the rank of the predicted binding score: strong binders (SB) were defined by having a %rank < 0.5 and weak binders (WB) a %rank < 2 [309]. The NetMHCIIpan-4.0 tool was used for predicting binding of peptides to HLA-DR molecules [314]. 13–25mer peptides were considered in the predictions and SB/WB were again defined using the %rank score: SB %rank < 1 and WB %rank < 5.

3.7 RNA techniques

3.7.1 RNA isolation from tissue

Tumor and normal colonic mucosa FFPE tissue sections were microdissected manually (see 3.2.4) and RNA was isolated from the obtained material. The automated Maxwell®16 research extraction system and the FFPE Plus LEV RNA Purification Kit were applied for RNA extraction adhering to the manufacturer's instructions. DNA digestion was conducted by using the TURBO DNA-free™ Kit and the concentration of DNA-free RNA was measured fluorimetrically with a Qubit fluorometer.

3.7.2 RNA isolation from cells

Total RNA from expanded and restimulated PBMCs (see 3.3.2, 3.3.3) was extracted using the RNeasy Mini Kit with several additions to the manufacturer's protocol. Briefly, the frozen cell pellet was thawed in 350 µl lysis buffer supplemented with β-Mercaptoethanol. Samples were vortexed intensively for around 30 sec before they were put through a 20 gauge needle in order to ensure proper cell lysis. Next, 350 µl cold 70 % ethanol were added, samples were resuspended properly and transferred to the provided spin column. Further steps were conducted in line with the manufacturer's recommendations. However, due to the often small amount of RNA, no on-column DNase treatment was performed. RNA was eluted from the column using 30 µl of DNase-/RNase-free water and the concentration was measured photospectrometically. Isolated RNA was stored at -80 °C until use.

3.7.3 Gene expression analysis

3.7.3.1 IFNγ reverse transcription-quantitative PCR

The FSP-specific activation of T cells was analyzed on the gene expression level by applying IFNγ RT-qPCR [315, 316]. 200 ng of isolated RNA (see 3.7.2) was used for cDNA synthesis in preparation for RT-qPCR. RNA was diluted with DNase-/RNase-free water resulting in 200 ng RNA in a total volume of 16 µl. Samples were treated with DNase I at a final concentration of 1 U/µl and incubated 15 min at room temperature. Subsequently, 2 µl of 25 mM EDTA were added to inactivate DNase I and avoid hydrolysis of RNA. After samples were incubated at 65 °C and 70 °C for 10 min each to further ensure DNase I inactivation, RNA was ready to be used in reverse transcription.
The SuperScript™ II Kit was applied for cDNA synthesis and 100 ng of DNase-treated RNA were reverse transcribed. Each reactions was performed in a total volume of 21 µl (Table 21). DNase-/RNase-free water was used as negative control, which was included in every run. In the establishing phase, one sample was processed without reverse transcriptase in order to assess DNA contamination and its impact. Lastly, samples were incubated in a thermal cycler (Table 21) and subsequently could be used for RT-qPCR.

Table 21: Setup of a cDNA synthesis reaction with first-strand reverse transcriptase (left) and thermocycling conditions (right). Final concentrations of reagents are provided in the square brackets.

reverse transcription		**program**	
cDNA [100 ng]	11 µl	37 °C	15 min
DNase-/RNase-free water	1.5 µl	42 °C	1 h
dNTPs [0.5 mM]	1 µl	90 °C	5 min
First-Strand buffer [1 x]	4 µl	4 °C	hold
Dithiothreitol (DTT) [10 mM]	2 µl		
Oligo(dT) 12–18 primer [0.01 µg/µl]	0.5 µl		
Random hexamer primer [0.01 µg/µl]	0.5 µl		
Reverse transcriptase [4.8 U/µl]	0.5 µl		

RT-qPCR reactions were set up in a total volume of 10 µl (Table 22) and, if possible, three technical replicates were added to a 96-well PCR plate.

Table 22: Composition of a RT-qPCR reaction (left) and the used PCR program (right). Final concentrations of reagents are provided in the square brackets.

RT-qPCR		program		
cDNA	1 µl	95 °C	5 min	
SYBR Green	5 µl	95 °C	30 sec	
β-actin/IFNγ primer reverse [0.5 µM]	each 0.5 µl	56 °C	1.5 min	50 x
β-actin/IFNγ primer forward [0.5 µM]	each 0.5 µl	72 °C	30 sec	
DNase-/RNase-free water	3 µl			

In addition to IFNγ, the expression of β-actin, as a stable reference gene, was assessed and used for normalization. PCR was performed in the StepOnePlus Real-Time PCR system with the established program (Table 22) and a melting curve analysis was performed to ensure the specificity of amplification. The generated data were analyzed using the StepOnePlus software and relative quantification of IFNγ expression was determined by applying the $\Delta\Delta$Ct method [317]. Overall, IFNγ expression between groups was compared using the -ΔC_t (-dC_t) value after normalization with β-actin.

3.7.3.2 NanoString nCounter®analysis

Gene expression analysis of tumor and normal mucosa tissue samples (see 3.7.1) using the NanoString nCounter®platform (PanCancer Human IO 360™ Panel) was performed by Dr. Martina Kirchner, Prof. Dr. Jan Budczies and Klaus Kluck at the Institute of Pathology, Heidelberg. The applied panel comprised 770 immune-relevant genes covering tumor microenvironment, tumor-immune cell interactions and immune evasion.

The obtained expression data first underwent background subtraction and subsequent sample normalization using 20 selected genes: *RELA*, *DNAJC14*, *AKT1*, *EIF2B4*, *PUM1*, *SF3A1*, *MAP3K7*, *GOT2*, *HDAC3*, *API5*, *OAZ1*, *TLK2*, *ALDOA*, *GLUD1*, *RBL2*, *CTNNB1*, *PSMC4*, *TWF1*, *TBP*, *TPI1* [318]. These housekeeping genes were chosen from the TCGA COAD-READ cohort based on a minimum expression level of 100 and the lowest coefficient of variation. Prior to statistical analysis, gene expression data were log2-transformed. The mRNA expression of marker genes was used to determine the abundance of 14 different immune cell populations (B cells, CD45-positive cells, CD56dim NK cells, CD8-positive T cells, cytotoxic cells, dendritic cells, exhausted CD8-positive T cells, macrophages, mast cells, neutrophils, NK cells, T cells, Th1 cells and regulatory T cells) [318, 319].

Non-scaled heatmaps were applied to display expression levels and the abundance of populations. Hierarchical clustering was conducted using Pearson correlations as similarity measure and the average linkage as measure of distances between clusters. Statistical testing for

changes between expression changes and immune population abundance was performed using the Kruskal-Wallis test as omnibus test and the Mann-Whitney test as post hoc test. Multiple hypothesis testing was corrected using the Benjamini-Hochberg method [320] with a 10 % false discovery rate (FDR). A potential correlation between principal components and different covariates was determined by applying a Wilcoxon test.

3.8 Protein techniques

3.8.1 Protein extraction

Proteins were extracted from cells and isolated EVs using RIPA buffer supplemented with a protease inhibitor cocktail. Cell samples were sonicated for 10 sec at 30 % power before being incubated on ice for 30 min. EV preparations did not undergo sonication due to the small sample volume and instead were only incubated on ice for at least 30 min. After incubation, samples were centrifuged at 17,000 x g for 15 min at 4 °C. The supernatant, containing proteins, was transferred to a new tube and stored at 4 °C for short-time use. Long-term, protein lysates were stored at -20 °C.

3.8.2 Determination of protein concentration

Protein content in the produced cellular and EV lysates was determined by applying a Bradford assay [321]. Depending on source and amount of starting material, protein samples were diluted 1:5 to 1:75 in DNase-/RNase-free water to avoid protein concentrations higher than the used standards. Bovine serum albumin (BSA) protein standards (0, 0.1, 0.25, 0.5 and 1 µg/µl) were prepared. 20 µl of each sample and standard were set up as duplicates and added individually to cuvettes. The Bradford solution was diluted 1:5 with water and 1 ml was added to each cuvette. After 5 min of incubation at room temperature, absorbance was measured at 595 nm using a photometer. The protein concentration was determined based on the produced standard curve.

3.8.3 Sodium dodecyl sulfate-polyacrylamide gel electrophoresis

Proteins were separated according to their size using sodium dodecyl sulfate-polyacrylamide gel electrophoresis (SDS-PAGE) [322]. 20–40 µg of protein lysates were filled up to a volume of 13 µl using water. 5 µl of 4 x lithiumdodecylsulfat (LDS) sample buffer and 2 µl 10 x reducing agent were added, resulting in a total volume of 20 µl. If higher volumes were used, the amount of LDS buffer and reducing agent were adjusted accordingly. Proteins were denatured by incubating the prepared samples at 95 °C for 5 min. Samples and 8 µl of a protein standard

were loaded onto 4–12 % Bis-Tris gels and run under reducing conditions with MES or MOPS buffer depending on the size of the protein of interest. MES buffer was applied for smaller proteins up to 50 kDa and MOPS buffer was used to separate higher molecular weight proteins. Around 600 ml of the respective SDS running buffer were added to the outer chamber of the electrophoresis system. 500 µl antioxidant were added to 200 ml running buffer and used for the inner chamber. The gel was run, following the manufacturer's instruction, at a constant voltage of 200 V for 40–50 min depending on the used running buffer.

3.8.4 Western blot

Proteins separated by SDS-PAGE (see 3.8.3) were transferred onto a PVDF membrane (pore size 0.45 µm) using a wet blotting system. The transfer buffer was prepared according to the manufacturer's instructions by adding methanol and antioxidant. The membrane was soaked in methanol for 1 min, washed in water for 5 min and placed in the transfer buffer until use. Additionally, two Whatman® filter papers were soaked in the prepared transfer buffer. The transfer sandwich was stacked as follows: anode (+), three blotting pads, filter paper, membrane, gel, filter paper, three blotting pads, cathode (-). The transfer was performed for 1 h at a constant voltage of 30 V.
Following, the membrane was briefly washed in TBS-T and then blocked in 5 % milk for 2 h at room temperature. The primary antibody (Table 5) was diluted in the blocking buffer and incubated with the membrane overnight at 4 °C. On the next day, the membrane was washed three times for 10 min each using TBS-T. Subsequently, the membrane was incubated with the suited HRP-labeled secondary antibody (Table 6), diluted in blocking buffer, for 1 h at room temperature. The membrane was washed again three times in TBS-T and proteins were visualized using enhanced chemiluminescence (ECL) and the ChemiDoc imaging system. The size of the detected proteins was determined with the pre-stained protein standard. After imaging, the membrane was washed again three times in TBS-T and either blocked again for incubation with another primary antibody or underwent Ponceau S staining. Briefly, all proteins were visualized by incubating the membrane for at least 30 min in Ponceau S solution and protein bands could be visualized after several washing steps in water.

3.8.5 Immunoprecipitation

In order to enrich A33-expressing, colon-derived EVs, IP was performed applying two different approaches. Both strategies were established by using cell culture-derived EVs.

3.8.5.1 Protein G

Dynabeads™ Protein G magnetic beads were prepared by thoroughly resuspending them for 15 min on a tube roller. 50 µl of resuspended beads were transferred to a new tube and washed twice with 250 µl citrate-phosphate buffer. Next, beads were resuspended in 250 µl citrate-phosphate buffer and 30 µg of mouse anti-A33 antibody were added. This was followed by 40 min incubation at room temperature on a rotator. The antibody-bound beads were then washed two times with 250 µl citrate-phosphate buffer and two times with 250 µl crosslinking buffer containing triethanolamine. The anti-A33 antibody was chemically crosslinked to the protein G beads by using dimethyl pimelimidate (DMP) which reacts with primary amines. Importantly, DMP is unstable in aqueous solution and was always freshly prepared immediately prior to use. 200 µl of DMP solution were added to the prepared beads and incubated for 30 min at room temperature on a rotator. Subsequently, beads were resuspended in 50 mM TRIS and incubated 15 min at room temperature on a rotator. After washing the crosslinked beads three times in 250 µl PBS with 0.05 % Tween 20, they were incubated with isolated EVs at 4 °C overnight on a rotator.

On the next day, beads were washed three times with 250 µl PBS and once with 250 µl water. Captured EVs were eluted using 15 µl 2 x LDS sample buffer (4 x buffer diluted 1:2 in H_2O). Doing so, beads were incubated in LDS for 10 min at room temperature and 450 rpm to ensure proper elution. After adding 1.5 µl reducing agent and 3.5 µl water, samples were used for SDS-PAGE and western blot (Wb) (see 3.8.3, 3.8.4).

3.8.5.2 Streptavidin/biotin

In order to use streptavidin-coated magnetic Dynabeads™, the anti-A33 antibody was biotinylated with the EZ-Link™ Sulfo-NHS-Biotin Kit. N-hydroxysulfosuccinimid (NHS) is a commonly used biotinylation reagent and reacts with primary amino groups on antibodies. The provided biotin reagent was dissolved in 224 µl water immediately before use, resulting in a 10 mM biotin solution which was added in a 20-fold molar excess to the anti-A33 antibody. The reaction was performed for 2 h on ice and the produced biotinylated antibody was stored at -20 °C. Successful antibody biotinylation was checked using ELISA and different concentrations of the biotinylated antibody (0, 0.01, 0.05, 0.1 µg/ml). 100 µl of each antibody dilution were incubated in a MaxiSorp™ ELISA plate overnight at 4 °C. After incubation, the anti-

body solution was removed and wells were washed three times with 200 µl PBS with 0.05 % Tween 20. Next, blocking was performed with 200 µl PBS supplemented with 0.1 % biotin-free BSA for 1 h at room temperature. 50 µl ExtrAvidin®-peroxidase, diluted 1:2,000 in PBS with 0.1 % biotin-free BSA, were added for 1 h at room temperature. The plate was washed again three times with 200 µl PBS with 0.05 % Tween 20 and peroxidase detection was performed by adding 50 µl 3,3´,5,5´-tetramethylbenzidine (TMB) substrate solution per well. Once the reaction turned blue, 50 µl 2 M HCl were added and the absorbance of the yellow product was measured at 450 nm.

Following, the biotinylated antibody was used for IP. First, streptavidin-coated magnetic Dynabeads™ were resuspended for around 15 min on a tube roller and washed two times with PBS. In parallel, non-reacted biotin and reaction byproducts were removed from the antibody solution by size exclusion using centrifugal filter units. Briefly, 30 µg of the biotinylated anti-A33 antibody were filled up to a total volume of 500 µl using PBS, transferred onto a centrifugal filter unit and centrifuged at 17,000 x g for 3 min. The flow-though was discarded and around 400 µl PBS were added to the filter unit to obtain a total volume of 500 µl. The tube was centrifuged again at 17,000 x g for 3 min and the step was repeated four times to ensure complete removal of excess biotin. The remaining antibody was then transferred to a new tube, 300 µl of washed streptavidin-coated magnetic Dynabeads™ were added and the mixture was incubated for 1 h on a rotator at room temperature. Following, the antibody-coupled beads were washed five times with PBS containing 0.1 % biotin-free BSA. The beads were resuspended in the prepared EV sample and incubated overnight at 4 °C on a rotator.

On the next day, beads were washed five times using 200 µl PBS. After washing the beads one final time in water, beads were resuspended in 12 µl 2 x LDS sample buffer and incubated at room temperature for 15 min on a shaker (450 rpm) to elute the captured EVs. Lastly and after adding 2 µl reducing agent and 6 µl water, elutes were used for SDS-PAGE and western blot (see 3.8.3, 3.8.4).

3.8.6 Indirect ELISA

The presence of A33-positive, colon-specific vesicles in EV preparations, obtained from cell culture supernatant and plasma, was assessed by an indirect ELISA. EVs were isolated as described previously (see 3.5.1, 3.5.2), resuspended in PBS and captured overnight at 4 °C on a 96-well MaxiSorp™ plate. Next, the EV solution was removed and each well was washed five times using 200 µl ELISA wash buffer containing 0.05 % Tween 20. Following, 100 µl anti-A33 antibody, diluted in PBS with 0.5 % BSA and in a concentration of 4 µg/ml, were added to each well. The subsequent antibody incubation was performed for 2 h at room temperature. After five wash steps, 100 µl/well of anti-IgG HRP-coupled secondary antibody, diluted 1:5,000 in

PBS with 0.5 % BSA, were applied for 1 h at room temperature. Lastly, 50 µl of TMB chromogenic substrate were applied to each well and 50 µl of 2 M HCl were added once the reaction turned blue. The absorbance of the resulting yellow product was measured at a wavelength of 450 nm using a spectrophotometer.

3.9 Peptide microarray

Plasma and serum samples were submitted to PEPperPRINT in Heidelberg, Germany. A neoepitope screening was conducted by assessing the humoral immune responses against 41 selected FSPs (Table 8) using a peptide microarray. All FSPs with more than 15 amino acids were translated into overlapping peptides. The resulting screening library, consisting of 124 peptides, was applied in duplicates. Briefly, plasma/serum samples were diluted 1:100 and incubated 16 h at 4°C on the generated PEPperCHIP®peptide microarray. Influenza virus hemagglutinin epitopes and polio peptides served as positive controls. The detection of IgA and IgG antibody responses was performed with anti-human IgG DyLight 680 and anti-human IgA DyLight 800 antibodies.
The obtained results, containing the background-corrected median fluorescence intensities for the different peptides and samples, were further processed for subsequent statistical analysis. Notably, all peptides displaying a fluorescence signal under 100 fluorescence units were removed. A non-parametric analysis was performed using the untransformed data, applying a Kruskal-Wallis test and a Dunn's multiple comparison post hoc test. The obtained data also underwent variance stabilizing normalization and the analyzed groups were compared applying ANOVA, controlling for multiple testing using a 10 % FDR. The peptide microarray as well as the statistical analysis was conducted by PEPperPRINT.

3.10 Statistical analysis

Statistical analysis was, if not stated otherwise, performed in GraphPad Prism (version 6.07) and R (version 3.6.1). All figures, if not stated otherwise, were produced using GraphPad Prism (version 6.07).

Statistical comparison of two groups was generally performed applying a Mann-Whitney test ($\alpha = 0.05$). Multiple groups were compared using a Kruskal-Wallis test and a Dunn's multiple comparison post hoc test ($\alpha = 0.05$). Testing the significance of a correlation between two continuous variables was performed with the Spearman's rank correlation ($\alpha = 0.05$). Statistical analysis of the NanoString-based gene expression data is described in 3.7.3.2. The analysis of the peptide microarray data was performed by PEPperPRINT and is described in 3.9.

Evaluation of data from the systematic literature search included the calculation of the 95 % confidence interval of the proportion of *B2M* mutations with the modified Wald method. The significance of the association between *B2M* mutation status and origin of MSI CRCs was tested using a Fisher's exact test ($\alpha = 0.05$). Odds ratios and the respective 95 % confidence intervals for the *B2M* mutation frequency in hereditary and sporadic MSI tumors were calculated and illustrated using the R Studio packages 'epitools' [323] and 'ggplot2' [324].

Age normalization of T cell counts was performed as follows: the expected count for the respective age was calculated based on linear regression and the obtained expected count was subtracted from the observed T cell number.

Statistical significance is indicated as follows: * $p < 0.05$; ** $p < 0.01$; *** $p < 0.001$; **** $p < 0.0001$; ns, non-significant.

4 Results

4.1 Characterization of local immune responses in LS carriers and MSI cancer patients

4.1.1 Systematic literature analysis of the immune phenotype of hereditary and sporadic MSI tumors

A pronounced immunogenicity is characteristic for MSI tumors and is typically accompanied by strong immune infiltration and frequent immune evasion events. However, the impact of the tumor's origin, hereditary (LS-associated) or sporadic, on local immune responses in MSI tumors has been insufficiently studied. For an overview of the current state of research, a systematic search of available literature was conducted to identify studies on immune infiltration and immune evasion in MSI tumors, distinguishing between hereditary and sporadic cases [304].

The systematic search in the MEDLINE database with defined search terms yielded 522 articles in total [304]. All publications were screened manually following the PRISMA guidelines (Figure 10) [305, 306].

The majority of articles were excluded based on the title (n = 364). The inter-rater reliability on the title level was determined to be adequate (Cohen's $\kappa = 0.7$). The abstracts of the remaining articles were assessed (n = 158) and 88 records were excluded. Several articles (n = 4) were not available in English and therefore excluded based on language. The eligibility of the remaining publications (n = 66) was examined on a full-text basis and 49 articles were found to be not suited for further analysis. The main exclusion criterion was the lacking distinction between hereditary and sporadic MSI tumors. Ultimately, 17 articles fulfilled the defined inclusion criteria and were analyzed qualitatively as well as quantitatively whenever possible. The identified articles mainly addressed immune infiltration and immune evasion in MSI CRCs, while ECs and premalignant lesions were analyzed to a lesser extent [304].

Notably, the analyzed studies were found to contain heterogeneous definitions of LS. While several studies only included proven pathogenic MMR gene variant carriers, others relied on IHC or fragment analysis and additional *MLH1* methylation as well as *BRAF* mutation analyses to identify 'suspected LS' individuals. As the expected percentage of wrongly classified specimens based on the existing literature is low, the respective studies were included in the systematic literature review [304].

4.1.1.1 Evidence for a more pronounced immune infiltration in hereditary MSI tumors

Eleven articles contained a quantitative analysis of the immune infiltration in MSI tumors (CRCs, ECs and premalignant lesions) applying IHC with various immune cell markers (CD3, CD4, CD8, PD-1) (Table S1). Importantly, all studies included a direct comparison between hereditary and sporadic MSI tumors [304]. Seven studies provided T cell counts in absolute numbers [113, 118, 209–211, 325, 326]. Notably, Takemoto et al. only reported exact T cell counts for stromal tumor areas and provided severity categories for intraepithelial TILs [210]. Four studies did not provide exact T cell counts but frequencies and defined immune infiltration categories [182, 327–329].

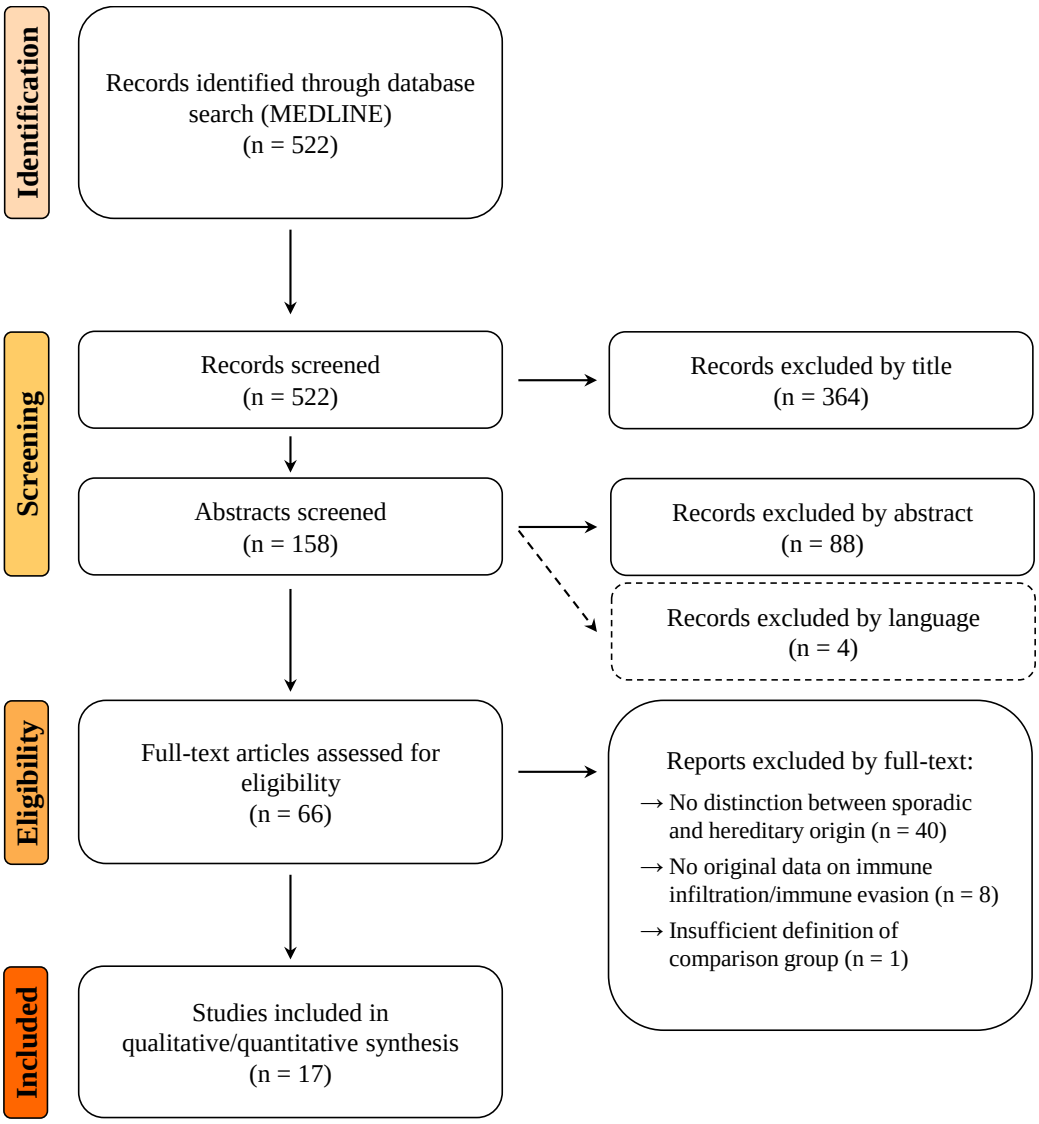

Figure 10: Flowchart illustrating the systematic literature search. The systematic search of the MEDLINE database was conducted adhering to the PRISMA guidelines [305, 306]. From 522 identified records, 17 were included in the final qualitative and quantitative analysis. Adapted from: [304].

Within the selected studies a total of 238 LS-associated and 250 sporadic MSI CRCs were analyzed. All studies reporting exact counts for intraepithelial T cells in MSI CRCs observed significantly higher numbers of CD3-positive pan T cells in LS-associated CRCs, compared to sporadic MSI CRCs [113, 209]. Moreover, Janikovits et al. found significantly more PD-1-positive T cells within LS-associated CRCs, compared to sporadic cases [113]. In line, the study by Young et al. reported higher numbers of T cells in hereditary CRCs, compared to sporadic MSI CRCs, using HE-stained sections [327]. A study by Jass et al., which was identified independently of the conducted search, observed a higher frequency of TILs and Crohn's-like reactions in LS-associated MSI CRCs [330]. However, studies not providing exact counts but using categorical data were not able to find statistically significant differences between hereditary and sporadic MSI CRCs [210, 328, 329]. Additionally, several publications comprised information on different T cell subpopulations (CD4- and CD8-positive T cells) and reported similar densities for both subsets in hereditary and sporadic MSI CRCs [118, 210, 211, 328].

Two studies, analyzing a total of 45 LS-associated and 71 sporadic cancers, focused on the local immune infiltration in MSI ECs and observed a trend towards a higher T cell density in LS-associated MSI ECs, compared to their sporadic counterparts [325, 326]. Pakish et al. found significantly elevated numbers of CD8-positive T cells in the stromal region of LS-associated MSI ECs, compared to sporadic cases. Similarly, LS ECs presented with more intraepithelial cytotoxic T cells without reaching statistical significance [325]. Ramchander et al. observed higher numbers of CD8-positive T cells in the tumor center of LS ECs, compared to sporadic tumors, not reaching statistical significance. However, significantly more CD8-positive T cells were found in the invasive margin of LS-associated ECs, compared to sporadic ECs [326].

In addition to the assessment of TILs, several identified studies comprised information on indirect markers of the tumoral immune status [304]. Pfuderer et al. examined the density of peritumoral high endothelial venules (HEV), which are specialized postcapillary venules crucial for lymphocyte trafficking and recruiting. A significantly higher HEV density was observed in the tissue adjacent to LS-associated CRCs, compared to sporadic MSI CRCs [331]. Moreover, the expression of PD-L1, a marker of prolonged immune activation, was examined in two of the selected studies and no significant difference between hereditary and sporadic MSI CRCs was detected [332, 333].

As opposed to multiple studies evaluating immunological characteristics of hereditary and sporadic MSI cancers, only very few articles focusing on precancerous lesions of hereditary and sporadic origin have been published so far. Two articles, which were identified through the systematic search, contained data on the immune infiltration in colorectal premalignant lesions and T cell densities were quantified in 91 LS-associated and 88 sporadic adenomas [304].

Koornstra et al., without specifying the lesions' MSI status, reported significantly higher numbers of CD8-positive T cells in LS-associated adenomas, compared to sporadic lesions [211]. Consistently, Meijer et al. observed higher lymphocyte densities (without providing absolute counts) in hereditary MMR-deficient adenomas, compared to sporadic adenomas. However, the MMR status of the sporadic colorectal adenomas was not provided [182].

In general, the qualitative analysis of the obtained immune infiltration data points towards more pronounced local immune responses in hereditary MSI CRCs and ECs, compared to sporadic counterparts (Figure 11) [304]. Moreover, hereditary MSI CRCs displayed higher HEV densities and hence enhanced lymphocyte recruitment, which would further reinforce local immune responses. Enhanced T cell infiltration associated with the hereditary origin was already observed in premalignant lesions and LS-associated colorectal adenomas presented with an increased number of infiltrating lymphocytes, compared to sporadic lesions [304].

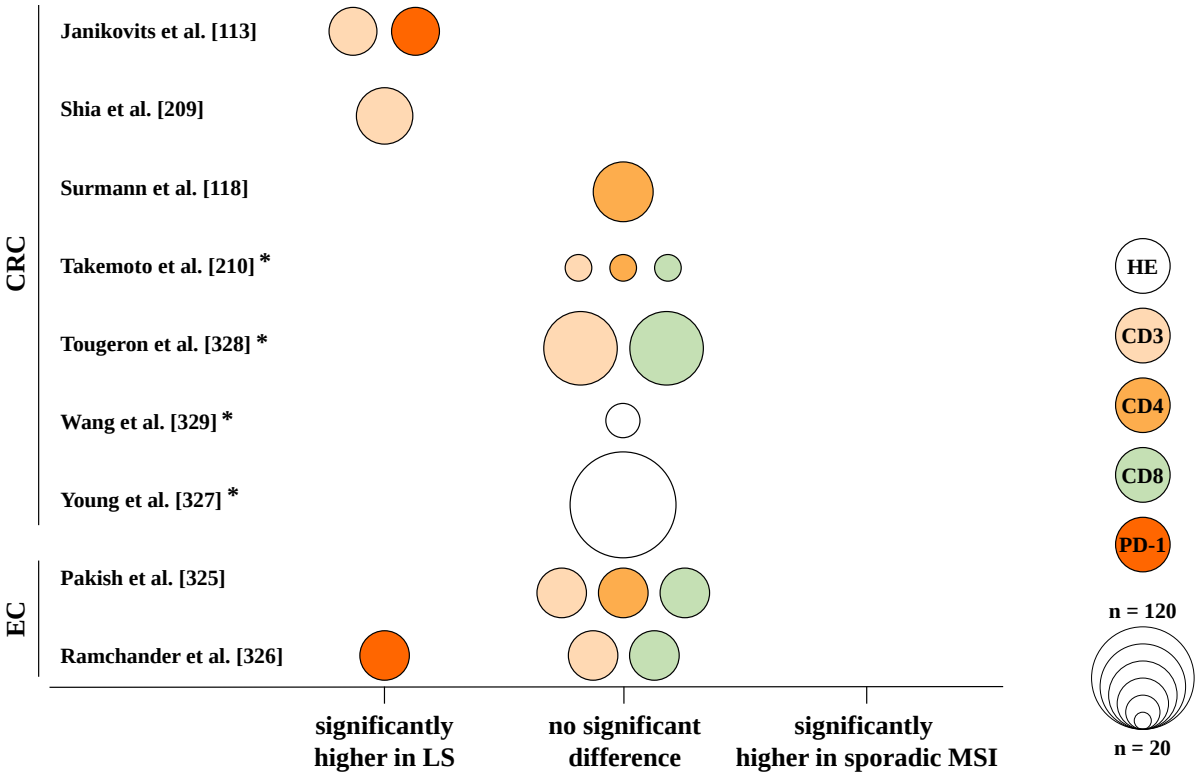

Figure 11: Graphical overview of the acquired data on immune infiltration in hereditary and sporadic MSI cancers. The identified articles on immune infiltration in MSI CRCs and ECs were divided into three groups: studies reporting significantly higher T cell numbers in LS-associated, compared to sporadic, MSI cancers ('significantly higher in LS'); studies finding no significant difference between the two groups ('no significance difference') and studies demonstrating significantly higher T cell counts in sporadic, compared to hereditary, MSI cancers ('significantly higher in sporadic MSI'). The cohort size is proportional to the depicted circle area. Asterisks indicate studies that did not provide exact T cell counts. Data on the immune infiltrate in stromal areas were not considered in this figure. Modified from: [304].

4.1.1.2 Higher frequency of immune evasion events in hereditary MSI tumors

The conducted literature search identified five studies analyzing immune evasion mechanisms affecting HLA class I and II-mediated antigen presentation in hereditary and sporadic MSI CRCs (Table S2) [111, 113, 118, 334, 335]. None of the studies provided data on immune evasion in MSI ECs [304].

The most common immune evasion mechanism reported for MSI CRCs is the abrogation of HLA class I antigen presentation by mutations in the *B2M* gene (see 1.2.3.2). *B2M* mutations were examined in four studies and in a total of 178 LS-associated and 166 sporadic MSI CRCs (Figure 12) [304]. The majority of selected studies (3/4) observed a higher rate of *B2M* mutations in hereditary MSI CRCs (ranging between 17–50 %), compared to sporadic MSI CRCs (3–29 %) [111, 113, 334]. However, one study reported the highest frequency of *B2M* mutations in sporadic, *MLH1*-methylated MSI CRCs and lower rates for LS-associated and suspected LS MSI CRCs [335].

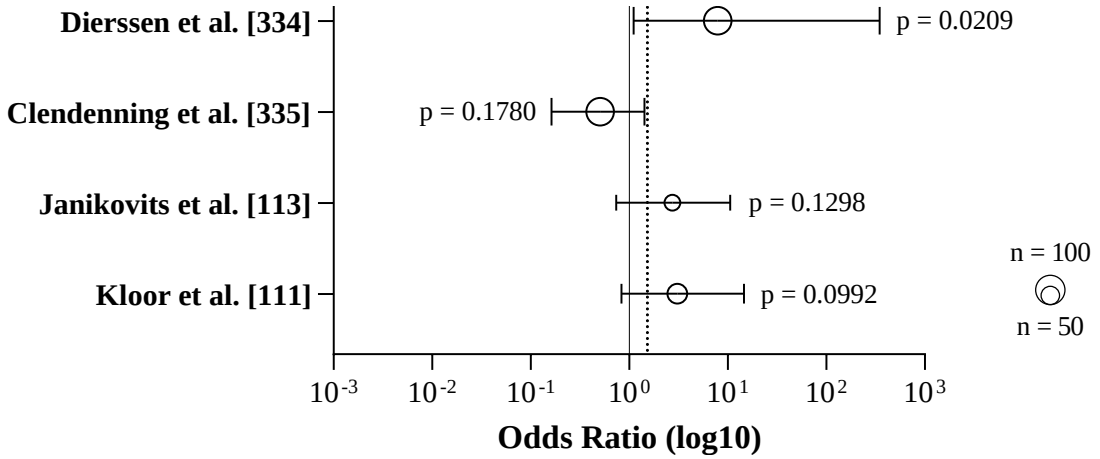

Figure 12: Forest plot summarizing the calculated odds ratios (OR) for the *B2M* mutation frequency in MSI CRC. OR (95 % CI) were calculated to assess the strength of the association between the origin of MSI CRC and the *B2M* mutation frequency. Data point size is proportional to the study size. The dashed vertical line indicates the calculated total OR. P-values for the Fisher's exact test are depicted for each study. Modified from: [304].

Two of the analyzed studies provided additional data on *B2M* mutations in colorectal premalignant lesions [111, 335]. In total, 80 MMR-deficient/MSI adenomas with an unclear LS status were analyzed within both studies. Even though the hereditary origin of the adenomas was not specified, MMR deficiency and the MSI phenotype in colorectal adenomas are commonly indicative of LS [336]. Kloor et al. observed a *B2M* mutation frequency of ca. 16 % in MSI adenomas [111]. In contrast, Clendenning et al. did not observe any *B2M* mutations in MMR-deficient colorectal premalignant lesions [335].

Only one study included in the systematic analysis provided data on HLA class II-mediated immune evasion mechanisms in MSI CRCs [118]. Surmann et al. examined the mutational pattern of two HLA class II regulatory genes (*CIITA* and *RFX5*) in 35 hereditary and 34 sporadic MSI CRCs. Without reaching statistical significance, *CIITA* mutations were observed more frequently in LS-associated MSI CRCs and sporadic cases more often displayed *RFX5* mutations [118].

In summary, the analysis of existing literature revealed a more pronounced local immune infiltration in hereditary MSI tumors, compared to their sporadic counterparts. This observation is possibly linked to the second finding of a higher frequency of acquired immune evasion mechanisms in LS-associated MSI CRCs. The observed differences indicate a distinct biology of hereditary and sporadic MSI tumors also reflected in their immune phenotypes, which may have clinical implications for therapy and prevention [304].

4.1.2 Profiling of local immune responses in LS individuals

The characteristic strong immune infiltration in MSI CRCs is well studied and known to be associated with an improved survival and patient outcome [133, 134]. As outlined above, several studies suggest immunological differences between LS-associated and sporadic MSI CRCs with a more active immune milieu in hereditary MSI CRCs (see 4.1.1) [304]. However, the conducted systematic literature search did not identify studies analyzing immune characteristics in the normal colorectal mucosa. Thus, an extensive characterization of the (tumor-distant) normal colonic mucosa, applying IHC and gene expression analysis, was conducted [318].

4.1.2.1 Increased immune infiltration in the normal colonic mucosa is associated with the MSI phenotype and LS

The infiltration with different T cell subpopulations was analyzed in the tumor-distant, normal mucosa of LS-associated MSI CRC, sporadic MSI CRC and MSS CRC patients. Further, T cell densities were quantified in biopsies of normal colonic mucosa from healthy LS carriers. IHC was conducted using three markers: CD3 (pan T cells), CD8 (cytotoxic T cells) and FOXP3 (regulatory T cells), and representative IHC stainings are shown in Figure 13 [318].

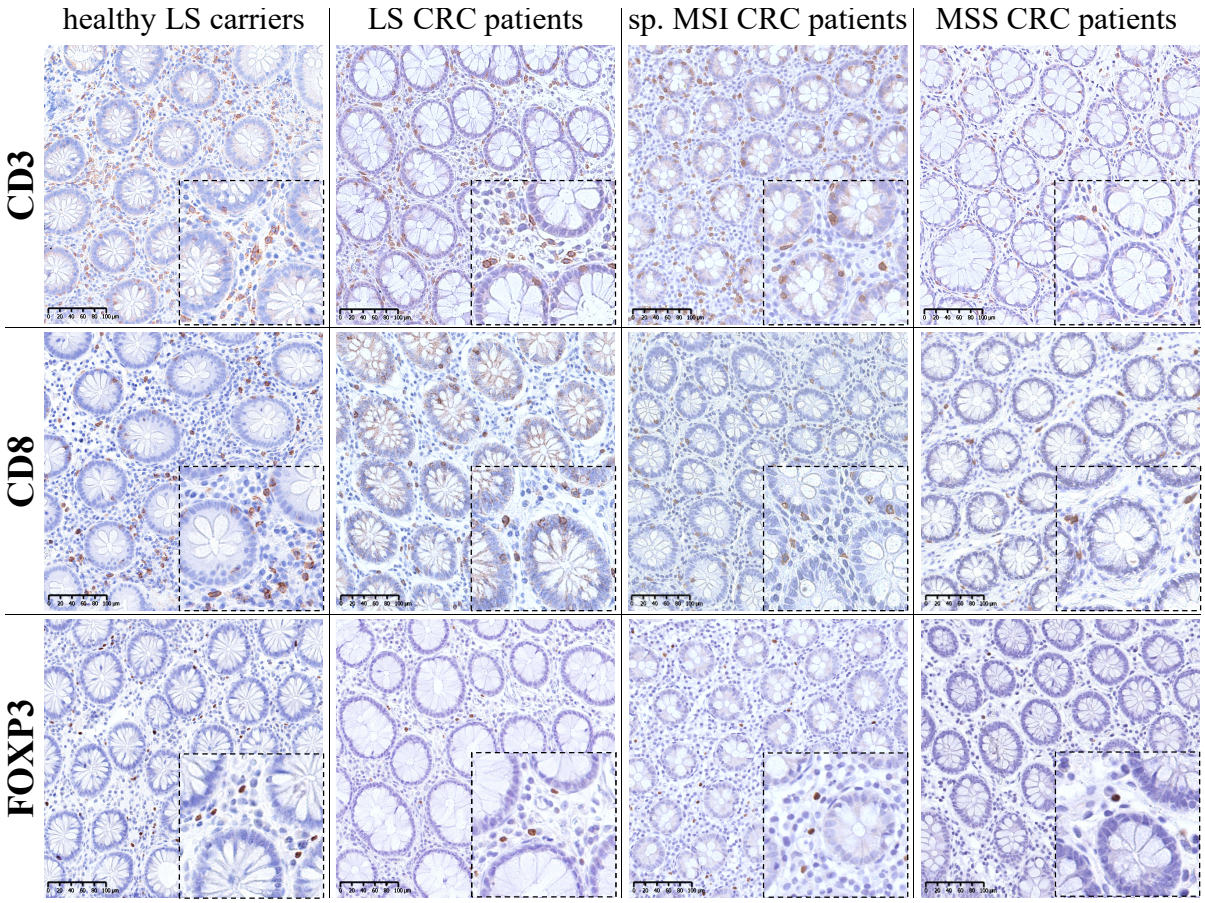

Figure 13: Representative IHC staining examples of normal colonic mucosa. CD3-, CD8- and FOXP3-positive T cells (20 x magnification) in the normal colonic mucosa from all four analyzed groups: healthy LS carriers, LS-associated CRC, sporadic (sp.) MSI CRC and MSS CRC patients. Modified from: [318].

CD3- and FOXP3-positive T cells were analyzed as previous studies suggested a functionally relevant role of these T cell types in LS colorectal immune surveillance [112, 113]. The prevalence of CD8-positive cells was assessed as they are characterized by their cytotoxic potential and consequently play a crucial role in CRC-associated immune responses [337].

If possible, all available tissue sections were analyzed using the three T cell markers (CD3, CD8, FOXP3). However, insufficient tissue and staining quality led to the exclusion of several samples during quality control, ensuring consistent and reliable quantification. Accordingly, the number of quantified samples varies for each marker. If more than one tissue block was available, all available blocks were used. For analysis T cell counts from all blocks were summarized as patient mean and the individual counts are shown in Figure S2, S3, S4, S5 [318].

Quantification of CD3-positive T cells was conducted in a total of 219 normal colonic mucosa sections from 124 individuals divided into to the four defined groups: healthy LS carriers (n = 43), LS-associated MSI CRC (n = 30), sporadic MSI CRC (n = 22) and MSS CRC (n = 29) patients [318]. The density of CD8-positive T cells was assessed in 201 normal mucosa samples coming from 120 individuals comprising: healthy LS carriers (n = 48), LS-associated MSI CRC (n = 28), sporadic MSI CRC (n = 23) and MSS CRC (n = 21) patients. FOXP3-positive T cells were quantified in 233 normal mucosa samples from 132 individuals of the same clinical groups: healthy LS carriers (n = 45), LS-associated MSI CRC (n = 32), sporadic MSI CRC (n = 26) and MSS CRC (n = 29) patients [318]. Clinical features of the analyzed patient cohort are summarized in Table S3.

The quantification of CD3-positive pan T cells revealed significantly higher numbers (median T cell density in 0.1 mm^2) in the tumor-distant, normal mucosa of MSI CRC patients (LS and sporadic), compared to the MSS patient group (LS/sporadic MSI CRC vs. MSS CRC: 60.38/64.88 vs. 37.75, p = 0.0050/0.0003) (Figure 14A). The normal mucosa of healthy LS carriers displayed the highest count of CD3-positive T cells, reaching statistical significance compared to the MSS CRC control group (healthy LS carriers vs. MSS CRC: 66.63 vs. 37.75, p < 0.0001) (Figure 14A) [318].

A similar pattern could be observed for FOXP3-positive regulatory T cells as the normal mucosa of MSI CRC patients, LS-associated as well as sporadic, presented with significantly higher counts compared to the MSS CRC group (LS/sporadic MSI CRC vs. MSS CRC: 5.50/4.13 vs. 2.63, p < 0.0001/p = 0.0222) (Figure 14C). The highest density of FOXP3-positive T cells was again observed in the normal mucosa of healthy LS carriers, being significantly higher compared to the MSS control group (healthy LS carriers vs. MSS CRC: 6.31 vs. 2.63, p < 0.0001) (Figure 14C) [318].

The cancer's MSI phenotype was not associated with a higher number of CD8-positive cytotoxic T cells in the tumor-distant, normal mucosa of CRC patients and no significant differences were detected between LS-associated MSI, sporadic MSI and MSS CRC patients (Figure 14B). However, the normal mucosa of healthy LS carriers presented with significantly higher CD8-positive T cell counts compared to all CRC patient groups (healthy LS carriers vs. LS/sporadic MSI/MSS CRC: 38.88 vs. 29/29/27.75, p = 0.0180/0.0041/0.0168) (Figure 14B) [318].

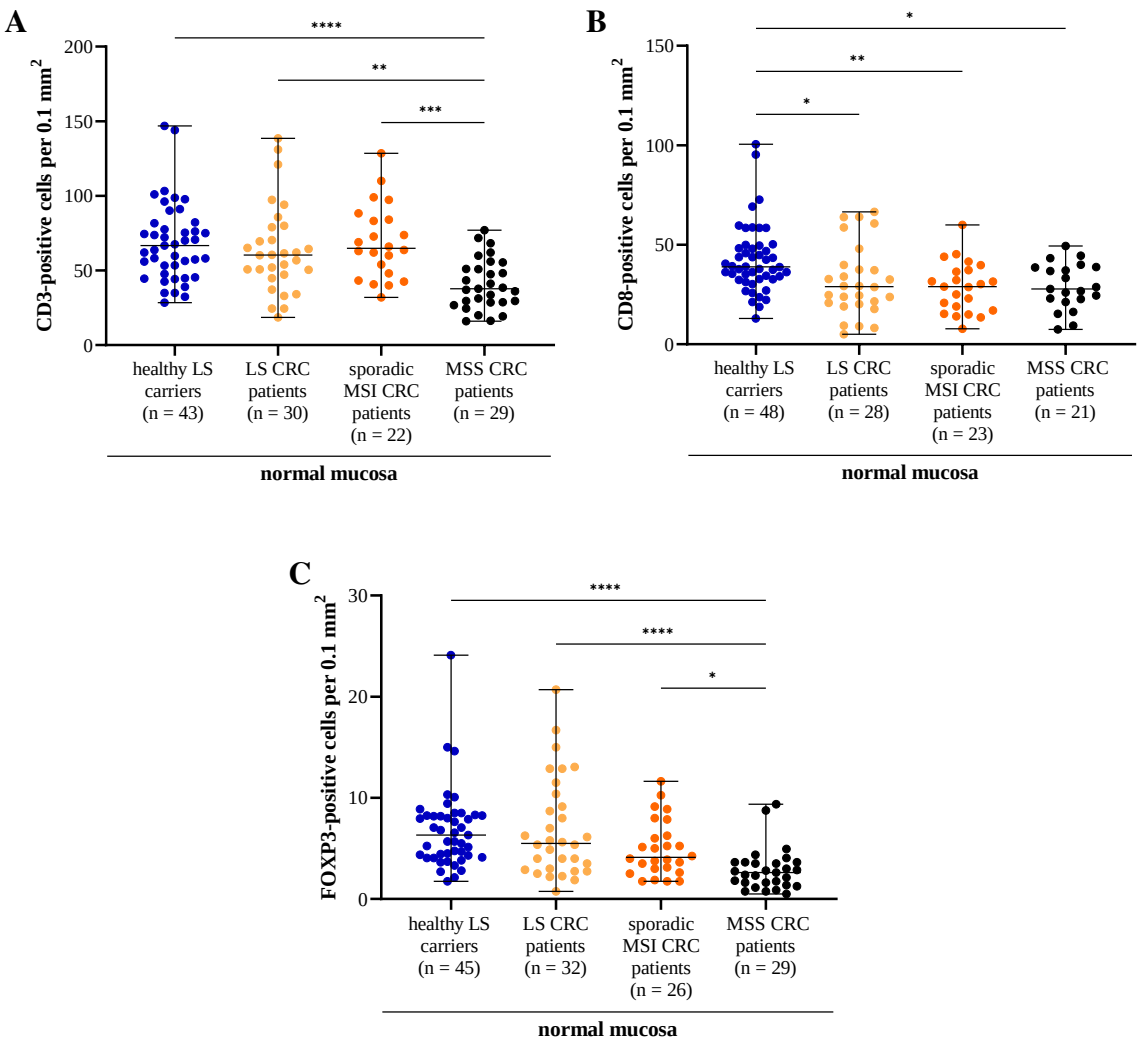

Figure 14: Quantification of T cell infiltration in the (tumor-distant) normal colonic mucosa. Density of CD3- (A), CD8- (B) and FOXP3-positive (C) T cells in the normal mucosa of CRC patients (LS, sporadic MSI and MSS) and healthy LS carriers. The highest counts for all three T cell markers were observed in the normal mucosa of healthy LS carriers. Increased densities of CD3- and FOXP3-positive T cells were associated with the MSI phenotype. Each data point represents the T cell count for one carrier/patient. The median T cell density in 0.1 mm^2 and data range are depicted. Asterisks (here and in the following) indicate statistical significance: * $p < 0.05$, ** $p < 0.01$, *** $p < 0.001$, **** $p < 0.0001$. Adapted from: [318].

T cell infiltration in the normal mucosa of healthy LS carriers and LS CRC patients was further analyzed considering the underlying MMR gene variant. The mucosal density of CD3-, CD8- and FOXP3-positive T cells was not found to be significantly different between healthy *MLH1*, *MSH2* and *MSH6* LS carriers (Figure 15A, 15B, 15C). Similarly, no significant differences were observed among *MLH1*, *MSH2* and *MSH6* LS CRC patients (Figure 15D, 15E, 15F) [318].

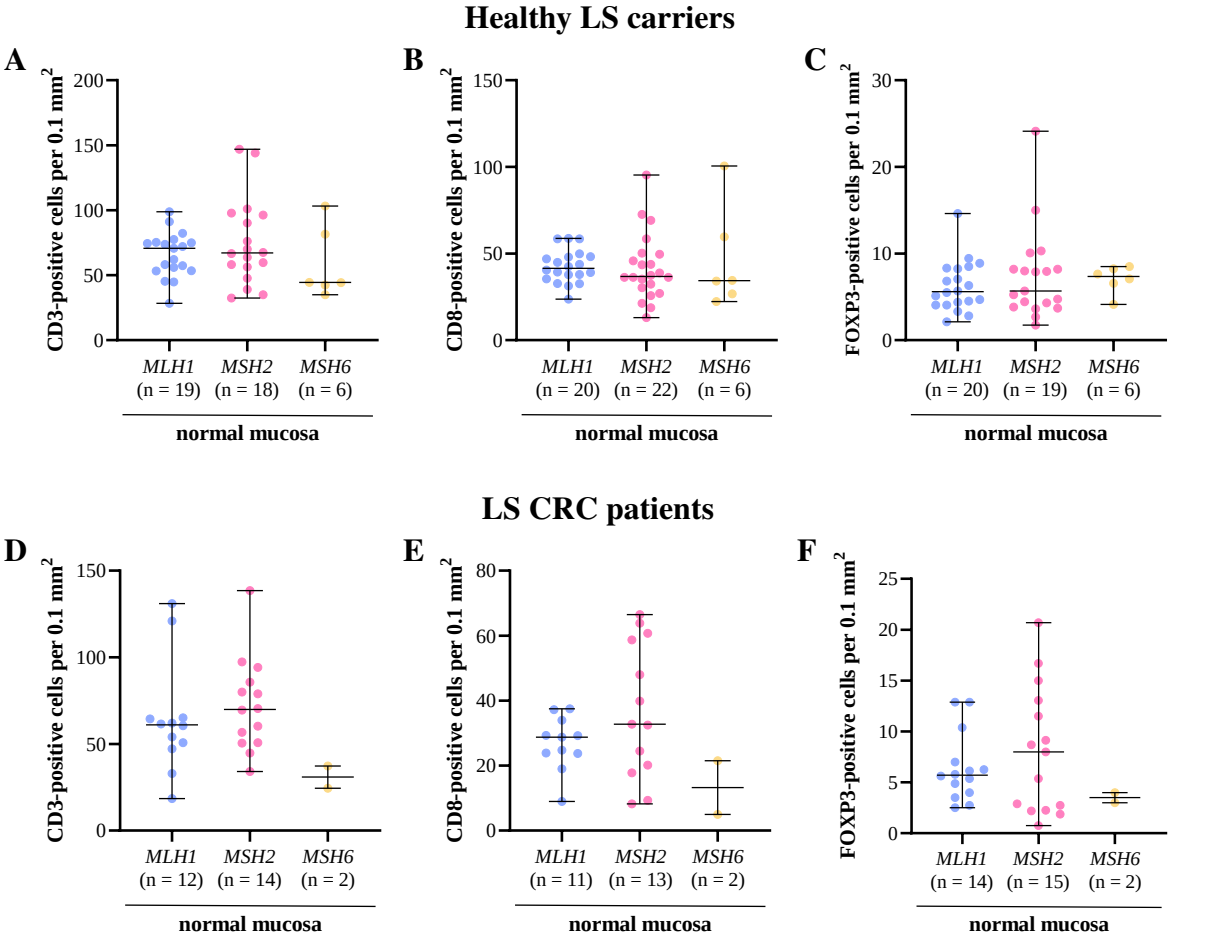

Figure 15: Stratification of T cell densities in the normal colonic mucosa according to the affected MMR gene. (A-C) Density of CD3-, CD8- and FOXP3-positive T cells in the normal colonic mucosa of healthy LS carriers stratified for the underlying MMR gene variant. No significant difference between the MMR genes could be detected (CD3: $p = 0.4534$, CD8: $p = 0.5909$, FOXP3: $p = 0.7011$). (D-F) Density of CD3-, CD8- and FOXP3-positive T cells in the tumor-distant, normal colonic mucosa of LS CRC patients stratified for the underlying MMR gene variant. No statistically significant difference between the analyzed groups was observed (CD3: $p = 0.0937$, CD8: $p = 0.142$ and FOXP3: $p = 0.6496$). Each data point depicts the T cell count for one individual. The median T cell density and its range are indicated. Adapted from: [318].

The age at sampling was not significantly correlated with the infiltration of CD3-, CD8- and FOXP3-positive T cells in the normal colonic mucosa of healthy LS carriers (Figure 16) [318].

Further, several healthy LS carriers within the analyzed cohort had a history of extracolonic cancer which was significantly associated with the individual's age ($p = 0.0280$) (Figure 17A). However, the age-normalized T cell densities in the normal mucosa were not found to be significantly different between LS carriers with and without previous extracolonic cancer (Figure 17B) [318].

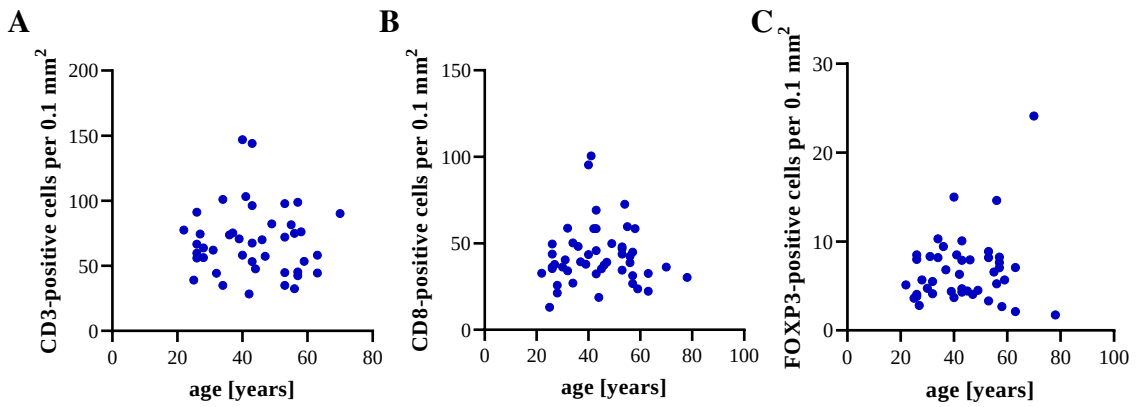

Figure 16: Correlation between T cell infiltration in the normal colonic mucosa of healthy LS carriers and the individuals' age. A non-significant correlation between the density of CD3- (A), CD8- (B) and FOXP3-positive (C) T cells and patients' age was detected (CD3: Spearman r = -0.0449, p = 0.7749; CD8: r = -0.0005, p = 0.9971; FOXP3: r = 0.0516, p = 0.7366). Each data point depicts the T cell count for one individual. Adapted from: [318]

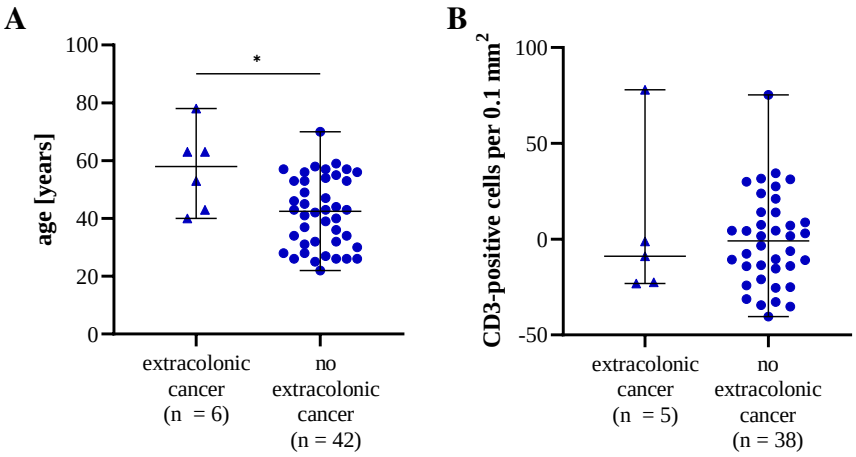

Figure 17: History of extracolonic cancer in healthy LS carriers. (A) Patients with a previous diagnosis of extracolonic cancer displayed a significantly higher age, compared to patients without a history of extracolonic cancer. Each data point indicates the age of one patient. (B) Age-normalized CD3-positive T cells counts for the normal mucosa of healthy LS carriers did not significantly differ between individuals with and without the history of extracolonic cancer (p = 0.8400). Each data point indicates the mean age-normalized T cell count per patient. Median T cell densities and data range are illustrated. Adapted from: [318]

Overall, the performed quantitative analysis of the mucosal immune infiltration in LS carriers and CRC patients demonstrated an elevated T cell density in healthy LS carriers prior to and potentially independent of tumor manifestation. Furthermore, the MSI phenotype was associated with a higher density of CD3- and FOXP3-positive T cells in the tumor-distant, normal mucosa of CRC patients [318].

4.1.2.2 Distinct immune profiles in LS patients with and without CRC manifestation

The mucosal immune milieu in healthy LS carriers and LS CRC patients was further assessed to evaluate a potential influence of a manifest CRC on immune infiltration in the normal colonic mucosa. First, the density of different T cell subpopulations in the normal colonic mucosa of LS individuals was compared to LS CRC tissue. Second, T cell infiltration was compared between the normal mucosa of LS individuals with and without CRC manifestation.

The local infiltration with CD3-, CD8- and FOXP3-positive T cells in LS-associated CRCs was evaluated immunohistochemically and representative IHC staining examples are shown in Figure 18. Clinical features of the respective patients are summarized in Table S4. Similarly to the analysis of normal mucosa sections, quality control excluded several CRC stainings and the number of quantified sections varied for each marker. If multiple tissue blocks from the same LS CRC were available, all blocks were analyzed and the obtained patient mean was used for all further analyses as described previously. The individual block counts for LS CRCs are shown in Figure S6 [318].

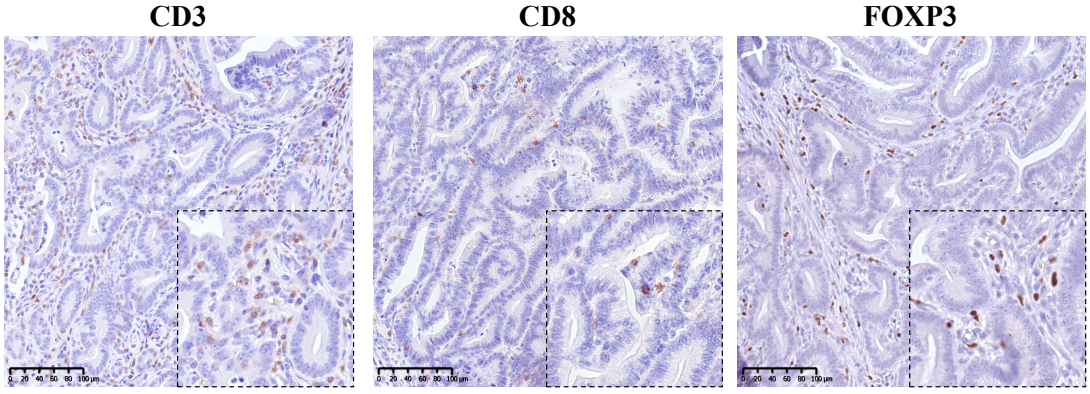

Figure 18: Representative IHC staining examples of LS-associated CRCs. CD3-, CD8- and FOXP3-positive T cells (20 x magnification) in cancer tissue of LS CRCs.

The density of CD3-positive T cells (median per 0.1 mm^2) was quantified in 26 LS CRCs, CD8-positive T cells were quantified in 22 CRC specimens and the density of FOXP3-positive T cells was assessed in 19 CRCs. LS CRCs displayed a significantly higher infiltration with CD3- and FOXP3-positive T cells, compared to the normal mucosa of healthy LS carriers and LS CRC patients (CD3: LS CRCs vs. healthy LS carriers/LS CRC patients: 119.6 vs. 66.63/60.38, $p = 0.0002/p > 0.0001$; FOXP3: LS CRCs vs. healthy LS carriers/LS CRC patients: 18.44 vs. 6.31/5.50, $p = 0.0001/p > 0.0001$) (Figure 19A, 19C). LS CRCs did not present with elevated numbers of CD8-positive T cells (Figure 19B) [318].
Importantly, the analysis of CD8-positive T cells revealed a significant difference between the normal mucosa of healthy LS carriers and LS CRC patients (healthy LS carriers vs. LS CRC patients: 38.88 vs. 29, $p = 0.0142$) (Figure 19B) [318].

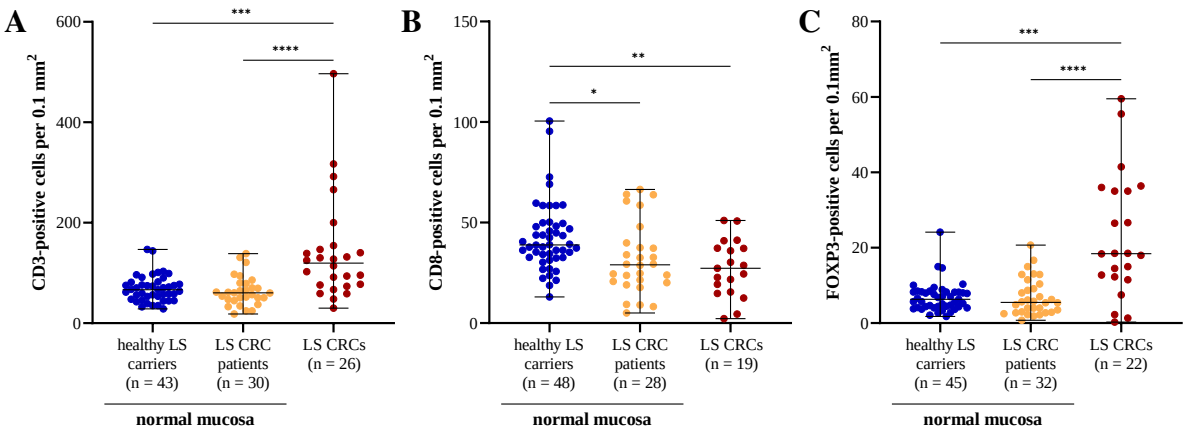

Figure 19: Quantification of T cell infiltration in the normal colonic mucosa of healthy LS carriers/LS CRC patients and LS CRC tissue. CD3- (A) and FOXP3-positive (C) T cells were significantly enriched in LS cancer tissue, compared to the normal mucosa. CD8-positive (B) T cells exhibited the highest density in the normal mucosa of healthy LS carriers, being significantly higher compared to the normal mucosa of LS CRC patients and LS CRC tissue. Each data point indicates the mean T cell count per patient. Median and range are illustrated. Adapted from: [318].

The described IHC results indicated an altered immune profile between LS individuals with and without CRC manifestation and an extensive gene expression analysis, using the NanoString nCounter®platform, was performed to obtain a more comprehensive picture of the mucosal immune processes in healthy LS carriers and LS CRC patients [318].

A subset (n = 10) of randomly selected samples of each LS group (normal mucosa of healthy LS carriers and LS CRC patients, and LS CRC tissue) was subjected to NanoString analysis. The obtained data were analyzed on two levels: mRNA expression of 770 immune-relevant genes and abundance of 14 different immune cell populations (B cells, CD45-positive cells, CD56dim NK cells, CD8-positive T cells, cytotoxic cells, dendritic cells, exhausted CD8-positive T cells, macrophages, mast cells, neutrophils, NK cells, T cells, Th1 cells and regulatory T cells) [318]. The gene expression data can be found under following link: `https://www.ncbi.nlm.nih.gov/geo/query/acc.cgi?acc=GSE178516`.

The preprocessed gene expression data underwent unsupervised hierarchical clustering analysis, which revealed a clear distinction between the analyzed groups. Importantly, the clustering did not only reveal a sharp differentiation between the normal colonic mucosa and LS cancer tissue, but also distinct expression patterns for the normal mucosa of LS individuals with and without cancer manifestation (Figure 20) [318]. Principle component analysis (PCA) of the gene expression data further confirmed the differential clustering of the three analyzed LS groups (Figure 21A). No significant correlation between PC1 and PC2 with any covariates (sex, age, affected MMR gene) was observed (Table S5) [318].

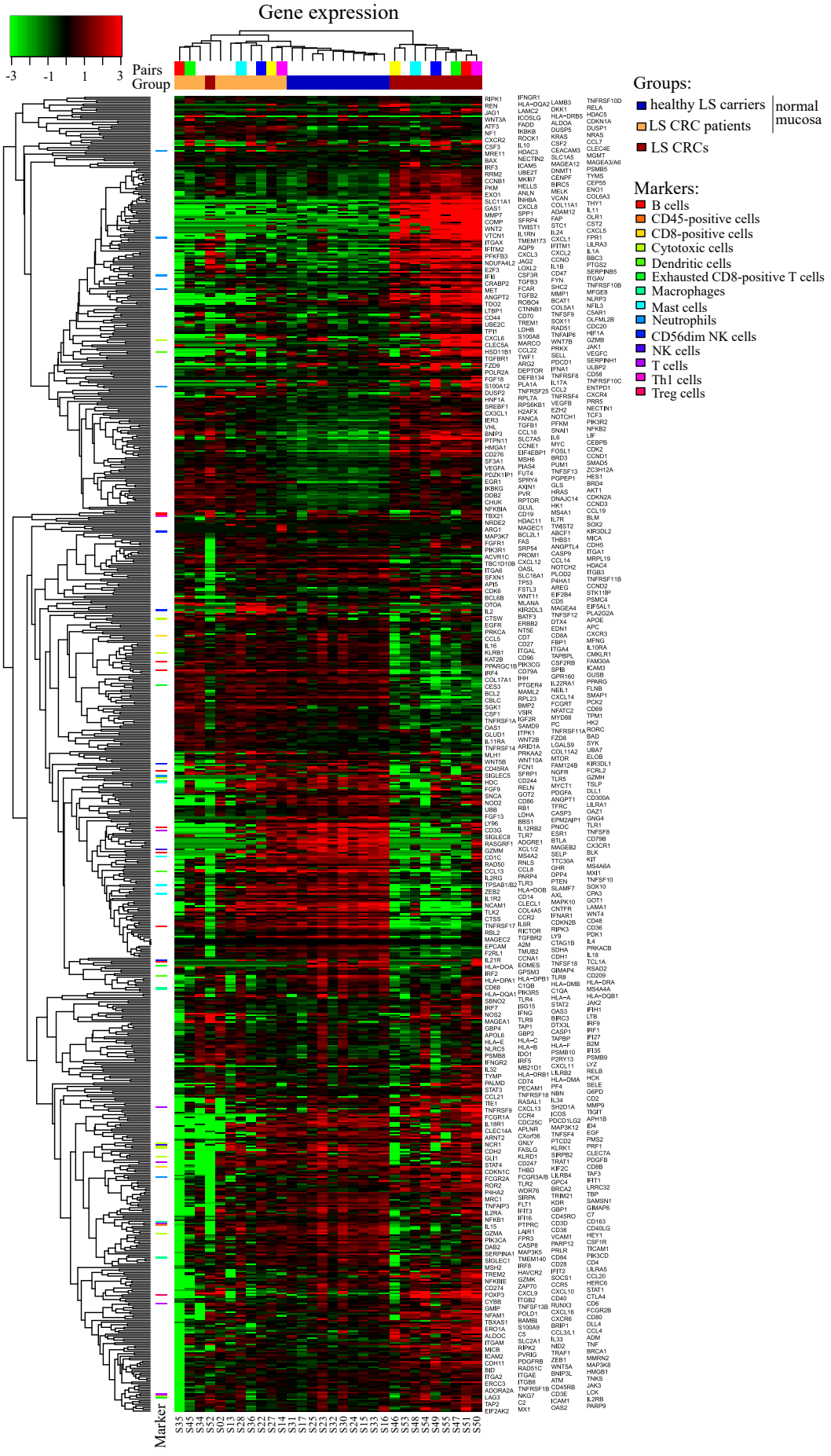
Gene expression
-3
-1
1
3
Pairs
Group
Groups:
healthy LS carriers
LS CRC patients
LS CRCs
normal mucosa
Markers:
B cells
CD45-positive cells
CD8-positive cells
Cytotoxic cells
Dendritic cells
Exhausted CD8-positive T cells
Macrophages
Mast cells
Neutrophils
CD56dim NK cells
NK cells
T cells
Th1 cells
Treg cells
Marker
S35 S45 S34 S52 S02 S12 S28 S36 S22 S27 S14 S31 S17 S25 S23 S32 S30 S24 S15 S16 S46 S53 S48 S54 S49 S55 S47 S51 S50

Figure 20: Gene expression data of the normal mucosa from LS carriers/LS CRC patients and LS CRC tissue. The unsupervised hierarchical clustering analysis revealed distinct expression profiles for the normal mucosa of healthy LS carriers and LS CRC patients as well as for cancer tissue from LS-associated CRCs. In the heatmap each gene was centered (but not scaled) with respect to the mean mRNA expression over all samples. Expression levels above the mean are depicted in red and levels below the mean are illustrated in green. Matched normal mucosa and cancer tissue samples from the same LS patient are labeled on top. Marker genes for different immune populations are indicated by color on the left margin. Modified from: [318].

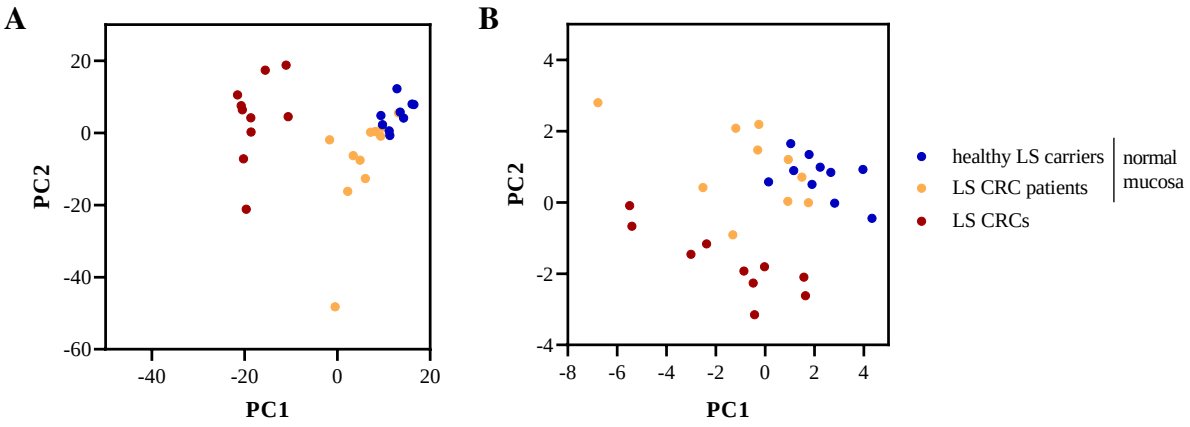

Figure 21: Principle component analysis. PCA for gene expression (A) and absolute markers (B) confirmed the distinct clustering of both normal mucosa groups (LS carriers/LS CRC patients) and LS cancer tissue. The variance explained by PC1 and PC2 amounts to 48 % for gene expression and to 68 % for absolute markers (Figure S7). Adapted from: [318].

The abundance of 14 different immune cell populations was estimated based on the mRNA expression profile of selected marker genes ('absolute markers') [319]. A subsequent unsupervised hierarchical clustering analysis showed that the majority of analyzed cell populations were overrepresented in the normal mucosa of healthy LS carriers, compared to the normal mucosa of LS CRC patients. The separation was even more distinct between the normal mucosa of healthy LS carriers and LS CRC tissue (Figure 22). The immune cell populations that were found to be overrepresented in the normal mucosa of healthy LS carriers were underrepresented in the LS CRC tissue. However, two populations (neutrophils and Treg cells) displayed the opposite pattern and were found to be more prevalent in LS CRCs (Figure 22) [318]. Similar to the gene expression data, the clustering of the absolute marker scores, representing the different immune cell populations, could be confirmed by PCA (Figure 21B). Further, no significant correlation between covariates and PC1/PC2 was observed (Table S5) [318].

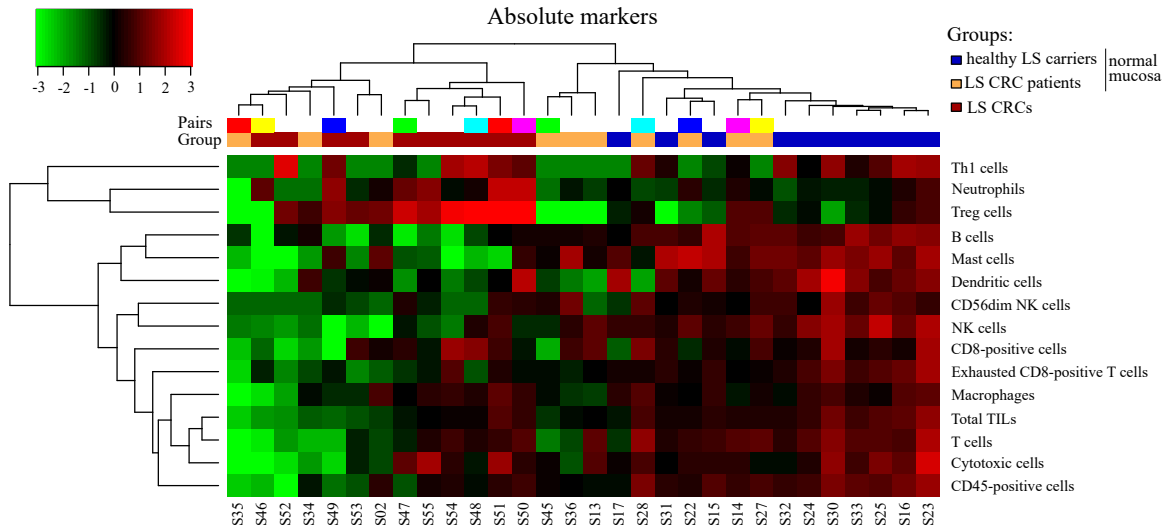

Figure 22: Abundance of 14 different immune cell populations in the normal mucosa of healthy LS carriers/LS CRC patients and LS CRC tissue. The unsupervised hierarchical clustering analysis of the absolute immune cell marker scores revealed distinct abundances of different immune cell populations for the analyzed groups. The majority of populations were overrepresented in the normal colonic mucosa of healthy LS carriers. The same populations displayed an underrepresentation in the cancer tissue. An opposite trend was observed for neutrophils and Treg cells. Each cell population in the heatmap was centered (but not scaled) according to the mean abundance over all samples. Abundances above the mean are depicted in red and abundances below the mean are illustrated in green. The analyzed immune cell populations are labeled on the right. Matched normal mucosa and cancer tissue samples from the same LS patient are indicated on top. Modified from: [318].

A supervised analysis was conducted to further examine differences in the abundance of immune cell populations. Ten out of 14 populations were found to be significantly changed between the three analyzed groups: B cells, crucial for the adaptive humoral immune system by generating and presenting antibodies; CD45-positive cells, including all leukocytes, e.g. B and T cells; dendritic cells, professional APCs that process and present antigens to lymphocytes; exhausted CD8-positive T cells, T cells that lost their effector function due to antigen overstimulation; mast cells, which release histamine containing granules thereby promoting inflammation; neutrophils, phagocytic granulocytes strongly associated with acute inflammation; NK cells, providing rapid cytotoxic response to virally infected and tumor cells; CD56dim NK cells, mature NK cells with great cytolytic activity; Th1 cells, a CD4-positive T cell subset that secretes IL-2 and IFNγ; and Treg cells, CD4-positive T cells paramount for immune suppression (Figure 23). The remaining four populations (CD8-positive T cells, cytotoxic cells, macrophages, T cells) did not present with statistically significant differences across the two normal mucosa groups and LS CRC tissue (Figure S8) [318].

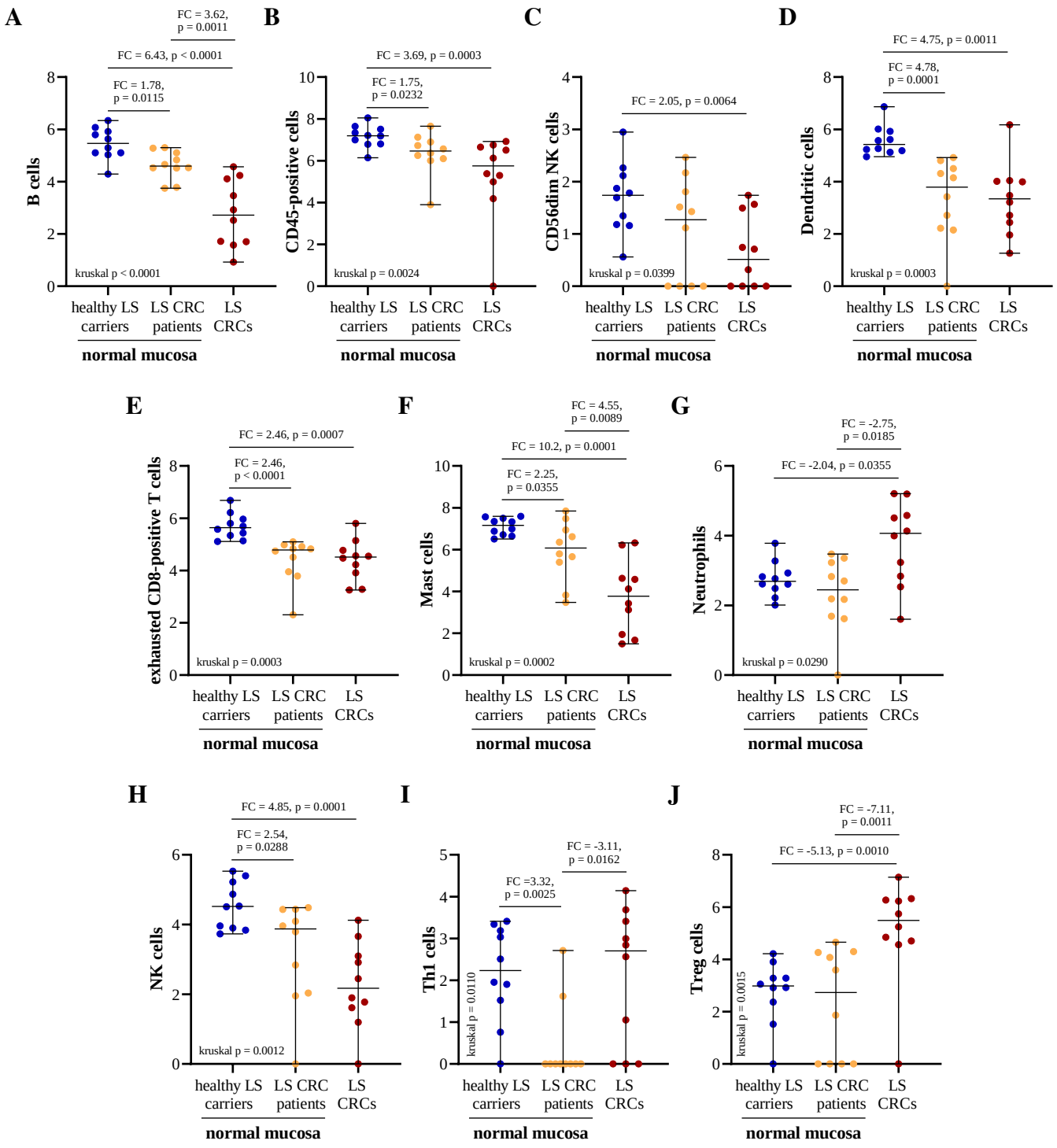

Figure 23: Supervised analysis of the abundance of different immune cell populations in the normal mucosa of healthy LS carriers/LS CRC patients and LS CRC tissue. Each beeswarm plot (A-J) depicts statistically significant changes in the abundance of ten different immune populations within the analyzed LS groups. The calculated absolute immune cell marker scores for each population are depicted on a log2 scale. FC indicates fold changes in immune cell abundance between two groups. P-values for the omnibus Kruskal-Wallis test and the post hoc Mann-Whitney test are indicated in the individual figures. Median and data range are depicted. Adapted from: [318].

Compared to the normal mucosa of LS CRC patients and cancer tissue, the normal mucosa of healthy LS carriers displayed a significantly higher prevalence of: B cells (Figure 23A), CD45-positive cells (Figure 23B), dendritic cells (Figure 23D), exhausted CD8-positive T cells (Figure 23E), mast cells (Figure 23F) and NK cells (Figure 23H). The abundance of CD56dim NK cells was higher in the normal mucosa of healthy LS carriers but only reached statistical significance when compared to LS CRC tissue (Figure 23C) [318].

Two populations (B and mast cells) were found to be significantly increased in the normal mucosa of LS cancer patients, compared to LS CRC tissue (Figure 23A, 23F) [318]. The obtained absolute marker scores for Th1 cells exhibited broad scattering across all three groups and consequently did not yield a clear picture. The lowest abundance of Th1 cells was identified in the normal mucosa of LS CRC patients, which was significantly lower compared to the normal mucosa of healthy LS carriers and LS CRC tissue (Figure 23I) [318]. Neutrophils and Treg cells were found to be enriched in LS cancer tissue and their abundance was significantly higher compared to both LS normal mucosa groups (Figure 23G, 23J) [318].

Additionally, matched samples of tumor-distant, normal mucosa and cancer tissue from the same LS CRC patients (n = 6) were analyzed pairwise (Figure 24). The observed higher abundance of several immune cell populations in the normal mucosa of LS patients was mostly represented in the pairwise analyses, e.g. for B, CD45-positive and mast cells (Figure 24A, 24B, 24F) [318]. Further, the previously observed high prevalence of neutrophils and Treg cells in LS CRC tissue (Figure 23G, 23J) was also illustrated by an increase of abundance in the cancer tissue, compared to the matched normal mucosa sample (Figure 24G, 24J) [318]. The estimated abundance of Th1 cells, which did not yield a clear picture in the group-wise analysis (Figure 23I), presented with an elevated prevalence in the cancer tissue, compared to the matched normal mucosa (Figure 24I) [318].

The pair-wise visualization of the remaining four immune cell populations without significant differences between the groups is depicted in Figure S9.

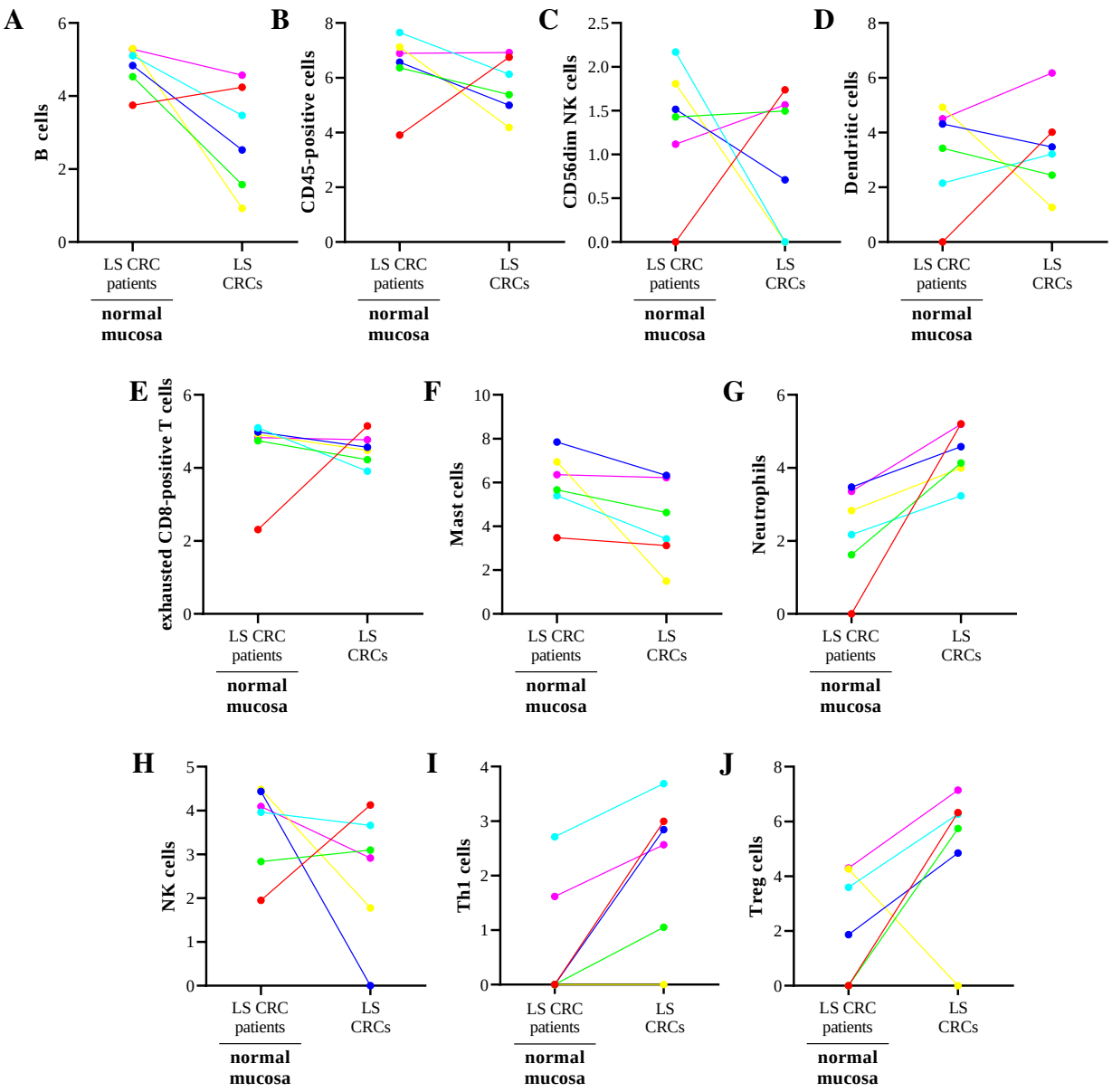

Figure 24: Pairwise comparison of the immune cell population abundance in matched normal mucosa and LS CRC tissue. Spaghetti plots (A-J) depict the estimated abundance of immune cell populations in matched tumor-distant, normal mucosa and cancer tissue samples from LS CRC patients (n = 6). Each pair is represented by one color. The y-axis shows the log2-transformed absolute marker scores.

Neutrophils and Treg cells are both associated with immunosuppressive properties and can counteract tumor immunity [338]. More recently, the role of TGFβ (TGFB) in the neutrophil-mediated suppression of TIL activity has been demonstrated in colon cancer [339]. In line with this observation and the described enrichment of neutrophils in LS CRC tissue, gene expression analysis revealed a significantly higher expression of all TGFB isoforms (1–3) in cancer tissue, compared to the normal mucosa of healthy LS carriers and LS CRC patients (Figure 25) [318].

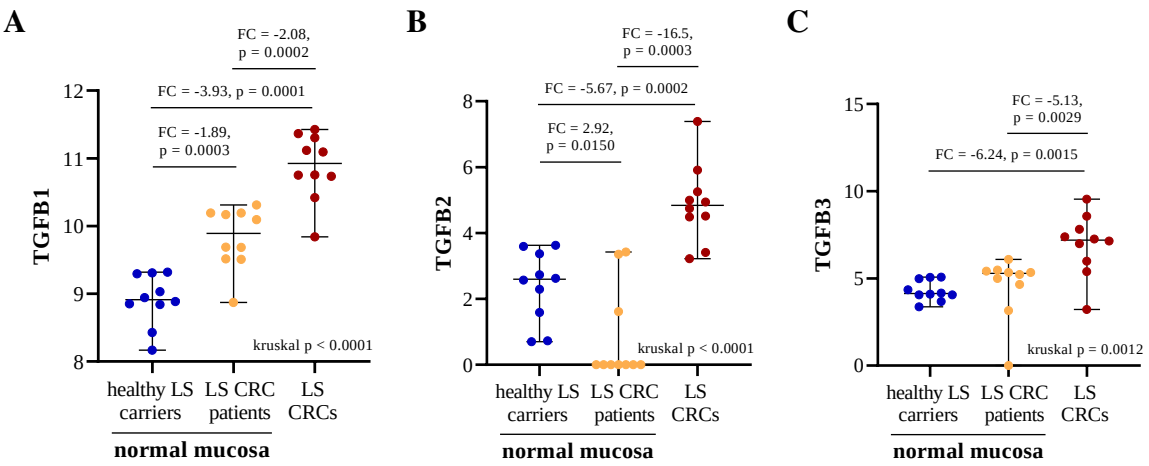

Figure 25: Expression of TGFB isoforms in the normal mucosa of healthy LS carriers/LS CRC patients and LS CRC tissue. Compared to the normal mucosa of healthy LS carriers and CRC patients, LS CRC tissue presented with a significantly higher expression of the TGFB isoforms 1 (A), 2 (B) and 3 (C). The y-axis depicts the normalized and log2-transformed expression data. FC indicates fold changes in gene expression between two groups. P-values for the omnibus Kruskal-Wallis test and the post hoc Mann-Whitney test are provided. Median and data range are indicated. Adapted from: [318].

The elevated expression of TGFB (1–3) in CRC tissue could also be observed in the pairwise comparison with the matched tumor-distant, normal mucosa samples from the same LS CRC patient (Figure 26) [318].

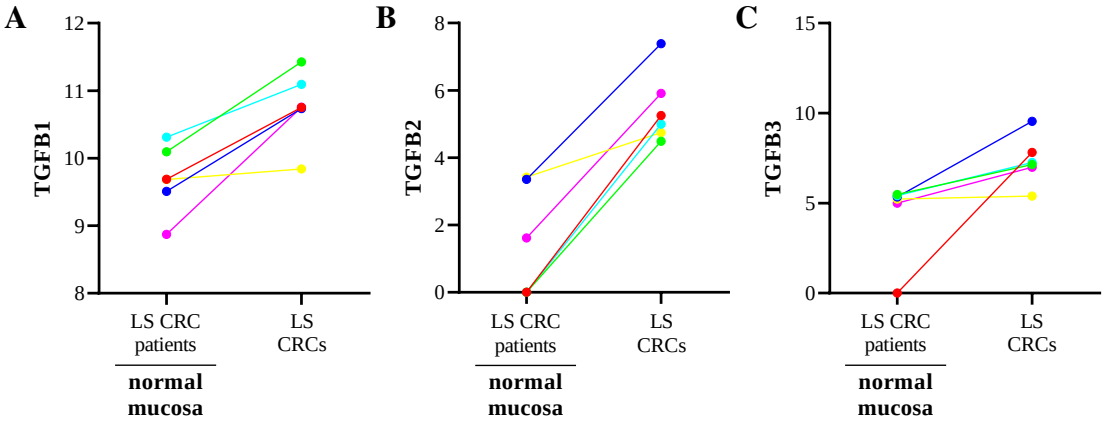

Figure 26: Pairwise comparison of TGFB expression in matched normal mucosa and LS CRC tissue. Spaghetti plots (A-C) depict the expression of all TGFB isoforms (1–3) in the normal colonic mucosa of LS CRC patients and matched samples of CRC tissue (n = 6). Each matched sample pair is depicted by one color. The log2-transformed and normalized expression data is shown on the y-axis. Modified from: [318].

The estimated abundance of immune cell populations in the normal colonic mucosa of healthy LS carriers and LS CRC patients, which is the result of deconvolution analysis, is concordant with the respective IHC-based quantification. A statistically significant correlation between IHC counts and NanoString scores was identified for CD8- (Spearman r = 0.68, p = 0.002) and FOXP3-positive (r = 0.50, p = 0.02) T cells (Figure S10) [318].

Overall, the analysis of the immunological milieu in the normal colonic mucosa of healthy LS carriers and LS CRC patients on the gene expression level revealed distinct immune profiles in LS individuals dependent on cancer manifestation. Furthermore, LS CRC tissue presented with a specific expression profile, particularly characterized by the pronounced abundance of neutrophils and Treg cells [318].

4.1.2.3 T cell infiltration in the normal rectal mucosa is associated with time to LS CRC manifestation

The observed immunological differences in the normal colonic mucosa of healthy LS carriers and LS CRC patients could point towards a role of the mucosal immune milieu in impacting LS CRC risk. This possibility was investigated by analyzing normal mucosa samples from individuals enrolled in the CAPP2 clinical trial, which assessed the effect of aspirin on CRC risk in LS carriers [247]. In contrast to the colonic mucosa specimens from the previously analyzed cohort (Table S3), the CAPP2 cohort solely included rectal mucosa samples. Notably, normal rectal mucosa samples were collected before the randomization to aspirin or placebo and the effect of aspirin on the CD3-positive T cell density could not be analyzed within this study. Contrary to the non-CAPP2 cohort described above, the limited availability of tissue samples only allowed the analysis of CD3-positive T cells and no further T cell subpopulations were quantified [318].

The density of CD3-positive T cells was assessed in 48 trial participants who developed CRC or a highly dysplastic colorectal adenoma (hereafter referred to as 'advanced neoplasia') within the follow-up period, and 49 participants who did not develop an advanced neoplasia. The median follow-up time for individuals with an advanced neoplasia was seven years (range: 0–10 years) and eight years for the participants without advanced neoplasia (range: 3–10 years). The two groups were age-matched and whenever possible sex-matched. The clinical characteristics of all included trial participants are summarized in Table S6.

Within the CAPP2 cohort a significant negative correlation between the number of CD3-positive T cells and the individuals' age was observed as younger age was associated with a higher density of CD3-positive T cells (Spearman r = -0.2819, p = 0.0052) (Figure 27A) [318].

Alike to the non-CAPP2 cohort, history of extracolonic cancer was significantly associated with older age (Figure S11A). After age-normalization the density of CD3-positive T cells was not found to be significantly different between CAPP2 LS carriers with and without a history of extracolonic cancer (Figure S11B) [318]. Comparing the CAPP2 and non-CAPP2 cohort according to anatomic location revealed a significantly lower number of CD3-positive T cells in the normal rectal mucosa, compared to colonic mucosa (Figure S12A). Therefore, any direct comparison of both cohorts, CAPP2 and non-CAPP2, was avoided in all aspects of the study. Notably, T cell infiltration did not differ significantly between the right and left hemicolon (Figure S12B) [318].

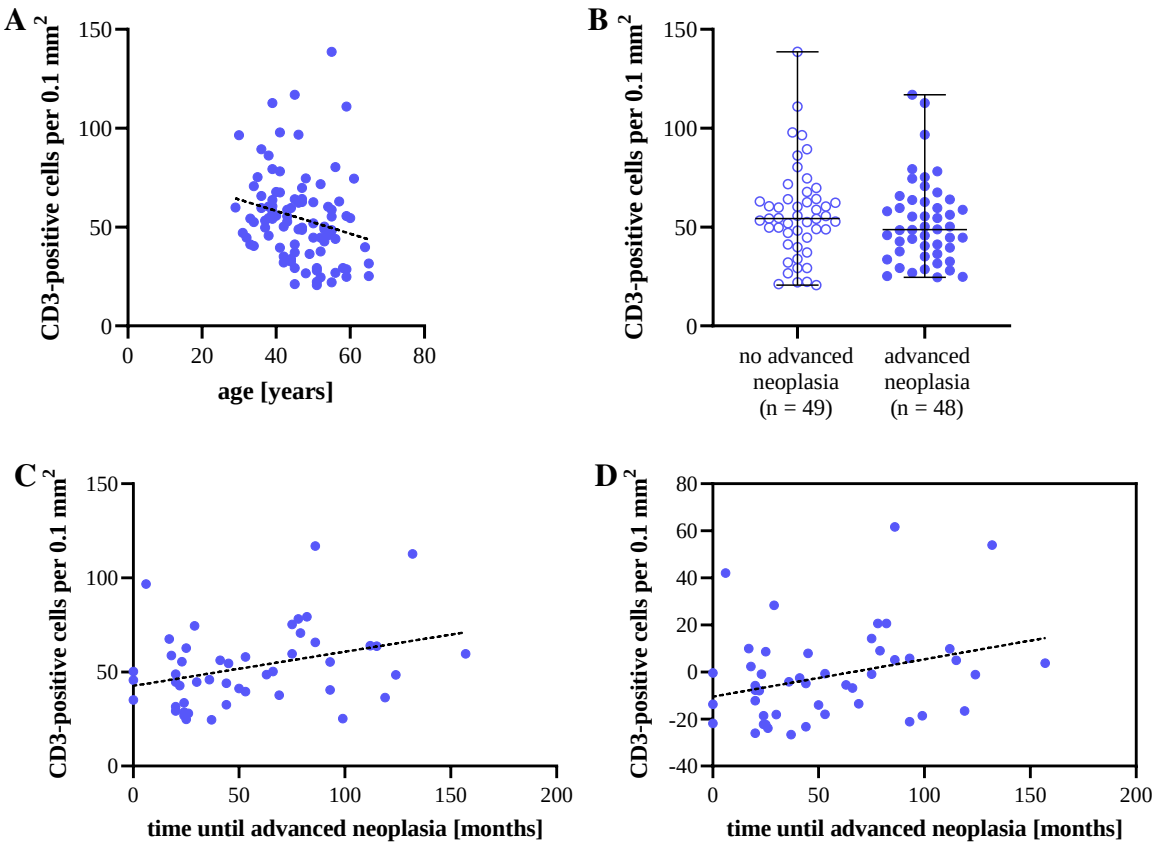

Figure 27: Quantification of T cell infiltration in the normal rectal mucosa of CAPP2 participants. (A) The individual's age was found to be significantly correlated with the density of CD3-positive T cells in the rectal mucosa. (B) No significant difference in CD3-positive T cell counts was observed between participants that developed an advanced lesions during follow-up and the ones that did not ($p = 0.2821$). Median and data range are depicted. (C) A significant correlation between the time from sampling to the diagnosis of an advanced lesion and the CD3-positive T cell infiltrate was found. (D) The age-normalized correlation between T cell density and time to advanced lesion remained statistically significant. Adapted from: [318].

The normal rectal mucosa of participants with and without an advanced neoplasia during follow-up presented with similar levels of CD3-positive T cells and no significant difference

was observed (Figure 27B) [318]. However, the time from the rectal biopsy at trial entry to diagnosis of an advanced lesion was significantly correlated with the density of CD3-positive T cells (Spearman r = 0.2888, p = 0.0465) and a more densely infiltrated mucosa was associated with a longer time until occurrence of an advanced lesion (Figure 27C). Importantly, the observed correlation remained statistically significant after normalization for the patients' age (Spearman r = 0.2949, p = 0.0419) (Figure 27D) [318].

In summary, the normal colonic mucosa of healthy LS carriers does not only present with elevated local T cell infiltration, it is further characterized by a distinct gene expression profile. The observed immunological differences between the normal mucosa of healthy LS carriers and LS CRC patients might indicate the mucosal immune milieu as a temporary or permanent tumor risk modifier in LS carriers. This hypothesis is supported by a long-term follow-up of LS carriers within the CAPP2 trial, which revealed a significant correlation between mucosal T cell infiltrate and time to subsequent tumor occurrence [318].

4.1.2.4 Altered T cell densities in LS-associated colorectal premalignant lesions

In addition to the quantification of immune infiltration in the normal colorectal mucosa of LS carriers, T cell densities were immunohistochemically assessed in LS-associated precancerous lesions. Clinical parameters of the analyzed patients are summarized in Table S7 and representative IHC stainings are presented in Figure 28. The densities of different T cell subpopulations were quantified in 140 adenomas from 74 LS patients. Notably, multiple adenomas from the same patient were analyzed individually. As described previously, insufficient staining and tissue quality led to the exclusion of certain samples for different T cell markers. CD3-positive T cells were quantified in 140 adenomas from 73 patients. The density of FOXP3-positive T cells was assessed in 124 adenomas from 64 patients. CD8-positive T cells were quantified in 81 adenomas from 57 patients.

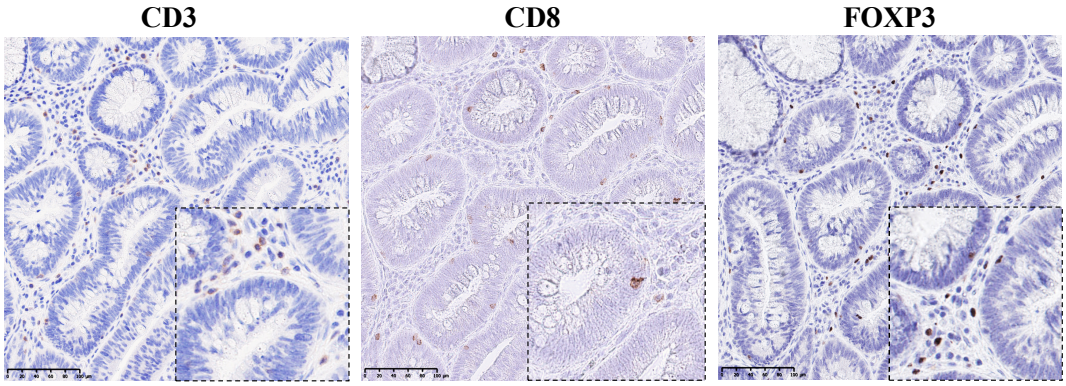

Figure 28: Representative IHC staining examples of LS-associated adenomas. CD3-, CD8- and FOXP3-positive T cells (20 x magnification) in adenomatous tissue of LS carriers.

The quantification of CD3-positive T cells (median per 0.1 mm^2) in LS-associated adenomatous tissue revealed similar T cell densities, compared to the normal colonic mucosa of healthy LS carriers (LS adenomas vs. healthy LS carriers: 73.88 vs. 66.63, $p = 0.3777$) (Figure 29A). The density of CD8-positive T cells was significantly lower in LS-associated adenomas, compared to the normal mucosa of healthy LS carriers (LS adenomas vs. healthy LS carriers: 30.75 vs. 38.88, $p = 0.0017$) (Figure 29B). The opposite was observed for FOXP3-positive T cells, which were significantly enriched in LS adenomas (LS adenomas vs. healthy LS carriers: 10.88 vs. 6.31, $p < 0.0001$) (Figure 29C).

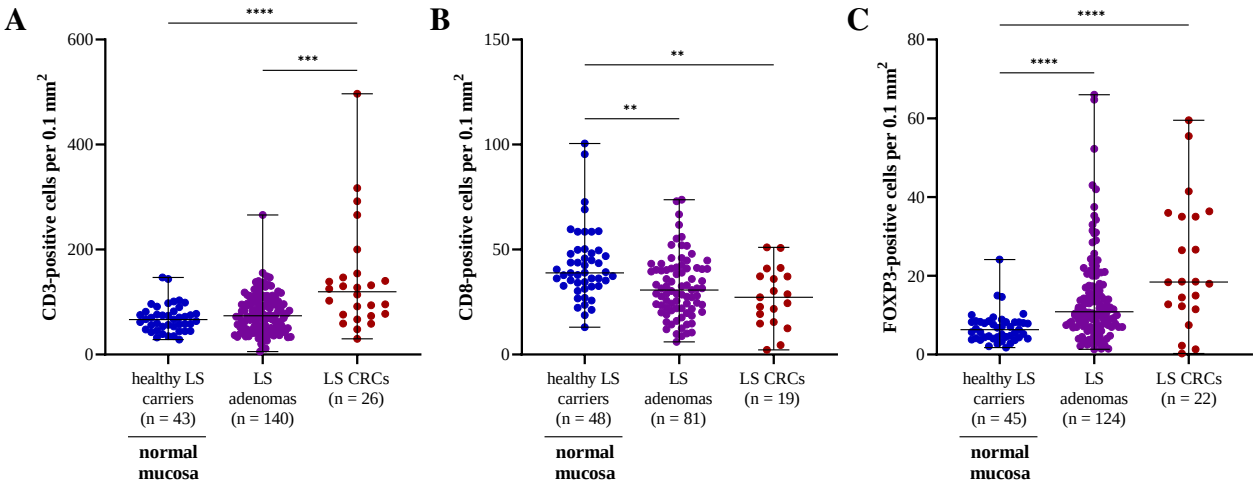

Figure 29: T cell infiltration in the normal mucosa of healthy LS carriers, LS-associated adenomas and LS CRCs. (A) The density of CD3-positive T cells was significantly higher in LS CRCs, compared to LS adenomas as well as LS normal mucosa. (B) CD8-positive T cells were significantly more prevalent in the normal mucosa of LS carriers, compared to LS adenomas and CRCs. No significant difference between adenomas and CRCs was observed. (C) FOXP3-positive T cell counts were significantly higher in LS-associated adenomas and CRCs, compared to the normal mucosa of LS carriers. No significant difference was observed between adenomas and CRCs. Each data point depicts the T cell count for one patient and one adenoma, respectively. The median T cell density and its range are depicted.

Additionally, the abundance of different T cell subpopulations in LS-associated precancerous lesions was compared to LS CRC tissue. The density of CD3-positive T cells was found to be significantly higher in LS CRC tissue, compared to adenomas (LS CRCs vs. LS adenomas: 119.60 vs. 73.88, $p = 0.0006$) (Figure 29A). Similarly, LS CRCs presented a more dense infiltration with FOXP3-positive T cells, compared to LS adenomas, but not reaching statistical significance (LS CRCs vs. LS adenomas: 18.44 vs 10.88, $p = 0.0618$) (Figure 29C). The density of CD8-positive T cells, which was found to be significantly lower in LS adenomas, compared to the normal colonic mucosa of LS carriers, was further reduced in LS CRCs without reaching statistical significance (LS CRCs vs. LS adenomas: 27.25 vs. 20.75, $p = 0.8922$) (Figure 29B).

Overall, LS-associated adenomas displayed intermediate numbers of CD3- and FOXP3-positive T cells, compared to the lower abundance in the normal colonic mucosa of healthy LS carriers and higher numbers in LS CRC tissue. However, the density of CD8-positive T cells in LS adenomas was found to be significantly reduced compared to the normal colonic mucosa of healthy LS carriers.

Stratification of the obtained T cell infiltration data for LS adenomas according to the underlying MMR gene germline variant did not show significant differences between *MLH1*, *MSH2* and *MSH6* LS carriers (Figure S13).

The assessment of the MMR status by IHC staining allowed the distinction between MMR-proficient (MMR-P) and MMR-deficient (MMR-D) adenomas. Approximately 60 % of adenomas in the analyzed cohort presented with a loss of the respective MMR protein, which is lower compared to previously reported frequencies (ranging between 70–79 % [175, 190, 340]). The infiltration with CD3-positive T cells was significantly higher in MMR-D adenomas, compared to their MMR-P counterparts (MMR-P vs. MMR-D: 63.00 vs. 87.29, $p = 0.0148$) (Figure 30A). Similarly, MMR-D adenomas displayed significantly higher counts of CD8- and FOXP3-positive T cells compared to adenomas retaining MMR protein expression (CD8: 24.25 vs. 36.00, $p = 0.0123$; FOXP3: 8.75 vs. 14.25, $p = 0.0008$) (Figure 30B, 30C).

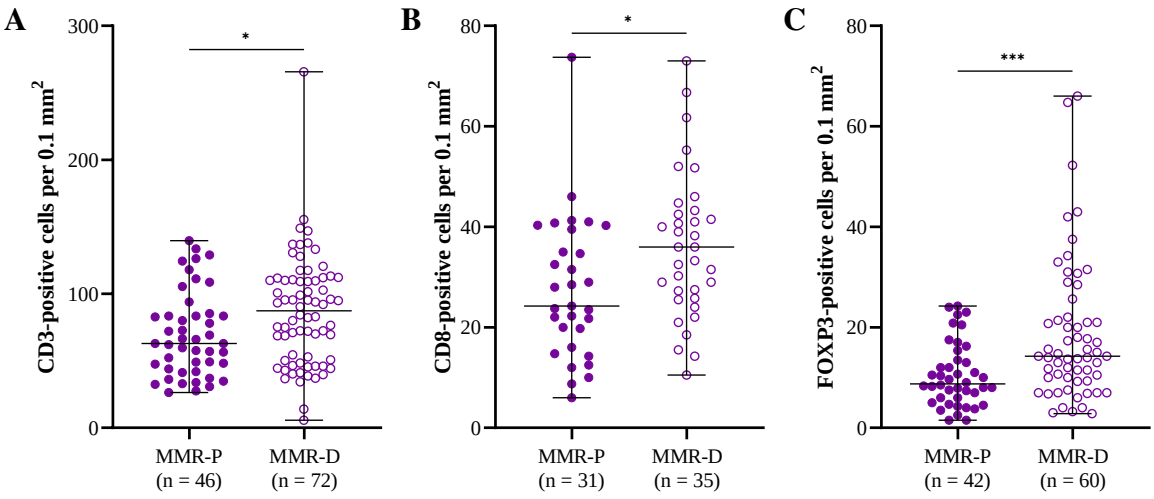

Figure 30: Quantification of T cell infiltration in LS-associated adenomas stratified for the MMR status. CD3- (A), CD8- (B) and FOXP3-positive (C) T cells were quantified in MMR-P and MMR-D LS adenomas. Significantly higher T cell densities for all markers were observed in MMR-D adenomas. Each data point represents the T cell counts for one adenoma. Median T cell density and range are indicated.

T cell densities in MMR-P and MMR-D LS adenomas were further stratified according to the affected MMR gene. Independent of the MMR gene, higher CD3-, CD8- and FOXP3-positive T cell counts were observed in MMR-D adenomas, reaching statistical significance for *MLH1* and *MSH2* LS carriers (Figure S14).

In summary, the quantitative analysis of different T cell subpopulations in LS-associated colorectal adenomas revealed altered T cell densities, compared to normal colonic mucosa and CRC tissue of LS individuals. Furthermore, T cell densities in MMR-D adenomas were found to be significantly higher, compared to MMR-P counterparts. The implications of the observed altered immune milieu in LS-associated adenomas could not be evaluated in the present thesis and have to be assessed in future studies.

4.2 Evaluation of systemic FSP-specific immune responses in LS carriers and MSI cancer patients

The described distinct mucosal immune profile in healthy LS carriers (see 4.1.2) and the observation of systemic FSP-specific T cell responses in LS carriers prior to cancer manifestation [80] point towards a life-long and tumor-independent activation of the immune system in those individuals. Hence, FSP-specific immune responses might hold potential to be utilized diagnostically as systemic LS markers enabling a tumor-independent immunological distinction between LS carriers and unaffected individuals. The feasibility of the proposed strategy was explored on the cellular and humoral level.

4.2.1 Elevated FSP-specific T cell responses in the blood of healthy LS carriers

FSP-specific immune responses in the peripheral blood of healthy LS carriers and cancer patients were characterized by IFNγ ELISpot assay and IFNγ RT-qPCR. The respective FSPs (resulting from the deletion of one nucleotide (-1)) were selected based on previous data reporting eight cMS that, despite their high immunogenicity, are frequently mutated in MSI cancers [79]. Two FSPs (SLC22A9 and MYH11) were used as two overlapping peptides (SLC22A9.1/SLC22A9.2 and MYH11.1/MYH11.2) due to their length. Additionally, three FSPs (HT001, TAF1B and AIM2), which were applied in the clinical trial investigating FSP vaccines in MSI cancer patients [81], were included. Thus, a panel of 13 FSPs (Table 7) was applied for all further analyses.
Blood samples were collected from four groups: healthy LS carriers, MSI cancer patients, MSS cancer patients and healthy non-LS controls. The clinical characteristics of all individuals are provided in Table S8. The analyzed cohort was heterogeneous and encompassed different cancer entities (57 % CRC, 29 % gastric cancer, 10 % EC,

5 % esophageal cancer), hereditary and sporadic cases, patients with prevalent cancer and post-surgery cancer patients. Several patients were also undergoing chemotherapy at the time of sampling. Notably, samples from MSI cancer patients eligible for ICB therapy were collected prior to therapy start and included in this analysis. FSP-specific T cell responses during ICB treatment have been analyzed as possible therapy success marker as part of a different research question (see 4.2.2).

PBMCs, isolated from the collected blood samples, underwent FSP-specific T cell expansion before being used for analysis. The upstream *in vitro* expansion enabled to overcome sensitivity issues resulting from the rarity of FSP-specific T cells in the peripheral blood. Systemic FSP-specific T cell responses were assessed by IFNγ ELISpot assay in a total of 55 individuals divided into the four groups: healthy LS carriers (n = 8), MSI cancer patients (LS and sporadic) (n = 21), MSS cancer patients (n = 7) and healthy non-LS controls (n = 19) (Figure 31). The obtained spot counts, representing the number of IFNγ-releasing cells per 100,000 PBMCs, were normalized by subtracting unspecific responses in the negative control from the FSP-specific counts. If possible, each FSP was analyzed in triplicates and the normalized mean was used for all further analyses. Notably, the individuals' age was not significantly correlated with the obtained IFNγ-spot counts for any of the used FSPs (Figure S15).

FSP-specific immune responses strongly varied within the analyzed groups and depending on the respective FSP. Broad data scattering was particularly observed in the cancer patient groups (MSI and MSS). MSS cancer patients were included as an additional control group and were not expected to show FSP-specific T cell responses. However, high IFNγ-spot counts were observed for the HT001 and AIM2 FSPs. 4/6 MSS cancer patients received chemotherapy at the time of sampling, which might have impacted the observed T cell responses. No statistically significant differences within the analyzed cohort were observed between both cancer patient groups and healthy controls. Further, the conducted analysis did not reveal significant differences between LS-associated and sporadic MSI cancer patients. However, a potential effect of the cancer's hereditary origin might not have been observable due to the low sample size (Figure S16).

Less variable FSP-specific immune responses were observed in healthy individuals (healthy LS carriers and non-LS controls) and overall significantly higher T cell responses were observed in LS carriers ($p < 0.0001$) (Figure 31). A statistically significant difference between healthy LS carriers and healthy controls as well as MSI cancer patients was observed for two FSPs (TGFBR2: healthy LS carriers vs. healthy controls/MSI cancer patients: 177.9 vs. 3.00/26.30, $p = 0.0010/0.0170$; SLC22A9.2: healthy LS carriers vs. healthy controls/MSI cancer patients: 99.65 vs. -2.00/5.00, $p = 0.0042/0.0074$). Hence, further analysis was conducted in the cancer-free scenario pursuing the aimed distinction between LS and non-LS individuals.

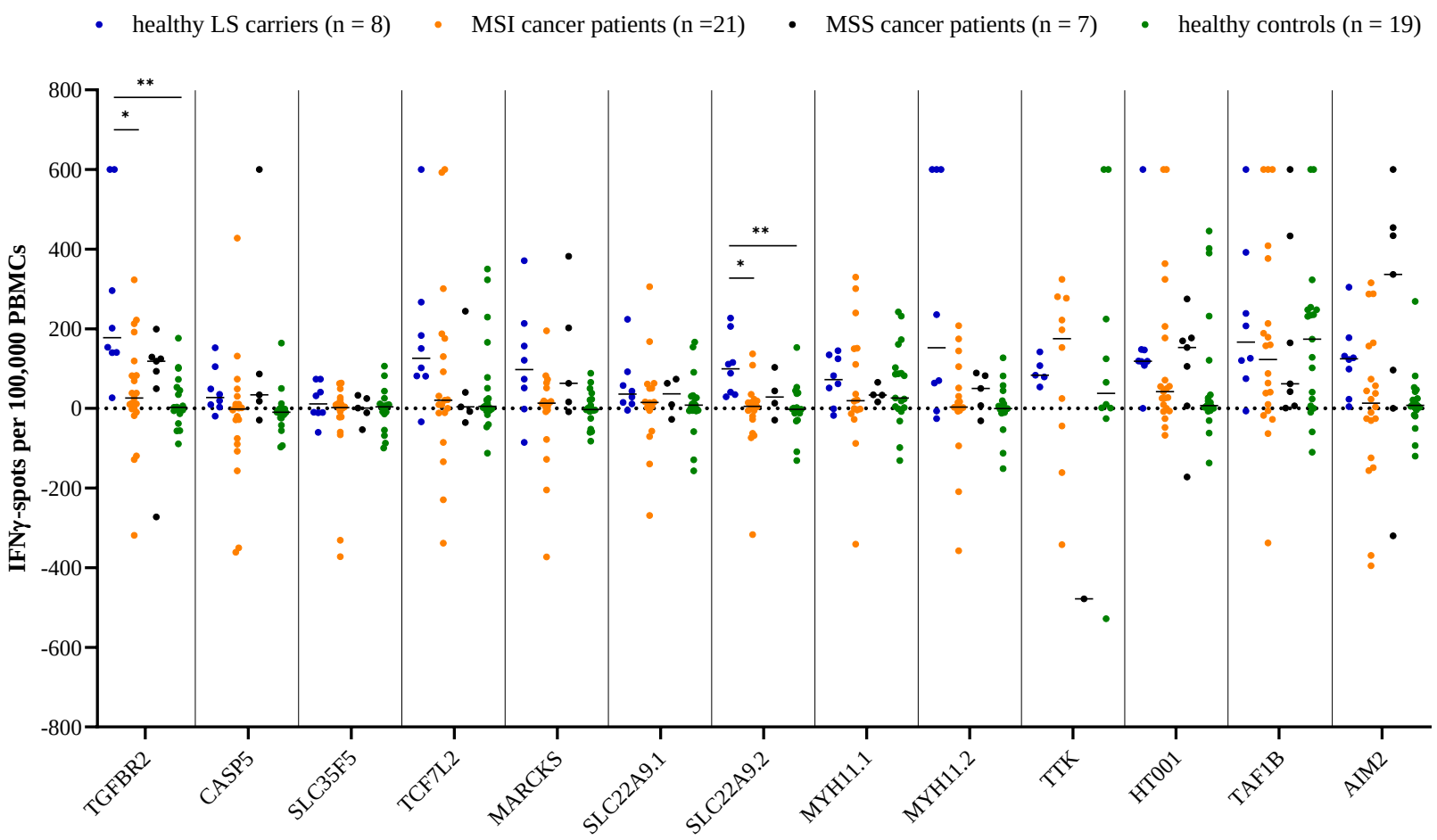

Figure 31: Systemic FSP-specific T cell responses in healthy LS carriers, MSI/MSS cancer patients and healthy controls. IFNγ-spots were quantified for each of the 13 different FSPs (two overlapping FSPs for SLC22A9 and MYH11) and all analyzed individuals. Significant differences between healthy LS carriers and healthy controls/MSI cancer patients were observed for TGFBR2 and SLC22A9.2. The depicted spot counts were normalized by subtracting the number of unspecific IFNγ-spots in the negative control from the FSP-specific counts. Each data point represents the mean normalized spot count for the respective FSP in one individual. The median for each group is indicated.

The direct comparison of IFNγ-spot counts between healthy LS carriers and non-LS controls yielded statistically significant differences for seven FSPs: TGFBR2 ($p = 0.0001$, Figure 32A) CASP5 ($p = 0.0079$, Figure 32B), TCF7L2 ($p = 0.0379$, Figure 32C), MARCKS ($p = 0.0158$, Figure 32D), SLC22A9.2 ($p = 0.0007$, Figure 32E), MYH11.2 ($p = 0.0208$, Figure 32F) and AIM2 ($p = 0.0029$, Figure 32G).

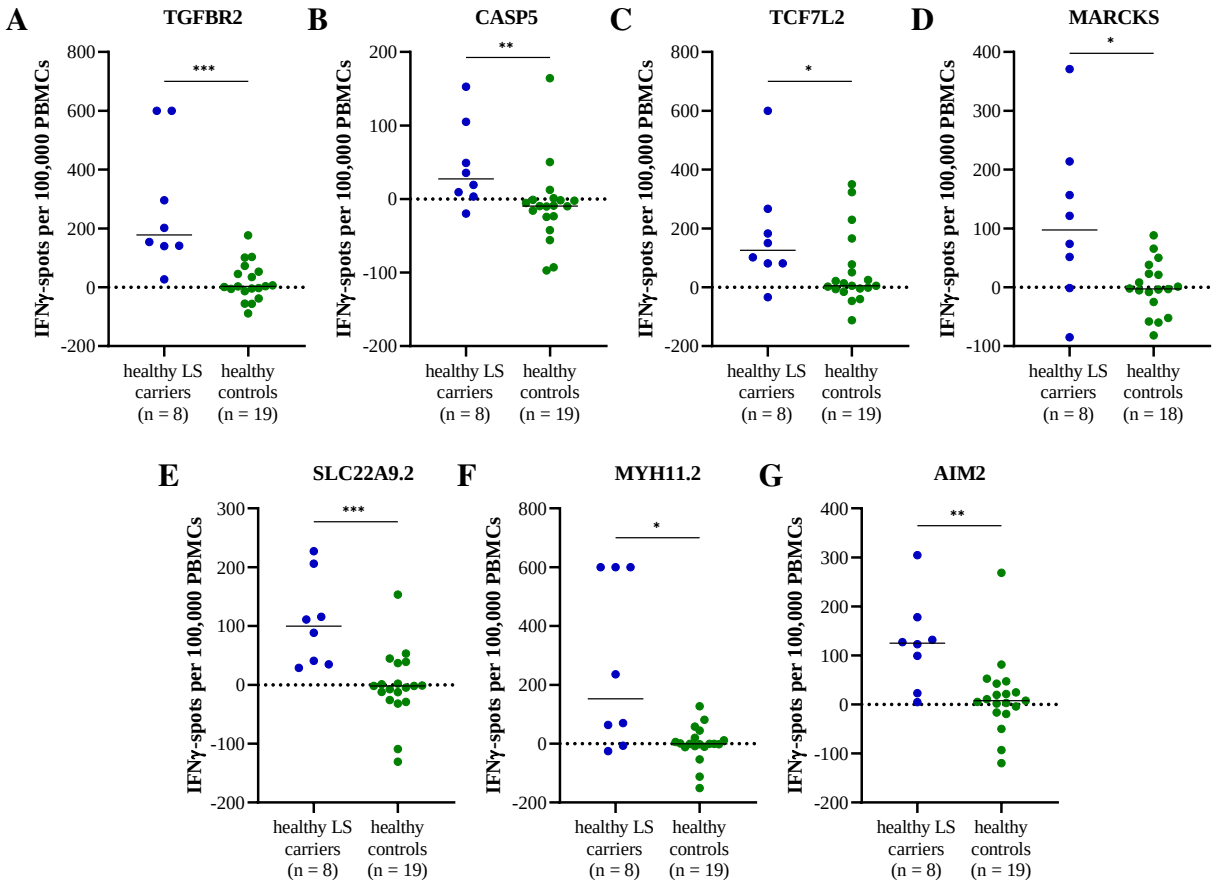

Figure 32: Systemic FSP-specific T cell responses in healthy LS carriers and healthy non-LS controls. (A-G) The direct comparison of IFNγ-spot counts between healthy LS carriers and controls revealed significantly higher T cell responses in LS carriers for seven FSPs. Each data point represents the normalized spot count mean for one individual. The median for both groups is depicted.

The remaining six FSPs (HT001, MYH11.1, SLC22A9.1, SLC35F5, TAF1B and TTK) did not display significant differences between the two analyzed groups. However, a trend towards higher FSP-specific T cell counts in healthy LS carriers was observed (Figure S17). Noteworthy, the analyzed cohort of healthy controls encompassed substantially more females compared to the group of healthy LS carriers. Thus, FSP-specific T cell responses between male and female healthy LS carriers and controls were compared revealing no significant difference ($p = 0.0963$).

In addition to the IFNγ ELISpot assay, which assessed the activation of specific T cells via the secretion of IFNγ, RT-qPCR was applied for quantifying IFNγ expression as a marker for specific T cell responses upon FSP stimulation (Figure 33). RT-qPCR could only be conducted if enough expanded cells from one individual were available after performing the ELISpot assay. Consequently, a smaller cohort of 25 individuals, containing healthy LS carriers (n = 6), MSI cancer patients (n = 11) and healthy non-LS controls (n = 8), was analyzed on the gene expression level. MSS cancer patients were excluded from this analysis due to insufficient RNA amounts. Similarly, the TTK FSP could not be assessed in the group of healthy LS carriers and was therefore not included in following analyses.

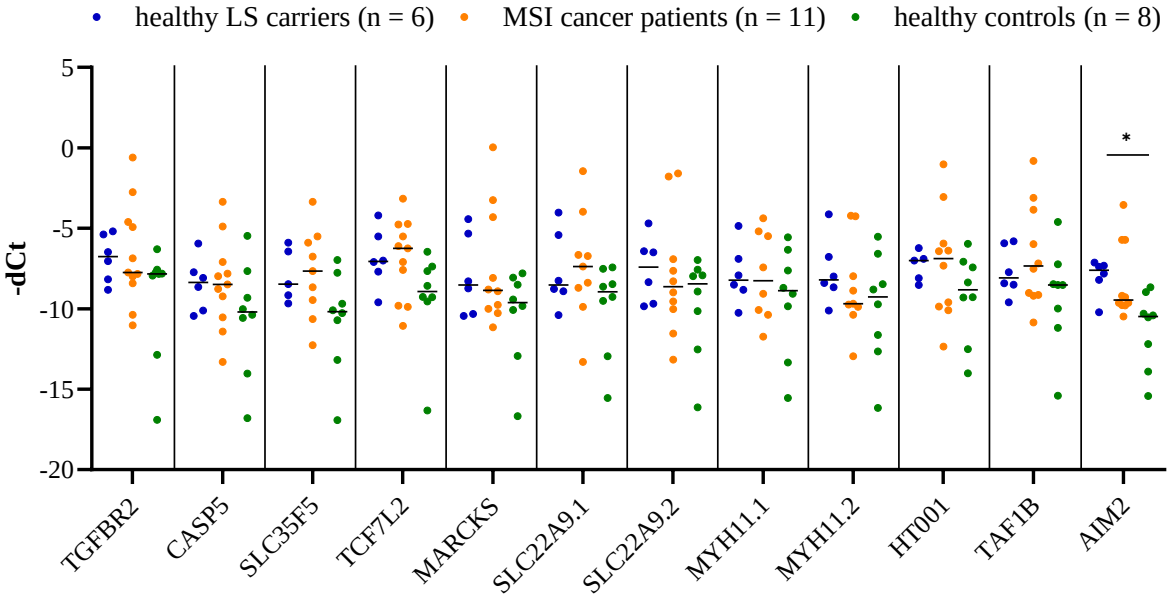

Figure 33: FSP-associated IFNγ expression in healthy LS carriers, MSI cancer patients and healthy controls. Expression of IFNγ in expanded and restimulated PBMCs was quantified using RT-qPCR. The highest IFNγ expression for all FSPs was detected in healthy LS carriers but only reaching statistical significance for AIM2. -dC_t values are given for each individual and FSP. The median is depicted for each group.

IFNγ expression was found to be highest in healthy LS carriers (Figure 33), concordant with the obtained ELISpot results. For several FSPs (SLC35F5, TCF7L2, SLC22A9.1 and HT001) MSI cancer patients exhibited an elevated IFNγ expression, compared to healthy controls. However, a statistically significant difference was only observed for the AIM2 FSP and between healthy LS carriers and non-LS controls ($p = 0.0170$) (Figure 33). Hence, IFNγ expression was again directly compared between healthy LS carriers and healthy non-LS controls. Overall and similar to IFNγ secretion, determined by the ELISpot assay, IFNγ expression upon FSP stimulation was found to be significantly higher in healthy LS carriers, compared to healthy controls ($p < 0.0001$) (Figure 34).

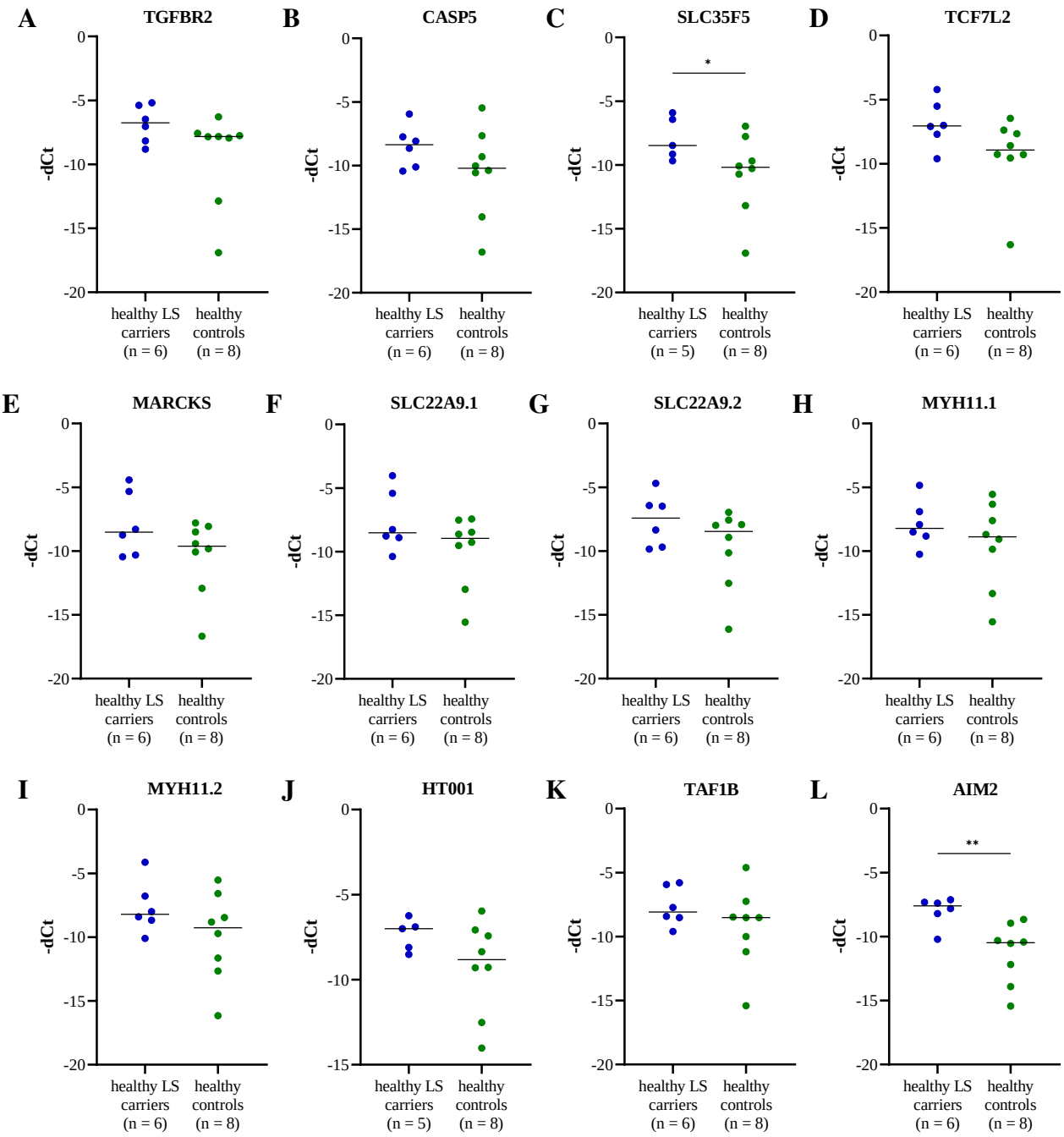

Figure 34: FSP-associated IFNγ expression in healthy LS carriers and healthy non-LS controls. A trend towards higher IFNγ expression was observed in healthy LS carriers but failed to reach statistical significance for the majority of analyzed FSPs: TGFBR2 ($p = 0.2284$, A), CASP5 ($p = 0.3450$, B), TCF7L2 ($p = 0.1419$, D), MARCKS ($p = 0.4136$, E), SLC22A9.1 ($p = 0.3450$, F), SLC22A9.2 ($p = 0.2284$, G), MYH11.1 ($p = 0.4908$, H), MYH11.2 ($p = 0.2284$, I), HT001 ($p = 0.1709$, J) and TAF1B ($p = 0.2284$, K). Compared to healthy non-LS controls, healthy LS carriers displayed significantly higher IFNγ expression for the FSPs SLC35F5 (C) and AIM2 (L). Each data point depicts the -dC_t value for each individual and FSP. The median for both groups is depicted.

A statistically significant difference between the two groups was observed for SLC35F5 ($p = 0.0451$, Figure 34C) and AIM2 ($p = 0.0027$, Figure 34L). The AIM2 FSP has already been identified as a FSP candidate using IFNγ ELISpot assay (Figure 32G). Overall, the analysis of FSP-specific T cell responses on the gene expression level pointed towards elevated responses in healthy LS carriers, supporting the previously described IFNγ ELISpot results. Importantly, the obtained IFNγ-spot counts and the corresponding -dC_t values from healthy LS carriers, MSI cancer patients and healthy controls were found to be significantly correlated (Spearman $r = 0.4375$, $p < 0.0001$), confirming the good concordance of both methods (Figure S18).

In summary, the observed elevated FSP-specific T cell responses in the peripheral blood of healthy LS carriers underpin the proposed life-long immune surveillance in LS. Such immunological characteristics might enable the distinction between LS and non-LS individuals on a functional level. Importantly, the present thesis identified seven FSPs, which were associated with significantly stronger systemic immune responses in healthy LS carriers, compared to healthy non-LS controls. The identification of these candidates laid the basis for future evaluation of their suitability as early, tumor-independent LS diagnostic markers.
The evaluation of systemic FSP-specific T cell responses in cancer patients did not yield a clear picture and no significant differences between MSI cancer patients and control groups (MSS cancer patients and healthy controls) were observed. This could be attributable to the heterogeneity of the analyzed group with regards to cancer manifestation, cancer origin and applied therapeutic interventions as these factors may greatly affect specific T cell responses in the peripheral blood. Hence, accounting for the influence of clinical characteristics and interventions is crucial when analyzing specific immune responses.

4.2.1.1 Detection of specific T cells using HLA class I tetramers

In addition to the analysis of IFNγ secretion and expression as indicators for T cell activation, the presence of FSP-specific T cells in peripheral blood was examined by using HLA-A*02:01 FSP-specific tetramers.

The successful formation of stable HLA-epitope monomers was confirmed by a complex formation assay. The binding affinity of 35 selected HLA-A*02:01 FSP epitopes, applied in three serial dilutions, was determined by flow cytometry. A negative control (no peptide) and the CMV pp65 peptide (a known HLA-A*02:01-restricted epitope) as positive control were included in the analysis. The applied gating strategy is shown in Figure 35.

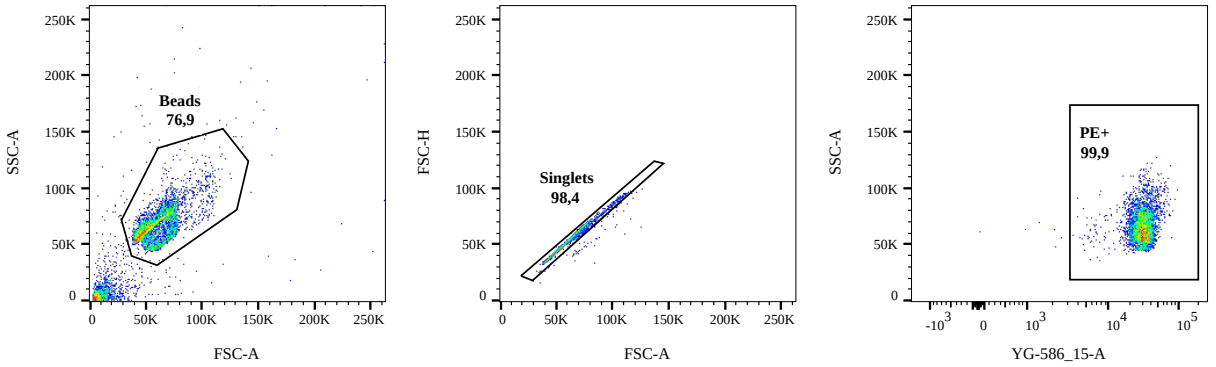

Figure 35: Gating strategy for the flow cytometry-based HLA class I complex formation assay. From left to right: identification of bead-bound HLA class I complexes, exclusion of doublets to ensure the analysis of single bead-bound complexes, gating of the PE-positive population. The percentage of the gated populations is shown next to the respective gate.

The geometric mean of the measured bead-associated fluorescence intensity (PE) for each dilution was calculated and plotted against the respective HLA complex concentration (Figure 36). Based on the obtained intensity values and an example provided by ImmunAware (Figure S19), the analyzed FSP epitopes could be categorized according to their HLA-A binding stability. No fluorescence intensity and hence no HLA binding was observed for the negative control (Figure 36A). Strong binding was detected for the positive control (CMV peptide pp65) demonstrating correct execution of the assay (Figure 36B). A total of ten FSP epitopes (TGFBR2 E3/E5, CASP5 E3, SLC35F5 E1, SLC22A9.1 E1/E3, SLC22A9.2 E2, MYH11.1 E2/E4 and TTK E3) were deemed stable binders and selected for subsequent tetramer production. HLA-A complexes with the selected FSP epitopes were tetramerized with fluorescently labeled streptavidin.

The suitability of all available patient samples was assessed by determining the HLA-A*02 status using Sanger sequencing. Within the analyzed cohort of healthy LS carriers and MSI cancer patients (Table S8) the proportion of HLA-A*02 alleles was 50 %, which was slightly higher compared to the general population (40 %) [313]. PBMCs from HLA-A*02-positive individuals were isolated and expanded as described previously. Following, the harvested cells were stained with the produced fluorescently labeled tetramers and an anti-CD8 antibody, enabling the identification of FSP-specific cytotoxic T cells.

The functionality of the produced tetramers and adequate flow cytometry analysis could be confirmed by the identification of CMV-specific T cells using pp65-specific tetramers (Figure 37). The applied gating strategy is also shown in Figure 37. However, the analysis of five samples, including three healthy LS carriers and two MSI cancer patients, with FSP-specific tetramers did not lead to the identification of FSP-specific T cell populations (representative example: Figure S20).

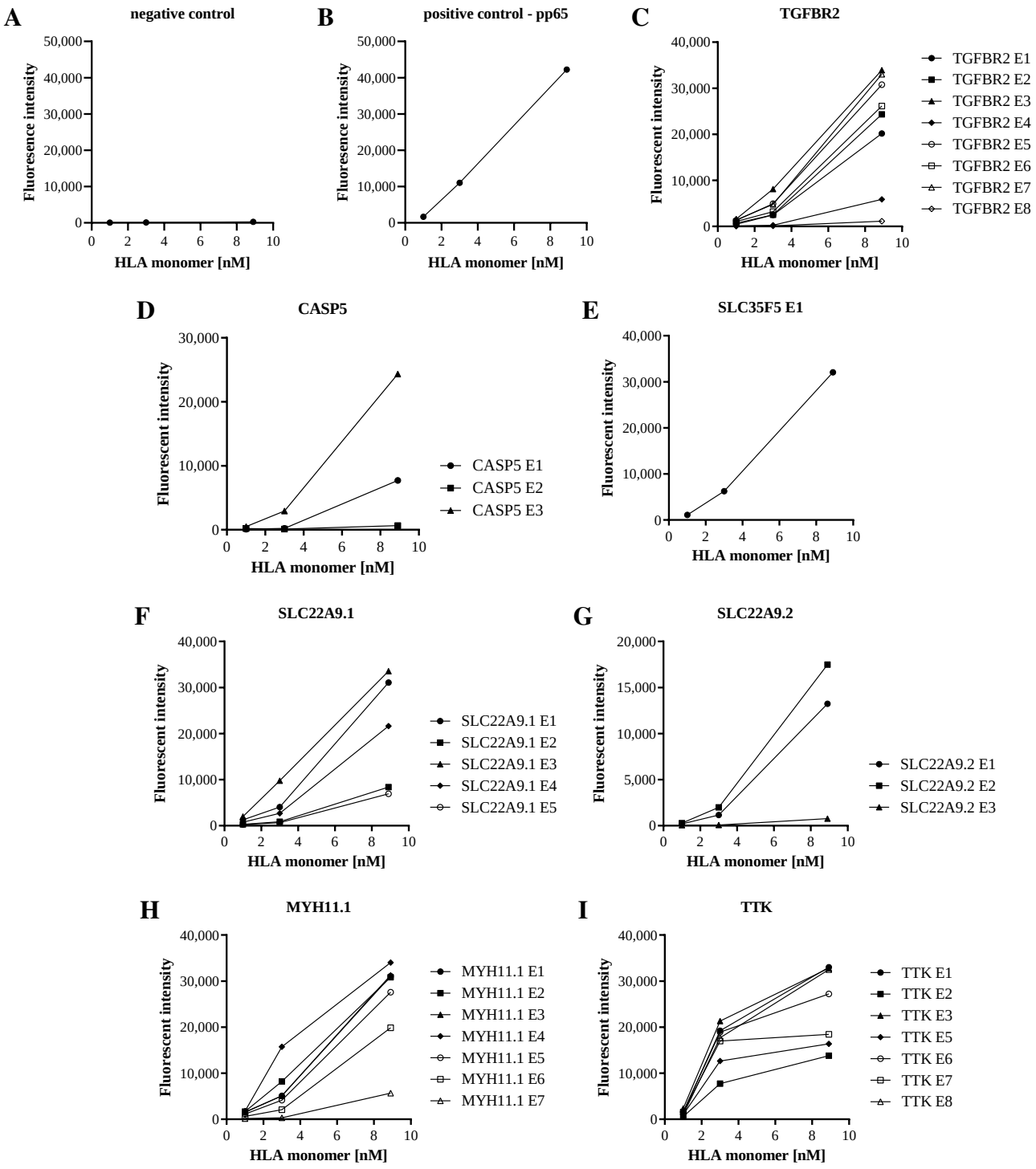

Figure 36: Selection of HLA-A*02:01 binding FSP epitopes for tetramer staining. To ensure correct execution of the assay negative (A) and positive (B) controls were analyzed. (C-I) HLA-A monomers were produced with different HLA-A*02:01-restricted FSP epitopes and stable complex formation was tested. Based on the determined binding stability epitopes were selected for tetramer production. All samples were analyzed as three serial dilutions (13.3 nM, 4.4 nM and 1.5 nM).

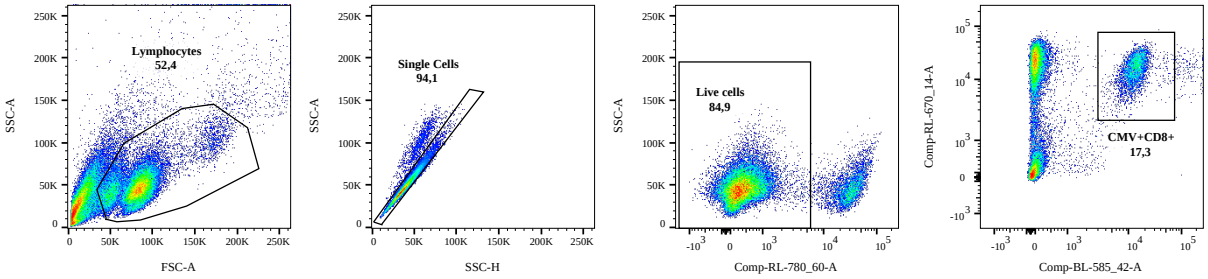

Figure 37: Identification of CMV-specific T cells in peripheral blood using HLA-A tetramers. The overall applicability of the produced tetramers could be demonstrated by the identification of CD8- and CMV-positive T cells. From left to right: gating for lymphocytes, exclusion of doublets by gating for single cells, gating for live cells and identification of CD8-, tetramer-positive cells. The percentage of the gated populations is shown next to the respective gate.

In summary, ten FSP epitopes were found to be strong binders of HLA-A*02:01 molecules and respective FSP-specific tetramers were successfully produced. The general applicability of the described protocol could be validated by the identification of CMV-positive T cells in peripheral blood with the corresponding tetramers. The limited availability of healthy LS carriers and MSI cancer patients with a confirmed HLA-A*02:01 allele hampered the application of the generated FSP-specific tetramers and their suitability remains to be determined.

4.2.2 Monitoring of FSP-specific T cell responses in MSI cancer patients during ICB therapy

Systemic FSP-specific immune responses may also show potential for other clinical applications such as therapy monitoring. ICB therapy has shown enormous success in treating MSI cancer patients (see 1.2.4.1) [139, 161]. However, a substantial proportion of patients do not respond to ICB treatment and reliable predictive markers are still lacking [163]. Hence, FSP-specific T cell responses were monitored prior to and during ICB therapy and their correlation with various clinical parameters, e.g. response to ICB and disease progression, was explored.

Blood samples from MSI cancer patients were processed and underwent *in vitro* expansion under FSP stimulation. Subsequently, IFNγ ELISpot assays and, whenever possible, IFNγ RT-qPCR were performed. FSP-specific T cell responses were quantified before therapy start and at several time points during ICB treatment. All analyses were conducted with the same FSP panel as described above. Clinical features of the analyzed patient cohort, containing seven CRC, two EC and one gastric cancer patients, are summarized in Table S9.

The quantification of FSP-specific T cell responses was conducted for ten different patients at 31 different time points before and during ICB therapy. Responses prior to ICB were quantified once immediately before treatment start (n = 10). The number of and intervals between the analyzed time points during ICB therapy varied between patients and a total of 21 samples were analyzed during ongoing ICB treatment. The overall comparison of FSP-specific T cell responses before and during ICB therapy did not yield statistically significant differences for any FSP (Figure 38). Individual IFNγ-spot counts for the analyzed patients are depicted in Figure S21.

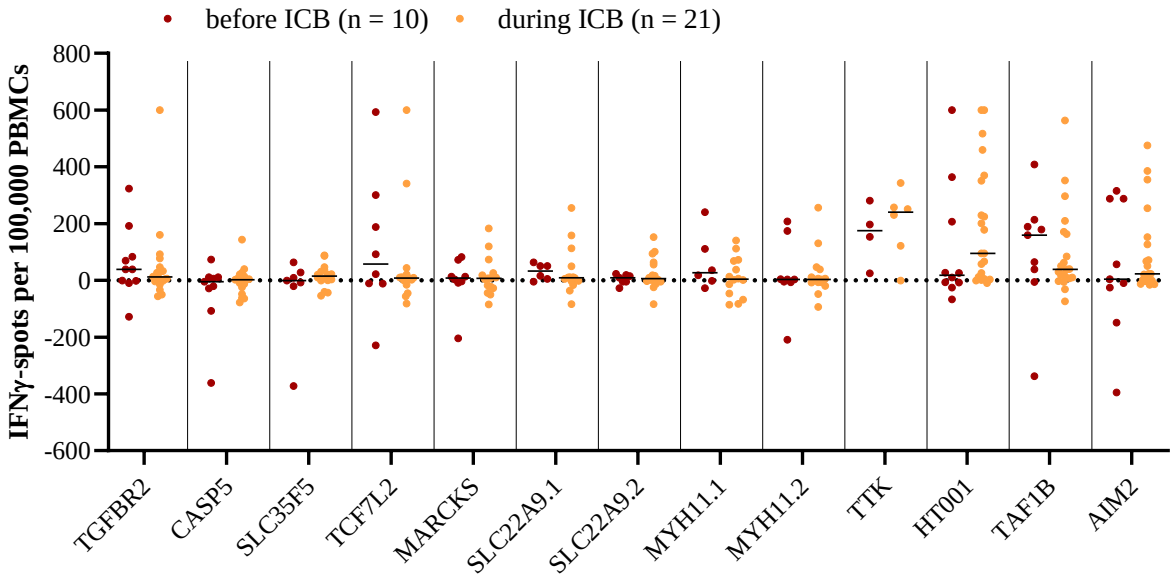

Figure 38: Quantification of FSP-specific T cell responses in MSI cancer patients before and during ICB therapy. IFNγ-spots were quantified for each of the 13 FSPs and all analyzed individuals of both groups (before and during ICB). Specific T cell responses were not found to be significantly different before and during ICB therapy: TGFBR2 ($p = 0.4352$), CASP5 ($p = 0.6314$), SLC35F5 ($p = 0.3680$), TCF7L2 ($p = 0.4167$), MARCKS ($p = 0.8626$), SLC22A9.1 ($p = 0.4940$), SLC22A9.2 ($p = 0.5454$), MYH11.1 ($p = 0.3970$), MYH11.2 ($p = 0.9639$), TTK ($p = 0.7619$), HT001 ($p = 0.1327$), TAF1B ($p = 0.3968$) and AIM2 ($p = 0.4377$). Each data point represents the mean normalized spot count for the respective FSP in one individual. The median for both groups is illustrated.

In order to obtain a clearer picture T cell responses throughout ICB treatment were monitored individually for each patient (P1-P10) (Figure 39).

The longest surveillance period of FSP-specific immune responses (305 days) and the highest number of analyzed samples at different time points was reported for patient P1. Within 40 days of ICB therapy T cell responses against the HT001 FSP greatly increased, supporting the idea of reactivation and expansion of FSP-specific T cells due to ICB treatment (Figure 39A).

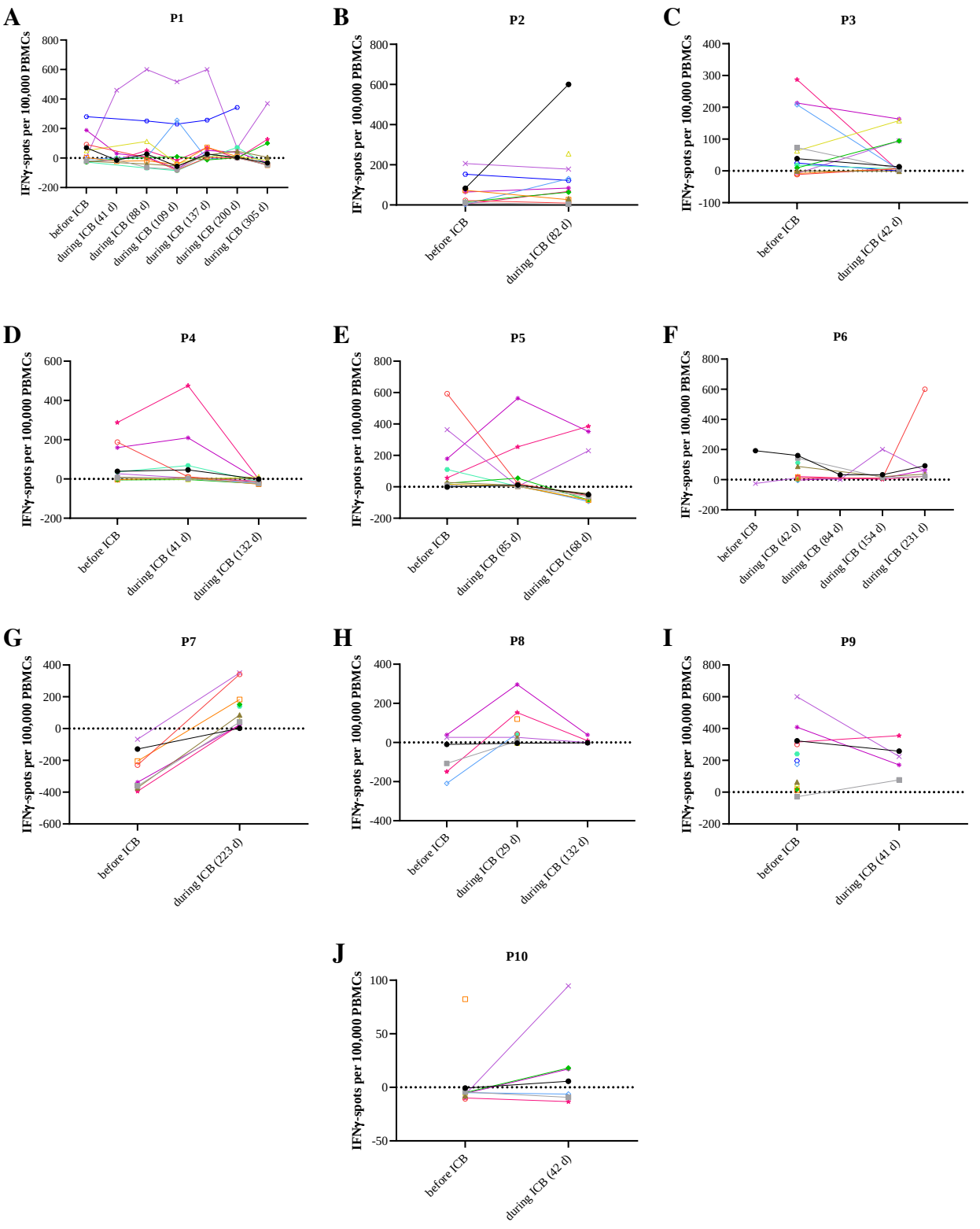
A
P1
IFNγ-spots per 100,000 PBMCs
800
600
400
200
0
-200
before ICB
during ICB (41 d)
during ICB (88 d)
during ICB (109 d)
during ICB (137 d)
during ICB (200 d)
during ICB (305 d)
B
P2
IFNγ-spots per 100,000 PBMCs
800
600
400
200
0
before ICB
during ICB (82 d)
C
P3
IFNγ-spots per 100,000 PBMCs
400
300
200
100
0
-100
before ICB
during ICB (42 d)
D
P4
IFNγ-spots per 100,000 PBMCs
600
400
200
0
-200
before ICB
during ICB (41 d)
during ICB (132 d)
E
P5
IFNγ-spots per 100,000 PBMCs
800
600
400
200
0
-200
before ICB
during ICB (85 d)
during ICB (168 d)
F
P6
IFNγ-spots per 100,000 PBMCs
800
600
400
200
0
-200
before ICB
during ICB (42 d)
during ICB (84 d)
during ICB (154 d)
during ICB (231 d)
G
P7
IFNγ-spots per 100,000 PBMCs
400
200
0
-200
-400
-600
before ICB
during ICB (223 d)
H
P8
IFNγ-spots per 100,000 PBMCs
400
200
0
-200
-400
before ICB
during ICB (29 d)
during ICB (132 d)
I
P9
IFNγ-spots per 100,000 PBMCs
800
600
400
200
0
-200
before ICB
during ICB (41 d)
J
P10
IFNγ-spots per 100,000 PBMCs
100
50
0
-50
before ICB
during ICB (42 d)
TGFBR2
CASP5
SLC35F5
TCF7L2
MARCKS
SLC22A9.1
SLC22A9.2
MYH11.1
MYH11.2
TTK
HT001
TAF1B
AIM2

Figure 39: Monitoring FSP-specific T cell responses in MSI cancer patients before and during ICB treatment. T cell responses against 13 FSPs were quantified using IFNγ ELISpot assay. Patient samples were obtained before ICB start and at several time points within the course of treatment. Varying patterns of FSP-specific T cell responses were observed for different patients (P1-P10). Several patients displayed an increase in FSP-specific T cell responses after receiving ICB treatment, potentially indicating a therapy-mediated reactivation of specific T cells. Each data point depicts the mean normalized IFNγ-spot count for the respective FSP and one time point. Each FSP is labeled in a different color and days (d) of ICB treatment are noted in the individual figures.

The response against the HT001 FSP remained stable for four months before decreasing on day 200. After 305 days of ICB treatment HT001-specific T cell responses were found to be elevated again (Figure 39A). T cell responses against the TTK FSP were at a similarly high level throughout the treatment period (Figure 39A).

Several patients (P2, P6, P7, P10) presented with an increase in T cell responses against one or multiple FSPs after starting ICB treatment (Figure 39B, 39F, 39G, 39J). P2 and P10 displayed elevated T cell responses against one FSP (TGFBR2 and HT001, respectively) within the first three months of treatment. The increase in responses against the TCF7L2 FSP in P6 was only observed after five months of ICB therapy. P7 exhibited an increase in T cell responses against all tested FSPs after 223 days of ICB treatment.

Three patients (P4, P5, P8) presented with a similar pattern of FSP-specific immune responses which was characterized by an increase in T cell responses within the first three months and a subsequent decrease of responses after approximately five months of therapy (Figure 39D, 39E, 39H).

No clear picture could be obtained for patients P3 and P9, which presented varying FSP-specific immune responses throughout ICB treatment. While T cell responses against some FSPs increased after therapy onset, responses against other FSPs decreased or remained unchanged (Figure 39C, 39I).

T cell responses against the selected FSP panel prior to ICB start and during the treatment phase were further assessed by measuring IFNγ expression using RT-qPCR. This additional analysis could be performed for five patients (P1, P2, P4, P7, P9) (Figure 40) and showed great concordance with the IFNγ ELISpot assay. Exemplarily, P1, in line with IFNγ secretion (Figure 39A), displayed a stable increase of IFNγ expression for the HT001 FSP (Figure 40A). Further, the previously observed decrease at day 200 and anew increase in HT001-specific T cell responses at day 305 (Figure 39A) were also confirmed by IFNγ RT-qPCR. Moreover, the TTK FSP was characterized by a constant IFNγ expression level for the observation period

(Figure 40A), confirming the described steady IFNγ secretion and inferred TTK-specific T cell responses (Figure 39A). Similarly coinciding patterns were observed for all analyzed patients (Figure 40). IFNγ-spot counts and IFNγ expression values were found to be significantly correlated (Spearman $r = 0.4375$, $p < 0.0001$) (Figure S22), suggesting feasibility of RT-qPCR-based T cell monitoring and an interconvertible character of IFNγ expression and IFNγ-spot results.

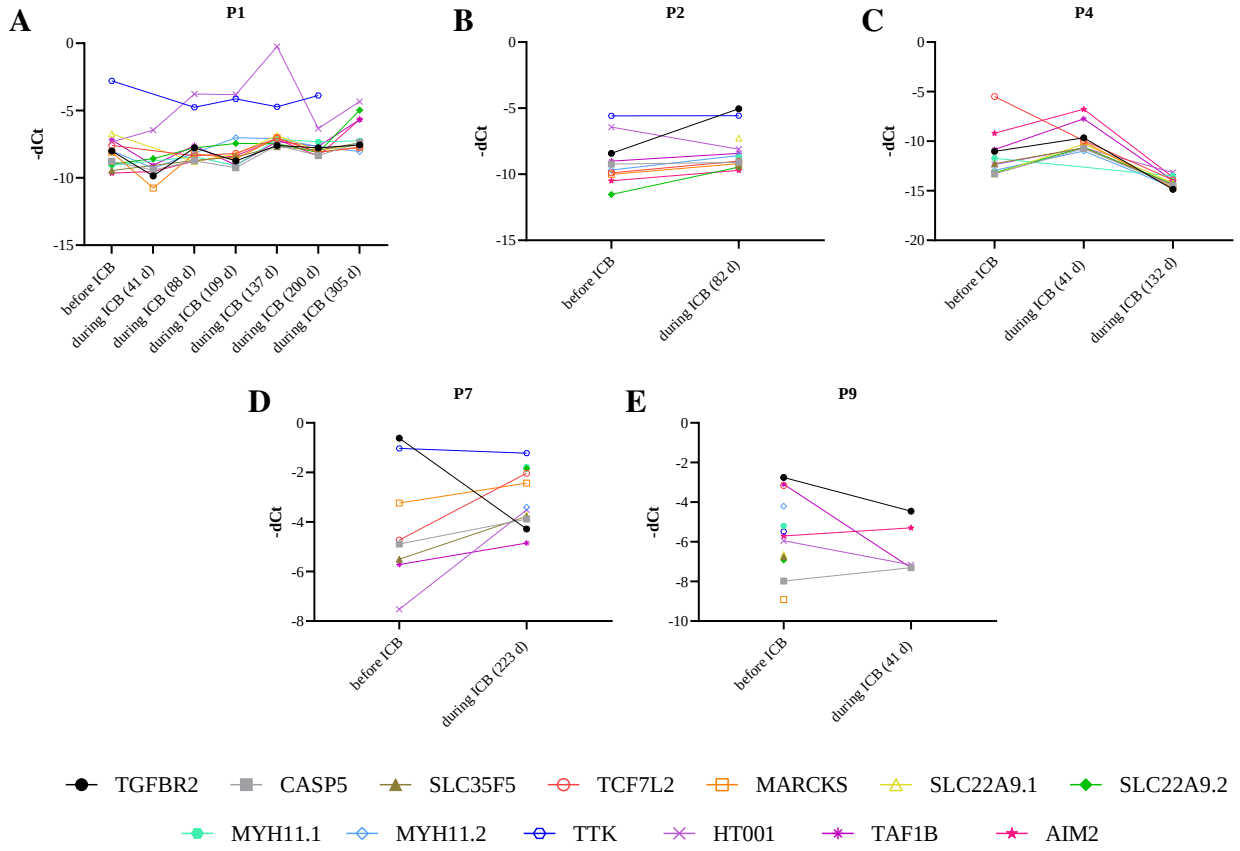

Figure 40: Monitoring FSP-associated IFNγ expression in MSI cancer patients before and during ICB therapy. Patients were analyzed individually and IFNγ expression, representing T cell activation, was assessed prior to ICB and within the course of the treatment. The observed increase in IFNγ expression for several FSPs in different patients might indicate FSP-specific T cell activation upon ICB therapy and was in concordance with the obtained IFNγ ELISpot results. Each FSP is labeled in a different color and days (d) of ICB treatment are noted in the figures.

Alterations of FSP-specific T cell responses during ICB treatment could reflect the disease course or therapy response. Thus, a potential correlation between FSP-specific T cell responses and the clinical course of MSI cancer patients undergoing ICB treatment was assessed (Figure 41). Follow-up and tumor assessment data during ICB therapy were available for seven patients. 2/7 patients presented with partial response (PR), disease stabilization (SD) was observed for 3/7 patients and two patients displayed progressive disease (PD). The first staging

after three months of treatment is still pending for one patient and the respective data could not be included in the present thesis. Overall, the median follow-up time was 7.4 months (range: 2.7–13.5 months).

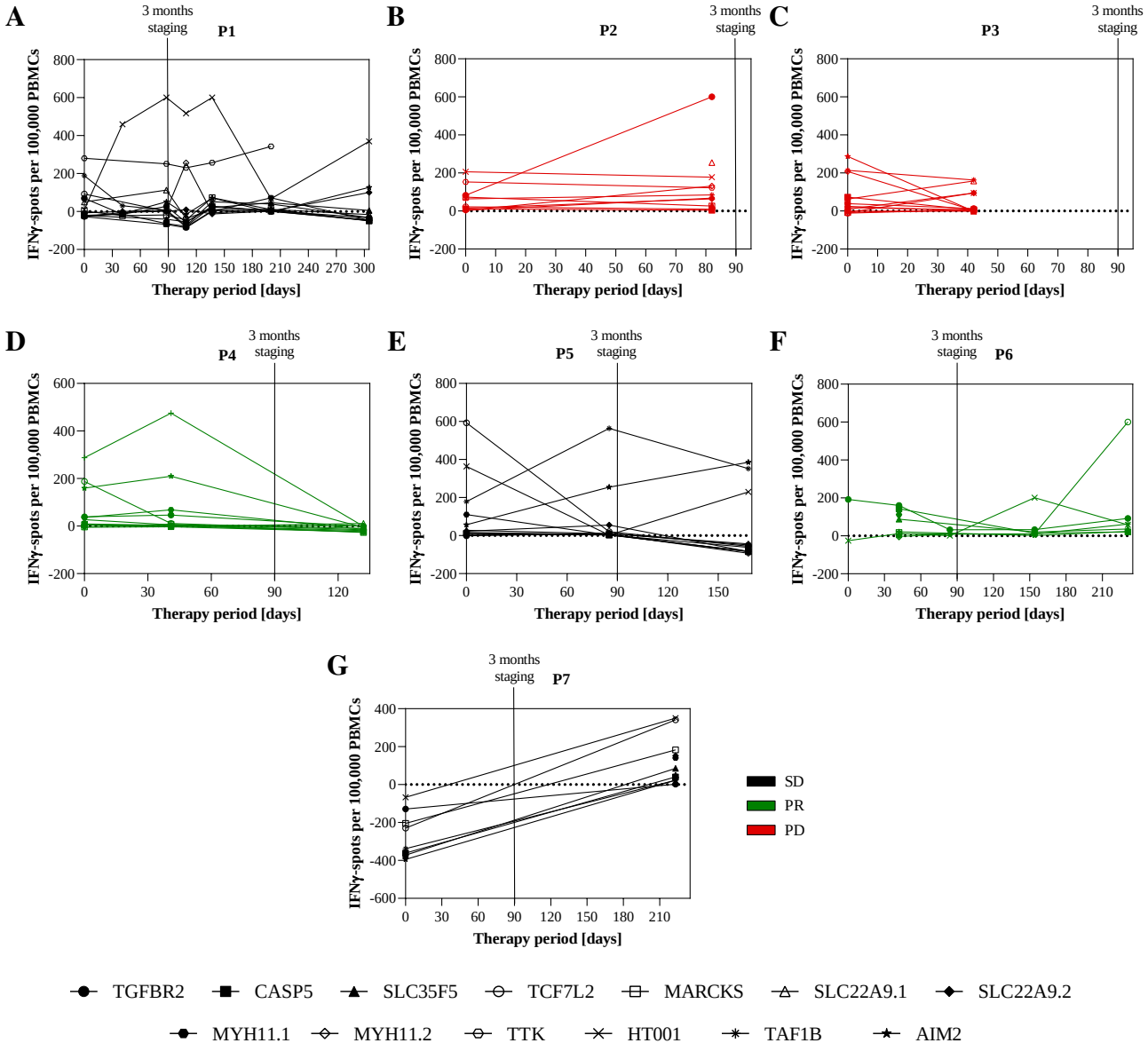

Figure 41: Correlation of FSP-specific T cell responses and the corresponding clinical course under ICB therapy. Available clinical data at the first staging after three months and FSP-specific T cell responses, determined by IFNγ ELISpot assay, are shown individually for seven patients. Overall, the conducted alignment did not yield a clear picture and therapy response or disease progression were not found to be correlated with specific T cell responses. Stable disease (SD), partial response (PR), progressive disease (PD).

The descriptive correlation did not reveal a substantial association between FSP-specific T cell responses and clinical course as neither response to ICB nor disease progression were clearly correlated with an increase or decrease in FSP-specific T cell responses. Briefly, in patient P1 an increase in HT001-specific T cell responses coincided with SD after three months of ICB (Figure 41A). P4 and P6, both displaying PR at the first staging, exhibited an increase in T cell responses against one or multiple FSPs (Figure 41D, 41F). However, the increase of immune responses in P6 was not detected until six months after treatment start. Moreover, progressive disease in P2 and P3 was not reflected by a decrease in FSP-specific T cell responses, but the respective immune responses were found to be increased or mixed (Figure 41B, 41C).

Taken together, an increase in FSP-specific immune responses against several FSPs after ICB therapy onset was observed for multiple patients, pointing towards ICB-mediated reactivation of specific T cells. However, no clear correlation between FSP-specific T cell responses and clinical therapy response or disease progression was observed. For future analyses a more rigorous patient follow-up and larger cohorts will be vital to reliably assess the predictive potential of FSP-specific T cell responses in the context of ICB therapy.

4.2.3 Correlation of host and somatic factors with FSP-specific T cell responses

The obtained data on systemic FSP-specific T cell responses in the peripheral blood of healthy LS carriers and MSI cancer patients was further explored with regards to different host and somatic factors. First, FSP-specific immune responses were correlated with the HLA type of the respective individual, accounting for a crucial host factor of neoantigen-specific immune responses. Second, specific T cell responses against the used FSPs in MSI cancer patients were correlated with the corresponding cMS mutation patterns of the underlying cancer. These additional analyses allowed a more comprehensive characterization of MSI cancers from immunological and mutational aspects.

4.2.3.1 HLA-FSP epitope binding predictions in LS carriers and MSI cancer patients

The HLA genotype is one of the most important factors determining the binding and presentation of epitopes and is a crucial aspect of specific T cell responses. Hence, HLA typing, covering HLA-A, -B and -C as well as -DRB1, -DQB1 and -DPB1, was conducted whenever possible. The binding of candidate FSP epitopes to the respective HLA types was determined by applying epitope binding prediction tools (NetMHCpan-4.1 and NetMHCIIpan-4.0). A potential correlation between the obtained epitope binding predictions and the previously described systemic FSP-specific T cell responses was descriptively assessed in a limited cohort.

HLA typing was performed for 38 individuals, including six healthy LS carriers and 32 MSI cancer patients. The majority of included cancer patients presented with CRC (78 %) and clinical characteristics are summarized in Table S10. HLA class I alleles can be distinguished in nine different supertypes which encompass alleles that share largely overlapping peptide repertoires due to similar molecular structures [312]. A classification of the identified HLA class I alleles into different supertypes allowed an initial evaluation of the HLA class I diversity in the described cohort (Figure S23). In contrast to the general German population in which A02 is the most frequent supertype (29 %), A01 was found to be the most prevalent HLA-A supertype in the analyzed cohort (ca. 30 %). Overall, the HLA-A supertype distribution in the analyzed cohort and the general population coincided adequately (Figure S23A). Moreover, B44 was the most common HLA-B supertype (30 %) in the respective cohort and higher frequencies of B27 and B44 alleles, compared to the general German population, were observed (Figure S23B). Notably, HLA-C molecules are thought to play a minor role in mediating antigen-specific T cell responses due to their limited polymorphism and low surface expression level [341] and were not included in the described analysis. HLA class II supertypes are less well studied due to the reduced availability of peptide binding data [342] and the prevalence of HLA class II supertypes was not specified within the analyzed cohort.

Epitope binding predictions for HLA-A and -B as well as -DR, covering all identified HLA types within the analyzed cohort, were obtained for the previously described FSP panel. Predicted epitopes for a specific HLA type were divided into strong binders (SB) and weak binders (WB). 'None' indicated no predicted binding epitopes for a certain FSP and HLA type, respectively. As reliable epitope predictions for HLA-DQ and -DP require typing of α- and β-chains, the respective data were not obtainable for the present thesis.
The predicted binding (SB, WB, none) of FSP epitopes to the individual's HLA type was aligned with the quantified IFNγ-spots indicating FSP-specific T cell responses. This correlation, covering HLA class I and II, could be performed for six healthy LS carriers and 15 MSI cancer patients (Table S11). Notably, samples from nine cancer patients eligible for ICB therapy were collected prior to treatment start and included in the described MSI cancer patient cohort.

In general, the used FSP panel and associated FSP epitopes indicated broad coverage of different HLA types in the analyzed cohort (Figure S24). Predicted epitope binding was only lacking for two individuals and their given HLA type. The respective analysis separate for HLA class I and II is shown in Figure S25. Further, each individual FSP was assessed regarding its predicted HLA binding epitopes in healthy LS carriers (Figure S26A) and MSI cancer patients (Figure S26B). The conducted peptide-wise correlation analysis revealed predicted SB and WB epitopes for all applied FSPs. The stratified analysis for HLA class I and II indicated that the majority of candidate epitopes bind HLA class I molecules (Figure S27).

FSP-specific immune response profiles determined over the course of ICB treatment were also correlated with the obtained epitope binding predictions (Figure S28). The increase in IFNγ-spots, indicating an ICB-mediated activation of FSP-specific T cells, was predominantly observed for FSPs harboring predicted SB and WB epitopes. The separate correlation results for HLA class I and II are shown in Figure S29.

Overall, the conducted HLA typing and the obtained epitope binding predictions for the analyzed cohort support the general suitability of the selected FSP panel. This observation indicates an efficient detection of the FSP-specific immune responses in individuals with different HLA genotypes. Consequently, the hampered presentation of the candidate FSP epitopes to the immune system due to HLA-restrictions is unlikely to explain the observed differences in FSP-specific immune responses in this cohort. However, the analysis of substantially larger cohorts is required to further examine the HLA-dependence of the used FSP panel.

4.2.3.2 Analysis of cMS mutation profiles in MSI cancers and correlation with systemic FSP-specific T cell responses

The examined FSP-specific immune responses in the peripheral blood of MSI cancer patients were further analyzed for a potential correlation with underlying cMS mutations in the respective cancer tissue. The mutation frequency of cMS, that were used as basis for the FSP selection (see 4.2.1), was determined by PCR-based fragment analysis and quantified by applying the ReFrame algorithm developed by Ballhausen et al. [79]. The obtained cMS mutation profiles, considering different indel mutation types, were correlated with the previously described IFNγ ELISpot data. Moreover, the *B2M* mutation status of the tumor was determined by Sanger sequencing to account for an important immune evasion mechanism in MSI cancers.

The cMS mutation pattern in MSI cancers was examined using 15 tumor tissue blocks from 12 different patients. The clinical characteristics of the analyzed patients are summarized in Table S12. The majority of included patients presented with CRC (n = 8), fewer patients were diagnosed with gastric (n = 3) and esophageal cancer (n = 1). Notably, seven patients of the described cohort were eligible for ICB therapy. However, samples prior to treatment start were included in the groups of MSI cancer patients and mutational analyses during the course of ICB treatment were conducted in a separate setting which is described later.

The average mutation frequencies for eleven cMS were calculated across all patient samples revealing the highest mutation rate of 39 % in the *HT001* cMS. Similarly, cMS in *SLC35F5*, *TGFBR2* and *SLC22A9* were found to be highly mutated and displayed a mutated proportion of 38 %, 35 % and 35 %, respectively (Figure 42). The *CASP5*, *TCF7L2* and *MYH11* genes displayed the lowest frequency of cMS mutations varying between 15–18 %. The mutated proportion for the remaining genes ranged between 20–30 % (Figure 42). A representative example of a cMS mutation and the respective calculated allele ratios is shown in Figure S30. Overall, the deletion of one nucleotide (-1) was the predominant indel mutation type observed across all analyzed cMS (Figure 42).

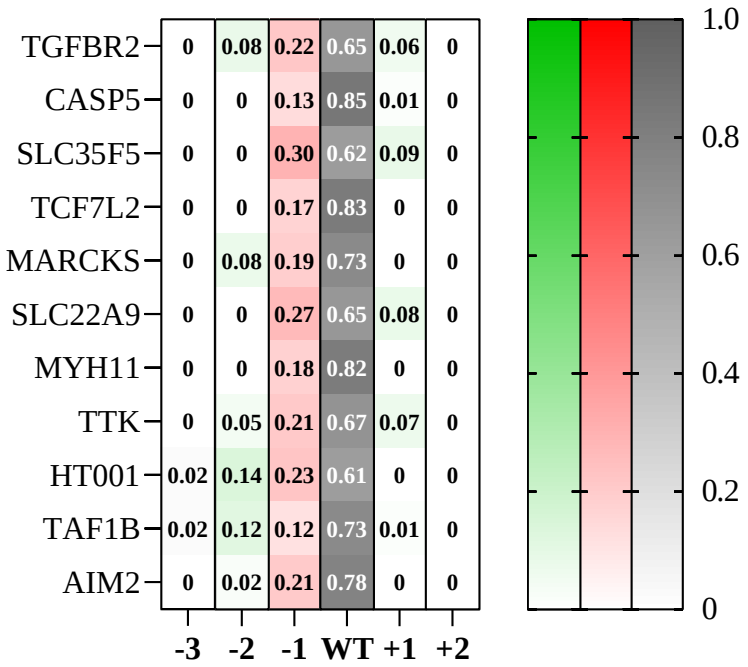

Figure 42: Average cMS mutation frequencies in MSI cancer tissue stratified for different indel mutation types. The average mutation frequency of eleven cMS in the analyzed MSI cancer patient cohort was determined by applying PCR-based fragment analysis and subsequent algorithm-based quantification [79]. Average frequencies of the different indel mutation types are given for each cMS.

The obtained cMS mutation profile for each patient was aligned with the corresponding FSP-specific T cell responses represented by IFNγ-spot counts (Figure 43). For the majority of analyzed patients (10/12) several cMS mutations were found to be associated with corresponding systemic FSP-specific immune responses in the peripheral blood. However, specific T cell responses against FSPs that were not underpinned by a mutated cMS in the respective cancer tissue were also observed in 10/12 patients.

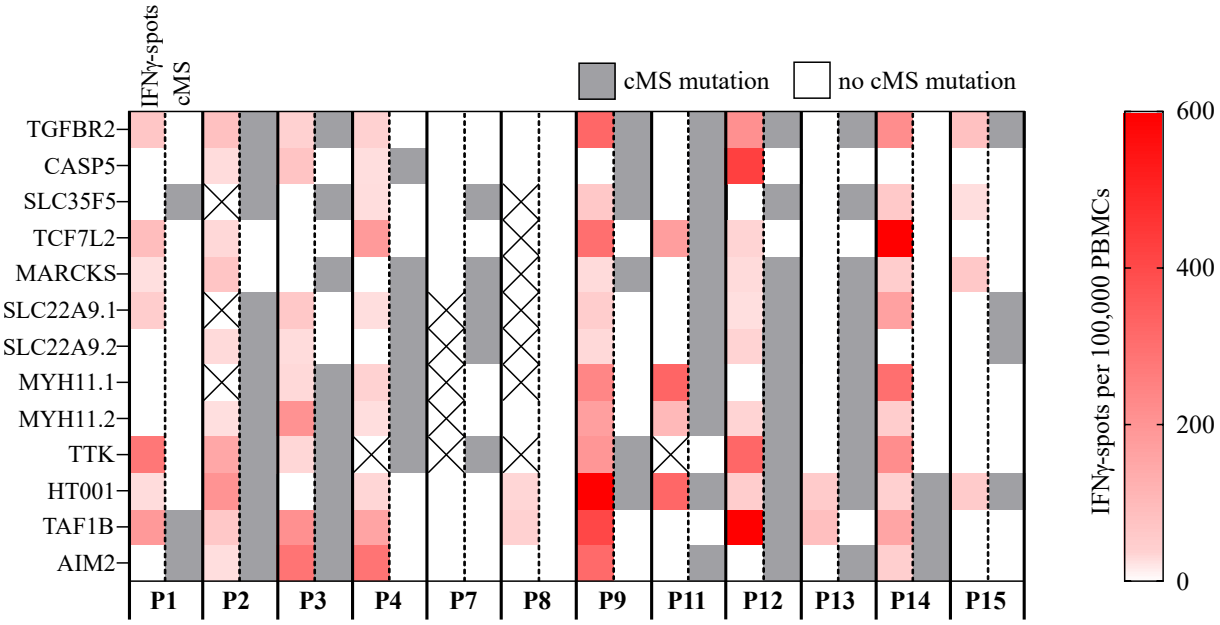

Figure 43: Correlation of FSP-specific T cell responses and corresponding cMS mutations in MSI cancer patients. Systemic FSP-specific T cell responses were aligned with cMS mutations in the underlying cancer tissue. In some cases, FSP-specific T cell responses in the blood were associated with the respective cMS mutation. In other cases, the corresponding cMS mutation to FSP-specific T cell responses was lacking. The magnitude of analyzed FSP-specific T cell responses (IFNγ-spots) is indicated for each patient by a color gradient in the left subcolumn: no responses (white) and maximal number of quantifiable IFNγ-spots (full intensity red). If no IFNγ ELISpot assay was conducted the respective FSP is marked with an X. The corresponding cMS status is provided in the right subcolumn, grey indicating a detected -1/+2 indel mutation and white no cMS mutation.

In addition to the described MSI cancer patient cohort, cMS mutations were correlated with the analyzed FSP-specific T cell responses in patients undergoing ICB therapy (Table S9). T cell responses were assessed prior to ICB therapy and at several time points during the ongoing treatment (see 4.2.2) and aligned with the corresponding cMS mutation patterns (Figure 44).

The two different observations described above were confirmed in MSI cancer patients under ICB. 6/7 patients displayed a correlating presence of a cMS mutation and T cell responses against the resulting FSP. Further, evidence for systemic FSP-specific T cell responses and the absence of corresponding cMS mutations was found in all patients (Figure 44).

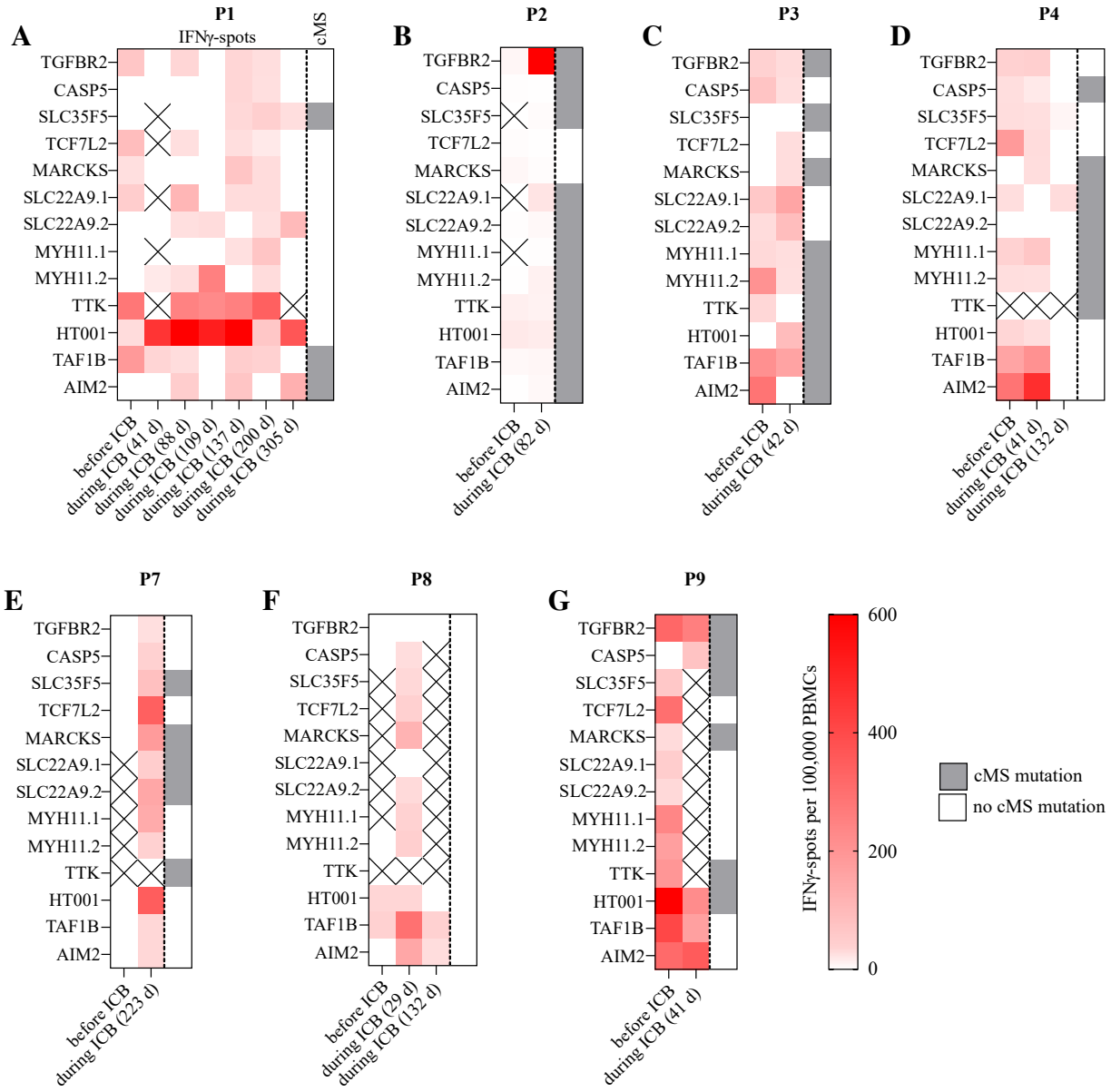

Figure 44: Correlation of FSP-specific T cell responses at different time points and corresponding cMS mutations in MSI cancer patients undergoing ICB therapy. The correlation analysis confirmed the two described observations described previously (Figure 43). The magnitude of the analyzed FSP-specific T cell responses (IFNγ-spots) is indicated by a color gradient in the left subcolumn for each patient: no responses (white) and the maximal number of quantifiable IFNγ-spots (full intensity red). If no IFNγ ELISpot was conducted the respective FSP is marked with an X. The corresponding cMS status is shown in the right subcolumn, grey indicating a detected -1/+2 indel mutation and white no cMS mutation.

Only one cancer (P15) within the analyzed cohort presented a *B2M* mutation, which precluded a reliable assessment of the impact of HLA class I antigen presentation loss in the context of systemic FSP-specific T cell responses. Further, as all patients included in the cMS mutation analysis possessed HLA types associated with predicted FSP epitope binding, no juxtaposed analysis of cMS mutations, corresponding FSP-specific immune responses and predicted FSP epitope binding could be conducted.

In summary, the analysis of cMS mutations in MSI cancer patients and the subsequent correlation with systemic FSP-specific T cell responses provided evidence for two different immunological observations. First, a mutated cMS leads to the generation of an immunogenic FSP and corresponding FSP-specific T cell responses are detectable in the peripheral blood. Second, the high immunogenicity of the produced FSP results in the elimination of cell clones harboring the respective cMS mutation.

4.2.4 Characterization of humoral FSP-specific immune responses in LS carriers and MSI cancer patients

In addition to cellular T cell responses, humoral immune responses in healthy LS carriers and MSI CRC patients were characterized by applying a peptide microarray provided by PEPperPRINT. Antibody reactivity against FSPs has already been described in serum from healthy LS carriers and MSI CRC patients [212]. However, the application of a microarray comprising an extensive number of different FSPs might be suited to further assess the diagnostic potential of humoral immune responses.

IgA and IgG antibody responses against 41 different FSPs (124 overlapping peptides), including the 13 FSPs applied for the analysis of cellular immune responses as described previously, were assessed (Table 8) [79, 81, 343]. Serum and plasma samples from 60 individuals (Table S13), including healthy LS carriers (n = 15), MSI CRC patients (n = 15), LS patients with a history of cancer (n = 15) and healthy non-LS controls (n = 15), were selected for the microarray-based analysis. The obtained microarray data were processed and analyzed applying parametric (ANOVA) and non-parametric approaches.

The parametric analysis revealed six FSPs displaying significantly different IgA antibody responses between the four groups (Figure 45). Importantly, the identified FSPs shared two common amino acid sequence motifs: VFQAERLLL and PGRKTCTPE. Four of these peptides were associated with significantly higher IgA responses in healthy controls, compared to MSI CRC patients and LS individuals with a history of cancer (Figure 45A, 45B, 45D, 45E). IgA responses against the LEGLEDVELLKMQMV (MYH11.1) FSP were found to be significantly elevated in healthy LS carriers, compared to the LS and MSI cancer groups (Figure 45C).

The non-parametric analysis of the microarray data identified eight FSPs with significantly different IgA responses between the groups (Figure 46). Two of those FSPs have already been identified in the described ANOVA (WPEDTYPGRKTCTPE (FLJ25378 (-2)_B) and LEGLEDVELLKMQMV (MYH11.1)) (Figure 45). The remaining six FSPs displayed overall low fluorescence intensity and did not yield a clear picture (Figure 46).

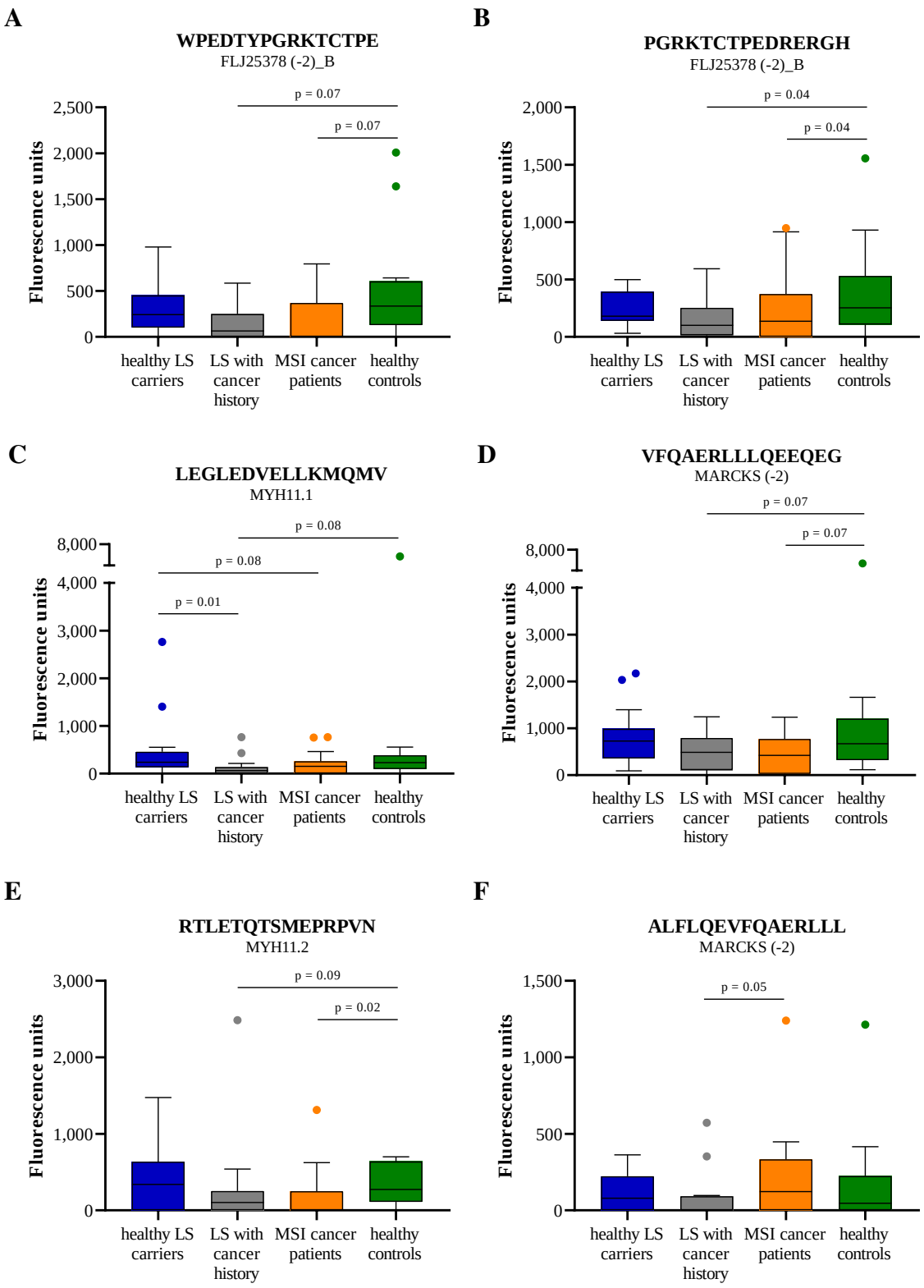

Figure 45: IgA antibody responses against relevant FSPs identified by ANOVA. (A-F) Six FSPs which presented significant differences between the four analyzed groups were identified by ANOVA. The background-corrected median intensities in fluorescence units are indicated on the y-axis. The amino acid sequence of each peptide is given in the respective figure. The adjusted p-values for the conducted ANOVA (FDR < 10 %) are provided in the individual figures.

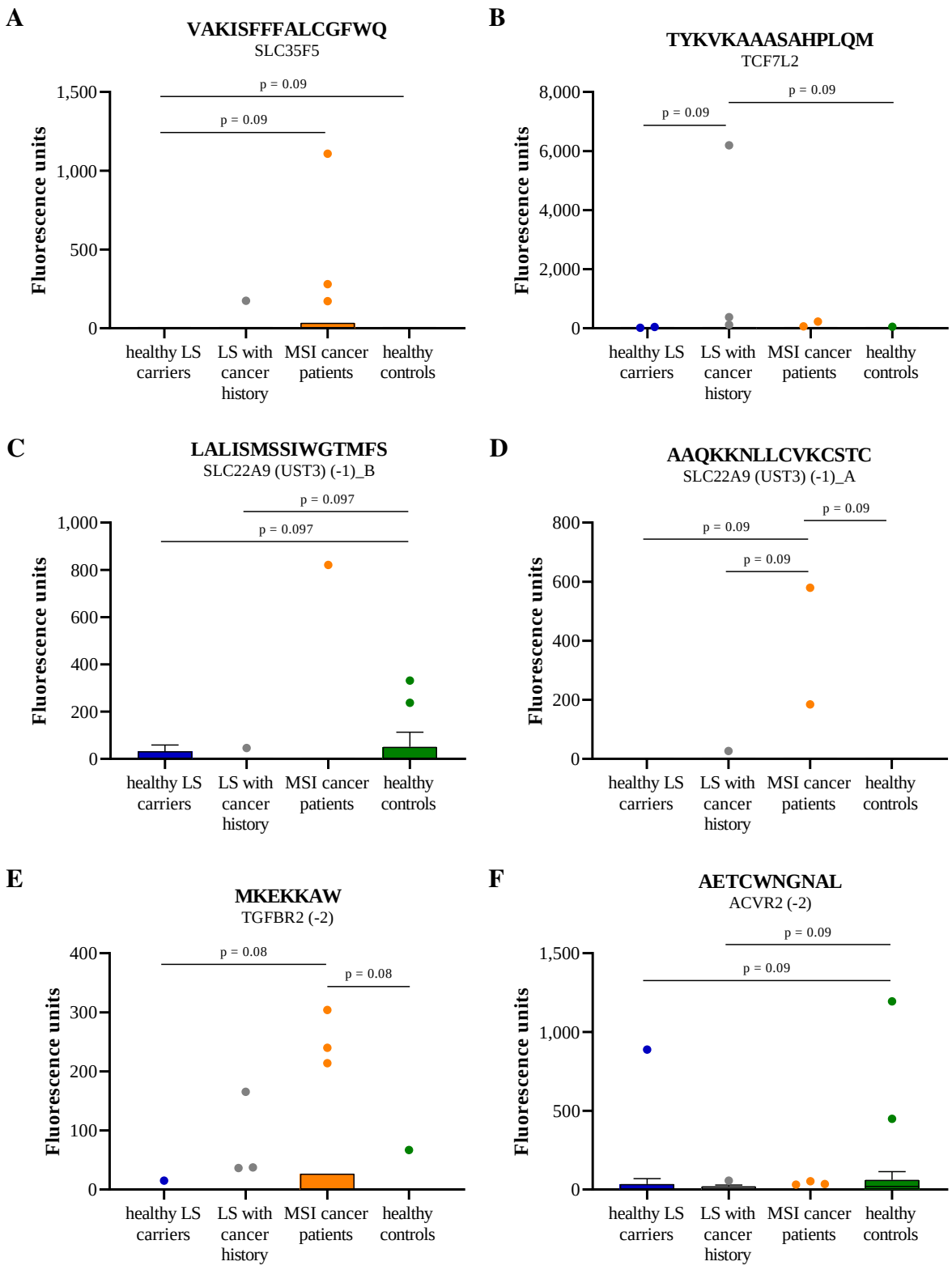

Figure 46: IgA antibody responses against relevant FSPs identified by non-parametric analysis. (A-F) Six FSPs which presented significant differences between the four analyzed groups were identified non-parametrically. Two additional FSPs (WPEDTYPGRKTCTPE (FLJ25378 (-2)_B) and LEGLEDVELLKMQMV (MYH11.1)) have already been identified by ANOVA (Figure 45A, 45C). The background-corrected median intensities in fluorescence units are indicated on the y-axis. The amino acid sequence of each peptide is given in the respective figures. The adjusted p-values for the performed post hoc Dunn's test are provided.

The detected IgG antibody reactivity was also assessed applying parametric and non-parametric strategies, identifying a total of six FSPs with significantly different IgG responses. Applying ANOVA three FSPs with differential IgG responses could be identified (Figure 47). Notably, no shared sequence motifs could be observed in these peptides. Two of the FSPs (KAKKKHREVKRTNSS (AIM2) and LEGLEDVELLKMQMV (MYH11.1)) displayed the highest IgG response in healthy LS carriers, reaching statistical significance compared to MSI CRC patients and LS patients with a history of cancer, respectively (Figure 47A, 47B). Moreover, LEGLEDVELLKMQMV (MYH11.1) has already been found to display significantly elevated IgA antibody responses in healthy LS carriers (Figure 45C).

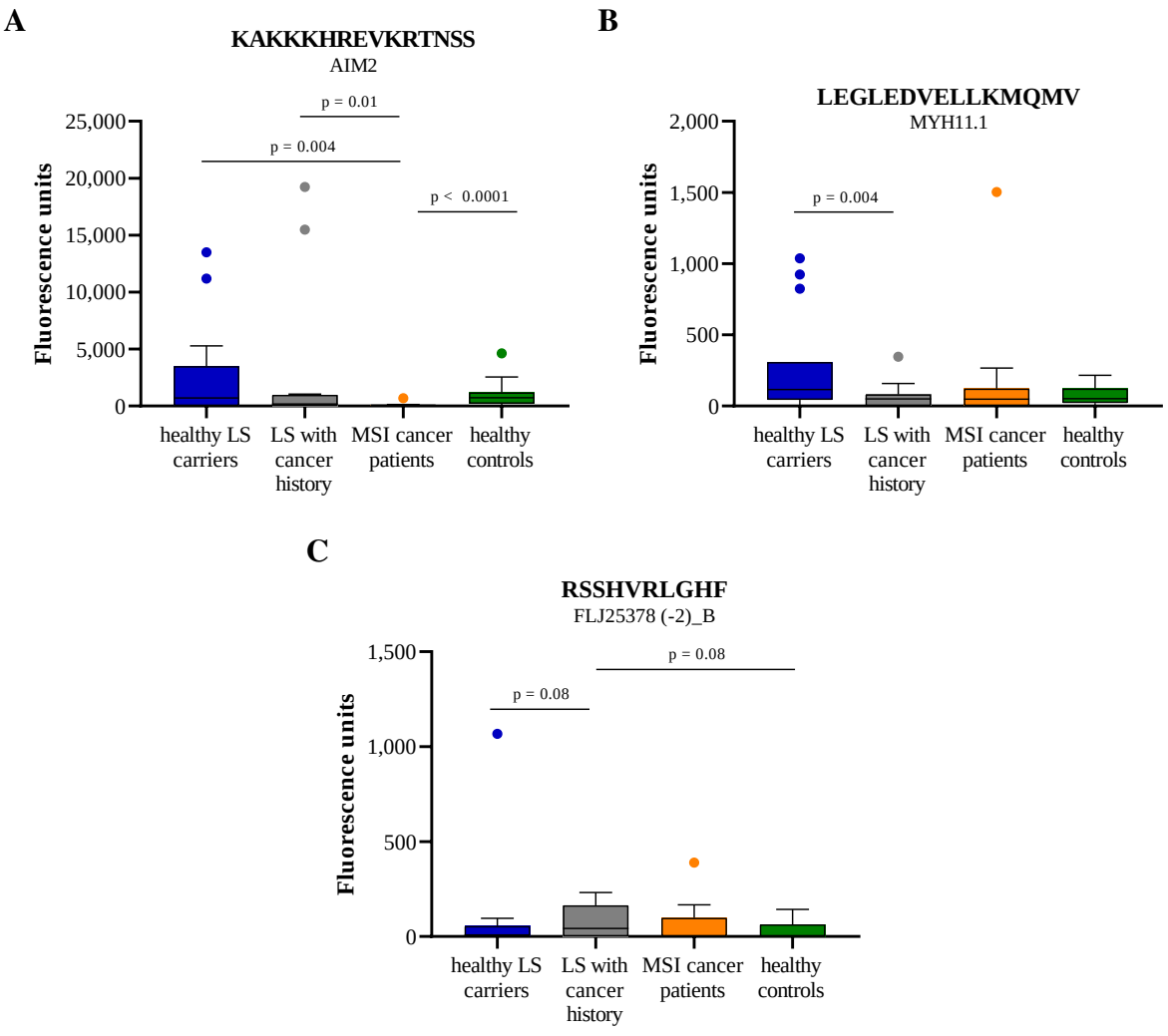

Figure 47: IgG antibody responses against relevant FSPs identified by ANOVA. (A-C) Three FSPs which presented significant differences between the four analyzed groups were identified by ANOVA. The background-corrected median intensities in fluorescence units are indicated on the y-axis. The amino acid sequence of each peptide is given in the respective figures. The adjusted p-values for the conducted ANOVA (FDR < 10 %) are provided in the individual figures.

Using the non-parametric approach, six FSPs with significantly different IgG responses between the analyzed groups could be identified (Figure 48). Three of these FSPs have already been found by the parametric analysis described above (KAKKKHREVKRTNSS (AIM2), LEGLEDVELLKMQMV (MYH11.1) and RSSHVRLGHF (FLJ25378 (-2)_B)) (Figure 47).

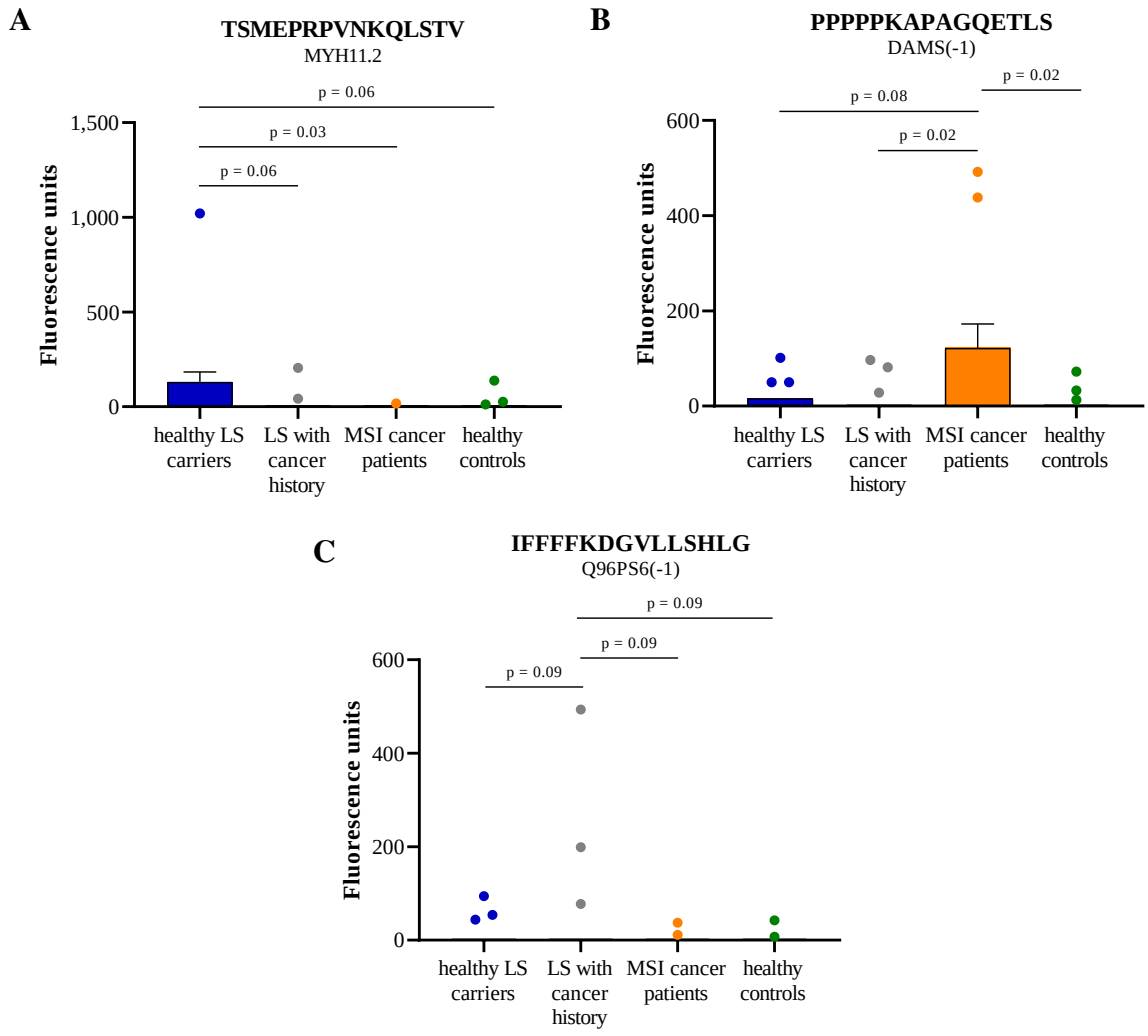

Figure 48: IgG antibody responses against relevant FSPs identified by non-parametric analysis. (A-C) Three FSPs which presented significant differences between the four analyzed groups were identified non-parametrically. Additionally, three FSPs (KAKKKHREVKRTNSS (AIM2), LEGLEDVELLKMQMV (MYH11.1) and RSSHVRLGHF (FLJ25378 (-2)_B)), that have already been identified by ANOVA (Figure 47), were associated with significantly different IgG responses between the groups. The background-corrected median intensities in fluorescence units are indicated on the y-axis. The amino acid sequence of each peptide is given in the respective figures. The adjusted p-values for the performed post hoc Dunn's test are provided.

The IgG antibody responses against the three remaining FSPs displayed low fluorescence intensity. However, the TSMEPRPVNKQLSTV (MYH11.2) FSP was associated with significantly higher IgG responses in healthy LS carriers, compared to both cancer groups and healthy non-LS controls (Figure 48A). In addition, the measured IgG responses against PPPPPKAPAGQETLS (DAMS (-1)) were predominantly observed in MSI cancer patients, reaching statistical significance compared to all other groups (Figure 48B).

Overall, the analysis of FSP-specific humoral immune responses in serum and plasma samples from LS individuals and MSI CRC patients enabled the identification of several FSPs potentially suited for diagnostic purposes.

4.3 Exploration of plasma-derived EVs for MSI detection

4.3.1 EV-based determination of the MSI status in cancer patients prior to ICB therapy

Extending beyond FSP-specific immune responses and their potential clinical use (see 4.2), the suitability of EVs to serve as source of circulating tumor DNA for MSI analysis was assessed. EVs are not only involved in various aspects of carcinogenesis, they also reflect the status of their parental cell and can carry cancer-associated cargo, including DNA. Importantly, EVs can be easily isolated from different bodily fluids, such as plasma [277, 287].
A hallmark of MSI cancers is the accumulation of indel mutations in microsatellite sequences [65] and the resulting MSI phenotype can be confirmed by PCR-based fragment analysis. Determining MSI via EV-transported DNA could possibly enable long-term, minimally invasive monitoring of MSI cancer patients and bear potential for various clinical aspects.

Plasma samples from MSI cancer patients and healthy controls were used first to optimize the isolation of EVs and second to evaluate the applicability of vesicular DNA for MSI analysis. EVs from plasma were isolated using two different approaches: differential ultracentrifugation and PEG-based precipitation. The presence and morphology of EVs in the obtained preparations were assessed by TEM. The typical cup-shaped morphology, described for EVs observed by TEM [344], could be confirmed for ultracentrifugation- and precipitation-based isolation (Figure 49A, 49B). Additionally, NTA analysis enabled the evaluation of the size distribution of isolated EVs. The plasma-derived particles' diameter ranged between 25–150 nm (Figure 49C).

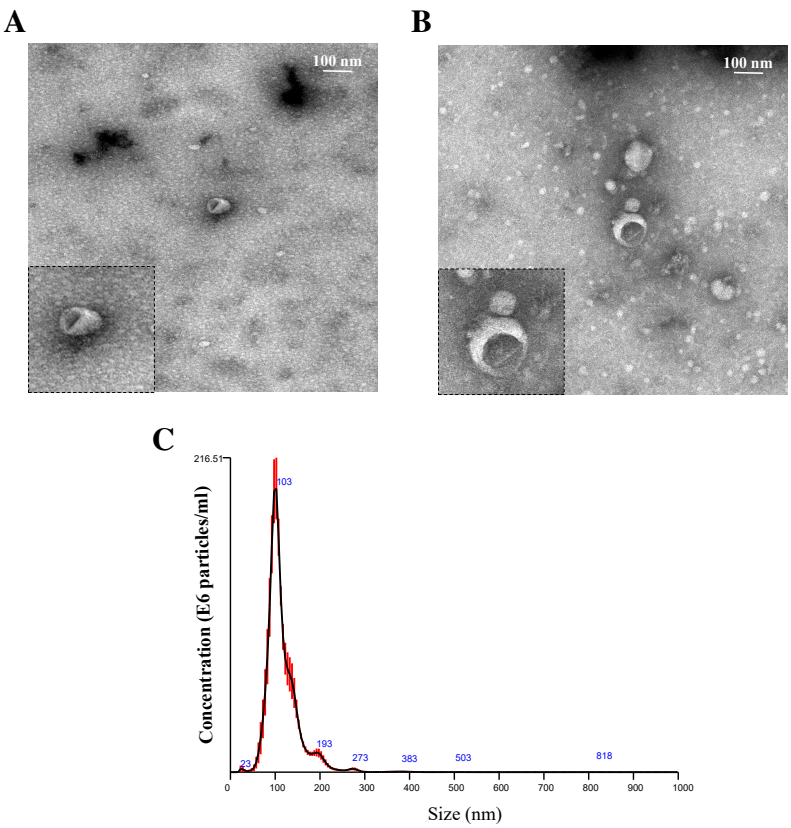

Figure 49: Characterization of plasma-derived EVs. Visualization of plasma EVs with TEM revealed the expected cup-shaped morphology for both isolation approaches: ultracentrifugation (A) and precipitation (B). (C) The diameter of isolated particles ranged between 25–150 nm and was determined through NTA measurement. The provided TEM and NTA results are representative for several independent analyses.

The successful isolation and characterization of EVs from human plasma enabled a preliminary analysis of the MSI phenotype in EV DNA from stage IV MSI cancer patients undergoing ICB therapy (n = 15). The analyzed cohort mostly consisted of MSI CRC patients (n = 13) and included a smaller number of gastric cancer patients (n = 2) (Table S14). For each patient multiple plasma samples were obtained at different time points before and during ICB treatment. Additionally, plasma samples from healthy controls were included and served as MSS controls (Table S14).

Isolated vesicular DNA from PEG-precipitated plasma EVs was subjected to fragment analysis and whole blood DNA from each individual was included serving as a normal tissue control and aiding the evaluation of allele shifts. The obtained fragment analysis results for four non-coding MSI markers (BAT25, BAT26, CAT25 and BAT40), which are routinely used for MSI diagnostics, were assessed and the vesicular MSI status was determined. Crucially, the experiment was conducted blinded and information on the analyzed individuals was only provided after complete assessment of the MSI status.

A total of 70 plasma samples from 15 MSI cancer patients receiving ICB therapy and 24 healthy controls were processed and analyzed as described. The EV DNA from the 24 healthy controls was found to be stable in all four microsatellite markers (exemplary: Figure 50A, 50B, 50C, 50D). 15 EV DNA samples from nine different MSI cancer patients displayed shifts and varying allele lengths in at least one of the four markers (exemplary: Figure 50E, 50F, 50G, 50H). Overall, the MSI status could be correctly determined in 60 % (9/15) of cancer patients using vesicular DNA from plasma-derived EVs.

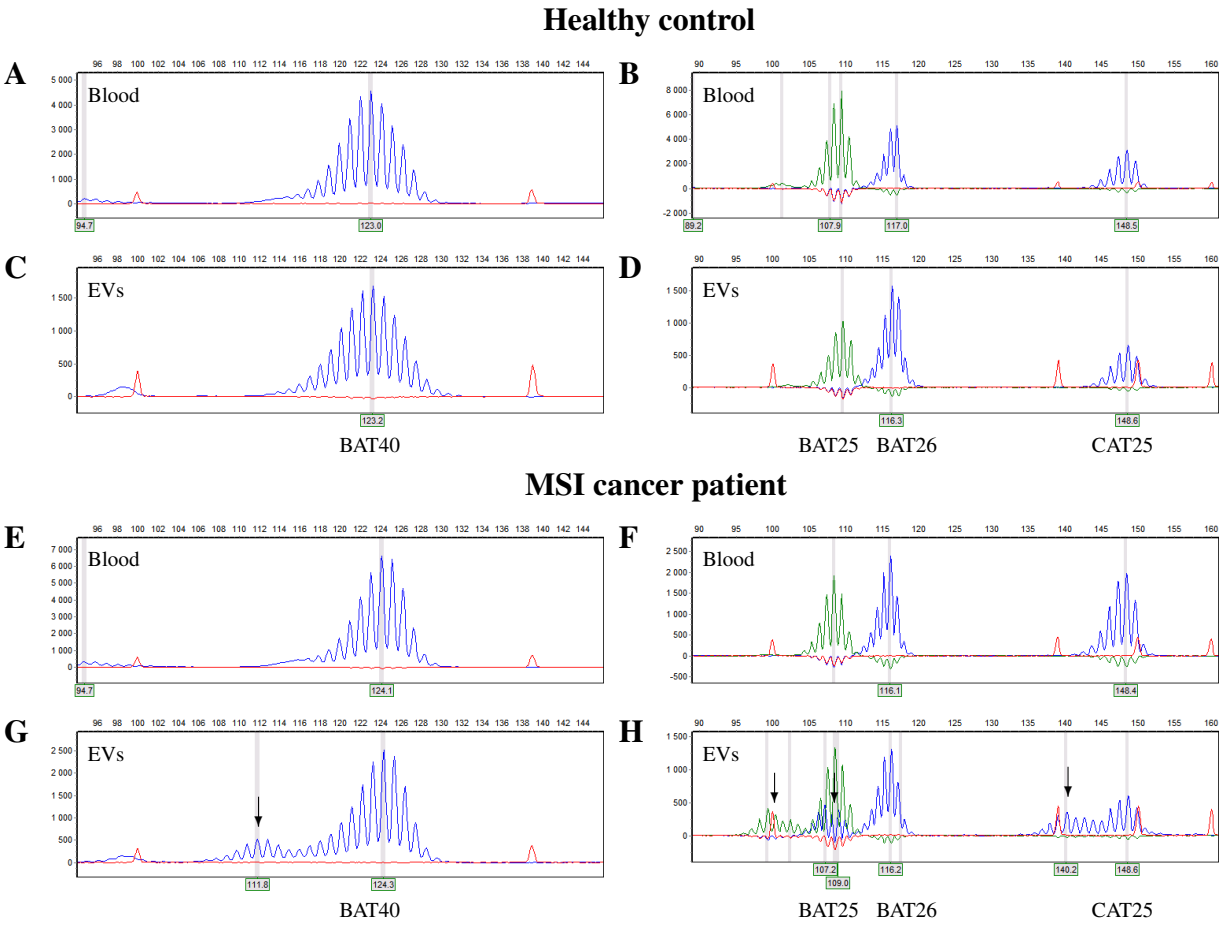

Figure 50: MSI fragment analysis of vesicular DNA from plasma-derived EVs. DNA was isolated from plasma EVs and corresponding whole blood samples serving as a normal tissue control. The obtained allelic profiles for BAT40, BAT25, BAT26 and CAT25 were compared between blood and EV samples. BAT25, BAT26 and CAT25 were analyzed in a multiplex PCR, BAT40 was assessed individually. (A-D) Representative electropherograms of healthy controls which all presented with non-MSI vesicular DNA. (E-H) Representative electropherograms of EV DNA from MSI cancer patients, 9/15 patients displayed MSI in at least one microsatellite marker. The amplicon length in base pairs (bp) is indicated on the top of each figure, the fluorescent signal intensity is provided on the left. The different MSI markers are labeled accordingly.

The allelic shifts in the MSI marker panel observed in vesicular DNA were compared to the allelic changes in the corresponding MSI cancer tissue. Importantly, the patterns of plasma EVs and cancer tissue derived from the same patient coincided well, indicating tumor origin of the isolated vesicles (representative examples: Figure 51).

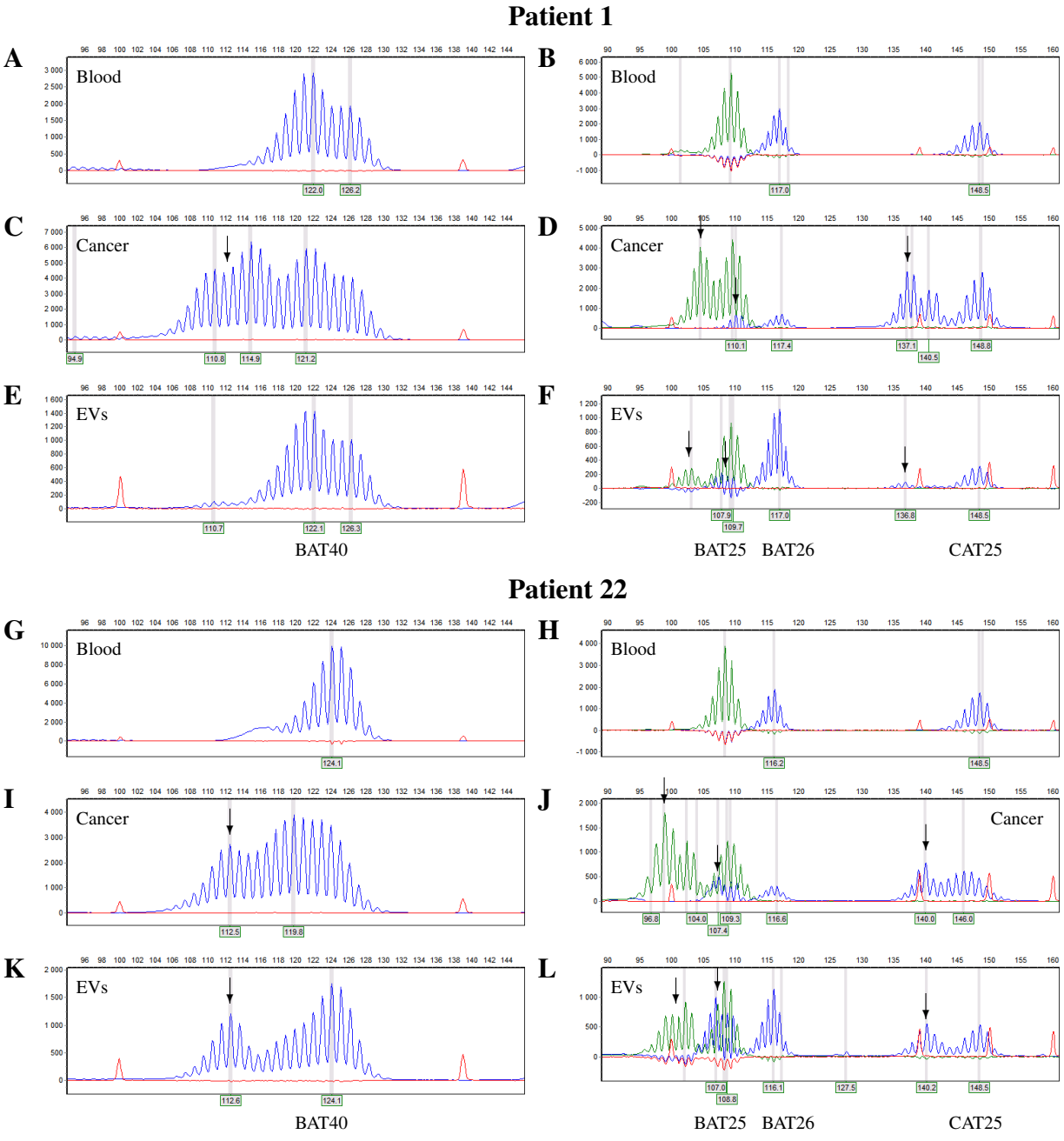

Figure 51: Similar allelic patterns of non-coding MSI markers in plasma-derived EVs and corresponding cancer tissue. MSI analysis was performed using vesicular DNA from plasma EVs and DNA from the underlying MSI cancer. The observed shifts and varying allele lengths coincided between vesicular DNA and cancer tissue, supporting the proposed tumor origin of plasma EVs. DNA from whole blood, displaying MSS, was used as normal tissue control. The amplicon length in bp is indicated on the top of each figure, the fluorescent signal intensity is provided on the left. The different MSI markers are labeled accordingly.

As plasma samples from different time points before and during ICB treatment were analyzed, the EVs' MSI status was correlated with the patients' clinical course (Figure 52). The MSI phenotype was most reliably detected prior to ICB therapy. Using plasma-derived EVs the MSI status was correctly determined before treatment onset in 6/7 cases.

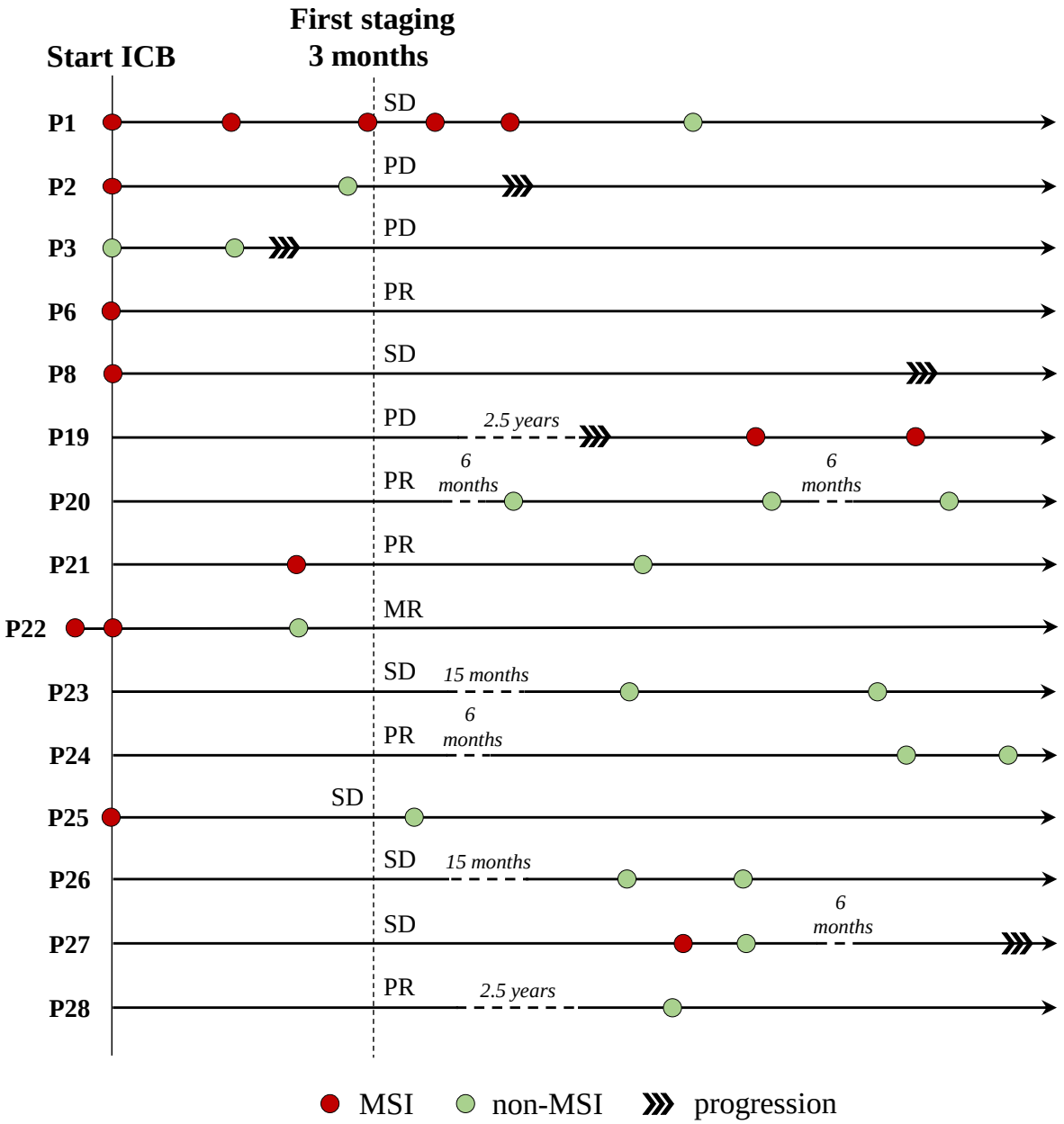

Figure 52: Correlation of the EV MSI status and clinical course of MSI cancer patients under ICB therapy. Assessment of the MSI status in EV DNA was performed at different time points before and during ICB therapy. The MSI phenotype was correctly identified prior to ICB treatment in 6/7 patients. The vesicular MSI status for each patient is indicated on the timeline. MSI/non-MSI is represented by red/green coloring. Disease assessment after three months of ICB therapy and time point of disease progression are also provided for each patient. Stable disease (SD), partial response (PR), progressive disease (PD), mixed response (MR).

Patient P3 was the only case in which MSI could not be observed in vesicular DNA prior to and shortly after therapy start. Plasma from patients in which the MSI status could not be determined using vesicular DNA was mostly sampled more than six months after starting ICB therapy. Further, patient P19 presented with the MSI phenotype in vesicular DNA shortly after disease progression. These findings could potentially indicate a correlation between the EVs' MSI status and cancer burden.

Moreover, plasma-derived EV DNA from various time points during ICB therapy was found to differ in its MSI status (Figure 52). Four patients (P1, P2, P22, P25) displayed the MSI phenotype in plasma-derived EVs before starting ICB therapy, which then disappeared with advancing treatment and could not be identified after several months. In P1, P22 and P25 the described change in the vesicular MSI status was associated with either SD or mixed response (MR) under ICB therapy. Representative electropherograms of P1 and P22, illustrating the change in the four used MSI markers during ICB therapy, are shown in Figure 53. In P2 non-MSI EV DNA was observed shortly before disease progression.

A subset of EV preparations from MSI cancer patients was treated with DNase I removing all external, surface-bound DNA and therefore enabling the isolation of solely intravesicular DNA. Importantly, the previously observed allelic shifts could also be detected in DNase-treated EVs, demonstrating that plasma-derived EVs carry DNA cargo in their lumen reflecting the MSI status of the parental cancer cell (Figure S31).
Additionally, the required volume of human plasma for reliably determining the MSI status using vesicular DNA was tested. All previously described experiments were standardly preformed with 1 ml of plasma. A potential reduction of the plasma volume might facilitate future clinical applications and different plasma volumes (500 µl, 250 µl, 125 µl) were tested. Allelic shifts in the MSI marker panel were observed in all preparations and as low as 125 µl of plasma (Figure S32).

Lastly, the presence of canonical driver mutations (*BRAF* and *KRAS*) in vesicular DNA was examined in patients presenting with an accordingly mutated tumor. The verification of such driver mutations in the EV cargo would support the proposed tumor origin of EVs presenting the MSI phenotype and might bear some clinical potential. For that purpose, DNA from cancer tissue and plasma EVs was isolated and *BRAF*/*KRAS* mutations were investigated by Sanger sequencing.

EVs from five cancer patients with a confirmed *BRAF* V600E mutation and two patients with a *KRAS* G12D mutation were subjected to further mutational analysis.

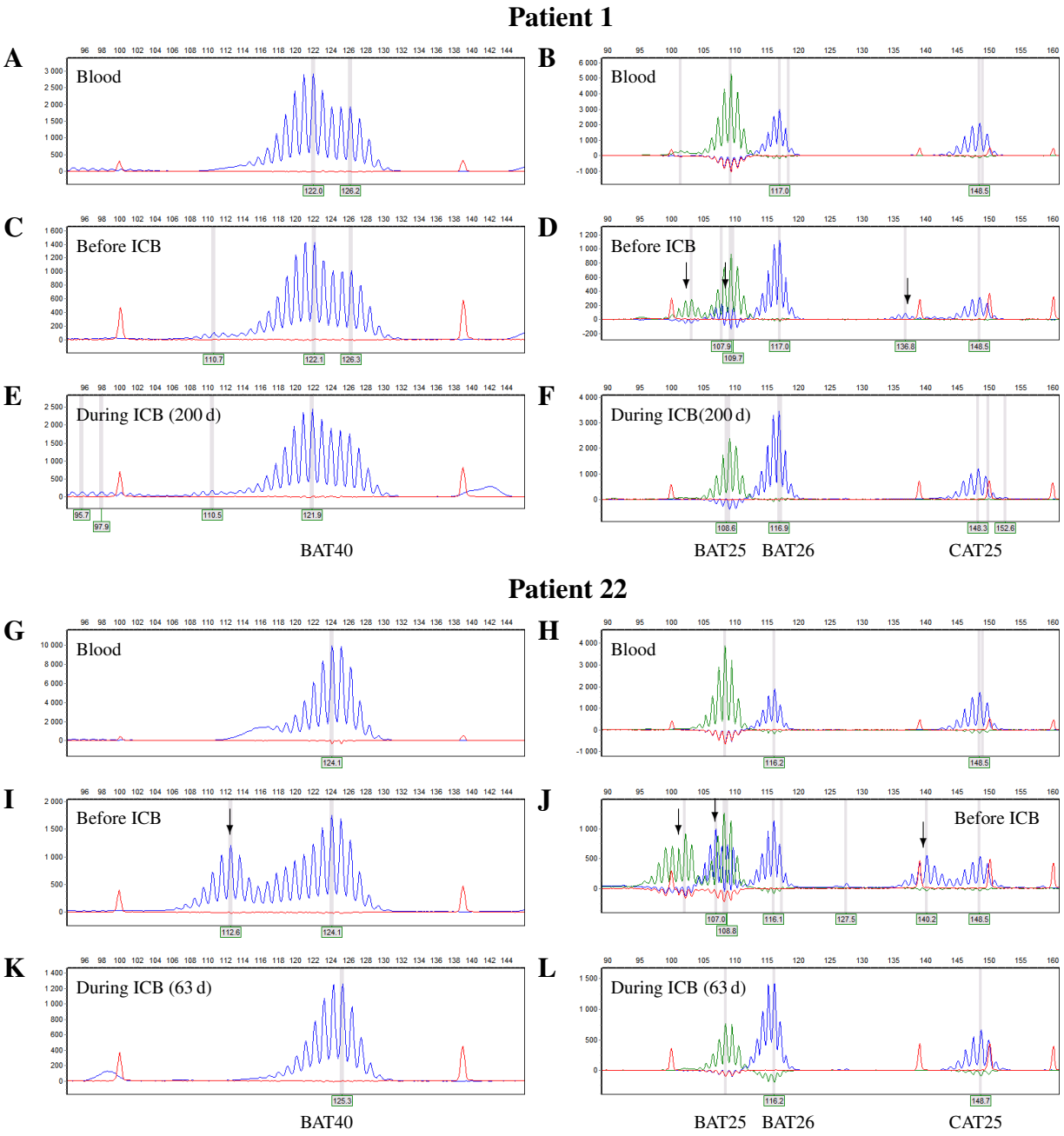

Figure 53: Changes in the vesicular MSI status of cancer patients during ICB therapy. DNA from plasma-derived EVs was examined for MSI in four markers at different time points before and during ICB therapy. Patients P1 (A-F) and P22 (G-L) displayed allelic length variations before starting ICB therapy. After 200 and 63 days of ICB therapy, respectively, no MSI-associated allelic shifts could be observed. DNA from whole blood, displaying MSS, was used as normal tissue control. The amplicon length in bp is indicated on the top of each figure, the fluorescent signal intensity is provided on the left. The different MSI markers are labeled accordingly.

Importantly, the relatively small amount of vesicular DNA did not hamper the applied Sanger sequencing protocol and sufficient signal intensities could be obtained for *BRAF* (Figure 54A) and *KRAS* (Figure 54B). However, none of the analyzed EV preparations displayed the respective mutation (Figure 54). This observation might suggest insufficient technical sensitivity.

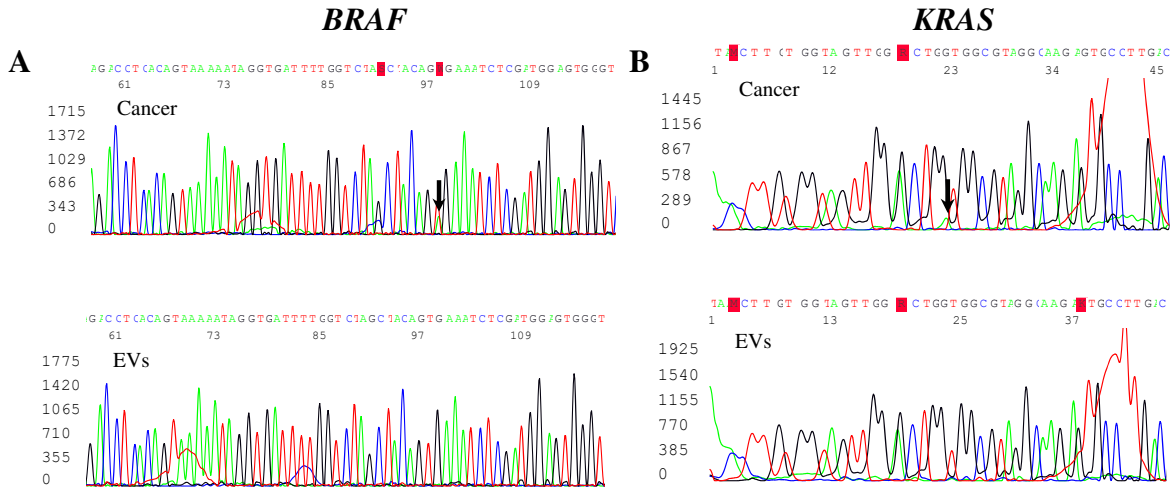

Figure 54: *BRAF* V600E/*KRAS* G12D mutation analysis in plasma-derived vesicular DNA from MSI cancer patients. Plasma EVs from patients presenting with a *BRAF*- (A) or *KRAS*-mutated (B) MSI cancer were assessed for the respective mutation. No mutations could be detected in vesicular DNA. The strength of the fluorescent signal is provided on the left. Called nucleotides and their position are labeled above each sequence.

In summary, EVs from human plasma were successfully isolated using differential ultracentrifugation and PEG-based precipitation. The suitability of the applied isolation protocols was confirmed by characterization of the particles' morphology and size. Importantly, the MSI phenotype was identified in plasma-derived vesicular DNA from MSI cancer patients under ICB therapy. Coinciding allelic patterns underpinned the vesicles' tumor origin. Further, the vesicular MSI status was found to change during the course of ICB treatment, suggesting a link between MSI detectability in EVs and cancer burden as well as a suitability of plasma-derived EVs in therapy monitoring.

4.3.2 Establishment of an enrichment strategy for A33-positive, colon-specific EVs

The enrichment of EVs from a particular organ system could potentially enable a more sensitive analysis of the MSI status and other cancer-associated biomarkers in plasma-derived vesicles. The glycoprotein A33 was selected as a possible candidate for the enrichment of colon-derived EVs. A33 is highly expressed in normal colonic epithelium and in over 95 % of CRCs [345]. IHC staining of exemplary normal colonic mucosa and MSI CRC tissue of the analyzed cohort (Table S14) confirmed the described expression of A33 (Figure 55).

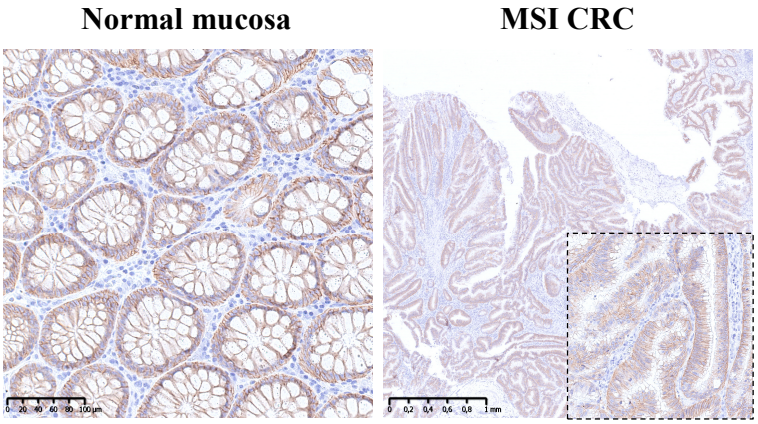

Figure 55: Representative IHC staining of A33 in normal colonic mucosa and MSI CRC. The expression of the glycoprotein A33 was confirmed in exemplary normal colonic mucosa and MSI CRC tissue. Normal mucosa: 20 x magnification, MSI CRC: 1.25 x and 20 x magnification.

An immunoaffinity-based EV enrichment strategy targeting A33 was established using EVs isolated from the MSI CRC cell line LIM1215, which is known to express high levels of A33 [346]. The use of EVs obtained from cell culture supernatant enabled the methodological establishment in a less complex setting and the optimization of various parameters. LIM1215 EVs isolated by PEG-based precipitation were characterized by TEM and NTA analysis (Figure 56) and used for all following experiments. Two different immunoprecipitation (IP) approaches using superparamagnetic beads were successfully established in the cell culture setting.

First, immunoaffinity-based capture of A33-positive LIM1215-derived EVs applying protein G magnetic beads could be confirmed by western blot analysis (A33: 45 kDa; Figure 57). The conducted western blot analysis also revealed the IgG heavy chain of the anti-A33 capture antibody at around 55 kDa, which could hamper the reliable detection of A33 at a similar size. Hence, the anti-A33 antibody was chemically linked to the protein G-coated beads using a DMP crosslinker, thereby avoiding the elution of the capture antibody during IP. DMP-mediated crosslinking did not impact the specificity of the anti-A33 antibody and A33-positive EVs could be efficiently captured (Figure 57).

Second, the enrichment of A33-positive EVs was conducted using streptavidin-coated magnetic beads. For that purpose, the anti-A33 capture antibody was biotinylated using a NHS reagent and effective biotinylation was confirmed by ELISA (Figure S33). Successful capture of A33-positive EVs could be confirmed by western blot (Figure 57).

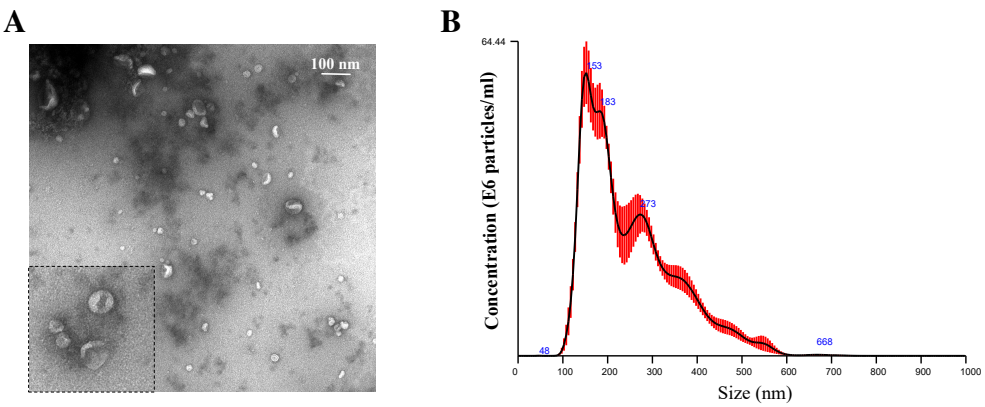

Figure 56: Characterization of LIM1215-derived EVs. EVs were isolated from LIM1215 cell culture supernatant applying PEG-based precipitation. (A) TEM analysis revealed the typical cup-shaped morphology of EVs. (B) The size distribution of isolated particles was determined by NTA analysis and the EVs' diameter ranged between 50–250 nm. The provided TEM and NTA results are representative for several independent analyses.

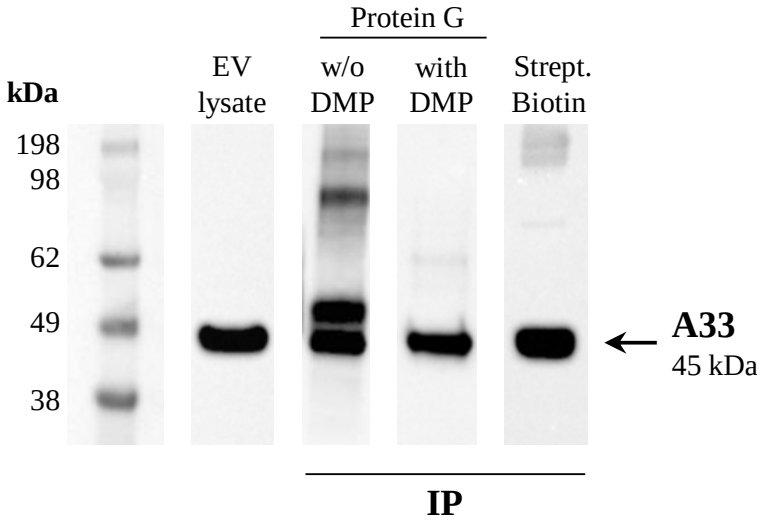

Figure 57: Immunoaffinity-based capture of A33-positive LIM1215-derived EVs. EVs were isolated from LIM1215 cells and A33-positive particles were enriched by IP. An A33 protein band at 45 kDa could be obtained for both IP strategies: protein G-coupled beads and streptavidin (Strept.)-coated beads in combination with a biotinylated anti-A33 antibody. Chemically crosslinking the anti-A33 antibody to the magnetic beads abolished the protein band of the capture antibody's heavy chain at 55 kDa. 20 µg protein lysate from the A33-positive LIM1215 cell line was used as positive control. All EV preparations were obtained from 136 ml cell culture medium. w/o: without.

The applicability of immunoprecipitated EVs for planned downstream analyses, particularly PCR-based fragment analysis for determination of the MSI status, was evaluated. Captured A33-positive EVs were eluted from the magnetic beads and isolated vesicular DNA was subjected to fragment analysis covering the described MSI marker panel (BAT40, BAT25, BAT26 and CAT25). Importantly, the MSI phenotype, characteristic for the LIM1215 cell line,

was observed in immunoprecipitated LIM1215-derived EVs. The obtained allelic patterns coincided well between the parental cell line and corresponding vesicular DNA (Figure 58).

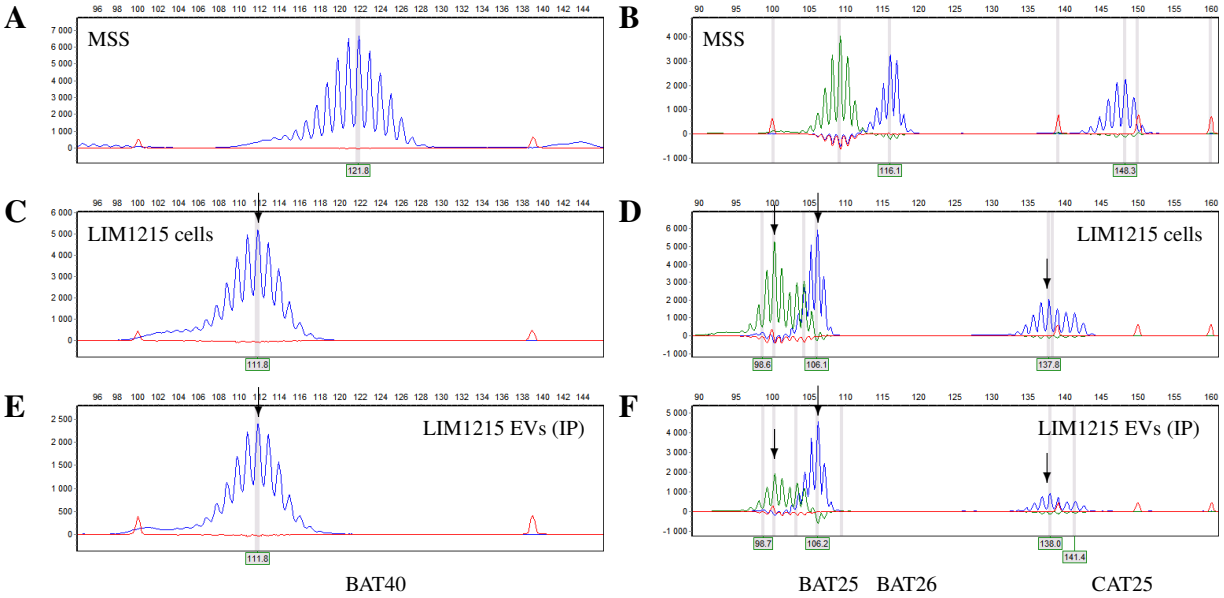

Figure 58: MSI fragment analysis of immunoprecipitated LIM1215-derived EVs. Captured A33-positive LIM1215-derived EVs were eluted from the magnetic beads. Vesicular DNA was isolated and PCR-based fragment analysis was conducted using four MSI markers. (A-B) MSS control. (C-D) DNA from the LIM1215 cell line presenting MSI in all markers. (E-F) The obtained allelic patterns for captured and eluted LIM1215 EVs coincided with the shifts of their parental cell line. The amplicon length in bp is indicated on the top of each figure, the fluorescent signal intensity is provided on the left.

Following, the established immunoaffinity-based EV enrichment approaches were tested with plasma EVs from healthy controls. Notably, even though EVs isolated by differential ultracentrifugation and PEG-based precipitation displayed similar size and morphology (Figure 49), successful western blot analysis was not achieved with plasma EVs isolated via precipitation. Thus, all following experiments were conducted with EV preparations obtained by ultracentrifugation.

None of the established IP strategies yielded a visible enrichment of A33-positive, colon-specific EVs (Figure 59A). Moreover and underpinning the need for a specific EV-enrichment, no specific A33 protein band was observed for the total protein lysate from plasma-derived EVs. These findings might indicate an insufficient technical sensitivity preventing the detection of EV-associated A33 via western blot.

In order to obtain information on the general capture of EVs using the described IP strategies, the presence of Alix, a commonly used EV marker protein, on A33-immunoprecipitated EVs was examined. Alix, detected in plasma EV protein lysate, could not be reliably verified for immunoprecipitated EVs using protein G beads. Instead, the undefined protein smear indicated a lack of specific capture of plasma EVs and potential unspecific interactions between protein G and residual plasma components (Figure 59B).
In contrast, EVs captured using streptavidin-coated beads yielded an Alix protein band (97 kDa), which indicated specific capture of A33-positive EVs with a concurrent insufficient amount of A33 protein preventing its detection via western blot (Figure 59B). However, using biotin-blocked streptavidin beads without an anti-A33 antibody also revealed an bead-associated Alix protein band, which pointed towards unspecific binding of plasma EVs to the beads independent of the coupled antibody (Figure 59B).

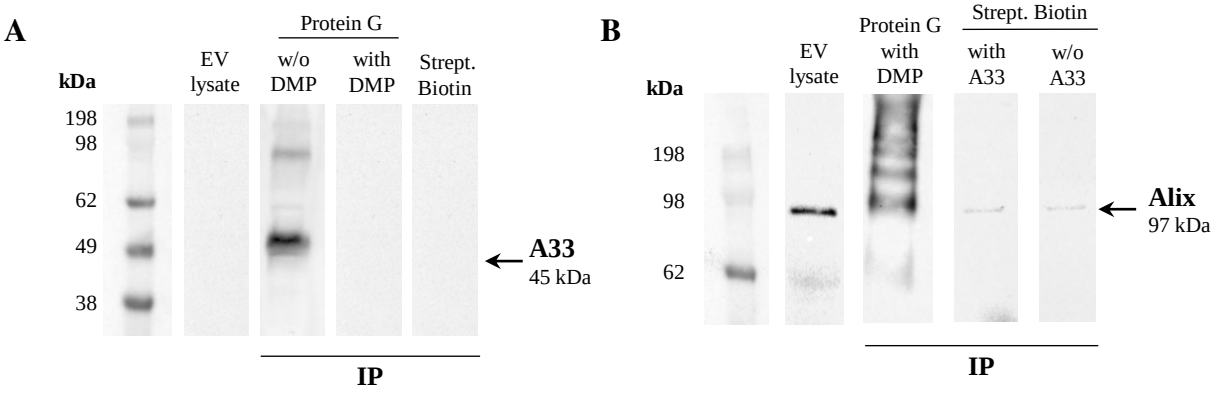

Figure 59: Immunoaffinity-based capture of plasma EVs. (A) The established IP strategies based on protein G and streptavidin magnetic beads did not yield an A33 protein band at the expected size of 45 kDa. A33 could also not be detected in plasma EV protein lysate. The visible protein band in the protein G (without crosslinking) sample represents the heavy chain of the used anti-A33 capture antibody. (B) Bead-mediated EV capture was assessed using Alix as a general EV marker (detected in plasma EV lysate). No clear Alix protein band was obtained by using protein G beads, indicating unspecific interactions and capture. The streptavidin/biotin approach with and without a coupled A33-antibody revealed similar Alix protein bands at 97 kDa, suggesting unspecific binding of plasma EVs to magnetic beads. 40 µg protein of plasma EV lysate were used as control. Plasma volume for EV isolation: 6 ml (protein G), 12 ml (streptavidin). w/o: without.

To overcome the limitations of detecting A33-positive EVs using western blot, a preliminary experiment was performed to evaluate the suitability of an indirect ELISA to identify plasma-derived A33-positive EVs. Importantly, this approach allowed the detection of A33 in cell culture- and plasma-derived EV preparations as an increase in optical density (OD) was associated with increasing EV concentrations (Figure 60). However, the applied EV concentrations were too high and led to a quick saturation of the protein-binding capacity of the ELISA plate, which is reflected by a plateauing OD curve.

This initial experiment was also conducted without the addition of the anti-A33 antibody. The measured OD for the respective controls was reduced compared to the A33-treated EV samples indicating specificity of the applied antibody and the chromogenic reaction (Figure 60). However, the increase of OD in plasma EV preparations without the presence of the anti-A33 antibody possibly points towards interactions between plasma residues and the secondary anti-IgG HRP-coupled detection antibody (Figure 60B). Nevertheless, the concentration-dependent signal increase and the observed difference between preparations with and without anti-A33 antibody indicate the suitability of ELISA to detect the colon-specific marker A33 on plasma-derived EVs.

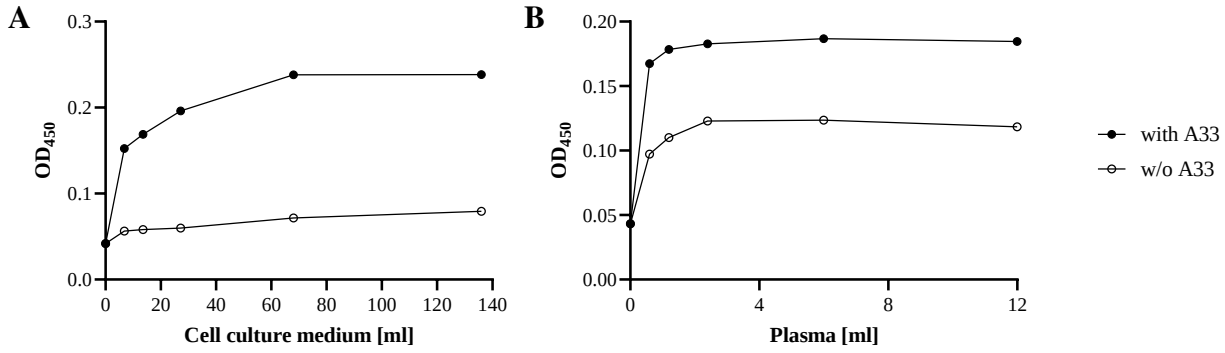

Figure 60: Detection of A33-positive EVs using an indirect ELISA. EVs were isolated from LIM1215 cell culture medium (A) or plasma (B) and applied to an ELISA plate in five different concentrations. As control EVs were treated with the detection antibody only, evaluating the specificity of the chromogenic reaction. An A33-associated signal was detected in LIM1215- and plasma-derived EVs. Unspecific interactions between EVs and the used detection antibody were observed in the plasma setting. w/o: without.

In summary, two IP-based enrichment strategies, targeting the glycoprotein A33, for colon-derived EVs were successfully established in the cell culture setting. Additionally, the feasibility of using immunoprecipitated EVs for PCR-based fragment analysis was confirmed. However, the methodological transfer of A33-mediated enrichment from cell culture to plasma EVs was hampered by the complex sample composition and limited technical sensitivity of western blot. A different approach applying an indirect ELISA yielded first promising results and indicated the presence and serological detectability of A33 on plasma-derived EVs. Further experiments are in order to reliably confirm the capture's specificity and optimize the ELISA for EV enrichment.

5 Discussion

LS, characterized by a monoallelic germline variant in one of the MMR genes, is the most common inherited cancer syndrome and associated with MSI cancer development [19]. As of yet, LS is largely underdiagnosed, which is partly attributable to the clinical heterogeneity and incomplete penetrance of the syndrome [239]. Moreover, reliance of currently applied LS diagnostic procedures on the molecular analysis of a manifest tumor impedes the identification of healthy LS carriers prior to tumor manifestation. Importantly, previous studies provided ample evidence for a life-long immune activation in LS carriers mediated by FSP neoantigens, which are the result of MMR deficiency and the consequential accumulation of indel mutations [65]. FSP-specific T cell and antibody responses have previously been observed in healthy LS carriers [80, 212]. The identification of MMR-DCF in the normal colonic mucosa of LS carriers provided a conceivable explanation for FSP-specific immune responses prior to tumor manifestation. MMR-DCF are characterized by a loss of MMR protein expression and have been described as LS-specific premalignant lesions as they frequently display the MSI phenotype and can harbor cMS mutations [185, 186]. MMR-DCF are not only involved in MSI carcinogenesis, they further constitute a cancer-independent source of FSPs and might prime the carrier's immune system prior to cancer development [175].

The proposed auto-immunization mechanism in LS carriers might provide sufficient immunological characteristics to enable the functional distinction between LS and non-LS individuals. Therefore, the present thesis aimed to evaluate the diagnostic potential of local and systemic immune responses in the context of LS. Simultaneously, the suitability of plasma-derived vesicular DNA as novel approach for minimally invasive MSI testing was explored.

The project's basis was laid by the characterization of local immune responses in MSI tumors and normal colonic mucosa. This included the systematic analysis of existing data on immune infiltration and immune evasion in hereditary and sporadic MSI tumors, and the comprehensive characterization of the immune milieu in the colorectal mucosa of healthy LS carriers and CRC patients. Systemic FSP-specific immune responses in LS carriers and MSI cancer patients were assessed on the cellular and humoral level, particularly aiming towards the diagnostic use of such. Complementing the exploration of MSI-associated immune responses, the clinical potential of plasma-derived EVs and their vesicular DNA was evaluated. In this context, an enrichment strategy for colon-derived EVs was established, aiming towards a sensitive liquid biopsy-based approach for MSI detection.

5.1 Mucosal immune infiltration in LS carriers and MSI cancer patients

5.1.1 Implications of the hereditary origin on the immune phenotype of MSI tumors

MSI cancers develop as a consequence of MMR deficiency and can have a hereditary background (LS) or occur sporadically. Regardless of their origin, MSI cancers are characterized by a high mutational load, particularly indel mutations in microsatellite regions, and pronounced immunogenicity which is mediated by FSP neoantigens [65]. The high immunogenicity in MSI cancers is paralleled by a strong infiltration with TILs and response to ICB therapy [124, 139, 161]. In spite of the described similarities, LS-associated and sporadic MSI cancers present with substantial differences in their pathogenesis, which might sculpt and be reflected by different immune phenotypes.
The conducted MEDLINE search allowed the comprehensive collection of existing data on immune infiltration and immune evasion mechanisms in MSI tumors. Ultimately, 17 articles fulfilled the defined inclusion criteria and were analyzed. Even though the used search terms were not restrictive of the organ system, the vast majority of identified articles focused on CRC. Only two of the selected publications contained information on EC. Data on premalignant lesions, stratified according to their origin, was also scarce and only two respective publications were identified. None of the studies provided information on immunological characteristics of the normal colonic mucosa, underlining the knowledge gap in the understanding of the immune cell composition in LS-associated normal tissue. Notably, studies with 'suspected LS' individuals were also included in the performed literature review as an omission of such would have reduced the comprehensiveness of the analysis [304].

Overall, the qualitative analysis indicated a more pronounced immune infiltration in hereditary MSI CRCs and ECs. This observation was further underpinned by evidence of enhanced lymphocyte recruitment, reflected by the increased density of HEV adjacent to LS-associated MSI CRCs. Such strong local immune responses can exert a potent selective pressure on precancerous cell clones and can trigger immune evasion, which allows tumor cells to escape immunological detection and destruction [347]. In line, hereditary MSI CRCs were also found to be more frequently associated with immune evasion phenomena. LS-associated MSI CRCs displayed a higher frequency of *B2M* mutations, compared to their sporadic counterparts.

The immunological differences between hereditary and sporadic MSI cancers identified in the present thesis might be explained by an ongoing FSP-associated immune stimulation in LS carriers prior to tumor manifestation [304]. However, alternative explanations for differing immune phenotypes have to be considered.

First, the host's immune status can greatly impact the interplay between immune and malignant cells, which is particularly reflected in individuals displaying immune dysfunction [348]. Immune-mediated diseases, such as rheumatoid arthritis, inflammatory bowel disease and psoriasis, are thought to affect around 10 % of the general population and were found to be associated with an increased cancer risk [349, 350]. Further, individuals affected from immunodeficiency disorders and transplant recipients, receiving immunosuppressive therapies, display a higher cancer risk [351–353]. In the LS setting, an increased rate of multiple cancers has been observed in LS carriers with autoimmune conditions or under immunosuppression [354]. However, data on the effect of immune dysfunctions or suppression on local immune responses is scarce and the host's immune status was not evaluated within the analyzed studies.

Second, the individual's age might contribute to the observed immunological differences as LS patients generally present with a younger age of cancer onset, compared to sporadic MSI cancer patients [19, 166]. Aging is associated with substantial immunological changes and a declining protective immunity [355, 356]. Consequently, the observed elevated immune activation in LS-associated MSI tumors might be affected by the patients' younger average age. However, the age-corrected HEV density, as an indicator for immune activation, remained significantly higher in LS MSI CRC patients, compared to sporadic MSI cases [331]. Hence, the younger age of LS individuals is unlikely to solely account for the described enhanced local immune responses in hereditary MSI tumors [304].

Third, sex has to be taken into account when comparing hereditary and sporadic MSI CRCs as in the general population tumors with the MSI phenotype are more frequently observed in female patients, especially at an older age [46, 357]. Further, a lack of estrogen was found to increase MSI cancer risk, which can be reduced by hormone replacement therapy in menopausal patients [358, 359]. None of the included studies explicitly considered the individuals' sex in their analyses.

Lastly, *BRAF* mutations and their immunosuppressive features have to be considered when comparing hereditary and sporadic MSI CRCs as over 60 % of sporadic MSI CRCs display a mutation in *BRAF* (mainly V600E), whereas LS-associated CRCs are rarely mutated (ca. 1.4 %) [174]. Previous studies in melanoma cells demonstrated an association between the *BRAF* V600E mutation and an increased production of immunosuppressive factors, such as IL-6, IL-10 and vascular endothelial growth factor (VEGF). These promote the recruitment of myeloid-derived suppressor cells (MDSCs) and Treg cells, facilitating immune escape [360–362]. However, additional evidence does not indicate *BRAF*-mediated immunosuppression in MSI CRCs. Specifically, *BRAF*-mutated MSI CRCs do not display significantly reduced densities of TILs and respond to ICB treatment with nivolumab plus ipilimumab as well as *BRAF*-WT MSI CRCs [363, 364]. Moreover, *BRAF* mutations in MSI CRCs were not found to be associated with a poorer prognosis, in contrast to MSS CRCs [365].

Based on the observed immunological differences between hereditary and sporadic MSI cancers and their differing pathogenesis, it seems conceivable that the cancer's origin also impacts therapy response [304]. Substantial differences between MSI and MSS CRCs have already been observed for 5-FU treatment, which can have detrimental effects on MSI CRC patients [136, 137]. However, only few studies examined a potentially differing responsiveness to chemotherapy in hereditary and sporadic MSI CRC patients. For instance, Sinicrope et al. found increased disease-free survival and reduction of distant recurrences in LS-associated, compared to sporadic, MSI CRC patients receiving 5-FU-based treatment [366]. A recent study by Zaanan et al. reported a significantly longer progression-free survival of LS-associated MSI CRC patients under chemotherapy combined with anti-EGFR, compared to sporadic cases [367].

In recent years, ICB therapy has achieved tremendous success in treating MSI cancers and its effectiveness for MSI CRCs was demonstrated in multiple studies [139, 161]. However, available data on differing ICB response rates between hereditary and sporadic MSI CRCs are scarce and Le et al. did not identify significant differences in the objective response rate between the two patient groups [139, 161]. This observation potentially reflects the net effect of two counteracting mechanisms positively or negatively impacting therapy response, supported by the results of the performed literature search. The observed elevated density of immune cells in LS-associated MSI CRCs, compared to sporadic cases, might provide a better prerequisite for ICB therapy response. Previous studies demonstrated local T cell infiltration to be a requirement for therapeutic response by enabling the reactivation of T cells during ICB treatment [162, 368, 369]. On the contrary, the described higher frequency of *B2M* mutations, abrogating HLA class I-mediated antigen presentation, in LS-associated MSI CRCs, compared to the sporadic group, might facilitate resistance towards ICB. Notably, the generally favorable prognosis of *B2M*-mutated MSI CRCs might mask ICB resistance [120, 121]. The reason for the reported favorable prognostic effect of *B2M* mutations in MSI CRCs is not fully clarified yet. However, a reduced metastatic potential, increased NK cell-mediated tumor cell killing or decreased platelet binding might be contributing factors [370–372].

In summary, the performed literature analysis revealed two potentially related findings: a more pronounced immune infiltration and a higher rate of immune evasion phenomena in hereditary, LS-associated MSI tumors. The more active immune milieu in the hereditary setting might be a result of the proposed life-long immune stimulation accomplished by recurrent encounters of immune cells with MMR-DCF [65]. Clinically, the reported findings may be of relevance to improve the delineation of ICB therapy response determinants [304]. Moreover, these findings encourage tumor-preventive immune approaches that could boost the pre-existing immune responses in LS carriers, preventing the outgrowth of tumors. Stimulation of immune responses may not only directly inhibit tumor outgrowth, but also force emerging

tumor cells to undergo immune evasion which is associated with an more favorable prognosis in MSI patients. Currently, respective strategies are being tested in the preclinical and clinical setting [81, 214].

5.1.2 The mucosal immune profile as a potential cancer risk modifier in LS

MSI CRCs can be distinguished from their MSS counterparts by dense immune infiltration and their immune landscape has been extensively studied. Numerous studies have reported strong infiltration with activated cytotoxic T cells and Crohn's-like lymphoid reactions, indicating pronounced intratumor immune reactions [124, 127, 128, 373, 374]. However, the immune status of the normal colonic mucosa is less well characterized, exemplified by the lack of respective articles on normal tissue in the performed systematic literature search outlined above. Thus, the immune infiltration in the (tumor-distant) normal colonic mucosa of LS-associated/sporadic MSI CRC and MSS CRC patients as well as healthy LS carriers was assessed, conducting quantitative T cell density analysis and expression analysis of immune-relevant genes [318]. Notably, the phenotypic description of T cell subpopulations via cell surface markers does not necessarily reflect the cell's functional state. However, for simplicity the present thesis refers to CD8- and FOXP3-positive T cells as cytotoxic and regulatory T cells, respectively.

The mucosal characterization revealed two major findings. First, the in the literature described differences between MSI and MSS CRCs go beyond the tumor area and the MSI phenotype was associated with significantly elevated densities of CD3- and FOXP3-positive T cells in the tumor-distant, normal mucosa [318]. Second, the normal mucosa of healthy LS carriers presented elevated T cell densities and a distinct gene expression profile. Compared to the normal mucosa of CRC patients, healthy LS carriers displayed the highest number of mucosal CD3-, CD8- and FOXP3-positive T cells. Importantly, the density of CD8-positive T cells was significantly different between the normal mucosa of healthy LS carriers and LS CRC patients. Gene expression analysis underpinned these observations and revealed significant differences between the normal mucosa of healthy LS carriers and LS CRC patients as well as LS CRC tissue in 552 genes. A significantly higher prevalence of CD8-positive exhausted T, Th1, CD45-positive, NK, mast and B cells was identified in the normal mucosa of healthy LS carriers, compared to LS CRC patients [318]. Notably, the prevalence of immune cell populations was determined by indirect methods using deconvolution algorithms of gene expression data and was not a result of direct measurement. However, the applied approach by Danaher et al. was specifically developed for FFPE tissue and NanoString nCounter®data, and has been thoroughly validated in previous studies [375–377]. Moreover, the applicability of this approach in the normal tissue context was confirmed in the present study, reflected by the significant concordance between IHC and NanoString deconvolution for CD8- and FOXP3-positive T cells which were included in both panels.

Overall, the latter finding points towards a compartment-wide local activation of the immune system independent of tumor manifestation and is supported by the detection of systemic FSP-specific T cell responses in healthy LS carriers [80]. Further, these observations indicate an association between cancer development or presence and alterations of the mucosal immune milieu, which is reflected by immunological differences between LS carriers with and without cancer manifestation [318]. Two different explanations are conceivable (Figure 61):

First, the cancer might stimulate an immunosuppressive environment beyond the boundaries of tumor and tumor-adjacent tissue, leading to the observed changes in certain immune cell populations [318]. In the context of MSI CRC, immunological changes in the tumor-adjacent colonic mucosa, dependent on the cancer's *B2M* mutation status, have already been observed [112]. Moreover, previous studies have demonstrated a systemic or organ-restricted immune suppression for different cancer types [338, 378–382]. The present study identified a significantly higher density of FOXP3-positive T cells in LS CRC tissue, compared to the normal colonic mucosa of LS individuals. In line, the conducted gene expression analysis revealed a significantly higher abundance of neutrophils and Treg cells in LS-associated CRC tissue, both populations being associated with immune suppression [318, 338]. A pairwise analysis of matched CRC tissue and normal mucosa samples from the same patient revealed more neutrophils, Treg and Th1 cells in the cancer tissue [318]. On the other side, the tumor-distant, normal mucosa of LS CRC patients displayed a higher prevalence of exhausted CD8-positive T, CD45-positive, mast and B cells [318].
The described immunological differences might arise through the release of immunosuppressive signals, e.g. IL-10 and TGFB, by the tumor and recruitment of specific immune cell populations, such as MDSCs and Treg cells, to the tumor site which counteract anti-tumor immunity [338]. The tumor microenvironment has also been shown to be shaped by the release of tumor-derived EVs. For instance, a study by Yamada et al. found an enrichment of TGFB-1 in CRC-derived EVs which was associated with an altered T cell phenotype and inhibition of T cell proliferation [383]. Fittingly, the expression of all TGFB isoforms was found to be significantly elevated in LS CRC tissue, compared to the normal colonic mucosa [318]. Further, TGFB is known to mediate the immunosuppressive role of neutrophils [339], an immune population that was also found to be significantly more abundant in LS CRCs. The observed higher prevalence of neutrophils in cancer tissue might also reflect their recruitment to areas of tumor-induced tissue damage [384]. Clinically, a cancer-mediated immunosuppressive milieu spreading beyond the manifest tumor and its surrounding tissue might offer an explanation for the slightly increased risk of subsequent cancers in LS patients with cancer history [385].

Second, the observed immunological differences in the normal mucosa between healthy LS carriers and LS CRC patients might be explained by a protective anti-tumor effect generated by mucosal T cells. Hence, the mucosal T cell infiltrate might impact the cancer risk of LS

individuals. Supposedly, a higher T cell density could facilitate the efficient recognition and elimination of MMR-deficient premalignant lesions, preventing malignant transformation and cancer manifestation. If this assumption is true, cancer susceptibility and risk of LS carriers might be affected by constitutional differences in the individual's mucosal immune status, rendering the T cell density in the normal colonic mucosa a permanent tumor risk modifier [318]. As described previously, multiple studies have already demonstrated that the underlying immune status can influence cancer risk, e.g. reflected by the increased cancer risk of immunosuppressed individuals [351–353, 386]. Importantly, the identified correlation between a higher density of CD3-positive T cells in the rectal mucosa and the prolonged time to subsequent tumor manifestation in LS carriers enrolled in the CAPP2 clinical trial supports the proposed tumor risk-modifying aspect of the mucosal immune composition.
In addition to constitutional differences, an individual's immune status might fluctuate throughout a life-time and can be influenced by various factors. Besides advancing age, which is associated with lower levels of lymphocytes and reduced diversity of T and B cell receptors [355, 356, 387–389], the immune system is influenced by environmental factors. For example, smokers have been shown to present with reduced levels of serum immunoglobulins and NK cell activity [390, 391]. Further, an individual's viral encounters and microbiota shape the immune system [389]. Overall, changes in the immune status, potentially reflected by an altered mucosal immune profile, might temporarily impact the cancer susceptibility of LS carriers. The observation that LS carriers with and without history of extracolonic cancer displayed similar CD3-positive T cell densities in their normal mucosa is in line with the hypothesis of the mucosal immune status as a temporary cancer risk modifier [318]. Thus, a comprehensive characterization of the colonic mucosa in LS carriers with and without previous extracolonic cancers should be addressed by future studies.

In general, CRC risk is influenced by genetic and different external risk factors, e.g. socio-economic conditions, alcohol consumption, smoking, diet and physical activity. Furthermore, several internal factors affecting the CRC risk have been identified, such as metabolic factors, hormones, oxidative stress and inflammation [392–395]. The gut microbiome is an additional internal factor and has been shown to impact intestinal carcinogenesis. Changes in the gut microbiome, e.g. induced by an extensive use of antibiotics and modern dietary regimens, are also suspected to contribute to the reported rising number of early onset CRCs in individuals younger than 50 years [396]. A decreased bacterial diversity and colonization of the gut with several bacterial species, e.g. *Fusobacterium nucleatum* and pathogenic *Escherichia coli* strains, have been connected to an increased CRC risk [397, 398]. A complex and strongly intertwined link has been described between the microbial colonization of the gut, host immunity and colorectal carcinogenesis. This observation is exemplified by the suspected downregulation of anti-tumor T cell responses by *Fusobacterium nucleatum* as elevated levels of this bacterium were associated with a lower density of CD3-positive T cells in CRC tissue [399]. Intriguingly,

alterations of the immune milieu in the colorectal mucosa might mediate the described relation between the gut microbiome and CRC risk. The obtained results underpin the importance of considering and accounting for the gut microbiome when studying immune infiltration in the colorectal mucosa and encourage further research on its immunomodulatory aspects.

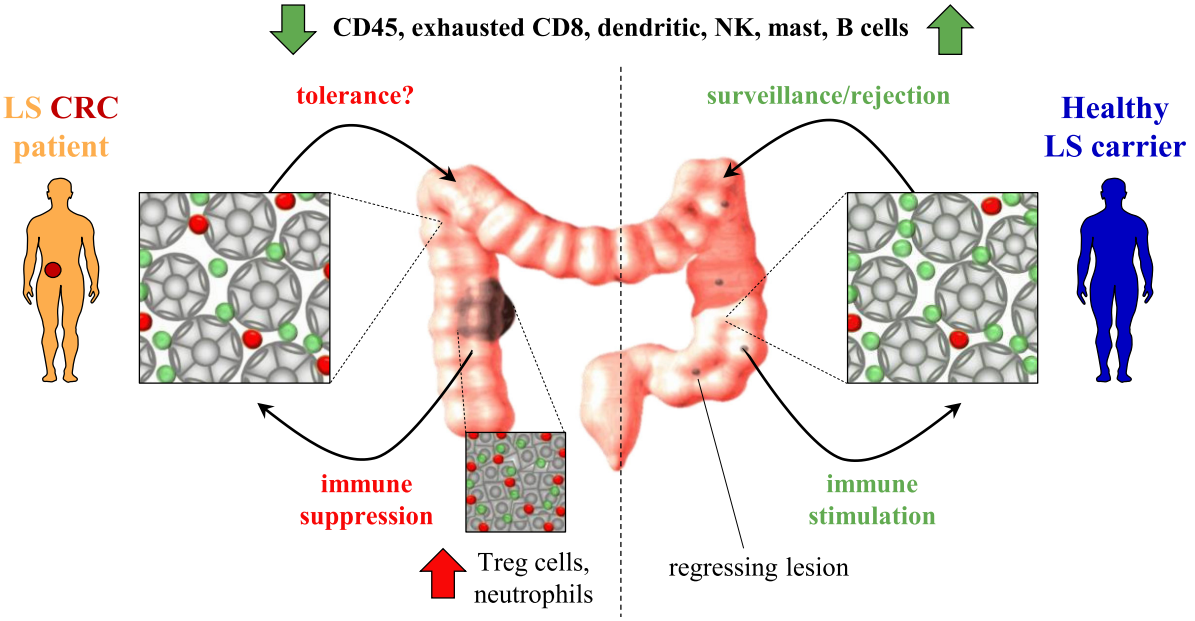

Figure 61: The immune profile of the normal colonic mucosa as potential cancer risk modifier in LS carriers. Healthy LS carriers and LS CRC patients present distinct immune profiles in the normal colonic mucosa. Higher mucosal T cell densities and the elevated abundance of several immune cell populations, e.g. CD45-positive, NK and B cells, might facilitate a protective anti-tumor immune milieu. The presence of a manifest cancer might impact the immune profile of the normal mucosa beyond the borders of cancer tissue and adjacent mucosa, representing an organ-wide field effect. Adapted from: [318].

The proposed concept of a permanent or temporary cancer-risk modifying potential of the mucosal immune profile would support the applicability of immune-based cancer-preventive strategies, which aim to induce alterations in the colorectal immune milieu and reduce cancer risk of LS carriers [81]. Moreover, increasing evidence suggests that modulation of the mucosal immune environment contributes to the observed cancer-preventive effects of NSAIDs in LS carriers [247]. Mechanistically, NSAIDs reduce the synthesis of prostaglandins by inhibiting the activity of the cyclooxygenase enzyme. Prostaglandins are biologically active lipids and proinflammatory prostaglandins, such as prostaglandin E_2 (PGE2), are associated with tumor growth and a poor prognosis in different malignancies, including CRC [400]. Prostaglandins have been shown to impact cancer growth via various mechanisms, e.g. by directly activating receptors on cancer cells impacting cell proliferation, apoptosis and migration, and inducing the secretion of growth and angiogenic factors [400]. Further, prostaglandins can facilitate a tumor-supportive, immunosuppressive microenvironment, e.g. PGE2 promotes the local accumulation of MDSCs and Treg cells [400, 401].

The beneficial immunomodulatory properties of NSAIDs have recently been demonstrated for naproxen and daily administration over a time span of six months led to the activation of different immune cell types in the intestinal mucosa [402]. Within the present study, biopsies from CAPP2 participants were taken prior to randomization to aspirin and none of the participants outside of the CAPP2 trial took aspirin for tumor prevention.
Additionally, a chemopreventive activity, concomitant with reduced tumor burden and improved survival, has been observed for *VCMsh2* mice receiving naproxen [402]. Naproxen has also been shown to potentiate immune responses in *VCMsh2* mice vaccinated with FSPs [214]. Importantly, FSP vaccination and NSAIDs were found to alter the intestinal tumor microenvironment by increasing the relative Th1 vs. Th2 immune responses, indicating that elevated Th1 T cell activation conveys the observed beneficial effects of FSP vaccination, NSAIDs and their combination [214]. These observations further encourage FSP vaccination approaches to boost immune surveillance and clinical trials for treatment of MSI tumors and cancer prevention are ongoing (NCT04041310, NCT05078866) [81].

Additional aspects of the performed mucosal characterization in LS carriers and CRC patients encompassed the analysis of T cell infiltration in varying anatomic locations and different MMR gene variant carriers.
Previous studies have already demonstrated that the distribution of immune cell populations varies along the intestine and anatomically defined segments are reflected by the compartmentalization of the intestinal immune system. The small intestine typically displays IL-17- and IL-22-producing T cells, innate lymphoid cells and the production of antimicrobial peptides. The colon is mainly characterized by IgA-producing plasma cells and larger numbers of Treg cells [403]. A study by Kirby et al. observed a linear decrease of intraepithelial T cells proceeding from the ascending colon and presenting the lowest number of T cells in the rectum [404]. In line, the conducted quantification of CD3-positive T cells in rectal and colonic normal mucosa revealed significantly lower T cell densities in the rectum, indicating an anatomically defined immune infiltration density. However, the direct comparison of rectal and colonic mucosa samples needs to be interpreted with caution due to the different sampling periods and was generally avoided within the conducted study.
Further, the abundance of different T cell subpopulations in the normal colonic mucosa of LS individuals was analyzed in a MMR gene-dependent manner. Importantly, substantial clinical and molecular differences have been reported for *MLH1*, *MSH2* and *MSH6* LS carriers, e.g. concerning cancer risk and pathogenic mechanisms [192, 193]. A recent study by Bajwaten Broeke et al. observed significantly lower numbers of CD3-positive TILs in *PMS2*-deficient CRCs, compared to CRCs from *MLH1* and *MSH2* carriers [405]. Moreover, several studies found a differing intratumoral immune milieu between *MLH1* and *MSH2* carriers, e.g. reflected by a higher frequency of *B2M* mutations in *MLH1* carriers [112, 335, 406]. In contrast to previous studies which mainly focused on intratumoral T cells, the conducted quantification of

T cell infiltration in the normal colonic mucosa of LS carriers and LS CRC patients did not reveal significant differences between *MLH1*, *MSH2* and *MSH6* carriers. Notably, only one patient in the analyzed cohort presented with a *PMS2* variant, which did not allow a reliable statistical analysis so that *PMS2* was not included in the MMR gene-dependent evaluation. The overall limited sample number within the present thesis might have been insufficient to discover subtle differences between MMR gene variant carriers and a potential correlation between LS genotype and immune phenotype remains to be elucidated.

Lastly, the present thesis comprised the quantification of local T cell infiltration in LS-associated adenomas. The density of CD3-positive T cells was found to be similar between LS adenomas and the normal colonic mucosa of healthy LS carriers. Interestingly, significant differences between adenomas and normal mucosa were observed in the infiltration with functionally different T cell subpopulations. Adenomas presented with a significantly reduced density of CD8-positive cytotoxic T cells and a significant enrichment with FOXP3-positive Treg cells. Potentially, such a shift in T cell subpopulations might indicate the establishment of an immunosuppressive and pro-tumor microenvironment, facilitating the development and progression into an invasive CRC. Treg cells can diminish anti-tumor immunity via multiple contact-dependent and -independent mechanisms, e.g. secretion of immunosuppressive cytokines (TGFB, IL-10 and IL-35), perforin/granzyme-mediated cytolysis of target T cells or downregulation of co-stimulatory molecules on APCs [407, 408]. A study by Cui et al. reported increased FOXP3 expression levels in colorectal adenomas, indicating Treg cells as important contributors to the formation of an immunosuppressive milieu during CRC carcinogenesis [409]. Moreover, a study in $APC^{Min/+}$ mice demonstrated an altered chemokine balance in adenomas, possibly contributing to the observed shift towards higher frequencies of Treg cells [410].
Additionally, immunological differences between MMR-proficient (MMR-P) and MMR-deficient (MMR-D) LS adenomas were assessed within the frame of the outlined study. MMR-D adenomas displayed a significantly higher density of CD3-, CD8- and FOXP3-positive T cells, compared to their MMR-P counterparts. In line, a previous study by Meijer et al. reported a correlation between MMR deficiency and lymphocytic response as well as increased TIL densities in MMR-D, compared to MMR-P, LS-associated adenomas [182]. On the contrary, Chang et al. described an active immune profile characterized by high expression of CD4, IFNγ, LAG3 and IL12A in LS adenomas independent of the adenoma's MMR-status [411]. However, the sample number analyzed in the latter study was low (4 MMR-D vs. 7 MMR-P polyps) and FAP adenomas, known to have different routes of progression and mutational drivers, were used as reference [411, 412]. Further research on the immune profile in LS-associated adenomas and its implications in CRC development is warranted.

In summary, the present thesis broadened the understanding of the immune landscape in LS and the obtained results allow two possible conclusions (Figure 61). First, they provide evidence for potential organ-wide changes in the immune status mediated by a manifest cancer. Second, they suggest a role of immune surveillance in impacting cancer risk and for the first time indicate the mucosal immune infiltration as cancer risk modifier in LS. The association between the mucosal immune profile and cancer risk in LS individuals, which shall be substantiated further in large prospective international studies, harbors potential for the development of cancer prediction and prevention strategies in LS [318, 413].

5.2 Systemic cellular and humoral FSP-specific immune responses in LS carriers and MSI cancer patients

5.2.1 FSP-specific immune responses as a potential diagnostic approach for healthy LS carriers

Besides the pronounced local immune activation in the colorectal mucosa of LS carriers as identified in the present thesis, systemic FSP-specific T cell and antibody responses had been previously reported in the peripheral blood of healthy LS carriers [80, 212]. Clinically, the enhancement of such pre-existing FSP-specific immune responses via vaccination approaches might improve MSI cancer patients' outcome in an adjuvant therapy setting or could be applied for cancer prevention in healthy LS carriers [65, 81]. Beyond their potential therapeutic and cancer-preventive significance, systemic FSP-specific immune responses may possess a diagnostic value and be suited for the immunological distinction between LS carriers and unaffected individuals. Within the present thesis, the suitability of FSP-specific immune responses as tumor-independent, diagnostic markers for LS was explored.

Systemic T cell responses against 13 FSPs, which were selected based on the mutational analysis of manifest tumors combined with the evaluation of their immune relevance during tumor evolution [79], were analyzed in healthy LS carriers and non-LS controls. Significantly stronger T cell responses in LS carriers were identified against seven FSPs (TGFBR2, CASP5, TCF7L2, MARCKS, SLC22A9.2, MYH11.2, AIM2) using an IFNγ ELISpot approach. Similarly, Schwitalle et al. have previously observed significantly elevated T cell responses against 7/13 FSPs in a cohort of 16 healthy LS carriers [80]. Despite applying a different IFNγ ELISpot approach as well as a mostly different FSP panel, Schwitalle et al. also reported significantly increased responses against the TGFBR2 and AIM2 FSPs in healthy LS carriers [80]. Moreover, the findings of the present study were validated by IFNγ RT-qPCR, which revealed overall increased IFNγ expression in healthy LS carriers, reaching statistical significance for the AIM2 FSP. The concordance of both methodological approaches (IFNγ ELISpot and RT-qPCR) was found to be statistically significant. Notably, a tetramer staining

approach for the identification of specific T cells was successfully established. However, the applicability of this method for the detection of FSP-specific T cell populations could not be evaluated due to limited availability of samples with suitable HLA type for this analysis and thus will not be discussed.

In contrast to the limited number of FSPs included in the cellular analysis, humoral immune responses were assessed against a broader FSP panel, based on similar selection criteria. Antibody responses against 41 different FSPs were evaluated in healthy LS carriers and healthy non-LS controls using a peptide microarray. The respective analysis was conducted by PEPperPRINT and revealed three FSPs (AIM2, MYH11.1 and MYH11.2) which were associated with increased IgA and IgG responses in healthy LS carriers and hence might be suited for the identification of such. Importantly, two identified candidate peptides (AIM2 and MYH11.2) have already been identified during the analysis of systemic FSP-specific T cell responses presented above. This finding also supports preliminary observations of FSP-specific antibody responses in LS carriers' sera reported by Reuschenbach et al. [212].

Until now, data on systemic FSP-specific immune responses, besides the mentioned studies by Schwitalle et al. [80] and Reuschenbach et al. [212], are scarce and immune responses have never been systematically assessed in healthy LS carriers with the proposed diagnostic objective. The independent identification of FSPs on the cellular and humoral level may indicate a particular suitability of these candidates for diagnostic applications. Further studies should implement these targets and focus on the evaluation of their performance in distinguishing LS carriers from non-carriers. Their successful prospective validation and implementation into routine procedures could improve LS diagnostics in the clinic by enabling the tumor tissue-independent identification of LS carriers.

Noteworthy, the observed responses were heterogeneous among analyzed samples and several aspects, such as age, sex and MMR gene variant, that may contribute to the heterogeneity of individual immune responses have to be considered when interpreting systemic immune response data. The analysis of FSP-specific T cell responses in healthy LS carriers (median age: 29 years) and older healthy non-LS controls (median age: 38 years) did not reveal a significant correlation between age and the respective number of IFNγ-spots. Also, IFNγ-spot counts were not found to vary significantly between male and female individuals. The influence of different MMR gene variants on FSP-specific immune responses and it's relevance should be evaluated in future studies.
Neoantigen-specific T cell responses might also be affected by the life-long microbial exposure and phenomena such as heterologous immunity, which describes encounters with a pathogen that alter immune responses to a second, related or completely unrelated, pathogen [414, 415]. The role of pre-existing heterologous immunity to microbial and viral

pathogens in impacting neoantigen-specific T cell responses is not fully understood yet [416]. However, cross-reactivity between peptide neoantigens and common viral pathogens, such as CMV, human papillomavirus (HPV) and hepatitis C virus, has been reported [417, 418].

The application of IFNγ-based assays (ELISpot and RT-qPCR) for the analysis of specific T cell responses is accompanied by several technical challenges that should be considered. For instance, present non-T cells in the culture can secrete cytokines which could impact the quantification and interpretation of the obtained results. Further, these assays typically do not provide information on the phenotype of the responding cell and the identification of cytokine-secreting cell subsets is challenging. Additionally, the amount of secreted cytokine per cell cannot be quantified and antigen-reactive cell populations that do not secret cytokines are not considered in the applied approaches [419–421].
Within the present thesis, several healthy non-LS controls presented with high numbers of IFNγ-spots and high IFNγ expression. Such spontaneous responses might be the result of previous T cell activation independent of the applied FSPs. Alternatively, T cell responses in healthy controls might be influenced by T cell cross-reactivity between neoantigens and microbial epitopes [416]. Moreover, the systemic T cell repertoire can be greatly affected by inflammatory and infectious diseases as well as vaccines, which could in turn impact the detection of FSP-specific T cells [422, 423]. The described methodological limitations may be overcome by alternative approaches, such as the already established FSP-specific tetramer staining approach.

Overall, the presented observations underscore tumor-independent, FSP-mediated immune responses in LS carriers which distinguish them from unaffected individuals. The diagnostic use of such immunological characteristics might aid to overcome known shortcomings of LS diagnostics. Despite the limited number of available samples, which also reflects the current diagnostic drawbacks in the identification of LS carriers prior to cancer manifestation, statistically significant differences between healthy LS carriers and non-LS controls were observed. The identification of candidate FSPs laid the foundation for the development of an applicable diagnostic approach, which will require longitudinal sampling to evaluate the variability of FSP-specific immune responses over time and in regard to immunomodulating aspects. Further, technical standardization and definition of cut-off criteria for LS identification will be essential to allow clinical translation.

5.2.2 Cancer- and chemotherapy-mediated effects on systemic FSP-specific immune responses

In addition to the analysis of systemic FSP-specific immune responses in healthy LS carriers and evaluation of their diagnostic potential (see 5.2.1), immune responses were also characterized in cancer patients. FSP-specific T cell responses were assessed in a heterogeneous group of cancer patients and allowed to evaluate the possible impact of cancer manifestation and therapeutic interventions on such. In addition, FSP-specific IgA and IgG antibody responses were examined in MSI CRC patients and LS carriers with a history of cancer.

The quantification of systemic FSP-specific T cell responses in cancer patients (MSI and MSS) yielded broadly scattered data and a wide range of immune responses against the applied 13 FSPs. Overall, no significant differences between MSI cancer patients, healthy controls and MSS cancer patients were detected. In contrast, Schwitalle et al. have reported significantly elevated T cell responses in the peripheral blood of MSI CRC patients, compared to healthy individuals and MSS CRC patients [80]. The observed discrepancy between both studies might be attributable to various factors. In addition to the technical differences in the IFNγ ELISpot protocol and FSP selection mentioned above, the group of patients described in Schwitalle et al. was more homogeneous and solely included MSI CRC patients after cancer resection. Cancer patients analyzed in the present study were heterogeneous regarding cancer entity/burden and therapy line. Several patients received chemotherapy at the time of sampling and patients with prevalent cancer as well as post-surgery patients were included.

The analysis of FSP-specific antibody responses in serum/plasma samples from MSI CRC patients and LS carriers with cancer history did not yield a clear picture and was hampered by overall low signal intensities. However, the DAMS (-1) FSP may be associated with manifest MSI cancer as respective IgG responses were significantly elevated in patients with prevalent cancer. In contrast to a study by Reuschenbach et al., demonstrating significantly elevated levels of FSP-specific antibody responses in LS carriers with a history of MSI cancer, the present study did not reveal distinct responses in the respective cohort [212]. However, Reuschenbach et al. observed the highest level of FSP-specific antibodies in patients with the shortest interval between cancer resection and sampling [212]. The present analysis could not account for this time period as the respective information was not available and the lack of substantial FSP-specific antibody responses might be attributable to a prolonged time between resection and sampling.

In general, various aspects may influence FSP-specific T cell and antibody responses. For instance, cancer-associated suppression of immune responses has been extensively studied and systemic perturbations of the immune system by cancer burden have been described for many different human cancer entities.

Importantly, the presence of manifest cancer influences immune responses across tissues, exceeding the local tumor microenvironment [424]. Cancer-bearing individuals can display disruption of hematopoiesis and often present with the peripheral expansion of immature neutrophils and monocytes, and subsequent accumulation of these populations in the tumor microenvironment [425–427]. Multiple factors, e.g. IL-17, IL-8, IL-1β and cancer-derived EVs, are thought to mediate the biased myeloid expansion associated with cancer burden [424]. Moreover, cancer manifestation can also affect other immune lineages and increased peripheral expansion of Treg cells, decreased TCR repertoires, perturbations of dendritic cells as well as phenotypic alterations of NK cells, have been observed in cancer patients [424, 428–432].
A manifest tumor might also affect systemic neoantigen-specific immune responses and interfere with the detection of FSP-specific T cell responses. The present analysis encompassed 12 cancer patients after cancer resection and 16 patients with prevalent cancer, but undefined tumor burden. Due to the main focus of the analysis on the potential exploitation of systemic cellular immune responses for specific detection of LS carriers as well as the small sample size, a stratified analysis of FSP-specific T cell responses in the aforementioned two groups was not possible and the impact of cancer prevalence was not determined. The analysis of systemic humoral responses included patients with prevalent MSI CRC and LS carriers with cancer history. Three FSPs (DAMS (-1), MARCKS (-2), AIM2) displayed significantly different antibody responses between both groups, indicating immunological alterations mediated by cancer manifestation.

Chemotherapy agents can also induce changes in circulating immune cell populations and multiple studies have demonstrated various immunosuppressive and immunostimulatory effects [433]. Chemotherapy can promote immunosuppression by inducing the acute release of pro-inflammatory molecules (e.g. IL-6, IL-8) by cancer-associated fibroblasts and endothelial cells, which in turn promote the expansion of immunosuppressive myeloid cells [434]. Moreover, EVs can exert chemotherapy-induced immunological changes, e.g. B cell-derived EVs have been shown to impair CD8-positive T cell function upon chemotherapy [435]. Oppositely, chemotherapy has also been reported to promote anti-tumor immune responses. For instance, dying cancer cells can stimulate dendritic and cytotoxic T cells, and downregulate the activity of MDSCs and Treg cells [436–438]. Further, the secretion of cyto- and chemokines upon chemotherapy can stimulate anti-tumor responses [439]. The immunomodulating effects of chemotherapy greatly depend on the cancer entity, therapy agent and context [424].
Therapy-related perturbations in various immune lineages may also have implications for FSP-specific immune responses and their *in vitro* analysis. The cohort, analyzed for cellular immune responses, included three cancer patients (MSI and MSS) who received chemotherapy at the time of blood sampling and eight patients with an undefined therapy line.

However, the overall small sample size did not justify a stratification of FSP-specific T cell responses according to chemotherapy status and no assessment of the potential chemotherapy-induced effects was performed.

Lastly, surgical cancer resection can affect an individual's immune responses and altered anti-tumor immunity after surgery has been indicated by various studies. For example, systemic wound healing programs, triggered upon cancer resection, have been shown to elevate the levels of IL-6, granulocyte-colony stimulating factor (G-CSF) and chemokine C-C motif ligand 2 (CCL2), facilitating immunosuppressive remodeling of myeloid cells [424, 440]. Cancer resection in CRC patients has been shown to significantly reduce IFNγ secretion by peripheral NK cells up to two months after surgery [441]. Similar mechanisms might directly impact the interpretation of specific T cell responses via IFNγ ELISpot assay.
The described analysis of FSP-specific T cell responses in MSI and MSS cancer patients included 12 patients after cancer resection, but stratification according to therapeutic intervention was outside the scope of the present thesis.

As an additional aspect of the present study, potential differences in systemic FSP-specific T cell responses between LS-associated and sporadic MSI cancer patients were assessed. The hereditary origin might be associated with elevated FSP-specific immune responses due to the proposed life-long immune stimulation in LS carriers [65]. This hypothesis is underpinned by results of the performed systematic literature search (see 5.1.1), which revealed evidence for a more pronounced immune infiltration and more frequent immune evasion phenomena in LS-associated, compared to sporadic, MSI cancers [304]. However, no significant difference between LS-associated and sporadic MSI cancer patients was observed in the analyzed patient cohort. Notably, the small sample size might have prevented the reliable observation of such and this question has to be addressed by future studies as immunological differences dependent on the cancer's origin might be of diagnostic and therapeutic relevance.

5.2.3 Suitability of FSP-specific immune responses as ICB therapy response markers

ICB therapy revolutionized the oncological treatment landscape and has shown tremendous success for various cancer types [141]. The high immunogenicity of MSI cancers renders them susceptible to ICB treatment and the MSI phenotype has been described as an important predictor for therapy response [65, 139, 160–162]. However, 10–40 % of MSI CRC patients present with primary therapy resistance and reliable predictive biomarkers are still lacking [162, 442, 443]. Hence, the present thesis aimed to explore the effects of ICB on FSP-specific T cell responses in order to generate first data informing about their potential suitability to be used in ICB therapy monitoring and as minimally invasive therapy success markers.

Systemic T cell responses against 13 FSPs were assessed in ten MSI cancer patients once before starting ICB therapy and at several time points during the course of treatment. Multiple MSI cancer patients presented with an increase in T cell responses against one or multiple FSPs after starting ICB treatment, which might point towards the ICB-induced reactivation of tumor-specific T cells. Le et al. has already demonstrated the ICB-mediated activation and expansion of FSP-specific T cells upon treatment with pembrolizumab *in vivo* [139]. Three patients displayed an initial increase of FSP-specific T cell responses upon treatment start and a decrease of such after 4–24 weeks. Interestingly, Le et al. observed a similar pattern and reported a rapid peripheral expansion of FSP-reactive TCRs after initiating ICB treatment and a subsequent normalization of the clone's frequency earlier than 14 weeks of ICB therapy [139]. However, previous analyses of FSP-specific immune responses were based on NGS-data, which have limited sensitivity for the detection of indel mutations at long microsatellites [79]. In the present thesis, the first analysis of specific immune responses directed against FSPs derived from common high frequency cMS mutation events has been performed.

Overall, no clear correlation between systemic FSP-specific immune responses and the patients' clinical course was observed within the analyzed cohort. The increase in specific immune responses during ICB therapy was not indicative of therapy response and only correlated with a clinically confirmed response in one patient. Further, disease progression was not explicitly associated with a lack or decrease of FSP-specific T cell responses and in one patient a substantial increase in T cell responses directly preceded disease progression. However, the observed changes in FSP-specific T cell responses during ICB treatment might also be influenced by other factors which potentially affect the interpretation of ICB-mediated effects.

Four cancer patients within the analyzed cohort received chemotherapy prior to starting ICB treatment and, as outlined above, chemotherapeutic agents are capable of exerting peripheral immunosuppressive effects, e.g. interfering with CD8-positive cytotoxic T cells [434]. Hence, preceding chemotherapy might impact the expansion of FSP-specific T cells and the magnitude of the respective responses.

Two patients presented with progressive disease during the course of ICB therapy. As different components of the immune system contribute to cancer progression, it seems conceivable that this might also impact FSP-specific T cell responses. Various immune cell populations, e.g. MDSCs, Treg cells and tumor-associated macrophages (TAMs), have been shown to promote progression via diverse mechanisms and on multiple levels. For instance, TAMs are known to stimulate angiogenesis, epithelial-mesenchymal transition, cancer cell proliferation and remodeling of the extracellular matrix. TAMs can also suppress the adaptive immune system, e.g. by secreting cytokines, such as IL-10 and TGFB, and thereby contribute to cancer growth and dissemination [444, 445].

The conducted immunological analysis revealed stagnating T cell responses against the majority of FSPs for both patients displaying disease progression at the first staging. However, this purely descriptive delineation warrants the evaluation of potential alterations in FSP-specific T cell responses related to cancer progression, which was outside the scope of this thesis.

Data on ICB-dependent FSP responses in the literature have been very scarce and limited to FSPs with likely low relevance in MSI cancer [139]. Moreover, the cohort size of respective studies was small and the expansion of FSP-specific T cells upon ICB treatment has only been assessed in three cancer patients [139]. The analyses in the present thesis significantly expanded available data and successfully prepared the ground for prospective multi-center studies on longitudinal patterns of FSP responses under ICB treatment. The present thesis also provides first qualitative results indicating that upon onset of ICB therapy increases of FSP-specific T cell responses occur in a subset of treated patients. The clinical significance of such alterations, also in comparison with dynamic decreases observed in other patients, needs to be addressed in future studies.

5.2.4 Correlation analysis of the HLA genotype and FSP-specific T cell responses

The recognition of FSP neoantigens by T cells requires the successful processing of the peptide and subsequent presentation of respective epitopes by HLA molecules. An individual's HLA type determines the repertoire of presented tumor-derived antigens and thereby shapes anti-tumor immunity [100, 101]. In order to account for this host factor, the analysis of FSP-specific T cell responses was complemented by HLA typing. Epitope binding for the 13 applied FSPs and the identified HLA types was predicted and combined with the obtained immunological data. As all analyses were performed with PBMCs and without separation of CD4- and CD8-positive T cells, combined predictions for HLA-A, -B and -DR were applied.

The performed correlation analysis revealed predicted binding of FSP epitopes for all analyzed individuals (healthy LS carriers and MSI cancer patients). FSPs that induced pronounced systemic immune responses encompassed at least one strong HLA binding peptide that corresponded to the patient's HLA genotype. Only two individuals displayed a lack of predicted binding for one FSP. In line, both individuals did not show measurable T cell responses against the given FSP. Overall, the analysis of this limited cohort did not yield substantial HLA-dependent inter-individual differences in FSP-specific T cell responses.
Additionally, a peptide-wise analysis displayed multiple predicted strong binding epitopes for 12/13 FSPs, which were only lacking for the CASP5 FSP. Accordingly, CASP5-specific T cell responses in healthy LS carriers and MSI cancer patients were found to be generally lower, compared to the remaining FSPs. However, weak binding FSP epitopes were apparently able to trigger measurable immune responses, which is in line with previous studies reporting

that peptides with weak or no binders were capable of initiating T cell responses [446, 447]. Notably, the present thesis has identified CASP5 as a potential candidate FSP for LS diagnostics, further supporting that predicted weak binding is an insufficient indicator for lack of immunogenicity. Further, the immunogenic properties of the CASP5 FSP have previously been described in MSI malignancies [78, 448].

In general, no clear consensus concerning the link between strong HLA binding and immunogenicity exists and opposing data are found in the existing literature. A study by Bjerregaard et al. showed that immunogenic peptides typically bind HLA molecules with a stronger affinity, compared to non-immunogenic peptides [449]. However, Duan et al. suggested that binding affinity scores alone are not an effective predictor of immunogenicity and identified weak binding epitopes were capable of eliciting CD8-dependent immunity [450]. In line, previous findings indicate that HLA ligands might be missed when applying the routinely used binding affinity threshold of $IC_{50} \leq 500$, corresponding to the percentile rank ≤ 2 [451–454], as it was done in the present thesis. Many prediction tools also display a less robust performance for non-canonical HLA class I sizes, shorter or longer than 9–10mers, which are known to be antigenic targets [455]. Further, predictive algorithms typically do not account for proteasomal antigen processing, peptide transport and T cell binding, which often results in a limited accuracy [452]. Noteworthy, prediction of HLA class II-binding epitopes is more complex and less accurate [452]. The limited correlation between epitope binding predictions and T cell activation should be considered when interpreting the obtained results.

In summary, the correlation analysis of HLA-peptide binding predictions and FSP-specific T cell responses indicated suitability of the selected FSP panel for the effective detection of FSP-specific immune responses in MSI cancer patients with different HLA types. Moreover, the obtained results supported the applicability of the described FSP panel for the identification of healthy LS carriers in the European Caucasian population. However, a reliable assessment of the used FSPs warrants the validation in substantially larger cohorts as an HLA-independent set of FSPs will be necessary to ensure the general applicability of a diagnostic tool based on FSP-specific T cell responses. In the future, large international studies should further investigate the HLA genotype's impact and relevance on LS carrier's cancer risk as well as on clinical prognosis in patients with immunogenic cancer types.

5.2.5 Analysis of cMS mutation patterns and corresponding peripheral T cell responses in MSI cancer patients

The comparative analysis of cMS mutations and FSP-specific immune responses did not reveal a significant correlation. This might be attributable to the interplay of mechanisms favoring negative and positive correlations and the performed analysis points towards two conceivable

scenarios. First, cancer-associated cMS mutations give rise to FSPs and corresponding T cell responses can be detected in the peripheral blood. Second, cell clones with cMS mutations giving rise to highly immunogenic FSPs are counterselected during MSI tumor development and specific T cell responses are reminiscent of such an immunoediting event. The given cMS mutation pattern possibly depends on the time point of sampling during tumor evolution, which would be an interesting aspect for future analyses. Moreover, the analysis of prior malignancies and metastases in these patients could be of value and provide additional information on the immunologically shaped mutational landscape of MSI cancers.

5.3 Plasma-derived EVs and their DNA cargo as novel MSI testing approach

Within recent years, the role of EVs in various aspects of tumorigenesis and their clinical potential have been the focus of extensive research. The value of EVs as potential clinical biomarkers is mainly based on their complex cargo reflecting the state of the parental cell and their easy accessibility via different bodily fluids [277, 288, 289]. The present thesis aimed to investigate the suitability of plasma-derived vesicular DNA as novel, tumor tissue-independent MSI detection approach, which could find valuable predictive or diagnostic application.

A study by Fricke et al. has previously reported that EVs can carry MSI-associated indel mutations and thereby mirror the mutational landscape of their parental MMR-D cell line [300]. However, successful determination of indel mutations in plasma-derived EVs from MSI cancer patients has not been shown so far. Importantly, the present thesis demonstrated the presence of MSI vesicular DNA in EVs from MSI cancer patients. The DNA cargo of plasma-derived EVs enabled the correct determination of the cancer's MSI status in 9/15 (60 %) patients. Moreover, the obtained allelic patterns for four non-coding microsatellite markers presented high concordance between vesicular DNA and the underlying cancer, indicating maintenance of the cancer's MSI phenotype in cancer-secreted plasma EVs.

The respective cohort of cancer patients was selected based on their high cancer burden (stage IV), presumably associated with a high number of circulating EVs, to facilitate the described proof-of-concept for MSI detectability in plasma EVs. The elevated number of EVs released by malignant cells has been demonstrated by multiple studies and a single cancer cell was estimated to release more than 10^4 EVs per day [456, 457]. In line, the present analysis indicated an association between cancer burden and MSI detectability in vesicular DNA as the MSI phenotype was particularly identified prior to ICB therapy start and soon after disease progression.

Furthermore, the EV-associated MSI status at different time points of ICB therapy was aligned with the clinical course of cancer patients, descriptively assessing the potential of plasma-derived EVs to be used as therapy response markers. The MSI phenotype in EVs disappeared with advancing therapy in three patients presenting stable disease or mixed responses. The observed loss of MSI signals in vesicular DNA might possibly be related to therapy response and an accompanying reduction of the cancer size, in turn leading to a decreased proportion of cancer-derived EVs in the plasma. The predictive potential of EVs in the context of MSI cancer and ICB therapy should be assessed via longitudinal analysis of larger cohorts.

As an additional aspect of the present study, the localization of EV-associated DNA was evaluated. In an explorative experiment, isolated EVs were treated with DNase I to remove all surface-bound DNA. Subsequent vesicular DNA extraction and fragment analysis revealed the persistence of the MSI phenotype in DNase-treated EVs. This indicates that MSI DNA is at least partly transported within the membrane-enclosed vesicular lumen of cancer-derived EVs. Several previous studies have reported that most of the EVs' DNA content is externally associated with the EV membrane and the distribution of surface-associated and internal DNA is thought to vary among different EV populations [458–460]. However, the implications of DNA location for various liquid biopsy applications remain to be elucidated.

Additional mutational analyses, covering canonical driver mutations in *BRAF* and *KRAS*, were conducted in order to substantiate the proposed tumor origin of EVs and further assess the sensitivity of the approach. Previous studies, using mutation-specific primers and NGS-based approaches, have already confirmed the presence of different point mutations, e.g. in *BRAF*, *KRAS*, *EGFR* and *p53*, in EVs derived from cultured cell lines, serum, plasma and lymphatic drainages [458, 461–465]. However, within the present analysis, no *BRAF* or *KRAS* mutations in vesicular DNA could be observed in patients with an accordingly mutated cancer. In rare cases, CRCs have been shown to present intratumoral heterogeneity of the *BRAF*/*KRAS* mutation status, which might affect the number of plasma-derived EVs carrying the respective mutation and hinder the detection of the respective mutations in vesicular DNA [466]. Another possible explanation for the discordant results might be the different time points of cancer tissue and plasma sampling. Möhrman et al. have reported discrepancy in the *BRAF*, *KRAS* and *EGFR* mutation status between archival tissue specimens and plasma-derived EVs with a median interval of 20 months between sample collection [461]. The respective time period between tissue and plasma sampling for the analyzed cohort was typically longer than the interval reported by Möhrmann et al. and could affect the mutation detectability. However, the observed absence of driver mutations in vesicular DNA might also point at insufficient technical sensitivity. Hence, the present thesis comprised the methodological establishment of organ-specific enrichment approaches for plasma-derived EVs.

The glycoprotein A33 was selected as a candidate for the enrichment of colon-specific EVs as it was shown to be highly expressed in colonic epithelium and 95 % of MSI CRCs [345]. Moreover, its suitability for the enrichment of CRC-derived EV subsets has been demonstrated before [346, 467]. Within the present thesis, two *in vitro* immunoaffinity-based strategies for an A33-targeting enrichment of EVs were successfully established using the MSI CRC cell line LIM1215. A33-based capture of EVs was achieved with protein G- as well as streptavidin-coated magnetic beads and demonstrated by western blot.
However, the established approach could not be directly transferred to plasma-derived EVs. Western blot analysis was found to be incompatible with EV isolation via PEG-based precipitation, which is possibly related to a high amount of co-precipitated non-EV material, such as lipoproteins [257, 468, 469]. Thus, all subsequent experiments were performed with EVs isolated by ultracentrifugation. Overall, several explanations for the failed detection of A33-positive plasma EVs are conceivable. First, the specific capture of A33-specific EVs might be hindered by unspecific interactions between the used anti-A33 antibody and plasma-associated components in EV preparations. Moreover, unspecific binding of plasma EVs to magnetic beads was observed. A33 might also be masked by other surface-bound molecules, preventing specific antibody binding. Second, the detection via western blot was unsuitable for the number of A33-positive EVs in plasma and the resulting protein amount. Notably, all immunoprecipitation experiments were conducted using EVs derived from healthy individuals. The detection of A33-positive EVs in MSI CRC patients, supposedly secreting more A33-positive EVs, was not conducted within the present thesis due to the limited volume of available plasma.

Ultimately, a different strategy, allowing easier quantification, for the detection and planned enrichment of colon-specific EVs was pursued. An indirect ELISA, performed with different concentrations of EVs, indicated the presence of A33-positive, colon-specific EVs in plasma from healthy controls. The potential of ELISA-based strategies for the detection of specific plasma-derived EVs has already been demonstrated by several studies [291, 470]. Prospectively, further experiments shall confirm the specificity of the described analysis and its suitability for enrichment of colon-specific EVs. Moreover, the applicability and potential superiority of other protein markers should be evaluated. For instance, guanylyl cyclase C (GUCY2C), a transmembrane protein with high expression in the intestinal epithelium and in nearly 100 % of CRCs, might be suited for EV enrichment approaches [471].

In summary, the present thesis, for the first time, identified the MSI phenotype in plasma-derived vesicular DNA from MSI cancer patients. The observed changes in the EVs' MSI status during the course of ICB therapy underlines the potential of vesicular DNA to be used clinically, e.g. as ICB therapy marker. The described findings further suggest a versatile suitability of plasma EVs, e.g. for the detection of tumor occurrence in LS individuals and

identification of LS carriers. It is expected that these applications require an increased technical sensitivity. Therefore, a novel approach to enrich specific plasma-derived EVs has been developed within the frame of the present project and preliminary data indicating its feasibility have been obtained. In the future, the clinical application of plasma-derived EVs as liquid biopsy-based MSI detection tool will demand standardized isolation of EVs, technical optimization and analysis of larger cohorts.

5.4 Outlook

The present thesis emphasizes three major findings. First, the normal colorectal mucosa was indicated as a possible cancer risk modifier in LS carriers. Second, candidate FSPs, associated with elevated T cell responses in healthy LS carriers, were identified and might be suited as tumor-independent LS diagnostic markers. Third, the MSI phenotype was detected in plasma-derived vesicular DNA from MSI cancer patients.

The systematic evaluation of the existing literature on immune infiltration and immune evasion phenomena in MSI tumors revealed evidence for immunological differences between hereditary and sporadic tumors. As previous studies focused on colorectal and rarely also on endometrial tissue, the characterization of the local immune phenotype in other tumors of the LS spectrum would clarify whether the observed differences are restricted to these entities or applicable to LS in general. Furthermore, the clinical relevance of the described immunological alterations should be evaluated in the future, particularly with regard to ICB therapy and guiding the respective patient selection.

Beyond the boundaries of the tumor, the presented analysis of immune profiles in the normal colonic mucosa identified the mucosal immune milieu as a novel potential risk factor for CRC development in LS carriers. Based on these findings, a multi-center European validation study has been initiated to assess the cancer-predictive potential of mucosal immune infiltration in a large cohort of LS carriers over a period of five years. Additionally, comprehensive immune profiling of other at-risk tissues in LS carriers, e.g. endometrium, is needed to affirm the general character of the proposed role of the local immune milieu. A comparative analysis with healthy non-LS controls will reveal whether the described mucosal characteristics of LS carriers are unique. If confirmed, this could further potentiate the possible clinical application of mucosal immune profiles for LS diagnostics. Further, single cell sequencing and multiplex flow cytometry approaches may further advance comprehensive immune profiling in the normal colorectal mucosa.

Prospectively and after successful validation in future studies, immune profiling of normal mucosa biopsies could be suitable for early LS diagnostics. The observed differences in the immune composition of normal mucosa in LS and non-LS individuals may serve, potentially in combination with systemic FSP-specific immune responses, as tumor-independent markers for LS. Ideally, the analysis of local immune cell profiles through routine surveillance colonoscopy in the general population could be used as a novel LS screening strategy. Based on the results of the present thesis, a study has been initiated to evaluate the diagnostic accuracy and clinical applicability of mucosa-based LS identification, also implementing cutting-edge technologies based on machine learning.
The observed immunological differences in the normal mucosa of healthy LS carriers and LS CRC patients could also provide insight into alterations of the immune cell composition which are indicative of an increased cancer risk and tumor development. Accordingly, longitudinal sampling of normal colorectal mucosa in identified LS carriers and monitoring of shifts in mucosal immune cell populations may be a valuable tool for dynamic tumor risk assessment.

The present thesis observed systemic FSP-specific immune responses in LS carriers prior to tumor manifestation, providing the first independent validation of a previous report by Schwitalle et al. [80]. These results suggest that systemic FSP-specific immune cells significantly contribute to the mucosal LS immune phenotype described above. The results also pave the way for prospective validation of the identified FSP candidates as early tumor-independent LS diagnostic markers in substantially larger cohorts, also accounting for the diversity of HLA genotypes. The transfer into the clinical setting will require the development of a simplified assay, e.g. delayed hypersensitivity assay, providing functional analysis of FSP-specific T cell responses. Moreover, peptide microarrays could enable a rapid serological identification of LS carriers and thereby improve LS diagnostics. Furthermore, longitudinal sampling and analysis of FSP-specific immune responses in LS individuals might provide insights into early LS-associated tumorigenesis and possibly guide strategies for prevention of MSI tumors. The impact of tumor manifestation on systemic FSP-specific immune responses will require extensive research to uncover the underlying mechanisms and eventually enable their application in different clinical settings, e.g. as ICB therapy response markers, in the future.

The present thesis is the first to provide unequivocal evidence for the presence of MSI in EVs isolated from MSI cancer patients. It also demonstrated that the vesicular MSI status may reflect ICB therapy response, highlighting EVs' great potential for non-invasive therapy monitoring. In the future, the enrichment of organ- and/or cancer-specific EVs will aid to broaden the area of clinical applications. This will require methodological adjustment of the indirect ELISA approach, which entails validation of the enrichment specificity, optimization of the assay's sensitivity, e.g. by applying a sandwich ELISA system, and evaluation of different marker proteins. Prospectively, capture of specific EV populations may further enable

minimally invasive early MSI cancer detection in LS individuals and identification of LS carriers. To exploit the full clinical potential of vesicular DNA the use of whole plasma, bypassing time-intensive EV isolation, should be facilitated to enable a rapid blood-based detection of MSI. Besides, the establishment of an ELISA-based quantification of cancer-derived EVs and associated marker proteins might serve as a potential tool for cancer screening, independent of the MSI status.

Taken together, the presented results demonstrate the significance of local and systemic immune responses in LS carriers and elucidate their clinical potential. Harnessing these immune responses and plasma-derived vesicular DNA for diagnostic purposes might aid the identification of LS carriers prior to tumor manifestation and thereby contribute to the reduction of LS-associated cancer risk and decrease the burden of preventable cancers.

Publications

Parts of this thesis have been published in:

Bohaumilitzky, L., Doeberitz, M. v. K., Kloor, M. Ahadova, A. Implications of Hereditary Origin on the Immune Phenotype of Mismatch Repair-Deficient Cancers: Systematic Literature Review. *J Clin Med.* **9**, 1741 (2020)

Bohaumilitzky, L., Kluck, K., Hüneburg, R., Gallon, R., Nattermann, J., Kirchner, M., Kristiansen, G., Hommerding, O., Pfuderer, P. L., Wagner, L., Echterdiek, F., Kösegi, S., Müller, N., Fischer, K., Nelius, N., Hartog, B., Borthwick, G., Busch, E., Haag, G. M., Bläker, H., Möslein, G., von Knebel Doeberitz, M., Seppälä, T. T., Ahtiainen, M., Meck- lin, J. P., Bishop, D. T., Burn, J., Stenzinger, A., Budczies, J., Kloor, M. Ahadova, A. The Different Immune Profiles of Normal Colonic Mucosa in Cancer-Free Lynch Syndrome Carriers and Lynch Syndrome Colorectal Cancer Patients. *Gastroenterology*, **162**, 907–919.e10 (2022)

References

[1] Sung, H., Ferlay, J., Siegel, R. L., Laversanne, M., Soerjomataram, I., Jemal, A. & Bray, F. Global Cancer Statistics 2020: GLOBOCAN Estimates of Incidence and Mortality Worldwide for 36 Cancers in 185 Countries. *CA Cancer J Clin.* **71,** 209–249 (2021).

[2] Bray, F., Laversanne, M., Weiderpass, E. & Soerjomataram, I. The ever-increasing importance of cancer as a leading cause of premature death worldwide. *Cancer.* **127,** 3029–3030 (2021).

[3] Fidler, M. M., Soerjomataram, I. & Bray, F. A global view on cancer incidence and national levels of the human development index. *Int J Cancer.* **139,** 2436–2446 (2016).

[4] Arnold, M., Sierra, M. S., Laversanne, M., Soerjomataram, I., Jemal, A. & Bray, F. Global patterns and trends in colorectal cancer incidence and mortality. *Gut.* **66,** 683–691 (2017).

[5] Siegel, R. L., Miller, K. D., Sauer, A. G., Fedewa, S. A., Butterly, L. F., Anderson, J. C., Cercek, A., Smith, R. A. & Jemal, A. Colorectal cancer statistics, 2020. *CA Cancer J Clin.* **70,** 145–164 (2020).

[6] Fedirko, V., Tramacere, I., Bagnardi, V., Rota, M., Scotti, L., Islami, F., Negri, E., Straif, K., Romieu, I., La Vecchia, C., Boffetta, P. & Jenab, M. Alcohol drinking and colorectal cancer risk: an overall and dose–response meta-analysis of published studies. *Ann Oncol.* **22,** 1958–1972 (2011).

[7] Botteri, E., Iodice, S., Bagnardi, V., Raimondi, S., Lowenfels, A. B. & Maisonneuve, P. Smoking and colorectal cancer: a meta-analysis. *JAMA.* **300,** 2765–2778 (2008).

[8] Schreuders, E. H., Ruco, A., Rabeneck, L., Schoen, R. E., Sung, J. J., Young, G. P. & Kuipers, E. J. Colorectal cancer screening: a global overview of existing programmes. *Gut.* **64,** 1637–1649 (2015).

[9] Keum, N. N. & Giovannucci, E. Global burden of colorectal cancer: emerging trends, risk factors and prevention strategies. *Nat Rev Gastroenterol Hepatol.* **16,** 713–732 (2019).

[10] Haggar, F. a., Boushey, R. P. & Ph, D. Colorectal Cancer Epidemiology: Incidence, Mortality, Survival, and Risk Factors. *Clin Colon Rectal Surg.* **22,** 191–197 (2009).

[11] O'Connell, J. B., Maggard, M. A. & Ko, C. Y. Colon cancer survival rates with the new American Joint Committee on Cancer sixth edition staging. *J Natl Cancer Inst.* **96,** 1420–1425 (2004).

[12] Buchner, A. M. The Role of Chromoendoscopy in Evaluating Colorectal Dysplasia. *Gastroenterol Hepatol (N Y).* **13,** 336–347 (2017).

[13] Xie, Y.-H., Chen, Y.-X. & Fang, J.-Y. Comprehensive review of targeted therapy for colorectal cancer. *Signal Transduct Target Ther.* **5** (2020).

[14] Brown, K. G., Solomon, M. J., Mahon, K. & O'Shannassy, S. Management of colorectal cancer. *BMJ.* **366,** 1–7 (2019).

[15] Biller, L. H. & Schrag, D. Diagnosis and Treatment of Metastatic Colorectal Cancer: A Review. *JAMA.* **325,** 669–685 (2021).

[16] Stoffel, E. M., Koeppe, E., Everett, J., Ulintz, P., Kiel, M., Osborne, J., Williams, L., Hanson, K., Gruber, S. B. & Rozek, L. S. Germline Genetic Features of Young Individuals with Colorectal Cancer. *Gastroenterology.* **154,** 897–905 (2018).

[17] Vuik, F. E., Nieuwenburg, S. A., Bardou, M., Lansdorp-Vogelaar, I., Dinis-Ribeiro, M., Bento, M. J., Zadnik, V., Pellisé, M., Esteban, L., Kaminski, M. F., Suchanek, S., Ngo, O., Májek, O., Leja, M., Kuipers, E. J. & Spaander, M. C. Increasing incidence of colorectal cancer in young adults in Europe over the last 25 years. *Gut.* **68,** 1820–1826 (2019).

[18] Grady, W. M. Genetic testing for high-risk colon cancer patients. *Gastroenterology.* **124,** 1574–1594 (2003).

[19] Jasperson, K. W., Tuohy, T. M., Neklason, D. W. & Burt, R. W. Hereditary and Familial Colon Cancer. *Gastroenterology.* **138,** 2044–2058 (2010).

[20] Monahan, K. J., Bradshaw, N., Dolwani, S., Desouza, B., Dunlop, M. G., East, J. E., Ilyas, M., Kaur, A., Lalloo, F., Latchford, A., Rutter, M. D., Tomlinson, I., Thomas, H. J. & Hill, J. Guidelines for the management of hereditary colorectal cancer from the British Society of Gastroenterology (BSG)/Association of Coloproctology of Great Britain and Ireland (ACPGBI)/United Kingdom Cancer Genetics Group (UKCGG). *Gut.* **69,** 411–444 (2020).

[21] Tariq, K. & Ghias, K. Colorectal cancer carcinogenesis: a review of mechanisms. *Cancer Biol Med.* **13,** 120–135 (2016).

[22] Grady, W. M. Genomic instability and colorectal cancer. *Curr Opin Gastroenterol.* **16,** 62–67 (2000).

[23] Pino, M. S. & Chung, D. C. The chromosomal instability pathway in colon cancer. *Gastroenterology.* **138,** 2059 (2010).

[24] Cahill, D. P., Lengauer, C., Yu, J., Riggins, G. J., Willson, J. K., Markowitz, S. D., Kinzler, K. W. & Vogelstein, B. Mutations of mitotic checkpoint genes in human cancers. *Nature* **392,** 300–303 (1998).

[25] Von Morgen, P. & Maciejowski, J. The ins and outs of telomere crisis in cancer. *Genome Med.* **10** (2018).

[26] Katona, B. W. & Lynch, J. P. in *Physiology of the Gastrointestinal Tract: Sixth Edition* Sixth Edit, 1615–1642 (2018).

[27] Shih, I.-M., Zhou, W., Goodman, S. N., Lengauer, C., Kinzler, K. W. & Vogelstein, B. Evidence That Genetic Instability Occurs at an Early Stage of Colorectal Tumorigenesis. *Cancer Res.* **61** (2001).

[28] Shen, L., Toyota, M., Kondo, Y., Lin, E., Zhang, L., Guo, Y., Hernandez, N. S., Chen, X., Ahmed, S., Konishi, K., Hamilton, S. R. & Issa, J. P. J. Integrated genetic and epigenetic analysis identifies three different subclasses of colon cancer. *Proc Natl Acad Sci U S A.* **104,** 18654 (2007).

[29] Fearon, E. R. & Vogelstein, B. A genetic model for colorectal tumorigenesis. *Cell* **61,** 759–767 (1990).

[30] Powell, S. M., Zilz, N., Beazer-Barclay, Y., Bryan, T. M., Hamihont, S. R., Thibodeau J, S. N., Vogelstein, B. & Kinzler, K. W. APC mutations occur early during colorectal tumorigenesis. *Nature.* **359,** 235–237 (1992).

[31] Kaplan, K. B., Burds, A. A., Swedlow, J. R., Bekir, S. S., Sorger, P. K. & Näthke, I. S. A role for the Adenomatous Polyposis Coli protein in chromosome segregation. *Nat Cell Biol.* **3,** 429–432 (2001).

[32] Fodde, R., Kuipers, J., Rosenberg, C., Smits, R., Kielman, M., Gaspar, C., Van Es, J. H., Breukel, C., Wiegant, J., Giles, R. H. & Clevers, H. Mutations in the APC tumour suppressor gene cause chromosomal instability. *Nat Cell Biol.* **3,** 433–438 (2001).

[33] Aoki, K., Aoki, M., Sugai, M., Harada, N., Miyoshi, H., Tsukamoto, T., Mizoshita, T., Tatematsu, M., Seno, H., Chiba, T., Oshima, M., Hsieh, C. L. & Taketo, M. M. Chromosomal instability by β-catenin/TCF transcription in APC or β-catenin mutant cells. *Oncogene.* **26,** 3511–3520 (2007).

[34] Hadjihannas, M. V., Brückner, M., Jerchow, B., Birchmeier, W., Dietmaier, W. & Behrens, J. Aberrant Wnt/β-catenin signaling can induce chromosomal instability in colon cancer. *Proc Natl Acad Sci U S A.* **103,** 10747–10752 (2006).

[35] Kinzler, K. W. & Vogelstein, B. Lessons from Hereditary Colorectal Cancer. *Cell.* **87,** 159–170 (1996).

[36] Fearon, E. R. Molecular Genetics of Colorectal Cancer. *Annu Rev Pathol.* **6,** 479–507 (2011).

[37] Santini, D., Loupakis, F., Vincenzi, B., Floriani, I., Stasi, I., Canestrari, E., Rulli, E., Maltese, P. E., Andreoni, F., Masi, G., Graziano, F., Baldi, G. G., Salvatore, L., Russo, A., Perrone, G., Tommasino, M. R., Magnani, M., Falcone, A., Tonini, G. & Ruzzo, A. High concordance of KRAS status between primary colorectal tumors and related metastatic sites: implications for clinical practice. *Oncologist.* **13,** 1270–1275 (2008).

[38] Ogino, S., Nosho, K., Irahara, N., Shima, K., Baba, Y., Kirkner, G. J., Meyerhardt, J. A. & Fuchs, C. S. Prognostic Significance and Molecular Associations of 18q Loss of Heterozygosity: A Cohort Study of Microsatellite Stable Colorectal Cancers. *J Clin Oncol.* **27,** 4591–4598 (2009).

[39] Nakayama, M. & Oshima, M. Mutant p53 in colon cancer. *J Mol Cell Biol.* **11,** 267–276 (2019).

[40] Lin, E. I., Tseng, L. H., Gocke, C. D., Reil, S., Le, D. T., Azad, N. S. & Eshleman, J. R. Mutational profiling of colorectal cancers with microsatellite instability. *Oncotarget.* **6,** 42334–42344 (2015).

[41] Nguyen, H. T. & Duong, H. Q. The molecular characteristics of colorectal cancer: Implications for diagnosis and therapy (review). *Oncol Lett.* **16,** 9–18 (2018).

[42] Mojarad, E. N., Kuppen, P. J., Aghdaei, H. A. & Zali, M. R. The CpG island methylator phenotype (CIMP) in colorectal cancer. *Gastroenterol Hepatol Bed Bench.* **6,** 120–128 (2013).

[43] Issa, J.-P. CpG island methylator phenotype in cancer. *Nat Rev Cancer.* **4,** 988–993 (2004).

[44] Lao, V. V. & Grady, W. M. Epigenetics and Colorectal Cancer. *Nat Rev Gastroenterol Hepatol.* **8,** 686–700 (2011).

[45] Esteller, M. CpG island hypermethylation and tumor suppressor genes: a booming present, a brighter future. *Oncogene.* **21,** 5427–5440 (2002).

[46] Ogino, S., Cantor, M., Kawasaki, T., Brahmandam, M., Kirkner, G. J., Weisenberger, D. J., Campan, M., Laird, P. W., Loda, M. & Fuchs, C. S. CpG island methylator phenotype (CIMP) of colorectal cancer is best characterised by quantitative DNA methylation analysis and prospective cohort studies. *Gut.* **55,** 1000–1006 (2006).

[47] Toyota, M., Ahuja, N., Ohe-Toyota, M., Herman, J. G., Baylin, S. B. & Issa, J. P. CpG island methylator phenotype in colorectal cancer. *Proc Natl Acad Sci U S A.* **96,** 8681–8686 (1999).

[48] Woerner, S. M., Kloor, M., von Knebel Doeberitz, M. & Gebert, J. F. Microsatellite instability in the development of DNA mismatch repair deficient tumors. *Cancer Biomark.* **2,** 69–86 (2006).

[49] Kunkel, T. A. & Erie, D. A. DNA mismatch repair. *Annu Rev Biochem.* **74,** 681–710 (2005).

[50] Arana, M. E. & Kunkel, T. A. Mutator phenotypes due to DNA replication infidelity. *Semin Cancer Biol.* **20,** 304–311 (2010).

[51] Modrich, P. Mechanisms in E. coli and Human Mismatch Repair. *Angew Chem Int Ed Engl.* **55,** 8490–8501 (2016).

[52] Yang, W. Structure and function of mismatch repair proteins. *Mutat Res.* **460,** 245–256 (2000).

[53] Modrich, P. Mechanisms and biological effects of mismatch repair. *Annu Rev Genet.* **25,** 229–53 (1991).

[54] Aravind, L., Walker, D. R. & Koonin, E. V. Conserved domains in DNA repair proteins and evolution of repair systems. *Nucleic Acids Res.* **27,** 1223–1242 (1999).

[55] Kolodner, R. Biochemistry and genetics of eukaryotic mismatch repair. *Genes Dev.* **10,** 1433–1442 (1996).

[56] Li, G. M. Mechanisms and functions of DNA mismatch repair. *Cell Res.* **18,** 85–98 (2008).

[57] Kadyrova, L. Y., Gujar, V., Burdett, V., Modrich, P. L. & Kadyrov, F. A. Human MutLγ, the MLH1-MLH3 heterodimer, is an endonuclease that promotes DNA expansion. *Proc Natl Acad Sci U S A.* **117,** 3535–3542 (2020).

[58] Hsieh, P. & Yamane, K. DNA mismatch repair: molecular mechanism, cancer, and ageing. *Mech Ageing Dev.* **129,** 391–407 (2008).

[59] Liu, D., Keijzers, G. & Rasmussen, L. J. DNA mismatch repair and its many roles in eukaryotic cells. *Mutat Res Rev Mutat Res.* **773,** 174–187 (2017).

[60] Sameer, A. S., Nissar, S. & Fatima, K. Mismatch repair pathway: Molecules, functions, and role in colorectal carcinogenesis. *Eur J Cancer Prev.* **23,** 246–257 (2014).

[61] Bhattacharyya, N. P., Skandalis, A., Ganesh, A., Groden, J. & Meuth, M. Mutator phenotypes in human colorectal carcinoma cell lines. *Proc Natl Acad Sci U S A.* **91,** 6319–6323 (1994).

[62] Parsons, R., Li, G. M., Longley, M. J., horng Fang, W., Papadopoulos, N., Jen, J., de la Chapelle, A., Kinzler, K. W., Vogelstein, B. & Modrich, P. Hypermutability and mismatch repair deficiency in RER+ tumor cells. *Cell* **75,** 1227–1236 (1993).

[63] Ellegren, H. Microsatellites: Simple sequences with complex evolution. *Nat Rev Genet.* **5,** 435–445 (2004).

[64] Thompson, R., Zoppis, S. & McCord, B. *An Overview of DNA Typing Methods for Human Identification: Past, Present, and Future* 3–16 (Humana Press, 2012).

[65] Kloor, M. & von Knebel Doeberitz, M. The immune biology of microsatellite unstable cancer. *Trends Cancer.* **2,** 121–133 (2016).

[66] Boland, C. R. & Goel, A. Microsatellite Instability in Colorectal Cancer. *Gastroenterology.* **138,** 2073–2087 (2010).

[67] Kim, T. M., Laird, P. W. & Park, P. J. The Landscape of Microsatellite Instability in Colorectal and Endometrial Cancer Genomes. *Cell.* **155,** 858–868 (2013).

[68] Alhopuro, P., Sammalkorpi, H., Niittymäki, I., Biström, M., Raitila, A., Saharinen, J., Nousiainen, K., Lehtonen, H. J., Heliövaara, E., Puhakka, J., Tuupanen, S., Sousa, S., Seruca, R., Ferreira, A. M., Hofstra, R. M., Mecklin, J. P., Järvinen, H., Ristimäki, A., Ørntoft, T. F., Hautaniemi, S., Arango, D., Karhu, A. & Aaltonen, L. A. Candidate driver genes in microsatellite-unstable colorectal cancer. *Int J Cancer.* **130,** 1558–1566 (2012).

[69] Markowitz, S., Wang, J., Myeroff, L., Parsons, R., Sun, L., Lutterbaugh, J., Fan, R. S., Zborowska, E., Kinzler, K. W., Brattain, M., Willson, J. K. V., Parsons, R., Sun, L., Lutterbaugh, J., Robert, S., Zborowska, E., Kinzler, K. W., Vogelstein, B., Brattain, M., Willson, J. K. V., Markowitz, S., Wang, J. & Myeroff, L. Inactivation of the Type II

TGF-β Receptor in Colon Cancer Cells with Microsatellite Instability. *Science.* **268,** 1336–1338 (1995).

[70] Parsons, R., Myeroff, L. L., Liu, B., Willson, J. K. V., Markowitz, S. D., Kinzler, K. W. & Vogelstein, B. Microsatellite Instability and Mutations of the Transforming Growth Factor beta Type II Receptor Gene in Colorectal Cancer. *Cancer Res.* **55,** 5548–5550 (1995).

[71] Rampino, N., Yamamoto, H., Li, Y., Sawai, H., Reed, J. C. & Perucho, M. Somatic Frameshift Mutations in the BAX Gene in Colon Cancers of the Microsatellite Mutator Phenotype. *Science.* **275,** 967–969 (1997).

[72] Townsend, A., Ohlen, C., Rogers, M., Edwards, J., Mukherjee, S. & Bastin, J. Source of unique tumour antigens. *Nature.* **371,** 662 (1994).

[73] Von Knebel Doeberitz, M. & Kloor, M. Towards a vaccine to prevent cancer in Lynch syndrome patients. *Fam Cancer.* **12,** 307–312 (2013).

[74] Linnebacher, M., Gebert, J., Rudy, W., Woerner, S., Yuan, Y. P., Bork, P. & von Knebel Doeberitz, M. Frameshift peptide-derived T-cell epitopes: a source of novel tumor-specific antigens. *Int J Cancer.* **93,** 6–11 (2001).

[75] Ripberger, E., Linnebacher, M., Schwitalle, Y., Gebert, J. & von Knebel Doeberitz, M. Identification of an HLA-A0201-restricted CTL epitope generated by a tumor-specific frameshift mutation in a coding microsatellite of the OGT gene. *J Clin Immunol.* **23,** 415–423 (2003).

[76] Sæterdal, I., Bjørheim, J., Lislerud, K., Gjertsen, M. K., Bukholm, I. K., Olsen, O. C., Nesland, J. M., Eriksen, J. A., Møller, M., Lindblom, A. & Gaudernack, G. Frameshift-mutation-derived peptides as tumor-specific antigens in inherited and spontaneous colorectal cancer. *Proc Natl Acad Sci U S A.* **98,** 13255–13260 (2001).

[77] Sæterdal, I., Gjertsen, M. K., Straten, P., Eriksen, J. A. & Gaudernack, G. A TFGβRII frameshift-mutation-derived CTL epitope recognised by HLA-A2-restricted CD8+T cells. *Cancer Immunol Immunother.* **50,** 469–476 (2001).

[78] Schwitalle, Y., Linnebacher, M., Ripberger, E., Gebert, J. & von Knebel Doeberitz, M. Immunogenic peptides generated by frameshift mutations in DNA mismatch repair-deficient cancer cells. *Cancer Immun.* **4,** 14 (2004).

[79] Ballhausen, A., Przybilla, M. J., Jendrusch, M., Haupt, S., Pfaffendorf, E., Seidler, F., Witt, J., Hernandez Sanchez, A., Urban, K., Draxlbauer, M., Krausert, S., Ahadova, A., Kalteis, M. S., Pfuderer, P. L., Heid, D., Stichel, D., Gebert, J., Bonsack, M., Schott, S., Bläker, H., Seppälä, T., Mecklin, J. P., Ten Broeke, S., Nielsen, M., Heuveline, V., Krzykalla, J., Benner, A., Riemer, A. B., von Knebel Doeberitz, M. & Kloor, M. The shared frameshift mutation landscape of microsatellite-unstable cancers suggests immunoediting during tumor evolution. *Nat Commun.* **11,** 4740 (2020).

[80] Schwitalle, Y., Kloor, M., Eiermann, S., Linnebacher, M., Kienle, P., Knaebel, H. P., Tariverdian, M., Benner, A. & von Knebel Doeberitz, M. Immune Response Against Frameshift-Induced Neopeptides in HNPCC Patients and Healthy HNPCC Mutation Carriers. *Gastroenterology.* **134,** 988–997 (2008).

[81] Kloor, M., Reuschenbach, M., Pauligk, C., Karbach, J., Rafiyan, M. R., Al-Batran, S. E., Tariverdian, M., Jäger, E. & von Knebel Doeberitz, M. A Frameshift Peptide Neoantigen-Based Vaccine for Mismatch Repair-Deficient Cancers: A Phase I/IIa Clinical Trial. *Clin Cancer Res.* **26,** 4503–4510 (2020).

[82] Klein, J. & Sato, A. The HLA System. First of two parts. *N Engl J Med.* **343,** 702–709 (2000).

[83] Choo, S. Y. The HLA System: Genetics, Immunology, Clinical Testing, and Clinical Implications. *Yonsei Med J.* **48,** 11–23 (2007).

[84] Gruen, J. R. & Weissman, S. M. Evolving Views of the Major Histocompatibility Complex. *Blood.* **90,** 4252–4265 (1997).

[85] Braud, V. M., Allan, D. S. & McMichael, A. J. Functions of nonclassical MHC and non-MHC-encoded class I molecules. *Curr Opin Immunol.* **11,** 100–108 (1999).

[86] Howell, W. M., Carter, V. & Clark, B. The HLA system: immunobiology, HLA typing, antibody screening and crossmatching techniques. *J Clin Pathol.* **63,** 387–390 (2010).

[87] Milner, C., Aguado, B., Campbell, R., Browning, M. & McMichael, A. in *HLA and MHC: genes, molecules and function* 39–75 (1996).

[88] Madden, K. & Chabot-Richards, D. HLA testing in the molecular diagnostic laboratory. *Virchows Arch.* **474,** 139–147 (2019).

[89] Pamer, E. & Cresswell, P. Mechanisms of MHC class I–restricted antigen processing. *Annu Rev Immunol.* **16,** 323–358 (1998).

[90] Rock, K. L. & Goldberg, A. L. Degradation of cell proteins and the generation of MHC class I-presented peptides. *Annu Rev Immunol.* **17,** 739–779 (1999).

[91] Kloetzel, P. M. The proteasome and MHC class I antigen processing. *Biochim Biophys Acta.* **1695,** 225–233 (2004).

[92] Cresswell, P. Assembly, transport, and function of MHC class II molecules. *Annu Rev Immunol.* **12,** 259–293 (1994).

[93] Pieters, J. MHC class II restricted antigen presentation. *Curr Opin Immunol.* **9,** 89–96 (1997).

[94] Trombetta, E. S. & Mellman, I. Cell biology of antigen processing in vitro and in vivo. *Annu Rev Immunol.* **23,** 975–1028 (2005).

[95] Leung, C. S. Endogenous antigen presentation of MHC class II epitopes through non-autophagic pathways. *Front Immunol.* **6,** 464 (2015).

[96] Joffre, O. P., Segura, E., Savina, A. & Amigorena, S. Cross-presentation by dendritic cells. *Nat Rev Immunol.* **12,** 557–569 (2012).

[97] Embgenbroich, M. & Burgdorf, S. Current concepts of antigen cross-presentation. *Front Immunol.* **9,** 1643 (2018).

[98] Zinkernagel, R. M. & Doherty, P. C. Restriction of in vitro T cell-mediated cytotoxicity in lymphocytic choriomeningitis within a syngeneic or semiallogeneic system. *Nature.* **248,** 701–702 (1974).

[99] Takaba, H. & Takayanagi, H. The Mechanisms of T Cell Selection in the Thymus. *Trends Immunol.* **38,** 805–816 (2017).

[100] Sebzda, E., Mariathasan, S., Ohteki, T., Jones, R., Bachmann, M. F. & Ohashi, P. S. Selection of the T cell repertoire. *Annu Rev Immunol.* **17,** 829–874 (1999).

[101] Košmrlj, A., Read, E. L., Qi, Y., Allen, T. M., Altfeld, M., Deeks, S. G., Pereyra, F., Carrington, M., Walker, B. D. & Chakraborty, A. K. Effects of thymic selection of the T cell repertoire on HLA-class I associated control of HIV infection. *Nature.* **465,** 350–354 (2010).

[102] Sommer, S. The importance of immune gene variability (MHC) in evolutionary ecology and conservation. *Front Zool.* **2,** 16 (2005).

[103] Markov, P. V. & Pybus, O. G. Evolution and Diversity of the Human Leukocyte Antigen (HLA). *Evol Med Public Health.* **1** (2015).

[104] Schumacher, T. N. & Schreiber, R. D. Neoantigens in cancer immunotherapy. *Science.* **348,** 69–74 (2015).

[105] Chowell, D., Morris, L. G., Grigg, C. M., Weber, J. K., Samstein, R. M., Makarov, V., Kuo, F., Kendall, S. M., Requena, D., Riaz, N., Greenbaum, B., Carroll, J., Garon, E., Hyman, D. M., Zehir, A., Solit, D., Berger, M., Zhou, R., Rizvi, N. A. & Chan, T. A. Patient HLA class I genotype influences cancer response to checkpoint blockade immunotherapy. *Science.* **359,** 582–587 (2018).

[106] Kloor, M., Michel, S. & von Knebel Doeberitz, M. Immune evasion of microsatellite unstable colorectal cancers. *Int J Cancer.* **127,** 1001–1010 (2010).

[107] Ozcan, M., Janikovits, J., von Knebel Doeberitz, M. & Kloor, M. Complex pattern of immune evasion in MSI colorectal cancer. *Oncoimmunology.* **7,** e1445453 (2018).

[108] Bicknell, D. C., Kaklamanis, L., Hampson, R., Bodmer, W. F. & Karran, P. Selection for β2-microglobulin mutation in mismatch repair-defective colorectal carcinomas. *Curr Biol.* **6,** 1695–1697 (1996).

[109] Cabrera, C. M., Jiménez, P., Cabrera, T., Esparza, C., Ruiz-Cabello, F. & Garrido, F. Total loss of MHC class I in colorectal tumors can be explained by two molecular pathways: β2-microglobulin inactivation in MSI-positive tumors and LMP7/TAP2 down-regulation in MSI-negative tumors. *Tissue Antigens.* **61,** 211–219 (2003).

[110] Wieczorek, M., Abualrous, E. T., Sticht, J., Álvaro-Benito, M., Stolzenberg, S., Noé, F. & Freund, C. Major Histocompatibility Complex (MHC) Class I and MHC Class

II Proteins: Conformational Plasticity in Antigen Presentation. *Front Immunol.* **8,** 292 (2017).

[111] Kloor, M., Michel, S., Buckowitz, B., Rüschoff, J., Büttner, R., Holinski-Feder, E., Dippold, W., Wagner, R., Tariverdian, M., Benner, A., Schwitalle, Y., Kuchenbuch, B. & von Knebel Doeberitz, M. Beta2-microglobulin mutations in microsatellite unstable colorectal tumors. *Int J Cancer.* **121,** 454–458 (2007).

[112] Echterdiek, F., Janikovits, J., Staffa, L., Müller, M., Lahrmann, B., Frühschütz, M., Hartog, B., Nelius, N., Benner, A., Tariverdian, M., von Knebel Doeberitz, M., Grabe, N. & Kloor, M. Low density of FOXP3-positive T cells in normal colonic mucosa is related to the presence of beta2-microglobulin mutations in Lynch syndrome-associated colorectal cancer. *Oncoimmunology.* **5,** e1075692 (2016).

[113] Janikovits, J., Müller, M., Krzykalla, J., Körner, S., Echterdiek, F., Lahrmann, B., Grabe, N., Schneider, M., Benner, A., von Knebel Doeberitz, M. & Kloor, M. High numbers of PDCD1 (PD-1)-positive T cells and B2M mutations in microsatellite-unstable colorectal cancer. *Oncoimmunology* **7,** e1390640 (2018).

[114] Dierssen, J. W. F., de Miranda, N. F. C. C., Ferrone, S., van Puijenbroek, M., Cornelisse, C. J., Fleuren, G. J., van Wezel, T. & Morreau, H. HNPCC versus sporadic microsatellite-unstable colon cancers follow different routes toward loss of HLA class I expression. *BMC Cancer.* **7,** 33 (2007).

[115] Wosen, J. E., Mukhopadhyay, D., MacAubas, C. & Mellins, E. D. Epithelial MHC class II expression and its role in antigen presentation in the gastrointestinal and respiratory tracts. *Front Immunol.* **9,** 2144 (2018).

[116] Løvig, T., Andersen, S. N., Thorstensen, L., Diep, C. B., Meling, G. I., Lothe, R. A. & Rognum, T. O. Strong HLA-DR expression in microsatellite stable carcinomas of the large bowel is associated with good prognosis. *Br J Cancer.* **87,** 756–762 (2002).

[117] Michel, S., Linnebacher, M., Alcaniz, J., Voss, M., Wagner, R., Dippold, W., Becker, C., von Knebel Doeberitz, M., Ferrone, S. & Kloor, M. Lack of HLA class II antigen expression in microsatellite unstable colorectal carcinomas is caused by mutations in HLA class II regulatory genes. *Int J Cancer.* **127,** 889–898 (2010).

[118] Surmann, E. M., Voigt, A. Y., Michel, S., Bauer, K., Reuschenbach, M., Ferrone, S., von Knebel Doeberitz, M. & Kloor, M. Association of high CD4-positive T cell infiltration with mutations in HLA class II-regulatory genes in microsatellite-unstable colorectal cancer. *Cancer Immunol Immunother.* **64,** 357–366 (2015).

[119] Koelzer, V. H., Baker, K., Kassahn, D., Baumhoer, D. & Zlobec, I. Prognostic impact of β-2-microglobulin expression in colorectal cancers stratified by mismatch repair status. *J Clin Pathol.* **65,** 996–1002 (2012).

[120] Tikidzhieva, A., Benner, A., Michel, S., Formentini, A., Link, K.-H., Dippold, W., von Knebel Doeberitz, M., Kornmann, M. & Kloor, M. Microsatellite instability and Beta2-

Microglobulin mutations as prognostic markers in colon cancer: results of the FOGT-4 trial. *Br J Cancer.* **106,** 1239–1245 (2012).

[121] Busch, E., Ahadova, A., Kosmalla, K., Bohaumilitzky, L., Pfuderer, P. L., Ballhausen, A., Witt, J., Wittemann, J. N., Bläker, H., Holinski-Feder, E., Jäger, D., von Knebel Doeberitz, M., Haag, G. M. & Kloor, M. Beta-2-microglobulin Mutations Are Linked to a Distinct Metastatic Pattern and a Favorable Outcome in Microsatellite-Unstable Stage IV Gastrointestinal Cancers. *Front Oncol.* **11,** 669774 (2021).

[122] Watson, N. F., Ramage, J. M., Madjd, Z., Spendlove, I., Ellis, I. O., Scholefield, J. H. & Durrant, L. G. Immunosurveillance is active in colorectal cancer as downregulation but not complete loss of MHC class I expression correlates with a poor prognosis. *Int J Cancer.* **118,** 6–10 (2006).

[123] Greenson, J. K., Bonner, J. D., Ben-Yzhak, O., Cohen, H. I., Miselevich, I., Resnick, M. B., Trougouboff, P., Tomsho, L. D., Kim, E., Low, M., Almog, R., Rennert, G. & Gruber, S. B. Phenotype of Microsatellite Unstable Colorectal Carcinomas: Well-Differentiated and Focally Mucinous Tumors and the Absence of Dirty Necrosis Correlate With Microsatellite Instability. *Am J Surg Pathol.* **27,** 563–570 (2003).

[124] Smyrk, T. C., Watson, P., Kaul, K. & Lynch, H. T. Tumor-Infiltrating Lymphocytes Are a Marker for Microsatellite Instability in Colorectal Carcinoma. *Cancer.* **91,** 2417–2422 (2001).

[125] Buckowitz, A., Knaebel, H.-P., Benner, A., Bläker, H., Gebert, J., Kienle, P., von Knebel Doeberitz, M. & Kloor, M. Microsatellite instability in colorectal cancer is associated with local lymphocyte infiltration and low frequency of distant metastases. *Br J Cancer.* **92,** 1746–1753 (2005).

[126] Galon, J., Costes, A., Sanchez-Cabo, F., Kirilovsky, A., Mlecnik, B., Lagorce-Pagès, C., Tosolini, M., Camus, M., Berger, A., Wind, P., Zinzindohoué, F., Bruneval, P., Cugnenc, P. H., Trajanoski, Z., Fridman, W. H. & Pagès, F. Type, density, and location of immune cells within human colorectal tumors predict clinical outcome. *Science.* **313,** 1960–1964 (2006).

[127] Dolcetti, R., Viel, A., Doglioni, C., Russo, A., Guidoboni, M., Capozzi, E., Vecchiato, N., Macrì, E., Fornasarig, M. & Boiocchi, M. High prevalence of activated intraepithelial cytotoxic T lymphocytes and increased neoplastic cell apoptosis in colorectal carcinomas with microsatellite instability. *Am J Pathol.* **154,** 1805–1813 (1999).

[128] Guidoboni, M., Gafà, R., Viel, A., Doglioni, C., Russo, A., Santini, A., Del Tin, L., Macrì, E., Lanza, G., Boiocchi, M. & Dolcetti, R. Microsatellite instability and high content of activated cytotoxic lymphocytes identify colon cancer patients with a favorable prognosis. *Am J Pathol.* **159,** 297–304 (2001).

[129] Llosa, N. J., Cruise, M., Tam, A., Wicks, E. C., Hechenbleikner, E. M., Taube, J. M., Blosser, R. L., Fan, H., Wang, H., Luber, B. S., Zhang, M., Papadopoulos, N., Kinzler,

K. W., Vogelstein, B., Sears, C. L., Anders, R. A., Pardoll, D. M. & Housseau, F. The vigorous immune microenvironment of microsatellite instable colon cancer is balanced by multiple counter-inhibitory checkpoints. *Cancer Discov.* **5,** 43–51 (2015).

[130] Xiao, Y. & Freeman, G. J. The Microsatellite Instable Subset of Colorectal Cancer Is a Particularly Good Candidate for Checkpoint Blockade Immunotherapy. *Cancer Discov.* **5,** 16–18 (2015).

[131] Graham, D. & Appelman, H. Crohn's-like lymphoid reaction and colorectal carcinoma: a potential histologic prognosticator. *Mod Pathol.* **3,** 332–335 (1990).

[132] Samowitz, W. S., Curtin, K., Ma, K.-N., Schaffer, D., Coleman, L. W., Leppert, M. & Slattery, M. L. Microsatellite Instability in Sporadic Colon Cancer Is Associated with an Improved Prognosis at the Population Level. *Cancer Epidemiol Biomarkers Prev.* **10,** 917–923 (2001).

[133] Gryfe, R., Kim, H., Hsieh, E. T., Aronson, M. D., Holowaty, E. J., Bull, S. B., Redston, M. & Gallinger, S. Tumor Microsatellite Instability and Clinical Outcome in Young Patients with Colorectal Cancer. *N Engl J Med.* **342,** 69–77 (2000).

[134] Mlecnik, B., Bindea, G., Angell, H. K., Maby, P., Angelova, M., Tougeron, D., Church, S. E., Lafontaine, L., Fischer, M., Fredriksen, T., Sasso, M., Bilocq, A. M., Kirilovsky, A., Obenauf, A. C., Hamieh, M., Berger, A., Bruneval, P., Tuech, J. J., Sabourin, J. C., Le Pessot, F., Mauillon, J., Rafii, A., Laurent-Puig, P., Speicher, M. R., Trajanoski, Z., Michel, P., Sesboüe, R., Frebourg, T., Pagès, F., Valge-Archer, V., Latouche, J. B. & Galon, J. Integrative Analyses of Colorectal Cancer Show Immunoscore Is a Stronger Predictor of Patient Survival Than Microsatellite Instability. *Immunity.* **44,** 698–711 (2016).

[135] Boland, C. R., Sinicrope, F. A., Brenner, D. E. & Carethers, J. M. Colorectal cancer prevention and treatment. *Gastroenterology.* **118,** S115–S128 (2000).

[136] Ribic, C. M., Sargent, D. J., Moore, M. J., Thibodeau, S. N., French, A. J., Goldberg, R. M., Hamilton, S. R., Laurent-Puig, P., Gryfe, R., Shepherd, L. E., Tu, D., Redston, M. & Gallinger, S. Tumor microsatellite-instability status as a predictor of benefit from fluorouracil-based adjuvant chemotherapy for colon cancer. *N Engl J Med.* **349,** 247–257 (2003).

[137] Sargent, D. J., Marsoni, S., Monges, G., Thibodeau, S. N., Labianca, R., Hamilton, S. R., French, A. J., Kabat, B., Foster, N. R., Torri, V., Ribic, C., Grothey, A., Moore, M., Zaniboni, A., Seitz, J. F., Sinicrope, F. & Gallinger, S. Defective Mismatch Repair As a Predictive Marker for Lack of Efficacy of Fluorouracil-Based Adjuvant Therapy in Colon Cancer. *J Clin Oncol.* **28,** 3219–3226 (2010).

[138] Jo, W. S. & Carethers, J. M. Chemotherapeutic implications in microsatellite unstable colorectal cancer. *Cancer Biomark.* **2,** 51–60 (2006).

[139] Le, D. T., Durham, J. N., Smith, K. N., Wang, H., Bjarne, R., Aulakh, L. K., Lu, S., Kemberling, H., Wilt, C., Brandon, S., Wong, F., Azad, N. S., Rucki, A. A., Laheru, D., Zaheer, A., Fisher, G. A., Crocenzi, T. S., Lee, J. J., Tim, F., Duffy, A. G., Ciombor, K. K., Eyring, A. D., Lam, B. H., Joe, A., Kang, S. P., Holdhoff, M., Danilova, L., Cope, L., Meyer, C., Zhou, S., Goldberg, R. M., Armstrong, D. K., Bever, K. M., Fader, A. N., Taube, J., Housseau, F., Xiao, N., Pardoll, D. M., Papadopoulos, N. & Kenneth, W. Mismatch-repair deficiency predicts response of solid tumors to PD-1. *Science* **357,** 409–413 (2017).

[140] He, X. & Xu, C. Immune checkpoint signaling and cancer immunotherapy. *Cell Res.* **30,** 660–669 (2020).

[141] Pardoll, D. M. The blockade of immune checkpoints in cancer immunotherapy. *Nat Rev Cancer.* **12,** 252–264 (2012).

[142] La-Beck, N. M., Jean, G. W., Huynh, C., Alzghari, S. K. & Lowe, D. B. Immune Checkpoint Inhibitors: New Insights and Current Place in Cancer Therapy. *Pharmacotherapy.* **35,** 963–976 (2015).

[143] Qin, S., Xu, L., Yi, M., Yu, S., Wu, K. & Luo, S. Novel immune checkpoint targets: moving beyond PD-1 and CTLA-4. *Mol Cancer.* **18,** 155 (2019).

[144] Sansom, D. M. CD28, CTLA-4 and their ligands: who does what and to whom? *Immunology.* **101,** 169–177 (2000).

[145] Lenschow, D. J., Walunas, T. L. & Bluestone, J. A. CD28/B7 system of T cell costimulation. *Annu Rev Immunol.* **14,** 233–258 (2003).

[146] Oyewole-Said, D., Konduri, V., Vazquez-Perez, J., Weldon, S. A., Levitt, J. M. & Decker, W. K. Beyond T-Cells: Functional Characterization of CTLA-4 Expression in Immune and Non-Immune Cell Types. *Front Immunol.* **11,** 608024 (2020).

[147] Qureshi, O. S., Zheng, Y., Nakamura, K., Attridge, K., Manzotti, C., Schmidt, E. M., Baker, J., Jeffery, L. E., Kaur, S., Briggs, Z., Hou, T. Z., Futter, C. E., Anderson, G., Walker, L. S. & Sansom, D. M. Trans-endocytosis of CD80 and CD86: a molecular basis for the cell extrinsic function of CTLA-4. *Science.* **332,** 600–603 (2011).

[148] Waldman, A. D., Fritz, J. M. & Lenardo, M. J. A guide to cancer immunotherapy: from T cell basic science to clinical practice. *Nat Rev Immunol.* **20,** 651–668 (2020).

[149] Tivol, E. A., Borriello, F., Schweitzer, A. N., Lynch, W. P., Bluestone, J. A. & Sharpe, A. H. Loss of CTLA-4 leads to massive lymphoproliferation and fatal multiorgan tissue destruction, revealing a critical negative regulatory role of CTLA-4. *Immunity.* **3,** 541–547 (1995).

[150] Leach, D. R., Krummel, M. F. & Allison, J. P. Enhancement of antitumor immunity by CTLA-4 blockade. *Science.* **271,** 1734–1736 (1996).

[151] Hodi, F. S., O'Day, S. J., McDermott, D. F., Weber, R. W., Sosman, J. A., Haanen, J. B., Gonzalez, R., Robert, C., Schadendorf, D., Hassel, J. C., Akerley, W., van den Eertwegh,

A. J., Lutzky, J., Lorigan, P., Vaubel, J. M., Linette, G. P., Hogg, D., Ottensmeier, C. H., Lebbé, C., Peschel, C., Quirt, I., Clark, J. I., Wolchok, J. D., Weber, J. S., Tian, J., Yellin, M. J., Nichol, G. M., Hoos, A. & Urba, W. J. Improved Survival with Ipilimumab in Patients with Metastatic Melanoma. *N Engl J Med.* **363,** 711–723 (2010).

[152] Han, Y., Liu, D. & Li, L. PD-1/PD-L1 pathway: current researches in cancer. *Am J Cancer Res.* **10,** 727–742 (2020).

[153] Yamazaki, T., Akiba, H., Iwai, H., Matsuda, H., Aoki, M., Tanno, Y., Shin, T., Tsuchiya, H., Pardoll, D. M., Okumura, K., Azuma, M. & Yagita, H. Expression of Programmed Death 1 Ligands by Murine T Cells and APC. *J Immunol.* **169,** 5538–5545 (2002).

[154] Sharpe, A. H. & Pauken, K. E. The diverse functions of the PD1 inhibitory pathway. *Nat Rev Immunol.* **18,** 153–167 (2017).

[155] Zou, W. & Chen, L. Inhibitory B7-family molecules in the tumour microenvironment. *Nat Rev Immunol.* **8,** 467–477 (2008).

[156] Dong, H., Strome, S. E., Salomao, D. R., Tamura, H., Hirano, F., Flies, D. B., Roche, P. C., Lu, J., Zhu, G., Tamada, K., Lennon, V. A., Cells, E. & Chen, L. Tumor-associated B7-H1 promotes T-cell apoptosis: a potential mechanism of immune evasion. *Nat Med.* **8,** 793–800 (2002).

[157] Iwai, Y., Ishida, M., Tanaka, Y., Okazaki, T., Honjo, T. & Minato, N. Involvement of PD-L1 on tumor cells in the escape from host immune system and tumor immunotherapy by PD-L1 blockade. *Proc Natl Acad Sci U S A.* **99,** 12293–12297 (2002).

[158] Hirano, F., Kaneko, K., Tamura, H., Dong, H., Wang, S., Ichikawa, M., Rietz, C., Flies, D. B., Lau, J. S., Zhu, G., Tamada, K. & Chen, L. Blockade of B7-H1 and PD-1 by monoclonal antibodies potentiates cancer therapeutic immunity. *Cancer Res.* **65,** 1089–1096 (2005).

[159] Weber, J. S., D'Angelo, S. P., Minor, D., Hodi, F. S., Gutzmer, R., Neyns, B., Hoeller, C., Khushalani, N. I., Miller, W. H., Lao, C. D., Linette, G. P., Thomas, L., Lorigan, P., Grossmann, K. F., Hassel, J. C., Maio, M., Sznol, M., Ascierto, P. A., Mohr, P., Chmielowski, B., Bryce, A., Svane, I. M., Grob, J. J., Krackhardt, A. M., Horak, C., Lambert, A., Yang, A. S. & Larkin, J. Nivolumab versus chemotherapy in patients with advanced melanoma who progressed after anti-CTLA-4 treatment (CheckMate 037): a randomised, controlled, open-label, phase 3 trial. *Lancet Oncol.* **16,** 375–384 (2015).

[160] Boyiadzis, M. M., Kirkwood, J. M., Marshall, J. L., Pritchard, C. C., Azad, N. S. & Gulley, J. L. Significance and implications of FDA approval of pembrolizumab for biomarker-defined disease. *J Immunother Cancer.* **6,** 35 (2018).

[161] Le, D. T., Uram, J. N., Wang, H., Bartlett, B. R., Kemberling, H., Eyring, A. D., Skora, A. D., Luber, B. S., Azad, N. S., Laheru, D., Biedrzycki, B., Donehower, R. C., Zaheer, A., Fisher, G. A., Crocenzi, T. S., Lee, J. J., Duffy, S. M., Goldberg, R. M., de la Chapelle, A., Koshiji, M., Bhaijee, F., Huebner, T., Hruban, R. H., Wood, L. D., Cuka,

N., Pardoll, D. M., Papadopoulos, N., Kinzler, K. W., Zhou, S., Cornish, T. C., Taube, J. M., Anders, R. A., Eshleman, J. R., Vogelstein, B. & Diaz, L. A. PD-1 Blockade in Tumors with Mismatch-Repair Deficiency. *N Engl J Med.* **372,** 2509–20 (2015).

[162] Cogdill, A. P., Andrews, M. C. & Wargo, J. A. Hallmarks of response to immune checkpoint blockade. *Br J Cancer.* **117,** 1–7 (2017).

[163] Bai, R., Lv, Z., Xu, D. & Cui, J. Predictive biomarkers for cancer immunotherapy with immune checkpoint inhibitors. *Biomark Res.* **8,** 1–17 (2020).

[164] Knudson, A. G. Mutation and cancer: statistical study of retinoblastoma. *Proc Natl Acad Sci U S A.* **68,** 820–823 (1971).

[165] Hampel, H., Frankel, W. L., Martin, E., Arnold, M., Khanduja, K., Kuebler, P., Nakagawa, H., Sotamaa, K., Prior, T. W., Westman, J., Panescu, J., Fix, D., Lockman, J., Comeras, I. & de la Chapelle, A. Screening for the Lynch Syndrome (Hereditary Nonpolyposis Colorectal Cancer). *N Engl J Med.* **352,** 1851–1860 (2005).

[166] Vasen, H. F. Clinical description of the Lynch syndrome [hereditary nonpolyposis colorectal cancer (HNPCC)]. *Fam Cancer.* **4,** 219–225 (2005).

[167] Talseth-Palmer, B. A., Wijnen, J. T., Grice, D. M. & Scott, R. J. Genetic modifiers of cancer risk in Lynch syndrome: a review. *Fam Cancer.* **12,** 207–216 (2013).

[168] Lynch, H. T., Snyder, C. L., Shaw, T. G., Heinen, C. D. & Hitchins, M. P. Milestones of Lynch syndrome: 1895–2015. *Nat Rev Cancer.* **15,** 181–194 (2015).

[169] Helderman, N. C., Bajwa-ten Broeke, S. W., Morreau, H., Suerink, M., Terlouw, D., van der Werf-' t Lam, A. S., van Wezel, T. & Nielsen, M. The diverse molecular profiles of lynch syndrome-associated colorectal cancers are (highly) dependent on underlying germline mismatch repair mutations. *Crit Rev Oncol Hematol.* **163,** 103338 (2021).

[170] Rustgi, A. K. The genetics of hereditary colon cancer. *Genes Dev.* **21,** 2525–2538 (2007).

[171] Park, J.-G., Park, Y. J., Wijnen, J. T. & Vasen, H. F. A. Gene-environment interaction in hereditary nonpolyposis colorectal cancer with implications for diagnosis and genetic testing. *Int J Cancer.* **82,** 516–519 (1999).

[172] Hampel, H., Stephens, J. A., Pukkala, E., Sankila, R., Aaltonen, L. A., Mecklin, J. P. & de la Chapelle, A. Cancer risk in hereditary nonpolyposis colorectal cancer syndrome: later age of onset. *Gastroenterology.* **129,** 415–421 (2005).

[173] Carethers, J. M. & Jung, B. H. Genetics and Genetic Biomarkers in Sporadic Colorectal Cancer. *Gastroenterology.* **149,** 1177–1190 (2015).

[174] Parsons, M. T., Buchanan, D. D., Thompson, B., Young, J. P. & Spurdle, A. B. Correlation of tumour BRAF mutations and MLH1 methylation with germline mismatch repair (MMR) gene mutation status: a literature review assessing utility of tumour features for MMR variant classification. *J Med Genet.* **49,** 151–157 (2012).

[175] Ahadova, A., Gallon, R., Gebert, J., Ballhausen, A., Endris, V., Kirchner, M., Stenzinger, A., Burn, J., von Knebel Doeberitz, M., Bläker, H. & Kloor, M. Three molecular pathways model colorectal carcinogenesis in Lynch syndrome. *Int J Cancer.* **143,** 139–150 (2018).

[176] Jass, J. R. Pathology of Hereditary Nonpolyposis Colorectal Cancer. *Ann N Y Acad Sci.* **14,** 1631–1634 (1994).

[177] Lindgren, G., Liljegren, A., Jaramillo, E., Rubio, C. & Lindblom, A. Adenoma prevalence and cancer risk in familial non-polyposis colorectal cancer. *Gut.* **50,** 228–234 (2002).

[178] De Jong, A. E., Morreau, H., Van Puijenbroek, M., Eilers, P. H., Wijnen, J., Nagengast, F. M., Griffioen, G., Cats, A., Menko, F. H., Kleibeuker, J. H. & Vasen, H. F. The role of mismatch repair gene defects in the development of adenomas in patients with HNPCC. *Gastroenterology.* **126,** 42–48 (2004).

[179] Vasen, H. F., Nagengast, F. M. & Meera Khan, P. Interval cancers in hereditary nonpolyposis colorectal cancer (Lynch syndrome). *Lancet.* **345,** 1183–1184 (1995).

[180] Winawer, S. J., Fletcher, R. H., Miller, L., Godlee, F., Stolar, M. H., Mulrow, C. D., Woolf, S. H., Glick, S. N., Ganiats, T. G., Bond, J. H., Rosen, L., Zapka, J. G., Olsen, S. J., Giardiello, F. M., Sisk, J. E., Van Antwerp, R., Brown-Davis, C., Marciniak, D. A. & Mayer, R. J. Colorectal cancer screening: clinical guidelines and rationale. *Gastroenterology.* **112,** 594–642 (1997).

[181] Halvarsson, B., Lindblom, A., Johansson, L., Lagerstedt, K. & Nilbert, M. Loss of mismatch repair protein immunostaining in colorectal adenomas from patients with hereditary nonpolyposis colorectal cancer. *Mod Pathol.* **18,** 1095–1101 (2005).

[182] Meijer, T. W., Hoogerbrugge, N., Nagengast, F. M., Ligtenberg, M. J. & van Krieken, J. H. In Lynch syndrome adenomas, loss of mismatch repair proteins is related to an enhanced lymphocytic response. *Histopathology.* **55,** 414–422 (2009).

[183] Vasen, H. F., Abdirahman, M., Brohet, R., Langers, A. M., Kleibeuker, J. H., van Kouwen, M., Koornstra, J. J., Boot, H., Cats, A., Dekker, E., Sanduleanu, S., Poley, J. W., Hardwick, J. C., de Vos Tot Nederveen Cappel, W. H., van der Meulen-de Jong, A. E., Tan, T. G., Jacobs, M. A., Mohamed, F. L. A., de Boer, S. Y., van de Meeberg, P. C., Verhulst, M. L., Salemans, J. M., van Bentem, N., Westerveld, B. D., Vecht, J. & Nagengast, F. M. One to 2-Year Surveillance Intervals Reduce Risk of Colorectal Cancer in Families With Lynch Syndrome. *Gastroenterology.* **138,** 2300–2306 (2010).

[184] Møller, P., Seppälä, T., Bernstein, I., Holinski-Feder, E., Sala, P., Evans, D. G., Lindblom, A., Macrae, F., Blanco, I., Sijmons, R., Jeffries, J., Vasen, H., Burn, J., Nakken, S., Hovig, E., Rødland, E. A., Tharmaratnam, K., de Vos Tot Nederveen Cappel, W. H., Hill, J., Wijnen, J., Green, K., Lalloo, F., Sunde, L., Mints, M., Bertario, L., Pineda, M., Navarro, M., Morak, M., Renkonen-Sinisalo, L., Frayling, I. M., Plazzer, J. P.,

Pylvanainen, K., Sampson, J. R., Capella, G., Mecklin, J. P. & Möslein, G. Cancer incidence and survival in Lynch syndrome patients receiving colonoscopic and gynaecological surveillance: First report from the prospective Lynch syndrome database. *Gut* **66,** 464–472 (2017).

[185] Kloor, M., Huth, C., Voigt, A. Y., Benner, A., Schirmacher, P., von Knebel Doeberitz, M. & Bläker, H. Prevalence of mismatch repair-deficient crypt foci in Lynch syndrome: A pathological study. *Lancet Oncol.* **13,** 598–606 (2012).

[186] Shia, J., Stadler, Z. K., Weiser, M. R., Vakiani, E., Mendelsohn, R., Markowitz, A. J., Shike, M., Boland, C. R. & Klimstra, D. S. Mismatch repair deficient-crypts in non-neoplastic colonic mucosa in Lynch syndrome: insights from an illustrative case. *Fam Cancer.* **14,** 61–68 (2015).

[187] Staffa, L., Echterdiek, F., Nelius, N., Benner, A., Werft, W., Lahrmann, B., Grabe, N., Schneider, M., Tariverdian, M., von Knebel Doeberitz, M., Bläker, H. & Kloor, M. Mismatch repair-deficient crypt foci in lynch syndrome-molecular alterations and association with clinical parameters. *PLoS One.* **10,** e0121980 (2015).

[188] Miyaki, M., Iijima, T., Kimura, J., Yasuno, M., Mori, T., Hayashi, Y., Koike, M., Shitara, N., Iwama, T. & Kuroki, T. Frequent Mutation of β-Catenin and APC Genes in Primary Colorectal Tumors from Patients with Hereditary Nonpolyposis Colorectal Cancer. *Cancer Res.* **59,** 4506–4509 (1999).

[189] White, B. D., Chien, A. J. & Dawson, D. W. Dysregulation of Wnt/β-catenin Signaling in Gastrointestinal Cancers. *Gastroenterology.* **142,** 219–232 (2012).

[190] Sekine, S., Mori, T., Ogawa, R., Tanaka, M., Yoshida, H., Taniguchi, H., Nakajima, T., Sugano, K., Yoshida, T., Kato, M., Furukawa, E., Ochiai, A. & Hiraoka, N. Mismatch repair deficiency commonly precedes adenoma formation in Lynch Syndrome-Associated colorectal tumorigenesis. *Mod Pathol.* **30,** 1144–1151 (2017).

[191] Ahadova, A., von Knebel Doeberitz, M., Bläker, H. & Kloor, M. CTNNB1-mutant colorectal carcinomas with immediate invasive growth: a model of interval cancers in Lynch syndrome. *Fam Cancer.* **15,** 579–586 (2016).

[192] Ten Broeke, S. W., van Bavel, T. C., Jansen, A. M., Gómez-García, E., Hes, F. J., van Hest, L. P., Letteboer, T. G., Olderode-Berends, M. J., Ruano, D., Spruijt, L., Suerink, M., Tops, C. M., van Eijk, R., Morreau, H., van Wezel, T. & Nielsen, M. Molecular Background of Colorectal Tumors From Patients With Lynch Syndrome Associated With Germline Variants in PMS2. *Gastroenterology.* **155,** 844–851 (2018).

[193] Engel, C., Ahadova, A., Seppälä, T., Aretz, S., Bigirwamungu-Bargeman, M., Bläker, H., Bucksch, K., Büttner, R., de Vos tot Nederveen Cappel, W., Endris, V., Holinski-Feder, E., Holzapfel, S., Hüneburg, R., Jacobs, M. A., Koornstra, J. J., Langers, A. M., Lepistö, A., Morak, M., Möslein, G., Peltomäki, P., Pylvänäinen, K., Rahner, N., Renkonen-Sinisalo, L., Schulmann, K., Steinke-Lange, V., Stenzinger, A., Strassburg,

C. P., van de Meeberg, P. C., van Kouwen, M., van Leerdam, M., Vangala, D. B., Vecht, J., Verhulst, M.-L., von Knebel Doeberitz, M., Weitz, J., Zachariae, S., Loeffler, M., Mecklin, J.-P., Kloor, M. & Vasen, H. F. Associations of Pathogenic Variants in MLH1, MSH2, and MSH6 With Risk of Colorectal Adenomas and Tumors and With Somatic Mutations in Patients With Lynch Syndrome. *Gastroenterology.* **158,** 1326–1333 (2020).

[194] Haanstra, J. F., Vasen, H. F., Sanduleanu, S., Van Der Wouden, E. J., Koornstra, J. J., Kleibeuker, J. H. & de Vos Tot Nederveen Cappel, W. H. Quality colonoscopy and risk of interval cancer in Lynch syndrome. *Int J Colorectal Dis.* **28,** 1643–1649 (2013).

[195] Møller, P., Seppälä, T. T., Bernstein, I., Holinski-Feder, E., Sala, P., Evans, D. G., Lindblom, A., Macrae, F., Blanco, I., Sijmons, R. H., Jeffries, J., Vasen, H. F., Burn, J., Nakken, S., Hovig, E., Rødland, E. A., Tharmaratnam, K., de Vos Tot Nederveen Cappel, W. H., Hill, J., Wijnen, J. T., Jenkins, M. A., Green, K., Lalloo, F., Sunde, L., Mints, M., Bertario, L., Pineda, M., Navarro, M., Morak, M., Renkonen-Sinisalo, L., Valentin, M. D., Frayling, I. M., Plazzer, J. P., Pylvanainen, K., Genuardi, M., Mecklin, J. P., Moeslein, G., Sampson, J. R. & Capella, G. Cancer risk and survival in path_MMR carriers by gene and gender up to 75 years of age: a report from the Prospective Lynch Syndrome Database. *Gut.* **67,** 1306–1316 (2018).

[196] Win, A. K., Jenkins, M. A., Dowty, J. G., Antoniou, A. C., Lee, A., Giles, G. G., Buchanan, D. D., Clendenning, M., Rosty, C., Ahnen, D. J., Thibodeau, S. N., Casey, G., Gallinger, S., Le Marchand, L., Haile, R. W., Potter, J. D., Zheng, Y., Lindor, N. M., Newcomb, P. A., Hopper, J. L. & MacInnis, R. J. Prevalence and Penetrance of Major Genes and Polygenes for Colorectal Cancer. *Cancer Epidemiol Biomarkers Previomarkers* **26,** 404–412 (2017).

[197] Peltomäki, P. Lynch Syndrome Genes. *Fam Cancer.* **4,** 227–232 (2005).

[198] Peltomäki, P. Role of DNA mismatch repair defects in the pathogenesis of human cancer. *J Clin Oncol.* **21,** 1174–1179 (2003).

[199] Tutlewska, K., Lubinski, J. & Kurzawski, G. Germline deletions in the EPCAM gene as a cause of Lynch syndrome – literature review. *Hered Cancer Clin Pract.* **11,** 9 (2013).

[200] Ligtenberg, M. J., Kuiper, R. P., Chan, T. L., Goossens, M., Hebeda, K. M., Voorendt, M., Lee, T. Y., Bodmer, D., Hoenselaar, E., Hendriks-Cornelissen, S. J., Tsui, W. Y., Kong, C. K., Brunner, H. G., Van Kessel, A. G., Yuen, S. T., Van Krieken, J. H. J., Leung, S. Y. & Hoogerbrugge, N. Heritable somatic methylation and inactivation of MSH2 in families with Lynch syndrome due to deletion of the 3 exons of TACSTD1. *Nat Genet.* **41,** 112–117 (2008).

[201] Kovacs, M. E., Papp, J., Szentirmay, Z., Otto, S. & Olah, E. Deletions removing the last exon of TACSTD1 constitute a distinct class of mutations predisposing to Lynch syndrome. *Hum Mutat.* **30,** 197–203 (2009).

[202] Dominguez-Valentin, M., Sampson, J. R., Seppälä, T. T., ten Broeke, S. W., Plazzer, J. P., Nakken, S., Engel, C., Aretz, S., Jenkins, M. A., Sunde, L., Bernstein, I., Capella, G., Balaguer, F., Thomas, H., Evans, D. G., Burn, J., Greenblatt, M., Hovig, E., de Vos tot Nederveen Cappel, W. H., Sijmons, R. H., Bertario, L., Tibiletti, M. G., Cavestro, G. M., Lindblom, A., Della Valle, A., Lopez-Köstner, F., Gluck, N., Katz, L. H., Heinimann, K., Vaccaro, C. A., Büttner, R., Görgens, H., Holinski-Feder, E., Morak, M., Holzapfel, S., Hüneburg, R., von Knebel Doeberitz, M., Loeffler, M., Rahner, N., Schackert, H. K., Steinke-Lange, V., Schmiegel, W., Vangala, D., Pylvänäinen, K., Renkonen-Sinisalo, L., Hopper, J. L., Win, A. K., Haile, R. W., Lindor, N. M., Gallinger, S., Le Marchand, L., Newcomb, P. A., Figueiredo, J. C., Thibodeau, S. N., Wadt, K., Therkildsen, C., Okkels, H., Ketabi, Z., Moreira, L., Sánchez, A., Serra-Burriel, M., Pineda, M., Navarro, M., Blanco, I., Green, K., Lalloo, F., Crosbie, E. J., Hill, J., Denton, O. G., Frayling, I. M., Rødland, E. A., Vasen, H., Mints, M., Neffa, F., Esperon, P., Alvarez, K., Kariv, R., Rosner, G., Pinero, T. A., Gonzalez, M. L., Kalfayan, P., Tjandra, D., Winship, I. M., Macrae, F., Möslein, G., Mecklin, J. P., Nielsen, M. & Møller, P. Cancer risks by gene, age, and gender in 6350 carriers of pathogenic mismatch repair variants: findings from the Prospective Lynch Syndrome Database. *Genet Med.* **22,** 15–25 (2020).

[203] Kempers, M. J., Kuiper, R. P., Ockeloen, C. W., Chappuis, P. O., Hutter, P., Rahner, N., Schackert, H. K., Steinke, V., Holinski-Feder, E., Morak, M., Kloor, M., Büttner, R., Verwiel, E. T., van Krieken, J. H., Nagtegaal, I. D., Goossens, M., van der Post, R. S., Niessen, R. C., Sijmons, R. H., Kluijt, I., Hogervorst, F. B., Leter, E. M., Gille, J. J., Aalfs, C. M., Redeker, E. J., Hes, F. J., Tops, C. M., van Nesselrooij, B. P., van Gijn, M. E., García, E. B., Eccles, D. M., Bunyan, D. J., Syngal, S., Stoffel, E. M., Culver, J. O., Palomares, M. R., Graham, T., Velsher, L., Papp, J., Oláh, E., Chan, T. L., Leung, S. Y., van Kessel, A. G., Kiemeney, L. A., Hoogerbrugge, N. & Ligtenberg, M. J. Risk of colorectal and endometrial cancers in EPCAM deletion-positive Lynch syndrome: a cohort study. *Lancet Oncol.* **12,** 49–55 (2011).

[204] Plaschke, J., Engel, C., Krüger, S., Holinski-Feder, E., Pagenstecher, C., Mangold, E., Moeslein, G., Schulmann, K., Gebert, J., von Knebel Doeberitz, M., Rüschoff, J., Loeffler, M. & Schackert, H. K. Lower incidence of colorectal cancer and later age of disease onset in 27 families with pathogenic MSH6 germline mutations compared with families with MLH1 or MSH2 mutations: The German Hereditary Nonpolyposis Colorectal Cancer Consortium. *J Clin Oncol.* **22,** 4486–4494 (2004).

[205] Ten Broeke, S. W., Brohet, R. M., Tops, C. M., Van Der Klift, H. M., Velthuizen, M. E., Bernstein, I., Munar, G. C., Garcia, E. G., Hoogerbrugge, N., Letteboer, T. G., Menko, F. H., Lindblom, A., Mensenkamp, A. R., Moller, P., Van Os, T. A., Rahner, N., Redeker, B. J., Sijmons, R. H., Spruijt, L., Suerink, M., Vos, Y. J., Wagner, A., Hes, F. J.,

Vasen, H. F., Nielsen, M. & Wijnen, J. T. Lynch syndrome caused by germline PMS2 mutations: Delineating the cancer risk. *J Clin Oncol.* **33,** 319–325 (2015).

[206] Ten Broeke, S. W., Klift, H. M., Tops, C. M., Aretz, S., Bernstein, I., Buchanan, D. D., Chapelle, A. D., Capella, G., Clendenning, M., Engel, C., Gallinger, S., Garcia, E. G., Figueiredo, J. C., Haile, R., Hampel, H. L., Hopper, J. L., Hoogerbrugge, N., von Knebel Doeberitz, M., Marchand, L. L., Letteboer, T. G., Jenkins, M. A., Lindblom, A., Lindor, N. M., Mensenkamp, A. R., Møller, P., Newcomb, P. A., Van Os, T. A., Pearlman, R., Pineda, M., Rahner, N., Redeker, E. J., Olderode-Berends, M. J., Rosty, C., Schackert, H. K., Scott, R., Senter, L., Spruijt, L., Steinke-Lange, V., Suerink, M., Thibodeau, S., Vos, Y. J., Wagner, A., Winship, I., Hes, J. F., Vasen, H. F., Wijnen, J. T., Nielsen, M. & Win, A. K. Cancer Risks for PMS2-Associated Lynch Syndrome. *J Clin Oncol.* **36,** 2961–2968 (2018).

[207] Hendriks, Y. M., Wagner, A., Morreau, H., Menko, F., Stormorken, A., Quehenberger, F., Sandkuijl, L., Møller, P., Genuardi, M., Van Houwelingen, H., Tops, C., Van Puijenbroek, M., Verkuijlen, P., Kenter, G., Van Mil, A., Meijers-Heijboer, H., Tan, G. B., Breuning, M. H., Fodde, R., Wijnen, J. T., Bröcker-Vriends, A. H. & Vasen, H. Cancer risk in hereditary nonpolyposis colorectal cancer due to MSH6 mutations: impact on counseling and surveillance. *Gastroenterology.* **127,** 17–25 (2004).

[208] Peltomäki, P. Update on Lynch syndrome genomics. *Fam Cancer.* **15,** 385–393 (2016).

[209] Shia, J., Ellis, N., Paty, P., Nash, G., Qin, J., Offit, K., Zhang, X.-M., Markowitz, A., Nafa, K., Guillem, J., Wong, W. D., Gerald, W. & Klimstra, D. Value of Histopathology in Predicting Microsatellite Instability. *Am J Surg Pathol.* **27,** 1407–1417 (2003).

[210] Takemoto, N., Konishi, F., Yamashita, K., Kojima, M., Furukawa, T., Miyakura, Y., Shitoh, K. & Nagai, H. The correlation of microsatellite instability and tumor-infiltrating lymphocytes in hereditary non-polyposis colorectal cancer (HNPCC) and sporadic colorectal cancers: the significance of different types of lymphocyte infiltration. *Jpn J Clin Oncol.* **34,** 90–98 (2004).

[211] Koornstra, J. J., De Jong, S., Boersma-Van Eck, W., Zwart, N., Hollema, H., De Vries, E. G. & Kleibeuker, J. H. Fas Ligand Expression in Lynch Syndrome-Associated Colorectal Tumours. *Pathol Oncol Res.* **15,** 399–406 (2009).

[212] Reuschenbach, M., Kloor, M., Morak, M., Wentzensen, N., Germann, A., Garbe, Y., Tariverdian, M., Findeisen, P., Neumaier, M., Holinski-Feder, E. & von Knebel Doeberitz, M. Serum antibodies against frameshift peptides in microsatellite unstable colorectal cancer patients with Lynch syndrome. *Fam Cancer.* **9,** 173–179 (2010).

[213] Mittal, D., Gubin, M. M., Schreiber, R. D. & Smyth, M. J. New insights into cancer immunoediting and its three component phases — elimination, equilibrium and escape. *Curr Opin Immunol.* **27,** 16–25 (2014).

[214] Gebert, J., Gelincik, O., Oezcan-Wahlbrink, M., Marshall, J. D., Hernandez-Sanchez, A., Urban, K., Long, M., Cortes, E., Tosti, E., Katzenmaier, E. M., Song, Y., Elsaadi, A., Deng, N., Vilar, E., Fuchs, V., Nelius, N., Yuan, Y. P., Ahadova, A., Sei, S., Shoemaker, R. H., Umar, A., Wei, L., Liu, S., Bork, P., Edelmann, W., von Knebel Doeberitz, M., Lipkin, S. M. & Kloor, M. Recurrent Frameshift Neoantigen Vaccine Elicits Protective Immunity With Reduced Tumor Burden and Improved Overall Survival in a Lynch Syndrome Mouse Model. *Gastroenterology.* **161,** 1288–1302 (2021).

[215] Yurgelun, M. B. & Hampel, H. Recent Advances in Lynch Syndrome: Diagnosis, Treatment, and Cancer Prevention. *Am Soc Clin Oncol Educ Book.* **38,** 101–109 (2018).

[216] Heinen, C. D. & Juel Rasmussen, L. Determining the functional significance of mismatch repair gene missense variants using biochemical and cellular assays. *Hered Cancer Clin Pract.* **10,** 9 (2012).

[217] Pritchard, C. C., Smith, C., Salipante, S. J., Lee, M. K., Thornton, A. M., Nord, A. S., Gulden, C., Kupfer, S. S., Swisher, E. M., Bennett, R. L., Novetsky, A. P., Jarvik, G. P., Olopade, O. I., Goodfellow, P. J., King, M. C., Tait, J. F. & Walsh, T. ColoSeq Provides Comprehensive Lynch and Polyposis Syndrome Mutational Analysis Using Massively Parallel Sequencing. *J Mol Diagn.* **14,** 357–366 (2012).

[218] Aaltonen, L. A., Peltomäki, P., Mecklin, J.-P., Järvinen, H., Jass, J. R., Green, J. S., Lynch, H. T., Watson, P., Tallqvist, G., Juhola, M., Sistonen, P., Hamilton, S. R., Kinzler, K. W., Vogelstein, B. & de la Chapelle, A. Replication Errors in Benign and Malignant Tumors from Hereditary Nonpolyposis Colorectal Cancer Patients. *Cancer Res.* **54,** 1645–1648 (1994).

[219] Vasen, H. F., Blanco, I., Aktan-Collan, K., Gopie, J. P., Alonso, A., Aretz, S., Bernstein, I., Bertario, L., Burn, J., Capella, G., Colas, C., Engel, C., Frayling, I. M., Maurizio Genuardi, K. H., Hes, F. J., Hodgson, S. V., Karagiannis, J. A., Lalloo, F., Lindblom, A., Mecklin, J. P., Møller, P., Myrhoj, T., Nagengast, F. M., Parc, Y., De Leon, M. P., Renkonen-Sinisalo, L., Sampson, J. R., Stormorken, A., Sijmons, R. H., Tejpar, S., Thomas, H. J., Rahner, N., Wijnen, J. T., Järvinen, H. J. & Möslein, G. Revised guidelines for the clinical management of Lynch syndrome (HNPCC): recommendations by a group of European experts. *Gut.* **62,** 812–823 (2013).

[220] Rodriguez-Bigas, M. A., Boland, C. R., Hamilton, S. R., Henson, D. E., Jass, J. R., Khan, P. M., Lynch, H., Perucho, M., Smyrk, T., Sobin, L. & Srivastava, S. A National Cancer Institute Workshop on Hereditary Nonpolyposis Colorectal Cancer Syndrome: meeting highlights and Bethesda guidelines. *J Natl Cancer Inst.* **89,** 1758–1762 (1997).

[221] Umar, A., Boland, C. R., Terdiman, J. P., Syngal, S., de la Chapelle, A., Rüschoff, J., Fishel, R., Lindor, N. M., Burgart, L. J., Hamelin, R., Hamilton, S. R., Hiatt, R. A., Jass, J., Lindblom, A., Lynch, H. T., Peltomaki, P., Ramsey, S. D., Rodriguez-Bigas, M. A., Vasen, H. F., Hawk, E. T., Barrett, J. C., Freedman, A. N. & Srivastava, S.

Revised Bethesda Guidelines for Hereditary Nonpolyposis Colorectal Cancer (Lynch Syndrome) and Microsatellite Instability. *J Natl Cancer Inst.* **96,** 261–268 (2004).

[222] Vasen, H. F., Mecklin, J. P., Meera Khan, P. & Lynch, H. T. The International Collaborative Group on Hereditary Non-Polyposis Colorectal Cancer (ICG-HNPCC). *Dis Colon Rectum.* **34,** 424–425 (1991).

[223] Vasen, H. F., Watson, P., Mecklin, J. P. & Lynch, H. T. New clinical criteria for hereditary nonpolyposis colorectal cancer (HNPCC, Lynch syndrome) proposed by the International Collaborative group on HNPCC. *Gastroenterology* **116,** 1453–1456 (1999).

[224] *Molecular testing strategies for Lynch syndrome in people with colorectal cancer | Guidance | NICE* `https://www.nice.org.uk/guidance/dg27` (Apr. 13, 2022).

[225] *NCCN (2021)* `https://www.nccn.org/professionals/physician_gls/pdf/colon.pdf`. (Apr. 13, 2022).

[226] Bellcross, C. A., Bedrosian, S. R., Daniels, E., Duquette, D., Hampel, H., Jasperson, K., Joseph, D. A., Kaye, C., Lubin, I., Meyer, L. J., Reyes, M., Scheuner, M. T., Schully, S. D., Senter, L., Stewart, S. L., St. Pierre, J., Westman, J., Wise, P., Yang, V. W. & Khoury, M. J. Implementing screening for Lynch syndrome among patients with newly diagnosed colorectal cancer: summary of a public health/clinical collaborative meeting. *Genet Med.* **14,** 152–162 (2012).

[227] Rahm, A. K., Cragun, D., Hunter, J. E., Epstein, M. M., Lowery, J., Lu, C. Y., Pawloski, P. A., Sharaf, R. N., Liang, S. Y., Burnett-Hartman, A. N., Gudgeon, J. M., Hao, J., Snyder, S., Gogoi, R., Ladd, I. & Williams, M. S. Implementing universal Lynch syndrome screening (IMPULSS): protocol for a multi-site study to identify strategies to implement, adapt, and sustain genomic medicine programs in different organizational contexts. *BMC Health Serv Res.* **18,** 824 (2018).

[228] Boland, C. R., Thibodeau, S. N., Hamilton, S. R., Sidransky, D., Eshleman, J. R., Burt, R. W., Meltzer, S. J., Rodriguez-Bigas, M. A., Fodde, R., Ranzani, G. N. & Srivastava, S. A National Cancer Institute Workshop on Microsatellite Instability for Cancer Detection and Familial Predisposition: Development of International Criteria for the Determination of Microsatellite Instability in Colorectal Cancer. *Cancer Res.* **58,** 5248–5257 (1998).

[229] Pagin, A., Zerimech, F., Leclerc, J., Wacrenier, A., Lejeune, S., Descarpentries, C., Escande, F., Porchet, N. & Buisine, M. P. Evaluation of a new panel of six mononucleotide repeat markers for the detection of DNA mismatch repair-deficient tumours. *Br J Cancer.* **108,** 2079–2087 (2013).

[230] Findeisen, P., Kloor, M., Merx, S., Sutter, C., Woerner, S. M., Dostmann, N., Benner, A., Dondog, B., Pawlita, M., Dippold, W., Wagner, R., Gebert, J. & von Knebel Doeberitz, M. T25 repeat in the 3' untranslated region of the CASP2 gene: a sensitive and specific

marker for microsatellite instability in colorectal cancer. *Cancer Res.* **65,** 8072–8078 (2005).

[231] Salipante, S. J., Scroggins, S. M., Hampel, H. L., Turner, E. H. & Pritchard, C. C. Microsatellite Instability Detection by Next Generation Sequencing. *Clin Chem.* **60,** 1192–1199 (2014).

[232] Nowak, J. A., Yurgelun, M. B., Bruce, J. L., Rojas-Rudilla, V., Hall, D. L., Shivdasani, P., Garcia, E. P., Agoston, A. T., Srivastava, A., Ogino, S., Kuo, F. C., Lindeman, N. I. & Dong, F. Detection of Mismatch Repair Deficiency and Microsatellite Instability in Colorectal Adenocarcinoma by Targeted Next-Generation Sequencing. *J Mol Diagn.* **19,** 84–91 (2017).

[233] Leclerc, J., Vermaut, C. & Buisine, M.-P. Diagnosis of Lynch Syndrome and Strategies to Distinguish Lynch-Related Tumors from Sporadic MSI/dMMR Tumors. *Cancers (Basel).* **13,** 467 (2021).

[234] Newton, K., Jorgensen, N. M., Wallace, A. J., Buchanan, D. D., Lalloo, F., McMahon, R. F., Hill, J. & Evans, D. G. Tumour MLH1 promoter region methylation testing is an effective prescreen for Lynch Syndrome (HNPCC). *J Med Genet.* **51,** 789–796 (2014).

[235] Balmaña, J., Stockwell, D. H., Steyerberg, E. W., Stoffel, E. M., Deffenbaugh, A. M., Reid, J. E., Ward, B., Scholl, T., Hendrickson, B., Tazelaar, J., Burbidge, L. A. & Syngal, S. Prediction of MLH1 and MSH2 mutations in Lynch syndrome. *JAMA* **296,** 1469–1478 (2006).

[236] Barnetson, R. A., Tenesa, A., Farrington, S. M., Nicholl, I. D., Cetnarskyj, R., Porteous, M. E., Campbell, H. & Dunlop, M. G. Identification and Survival of Carriers of Mutations in DNA Mismatch-Repair Genes in Colon Cancer. *N Engl J Med.* **354,** 2751–2763 (2006).

[237] Chen, S., Wang, W., Lee, S., Nafa, K., Lee, J., Romans, K., Watson, P., Gruber, S. B., Euhus, D., Kinzler, K. W., Jass, J., Gallinger, S., Lindor, N. M., Casey, G., Ellis, N., Giardiello, F. M., Offit, K. & Parmigiani, G. Prediction of germline mutations and cancer risk in the Lynch syndrome. *JAMA.* **296,** 1479–1487 (2006).

[238] Hampel, H. Genetic counseling and cascade genetic testing in Lynch syndrome. *Fam Cancer.* **15,** 423–427 (2016).

[239] Lynch, H. T., Boland, C. R., Gong, G., Shaw, T. G., Lynch, P. M., Fodde, R., Lynch, J. F. & de la Chapelle, A. Phenotypic and genotypic heterogeneity in the Lynch syndrome: diagnostic, surveillance and management implications. *Eur J Hum Genet.* **14,** 390–402 (2006).

[240] Moiel, D. & Thompson, J. Early detection of colon cancer-the kaiser permanente northwest 30-year history: how do we measure success? Is it the test, the number of tests, the stage, or the percentage of screen-detected patients? *Perm J.* **15,** 30–38 (2011).

[241] Järvinen, H. J., Mecklin, J. P. & Sistonen, P. Screening reduces colorectal cancer rate in families with hereditary nonpolyposis colorectal cancer. *Gastroenterology.* **108,** 1405–1411 (1995).

[242] Järvinen, H. J., Aarnio, M., Mustonen, H., AktanCollan, K., Aaltonen, L. A., Peltomäki, P., Chapelle, A. D. L. & Mecklin, J. P. Controlled 15-year trial on screening for colorectal cancer in families with hereditary nonpolyposis colorectal cancer. *Gastroenterology.* **118,** 829–834 (2000).

[243] Kim, J. Y. & Byeon, J.-S. Genetic Counseling and Surveillance Focused on Lynch Syndrome. *J Anus Rectum Colon.* **3,** 60–68 (2019).

[244] Engel, C., Vasen, H. F., Seppälä, T., Aretz, S., Bigirwamungu-Bargeman, M., de Boer, S. Y., Bucksch, K., Büttner, R., Holinski-Feder, E., Holzapfel, S., Hüneburg, R., Jacobs, M. A., Järvinen, H., Kloor, M., von Knebel Doeberitz, M., Koornstra, J. J., van Kouwen, M., Langers, A. M., van de Meeberg, P. C., Morak, M., Möslein, G., Nagengast, F. M., Pylvänäinen, K., Rahner, N., Renkonen-Sinisalo, L., Sanduleanu, S., Schackert, H. K., Schmiegel, W., Schulmann, K., Steinke-Lange, V., Strassburg, C. P., Vecht, J., Verhulst, M. L., de Vos tot Nederveen Cappel, W., Zachariae, S., Mecklin, J. P. & Loeffler, M. No Difference in Colorectal Cancer Incidence or Stage at Detection by Colonoscopy Among 3 Countries With Different Lynch Syndrome Surveillance Policies. *Gastroenterology.* **155,** 1400–1409.e2 (2018).

[245] Seppälä, T. T., Ahadova, A., Dominguez-Valentin, M., Macrae, F., Evans, D. G., Therkildsen, C., Sampson, J., Scott, R., Burn, J., Möslein, G., Bernstein, I., Holinski-Feder, E., Pylvänäinen, K., Renkonen-Sinisalo, L., Lepistö, A., Lautrup, C. K., Lindblom, A., Plazzer, J. P., Winship, I., Tjandra, D., Katz, L. H., Aretz, S., Hüneburg, R., Holzapfel, S., Heinimann, K., Valle, A. D., Neffa, F., Gluck, N., de Vos Tot Nederveen Cappel, W. H., Vasen, H., Morak, M., Steinke-Lange, V., Engel, C., Rahner, N., Schmiegel, W., Vangala, D., Thomas, H., Green, K., Lalloo, F., Crosbie, E. J., Hill, J., Capella, G., Pineda, M., Navarro, M., Blanco, I., Ten Broeke, S., Nielsen, M., Ljungmann, K., Nakken, S., Lindor, N., Frayling, I., Hovig, E., Sunde, L., Kloor, M., Mecklin, J. P., Kalager, M. & Møller, P. Lack of association between screening interval and cancer stage in Lynch syndrome may be accounted for by over-diagnosis; a prospective Lynch syndrome database report. *Hered Cancer Clin Pract.* **17,** 8 (2019).

[246] Kune, G. A., Kune, S. & Watson, L. F. Colorectal Cancer Risk, Chronic Illnesses, Operations, and Medications: Case Control Results from the Melbourne Colorectal Cancer Study. *Cancer Res.* **48,** 4399–4404 (1988).

[247] Burn, J., Sheth, H., Elliott, F., Reed, L., Macrae, F., Mecklin, J. P., Möslein, G., McRonald, F. E., Bertario, L., Evans, D. G., Gerdes, A. M., Ho, J. W., Lindblom, A., Morrison, P. J., Rashbass, J., Ramesar, R., Seppälä, T., Thomas, H. J., Pylvänäinen, K., Borthwick, G. M., Mathers, J. C., Bishop, D. T., Boussioutas, A., Brewer, C., Cook,

J., Eccles, D., Ellis, A., Hodgson, S. V., Lubinski, J., Maher, E. R., Porteous, M. E., Sampson, J., Scott, R. J. & Side, L. Cancer prevention with aspirin in hereditary colorectal cancer (Lynch syndrome), 10-year follow-up and registry-based 20-year data in the CAPP2 study: a double-blind, randomised, placebo-controlled trial. *Lancet.* **395,** 1855–1863 (2020).

[248] Schmeler, K. M., Lynch, H. T., Chen, L.-m., Munsell, M. F., Soliman, P. T., Clark, M. B., Daniels, M. S., White, K. G., Boyd-Rogers, S. G., Conrad, P. G., Yang, K. Y., Rubin, M. M., Sun, C. C., Slomovitz, B. M., Gershenson, D. M. & Lu, K. H. Prophylactic Surgery to Reduce the Risk of Gynecologic Cancers in the Lynch Syndrome. *N Engl J Med* . **354,** 261–269 (2009).

[249] Siravegna, G., Mussolin, B., Venesio, T., Marsoni, S., Seoane, J., Dive, C., Papadopoulos, N., Kopetz, S., Corcoran, R. B., Siu, L. L. & Bardelli, A. How liquid biopsies can change clinical practice in oncology. *Ann Oncol.* **30,** 1580–1590 (2019).

[250] Ignatiadis, M., Sledge, G. W. & Jeffrey, S. S. Liquid biopsy enters the clinic – implementation issues and future challenges. *Nat Rev Clin Oncol.* **18,** 297–312 (2021).

[251] Van Niel, G. & Raposo, G. Shedding light on the cell biology of extracellular vesicles. *Nat Rev Mol Cell Biol.* **19,** 213–228 (2018).

[252] Deatheragea, B. L. & Cooksona, B. T. Membrane Vesicle Release in Bacteria, Eukaryotes, and Archaea: a Conserved yet Underappreciated Aspect of Microbial Life. *Infect Immun.* **80,** 1948–57 (2012).

[253] Mathieu, M., Martin-Jaular, L., Lavieu, G. & Théry, C. Specificities of secretion and uptake of exosomes and other extracellular vesicles for cell-to-cell communication. *Nat Cell Biol.* **21,** 9–17 (2019).

[254] Maas, S. L., Breakefield, X. O. & Weaver, A. M. Extracellular vesicles: unique intercellular delivery vehicles. *Trends Cell Biol.* **27,** 172–188 (2017).

[255] Yáñez-Mó, M., Siljander, P. R., Andreu, Z., Zavec, A. B., Borràs, F. E., Buzas, E. I., Buzas, K., Casal, E., Cappello, F., Carvalho, J., Colás, E., Cordeiro-Da Silva, A., Fais, S., Falcon-Perez, J. M., Ghobrial, I. M., Giebel, B., Gimona, M., Graner, M., Gursel, I., Gursel, M., Heegaard, N. H., Hendrix, A., Kierulf, P., Kokubun, K., Kosanovic, M., Kralj-Iglic, V., Krämer-Albers, E. M., Laitinen, S., Lässer, C., Lener, T., Ligeti, E., Line, A., Lipps, G., Llorente, A., Lötvall, J., Manček-Keber, M., Marcilla, A., Mittelbrunn, M., Nazarenko, I., Nolte-'t Hoen, E. N., Nyman, T. A., O'Driscoll, L., Olivan, M., Oliveira, C., Pállinger, É., Del Portillo, H. A., Reventós, J., Rigau, M., Rohde, E., Sammar, M., Sánchez-Madrid, F., Santarém, N., Schallmoser, K., Ostenfeld, M. S., Stoorvogel, W., Stukelj, R., Van Der Grein, S. G., Helena Vasconcelos, M., Wauben, M. H. & De Wever, O. Biological properties of extracellular vesicles and their physiological functions. *J Extracell Vesicles.* **4,** 1–60 (2015).

[256] Mathieu, M., Névo, N., Jouve, M., Valenzuela, J. I., Maurin, M., Verweij, F. J., Palmulli, R., Lankar, D., Dingli, F., Loew, D., Rubinstein, E., Boncompain, G., Perez, F. & Théry, C. Specificities of exosome versus small ectosome secretion revealed by live intracellular tracking of CD63 and CD9. *Nat Commun.* **12,** 4389 (2021).

[257] Théry, C. *et al.* Minimal information for studies of extracellular vesicles 2018 (MISEV2018): a position statement of the International Society for Extracellular Vesicles and update of the MISEV2014 guidelines. *J Extracell Vesicles.* **7,** 1535750 (2018).

[258] Colombo, M., Raposo, G. & Théry, C. Biogenesis, Secretion, and Intercellular Interactions of Exosomes and Other Extracellular Vesicles. *Annu Rev Cell Dev Biol.* **30,** 255–289 (2014).

[259] Henne, W. M., Stenmark, H. & Emr, S. D. Molecular Mechanisms of the Membrane Sculpting ESCRT Pathway. *Cold Spring Harb Perspect Biol.* **5,** a016766 (2013).

[260] Trajkovic, K., Hsu, C., Chiantia, S., Rajendran, L., Wenzel, D., Wieland, F., Schwille, P., Brügger, B. & Simons, M. Ceramide triggers budding of exosome vesicles into multivesicular endosomes. *Science.* **319,** 1244–1247 (2008).

[261] Anand, S., Samuel, M., Kumar, S. & Mathivanan, S. Ticket to a bubble ride: Cargo sorting into exosomes and extracellular vesicles. *Biochim Biophys Acta Proteins Proteom.* **1867,** 140203 (2019).

[262] Cocucci, E. & Meldolesi, J. Ectosomes and exosomes: shedding the confusion between extracellular vesicles. *Trends Cell Biol.* **25,** 364–372 (2015).

[263] Juan, T. & Fürthauer, M. Biogenesis and function of ESCRT-dependent extracellular vesicles. *Semin Cell Dev Biol.* **74,** 66–77 (2018).

[264] Atkin-Smith, G. K., Tixeira, R., Paone, S., Mathivanan, S., Collins, C., Liem, M., Goodall, K. J., Ravichandran, K. S., Hulett, M. D. & Poon, I. K. A novel mechanism of generating extracellular vesicles during apoptosis via a beads-on-a-string membrane structure. *Nat Commun.* **6,** 7439 (2015).

[265] Santavanond, J. P., Rutter, S. F., Atkin-Smith, G. K. & Poon, I. K. H. Apoptotic Bodies: Mechanism of Formation, Isolation and Functional Relevance. *Subcell Biochem.* **97,** 61–88 (2021).

[266] Crescitelli, R., Lässer, C., Szabó, T. G., Kittel, A., Eldh, M., Dianzani, I., Buzás, E. I. & Lötvall, J. Distinct RNA profiles in subpopulations of extracellular vesicles: apoptotic bodies, microvesicles and exosomes. *J Extracell Vesicles.* **2** (2013).

[267] Hanahan, D. & Weinberg, R. A. The Hallmarks of Cancer. *Cell.* **100,** 57–70 (2000).

[268] Hanahan, D. & Weinberg, R. A. Hallmarks of Cancer: The Next Generation. *Cell.* **144,** 646–674 (2011).

[269] Meehan, K. & Vella, L. J. The contribution of tumour-derived exosomes to the hallmarks of cancer. *Crit Rev Clin Lab Sci.* **53,** 121–31 (2015).

[270] Han, L., Lam, E. W. & Sun, Y. Extracellular vesicles in the tumor microenvironment: old stories, but new tales. *Mol Cancer.* **18,** 59 (2019).

[271] Bebelman, M. P., Janssen, E., Pegtel, D. M. & Crudden, C. The forces driving cancer extracellular vesicle secretion. *Neoplasia.* **23,** 149–157 (2021).

[272] Bebelman, M. P., Smit, M. J., Pegtel, D. M. & Baglio, S. R. Biogenesis and function of extracellular vesicles in cancer. *Pharmacol Ther.* **188,** 1–11 (2018).

[273] Lee, T. H., Chennakrishnaiah, S., Audemard, E., Montermini, L., Meehan, B. & Rak, J. Oncogenic ras-driven cancer cell vesiculation leads to emission of double-stranded DNA capable of interacting with target cells. *Biochem Biophys Res Commun.* **451,** 295–301 (2014).

[274] King, H. W., Michael, M. Z. & Gleadle, J. M. Hypoxic enhancement of exosome release by breast cancer cells. *BMC Cancer.* **12,** 421 (2012).

[275] Al-Nedawi, K., Meehan, B., Micallef, J., Lhotak, V., May, L., Guha, A. & Rak, J. Intercellular transfer of the oncogenic receptor EGFRvIII by microvesicles derived from tumour cells. *Nat Cell Biol.* **10,** 619–624 (2008).

[276] Beckler, M. D., Higginbotham, J. N., Franklin, J. L., Ham, A. J., Halvey, P. J., Imasuen, I. E., Whitwell, C., Li, M., Liebler, D. C. & Coffey, R. J. Proteomic Analysis of Exosomes from Mutant KRAS Colon Cancer Cells Identifies Intercellular Transfer of Mutant KRAS. *Mol Cell Proteomics.* **12,** 343–55 (2013).

[277] Becker, A., Thakur, B. K., Weiss, J. M., Kim, H. S., Peinado, H. & Lyden, D. Extracellular vesicles in cancer: cell-to-cell mediators of metastasis. *Cancer Cell.* **30,** 836–848 (2016).

[278] Zhang, D. X., Vu, L. T., Ismail, N. N., Le, M. T. & Grimson, A. Landscape of extracellular vesicles in the tumour microenvironment: Interactions with stromal cells and with non-cell components, and impacts on metabolic reprogramming, horizontal transfer of neoplastic traits, and the emergence of therapeutic resistance. *Semin Cancer Biol.* **74,** 24–44 (2021).

[279] Jabalee, J., Towle, R. & Garnis, C. The Role of Extracellular Vesicles in Cancer: Cargo, Function, and Therapeutic Implications. *Cells.* **7,** 93 (2018).

[280] Webber, J. P., Spary, L. K., Sanders, A. J., Chowdhury, R., Jiang, W. G., Steadman, R., Wymant, J., Jones, A. T., Kynaston, H., Mason, M. D., Tabi, Z. & Clayton, A. Differentiation of tumour-promoting stromal myofibroblasts by cancer exosomes. *Oncogene.* **34,** 290–302 (2014).

[281] Treps, L., Perret, R., Edmond, S., Ricard, D. & Gavard, J. Glioblastoma stem-like cells secrete the pro-angiogenic VEGF-A factor in extracellular vesicles. *J Extracell Vesicles.* **6,** 1359479 (2017).

[282] Zeng, Z., Li, Y., Pan, Y., Lan, X., Song, F., Sun, J., Zhou, K., Liu, X., Ren, X., Wang, F., Hu, J., Zhu, X., Yang, W., Liao, W., Li, G., Ding, Y. & Liang, L. Cancer-derived exoso-

mal miR-25-3p promotes pre-metastatic niche formation by inducing vascular permeability and angiogenesis. *Nat Commun.* **9,** 5395 (2018).

[283] Lundholm, M., Schröder, M., Nagaeva, O., Baranov, V., Widmark, A., Mincheva-Nilsson, L. & Wikström, P. Prostate Tumor-Derived Exosomes Down-Regulate NKG2D Expression on Natural Killer Cells and CD8+ T Cells: Mechanism of Immune Evasion. *PLoS One.* **9,** e108925 (2014).

[284] Lobb, R. J., Lima, L. G. & Möller, A. Exosomes: Key mediators of metastasis and pre-metastatic niche formation. *Semin Cell Dev Biol.* **67,** 3–10 (2017).

[285] Vasconcelos, M. H., Caires, H. R., Ābols, A., Xavier, C. P. & Linē, A. Extracellular vesicles as a novel source of biomarkers in liquid biopsies for monitoring cancer progression and drug resistance. *Drug Resist Updat.* **47,** 100647 (2019).

[286] Dong, H., Wang, W., Chen, R., Zhang, Y., Zou, K., Ye, M., He, X., Zhang, F. & Han, J. Exosome-mediated transfer of lncRNA-SNHG14 promotes trastuzumab chemoresistance in breast cancer. *Int J Oncol.* **53,** 1013–1026 (2018).

[287] Xu, R., Rai, A., Chen, M., Suwakulsiri, W., Greening, D. W. & Simpson, R. J. Extracellular vesicles in cancer – implications for future improvements in cancer care. *Nat Rev Clin Oncol.* **15,** 617–638 (2018).

[288] Lane, R. E., Korbie, D., Hill, M. M. & Trau, M. Extracellular vesicles as circulating cancer biomarkers: opportunities and challenges. *Clin Transl Med.* **7,** 14 (2018).

[289] Kosaka, N., Kogure, A., Yamamoto, T., Urabe, F., Usuba, W., Prieto-Vila, M. & Ochiya, T. Exploiting the message from cancer: the diagnostic value of extracellular vesicles for clinical applications. *Exp Mol Med.* **51,** 1–9 (2019).

[290] Yoshioka, Y., Kosaka, N., Konishi, Y., Ohta, H., Okamoto, H., Sonoda, H., Nonaka, R., Yamamoto, H., Ishii, H., Mori, M., Furuta, K., Nakajima, T., Hayashi, H., Sugisaki, H., Higashimoto, H., Kato, T., Takeshita, F. & Ochiya, T. Ultra-sensitive liquid biopsy of circulating extracellular vesicles using ExoScreen. *Nat Commun.* **5,** 3591 (2014).

[291] Logozzi, M., De Milito, A., Lugini, L., Borghi, M., Calabrò, L., Spada, M., Perdicchio, M., Marino, M. L., Federici, C., Iessi, E., Brambilla, D., Venturi, G., Lozupone, F., Santinami, M., Huber, V., Maio, M., Rivoltini, L. & Fais, S. High Levels of Exosomes Expressing CD63 and Caveolin-1 in Plasma of Melanoma Patients. *PLoS One.* **4,** e5219 (2009).

[292] Bhagirath, D., Yang, T. L., Bucay, N., Sekhon, K., Majid, S., Shahryari, V., Dahiya, R., Tanaka, Y. & Saini, S. microRNA-1246 is an exosomal biomarker for aggressive prostate cancer. *Cancer Res.* **78,** 1833–1844 (2018).

[293] Allenson, K., Castillo, J., San Lucas, F. A., Scelo, G., Kim, D. U., Bernard, V., Davis, G., Kumar, T., Katz, M., Overman, M. J., Foretova, L., Fabianova, E., Holcatova, I., Janout, V., Meric-Bernstam, F., Gascoyne, P., Wistuba, I., Varadhachary, G., Brennan, P., Hanash, S., Li, D., Maitra, A. & Alvarez, H. High prevalence of mutant KRAS

in circulating exosome-derived DNA from early-stage pancreatic cancer patients. *Ann Oncol.* **28,** 741–747 (2017).

[294] Lucchetti, D., Zurlo, I. V., Colella, F., Ricciardi-Tenore, C., Di Salvatore, M., Tortora, G., De Maria, R., Giuliante, F., Cassano, A., Basso, M., Crucitti, A., Laurenzana, I., Artemi, G. & Sgambato, A. Mutational status of plasma exosomal KRAS predicts outcome in patients with metastatic colorectal cancer. *Sci Rep.* **11,** 22686 (2021).

[295] Costa-Silva, B., Aiello, N. M., Ocean, A. J., Singh, S., Zhang, H., Thakur, B. K., Becker, A., Hoshino, A., Mark, M. T., Molina, H., Xiang, J., Zhang, T., Theilen, T. M., García-Santos, G., Williams, C., Ararso, Y., Huang, Y., Rodrigues, G., Shen, T. L., Labori, K. J., Lothe, I. M. B., Kure, E. H., Hernandez, J., Doussot, A., Ebbesen, S. H., Grandgenett, P. M., Hollingsworth, M. A., Jain, M., Mallya, K., Batra, S. K., Jarnagin, W. R., Schwartz, R. E., Matei, I., Peinado, H., Stanger, B. Z., Bromberg, J. & Lyden, D. Pancreatic cancer exosomes initiate pre-metastatic niche formation in the liver. *Nat Cell Biol.* **17,** 816–26 (2015).

[296] König, L., Kasimir-Bauer, S., Bittner, A. K., Hoffmann, O., Wagner, B., Santos Manvailer, L. F., Kimmig, R., Horn, P. A. & Rebmann, V. Elevated levels of extracellular vesicles are associated with therapy failure and disease progression in breast cancer patients undergoing neoadjuvant chemotherapy. *Oncoimmunology* **7,** e1376153 (2017).

[297] Shukuya, T., Ghai, V., Amann, J. M., Okimoto, T., Shilo, K., Kim, T. K., Wang, K. & Carbone, D. P. Circulating MicroRNAs and Extracellular Vesicle-Containing MicroRNAs as Response Biomarkers of Anti-programmed Cell Death Protein 1 or Programmed Death-Ligand 1 Therapy in NSCLC. *J Thorac Oncol.* **15,** 1773–1781 (2020).

[298] Shehzad, A., Islam, S. U., Shahzad, R., Khan, S. & Lee, Y. S. Extracellular vesicles in cancer diagnostics and therapeutics. *Pharmacol Ther.* **223,** 107806 (2021).

[299] Schubert, A. & Boutros, M. Extracellular vesicles and oncogenic signaling. *Mol Oncol.* **15,** 3–26 (2021).

[300] Fricke, F., Lee, J., Michalak, M., Warnken, U., Hausser, I., Suarez-Carmona, M., Halama, N., Schnölzer, M., Kopitz, J. & Gebert, J. TGFBR2-dependent alterations of exosomal cargo and functions in DNA mismatch repair-deficient HCT116 colorectal cancer cells. *Cell Commun Signal.* **15,** 14 (2017).

[301] Fricke, F., Mussack, V., Buschmann, D., Hausser, I., Pfaffl, M. W., Kopitz, J. & Gebert, J. TGFBR2-dependent alterations of microRNA profiles in extracellular vesicles and parental colorectal cancer cells. *Int J Oncol.* **55,** 925–937 (2019).

[302] Bankhead, P., Loughrey, M. B., Fernández, J. A., Dombrowski, Y., McArt, D. G., Dunne, P. D., McQuaid, S., Gray, R. T., Murray, L. J., Coleman, H. G., James, J. A., Salto-Tellez, M. & Hamilton, P. W. QuPath: Open source software for digital pathology image analysis. *Sci Rep.* **7,** 16878 (2017).

[303] R Core Team. *R: A Language and Environment for Statistical Computing* R Foundation for Statistical Computing (2021).

[304] Bohaumilitzky, L., von Knebel Doeberitz, M., Kloor, M. & Ahadova, A. Implications of Hereditary Origin on the Immune Phenotype of Mismatch Repair-Deficient Cancers: Systematic Literature Review. *J Clin Med.* **9,** 1741 (2020).

[305] Page, M. J., McKenzie, J. E., Bossuyt, P. M., Boutron, I., Hoffmann, T. C., Mulrow, C. D., Shamseer, L., Tetzlaff, J. M., Akl, E. A., Brennan, S. E., Chou, R., Glanville, J., Grimshaw, J. M., Hróbjartsson, A., Lalu, M. M., Li, T., Loder, E. W., Mayo-Wilson, E., McDonald, S., McGuinness, L. A., Stewart, L. A., Thomas, J., Tricco, A. C., Welch, V. A., Whiting, P. & Moher, D. The PRISMA 2020 statement: an updated guideline for reporting systematic reviews. *BMJ.* **372,** n71 (2021).

[306] Page, M. J., Moher, D., Bossuyt, P. M., Boutron, I., Hoffmann, T. C., Mulrow, C. D., Shamseer, L., Tetzlaff, J. M., Akl, E. A., Brennan, S. E., Chou, R., Glanville, J., Grimshaw, J. M., Hróbjartsson, A., Lalu, M. M., Li, T., Loder, E. W., Mayo-Wilson, E., Mcdonald, S., Mcguinness, L. A., Stewart, L. A., Thomas, J., Tricco, A. C., Welch, V. A., Whiting, P. & Mckenzie, J. E. PRISMA 2020 explanation and elaboration: updated guidance and exemplars for reporting systematic reviews. *BMJ* **372,** n160 (2021).

[307] Currier, J. R., Kuta, E. G., Turk, E., Earhart, L. B., Loomis-Price, L., Janetzki, S., Ferrari, G., Birx, D. L. & Cox, J. H. A panel of MHC class I restricted viral peptides for use as a quality control for vaccine trial ELISPOT assays. *J Immunol Methods.* **260,** 157–172 (2002).

[308] Czerkinsky, C. C., Nilsson, L. Å., Nygren, H., Ouchterlony, Ö. & Tarkowski, A. A solid-phase enzyme-linked immunospot (ELISPOT) assay for enumeration of specific antibody-secreting cells. *J Immunol Methods.* **65,** 109–121 (1983).

[309] Reynisson, B., Alvarez, B., Paul, S., Peters, B. & Nielsen, M. NetMHCpan-4.1 and NetMHCIIpan-4.0: improved predictions of MHC antigen presentation by concurrent motif deconvolution and integration of MS MHC eluted ligand data. *Nucleic Acids Res.* **48,** W449–W454 (2020).

[310] Villabona, L., Rodriguez, D. A., Andersson, E. K., Seliger, B., Dalianis, T. & Masucci, G. V. A novel approach for HLA-A typing in formalin-fixed paraffin-embedded-derived DNA. *Mod Pathol.* **27,** 1296–1305 (2014).

[311] Witt, J., Haupt, S., Ahadova, A., Bohaumilitzky, L., Fuchs, V., Ballhausen, A., Przybilla, M. J., Jendrusch, M., Seppälä, T. T., Fürst, D., Walle, T., Busch, E., Haag, G. M., Hüneburg, R., von Knebel Doeberitz, M., Heuveline, V. & Kloor, M. An easy-to-use approach for detecting HLA-A*02 alleles in archival formalin-fixed paraffin-embedded tissue samples and an application example for studying cancer immunoediting. *Submitted* (2022).

[312] Sidney, J., Peters, B., Frahm, N., Brander, C. & Sette, A. HLA class I supertypes: A revised and updated classification. *BMC Immunol.* **9,** 1 (2008).

[313] Gonzalez-Galarza, F. F., McCabe, A., Santos, E. J. D., Jones, J., Takeshita, L., Ortega-Rivera, N. D., Cid-Pavon, G. M., Ramsbottom, K., Ghattaoraya, G., Alfirevic, A., Middleton, D. & Jones, A. R. Allele frequency net database (AFND) 2020 update: gold-standard data classification, open access genotype data and new query tools. *Nucleic Acids Res.* **48,** D783–D788 (2020).

[314] Reynisson, B., Barra, C., Kaabinejadian, S., Hildebrand, W. H., Peters, B., Peters, B., Nielsen, M. & Nielsen, M. Improved Prediction of MHC II Antigen Presentation through Integration and Motif Deconvolution of Mass Spectrometry MHC Eluted Ligand Data. *J Proteome Res.* **19,** 2304–2315 (2020).

[315] Gibson, U. E., Heid, C. A. & Williams, P. M. A novel method for real time quantitative RT-PCR. *Genome Res.* **6,** 995–1001 (1996).

[316] Heid, C. A., Stevens, J., Livak, K. J. & Williams, P. M. Real time quantitative PCR. *Genome Res.* **6,** 986–994 (1996).

[317] Livak, K. J. & Schmittgen, T. D. Analysis of relative gene expression data using real-time quantitative PCR and the 2(-Delta Delta C(T)) Method. *Methods* **25,** 402–408 (2001).

[318] Bohaumilitzky, L., Kluck, K., Hüneburg, R., Gallon, R., Nattermann, J., Kirchner, M., Kristiansen, G., Hommerding, O., Pfuderer, P. L., Wagner, L., Echterdiek, F., Kösegi, S., Müller, N., Fischer, K., Nelius, N., Hartog, B., Borthwick, G., Busch, E., Haag, G. M., Bläker, H., Möslein, G., von Knebel Doeberitz, M., Seppälä, T. T., Ahtiainen, M., Macklin, J. P., Bishop, D. T., Burn, J., Stenzinger, A., Budczies, J., Kloor, M. & Ahadova, A. The Different Immune Profiles of Normal Colonic Mucosa in Cancer-Free Lynch Syndrome Carriers and Lynch Syndrome Colorectal Cancer Patients. *Gastroenterology.* **162,** 907–919.e10 (2022).

[319] Danaher, P., Warren, S., Dennis, L., D'Amico, L., White, A., Disis, M. L., Geller, M. A., Odunsi, K., Beechem, J. & Fling, S. P. Gene expression markers of Tumor Infiltrating Leukocytes. *J Immunother Cancer.* **5,** 18 (2017).

[320] Benjamini, Y. & Hochberg, Y. Controlling the False Discovery Rate: A Practical and Powerful Approach to Multiple Testing. *J R Stat Soc: series B (Methodological).* **57,** 289–300 (1995).

[321] Bradford, M. M. A rapid and sensitive method for the quantitation of microgram quantities of protein utilizing the principle of protein-dye binding. *Anal Biochem.* **72,** 248–254 (1976).

[322] Laemmli, U. K. Cleavage of Structural Proteins during the Assembly of the Head of Bacteriophage T4. *Nature.* **227,** 680–685 (1970).

[323] Aragon, T. J. *epitools: Epidemiology Tools* (2020).

[324] Wickham, H. *ggplot2: Elegant Graphics for Data Analysis* (2016).

[325] Pakish, J. B., Zhang, Q., Chen, Z., Liang, H., Chisholm, G. B., Yuan, Y., Mok, S. C., Broaddus, R. R., Lu, K. H. & Yates, M. S. Immune microenvironment in microsatellite instable endometrial cancers: Hereditary or sporadic origin matters. *Clin Cancer Res.* **23,** 4473–4481 (2017).

[326] Ramchander, N. C., Ryan, N. A., Walker, T. D., Harries, L., Bolton, J., Bosse, T., Evans, D. G. & Crosbie, E. J. Distinct Immunological Landscapes Characterize Inherited and Sporadic Mismatch Repair Deficient Endometrial Cancer. *Front Immunol.* **10,** 3023 (2020).

[327] Young, J., Simms, L. A., Biden, K. G., Wynter, C., Whitehall, V., Karamatic, R., George, J., Goldblatt, J., Walpole, I., Robin, S.-A., Borten, M. M., Stitz, R., Searle, J., McKeone, D., Fraser, L., Purdie, D. R., Podger, K., Price, R., Buttenshaw, R., Walsh, M. D., Barker, M., Leggett, B. A. & Jass, J. R. Features of Colorectal Cancers with High-Level Microsatellite Instability Occurring in Familial and Sporadic Settings Parallel Pathways of Tumorigenesis. *Am J Pathol.* **159,** 2107–2116 (2001).

[328] Tougeron, D., Maby, P., Elie, N., Fauquembergue, É., Le Pessot, F., Cornic, M., Sabourin, J.-C., Michel, P., Frébourg, T. & Latouche, J.-B. Regulatory T Lymphocytes Are Associated with Less Aggressive Histologic Features in Microsatellite-Unstable Colorectal Cancers. *PLoS One.* **8,** e61001 (2013).

[329] Wang, T., Lik, Lee, H., Vyas, M., Zhang, L., Ganesh, K., Firat, C., Segal, N. H., Desai, A., Hechtman, J. F., Ntiamoah, P., Weiser, M. R., Arnold, Markowitz, J., Efsevia Vakiani, David, Klimstra, S., Stadler, Z. K. & Shia, J. Colorectal carcinoma with double somatic mismatch repair gene inactivation: clinical and pathological characteristics and response to immune checkpoint blockade. *Mod Pathol.* **32,** 1551–1562 (2019).

[330] Jass, J. R., Walsh, M. D., Barker, M., Simms, L. A., Young, J. & Leggett, B. A. Distinction between familial and sporadic forms of colorectal cancer showing DNA microsatellite instability. *Eur J Cancer.* **38,** 858–866 (2002).

[331] Pfuderer, P. L., Ballhausen, A., Seidler, F., Stark, H.-J., Grabe, N., Frayling, I. M., Ager, A., von Knebel Doeberitz, M., Kloor, M. & Ahadova, A. High endothelial venules are associated with microsatellite instability, hereditary background and immune evasion in colorectal cancer. *Br J Cancer.* **121,** 395–404 (2019).

[332] Lee, K. S., Kwak, Y., Ahn, S., Shin, E., Oh, H.-K., Kim, D.-W., Kang, S.-B., Choe, G., Kim, W. H. & Lee, H. S. Prognostic implication of CD274 (PD-L1) protein expression in tumor-infiltrating immune cells for microsatellite unstable and stable colorectal cancer. *Cancer Immunol Immunother.* **66,** 927–939 (2017).

[333] Ahtiainen, M., Erkki-Ville Wirta, Kuopio, T., Seppälä, T., Rantala, J., Mecklin, J.-P. & Böhm, J. Combined prognostic value of CD274 (PD-L1)/PDCDI (PD-1) expression and

immune cell infiltration in colorectal cancer as per mismatch repair status. *Mod Pathol.* **32,** 866–883 (2019).

[334] Dierssen, J. W. F., de Miranda, N. F., Mulder, A., van Puijenbroek, M., Verduyn, W., Claas, F. H., van de Velde, C. J., Fleuren, G. J., Cornelisse, C. J., Corver, W. E. & Morreau, H. High-resolution analysis of HLA class I alterations in colorectal cancer. *BMC Cancer.* **6,** 233 (2006).

[335] Clendenning, M., Huang, A., Jayasekara, H., Lorans, M., Preston, S., O'Callaghan, N., Pope, B. J., Macrae, F. A., Winship, I. M., Milne, R. L., Giles, G. G., English, D. R., Hopper, J. L., Win, A. K., Jenkins, M. A., Southey, M. C., Rosty, C. & Buchanan, D. D. Somatic mutations of the coding microsatellites within the beta-2-microglobulin gene in mismatch repair-deficient colorectal cancers and adenomas. *Fam Cancer.* **17,** 91–100 (2018).

[336] Dabir, P. D., Bruggeling, C. E., van der Post, R. S., Dutilh, B. E., Hoogerbrugge, N., Ligtenberg, M. J., Boleij, A. & Nagtegaal, I. D. Microsatellite instability screening in colorectal adenomas to detect Lynch syndrome patients? A systematic review and meta-analysis. *Eur J Hum Genet.* **28,** 277–286 (2020).

[337] Mlecnik, B., Bifulco, C., Bindea, G., Marliot, F., Lugli, A., Lee, J. J., Zlobec, I., Rau, T. T., Berger, M. D., Nagtegaal, I. D., Vink-Börger, E., Hartmann, A., Geppert, C., Kolwelter, J., Merkel, S., Gru tzmann, R., Van den Eynde, M., Jouret-Mourin, A., Kartheuser, A., Léonard, D., Remue, C., Wang, J. Y., Bavi, P., Roehrl, M. H., Ohashi, P. S., Nguyen, L. T., Han, S. J., MacGregor, H. L., Hafezi-Bakhtiari, S., Wouters, B. G., Masucci, G. V., Andersson, E. K., Zavadova, E., Vocka, M., Spacek, J., Petruzelka, L., Konopasek, B., Dundr, P., Skalova, H., Nemejcova, K., Botti, G., Tatangelo, F., Delrio, P., Ciliberto, G., Maio, M., Laghi, L., Grizzi, F., Fredriksen, T., Buttard, B., Lafontaine, L., Bruni, D., Lanzi, A., El Sissy, C., Haicheur, N., Kirilovsky, A., Berger, A., Lagorce, C., Paustian, C., Ballesteros-Merino, C., Dijkstra, J., Van De Water, C., Van Lent-Van Vliet, S., Knijn, N., Muşină, A. M., Scripcariu, D. V., Popivanova, B., Xu, M., Fujita, T., Hazama, S., Suzuki, N., Nagano, H., Okuno, K., Torigoe, T., Sato, N., Furuhata, T., Takemasa, I., Itoh, K., Patel, P. S., Vora, H. H., Shah, B., Patel, J. B., Rajvik, K. N., Pandya, S. J., Shukla, S. N., Wang, Y., Zhang, G., Kawakami, Y., Marincola, F. M., Ascierto, P. A., Fox, B. A., Pagès, F. & Galon, J. Multicenter International Society for Immunotherapy of Cancer Study of the Consensus Immunoscore for the Prediction of Survival and Response to Chemotherapy in Stage III Colon Cancer. *J Clin Oncol.* **38,** 3638–3651 (2020).

[338] Labani-Motlagh, A., Ashja-Mahdavi, M. & Loskog, A. The Tumor Microenvironment: A Milieu Hindering and Obstructing Antitumor Immune Responses. *Front Immunol.* **11,** 940 (2020).

[339] Germann, M., Zangger, N., Sauvain, M.-O., Sempoux, C., Bowler, A. D., Wirapati, P., Kandalaft, L. E., Delorenzi, M., Tejpar, S., Coukos, G. & Radtke, F. Neutrophils suppress tumor-infiltrating T cells in colon cancer via matrix metalloproteinase-mediated activation of TGFβ. *EMBO Mol Med.* **12,** e10681 (2020).

[340] Pino, M. S., Mino-Kenudson, M., Wildemore, B. M., Ganguly, A., Batten, J., Sperduti, I., Iafrate, A. J. & Chung, D. C. Deficient DNA Mismatch Repair Is Common in Lynch Syndrome-Associated Colorectal Adenomas. *J Mol Diagn.* **11,** 238–247 (2009).

[341] Blais, M. E., Dong, T. & Rowland-Jones, S. HLA-C as a mediator of natural killer and T-cell activation: spectator or key player? *Immunology.* **133,** 1–7 (2011).

[342] Wang, M. & Claesson, M. H. Classification of Human Leukocyte Antigen (HLA) Supertypes. *Methods Mol Biol.* **1184,** 309–317 (2014).

[343] Woerner, S. M., Yuan, Y. P., Benner, A., Korff, S., von Knebel Doeberitz, M. & Bork, P. SelTarbase, a database of human mononucleotide-microsatellite mutations and their potential impact to tumorigenesis and immunology. *Nucleic Acids Res.* **38,** D682–D689 (2010).

[344] Chuo, S. T. Y., Chien, J. C. Y. & Lai, C. P. K. Imaging extracellular vesicles: Current and emerging methods. *J Biomed Sci.* **25,** 91 (2018).

[345] Heath, J. K., White, S. J., Johnstone, C. N., Catimel, B., Simpson, R. J., Moritz, R. L., Tu, G. F., Ji, H., Whitehead, R. H., Groenen, L. C., Scott, A. M., Ritter, G., Cohen, L., Welt, S., Old, L. J., Nice, E. C. & Burgess, A. W. The human A33 antigen is a transmembrane glycoprotein and a novel member of the immunoglobulin superfamily. *Proc Natl Acad Sci U S A.* **94,** 469–474 (1997).

[346] Mathivanan, S., Lim, J. W., Tauro, B. J., Ji, H., Moritz, R. L. & Simpson, R. J. Proteomics analysis of A33 immunoaffinity-purified exosomes released from the human colon tumor cell line LIM1215 reveals a tissue-specific protein signature. *Mol Cell Proteomics.* **9,** 197–208 (2010).

[347] Dunn, G. P., Bruce, A. T., Ikeda, H., Old, L. J. & Schreiber, R. D. Cancer immunoediting: from immunosurveillance to tumor escape. *Nat Immunol.* **3,** 991–998 (2002).

[348] Calì, B., Molon, B. & Viola, A. Tuning cancer fate: the unremitting role of host immunity. *Open Biol.* **7,** 170006 (2017).

[349] El-Gabalawy, H., Guenther, L. C. & Bernstein, C. N. Epidemiology of Immune-Mediated Inflammatory Diseases: Incidence, Prevalence, Natural History, and Comorbidities. *J Rheumatol Suppl.* **85,** 2–10 (2010).

[350] He, M. M., Lo, C. H., Wang, K., Polychronidis, G., Wang, L., Zhong, R., Knudsen, M. D., Fang, Z. & Song, M. Immune-Mediated Diseases Associated With Cancer Risks. *JAMA Oncol.* **8,** 209–219 (2022).

[351] Vajdic, C. M. & Leeuwen, M. T. V. Cancer incidence and risk factors after solid organ transplantation. *Int J Cancer.* **125,** 1747–1754 (2009).

[352] Mortaz, E., Tabarsi, P., Mansouri, D., Khosravi, A., Garssen, J., Velayati, A. & Adcock, I. M. Cancers Related to Immunodeficiencies: Update and Perspectives. *Front Immunol.* **7,** 365 (2016).

[353] Huo, Z., Li, C., Xu, X., Ge, F., Wang, R., Wen, Y., Peng, H., Wu, X., Liang, H., Peng, G., Li, R., Huang, D., Chen, Y., Zhong, R., Cheng, B., Xiong, S., Lin, W., He, J. & Liang, W. Cancer Risks in Solid Organ Transplant Recipients: Results from a Comprehensive Analysis of 72 Cohort Studies. *Oncoimmunology.* **9,** 1848068. (2020).

[354] Bari, S., Wang, X., Ajose, T. & Muzaffar, J. Characterization of Lynch syndrome (LS) associated cancers in patients with immune dysfunction. *J Clin Oncol.* **37,** 1532–1532 (2019).

[355] Foster, A. D., Sivarapatna, A. & Gress, R. E. The aging immune system and its relationship with cancer. *Aging health.* **7,** 707–718 (2011).

[356] Weyand, C. M. & Goronzy, J. J. Aging of the immune system: Mechanisms and therapeutic targets. *Ann Am Thorac Soc.* **13,** S422–S428 (2016).

[357] Tsai, Y. J., Huang, S. C., Lin, H. H., Lin, C. C., Lan, Y. T., Wang, H. S., Yang, S. H., Jiang, J. K., Chen, W. S., chen Lin, T., Lin, J. K. & Chang, S. C. Differences in gene mutations according to gender among patients with colorectal cancer. *World J Surg Oncol.* **16,** 128 (2018).

[358] Slattery, M. L., Potter, J. D., Curtin, K., Edwards, S., Ma, K. N., Anderson, K., Schaffer, D. & Samowitz, W. S. Estrogens reduce and withdrawal of estrogens increase risk of microsatellite instability-positive colon cancer. *Cancer Res.* **61,** 126–130 (2001).

[359] Rossouw, J. E., Anderson, G. L., Prentice, R. L., LaCroix, A. Z., Kooperberg, C., Stefanick, M. L., Jackson, R. D., Beresford, S. A., Howard, B. V., Johnson, K. C., Kotchen, J. M. & Ockene, J. Risks and Benefits of Estrogen Plus Progestin in Healthy Postmenopausal Women: Principal Results From the Women's Health Initiative Randomized Controlled Trial. *JAMA.* **288,** 321–333 (2002).

[360] Sumimoto, H., Imabayashi, F., Iwata, T. & Kawakami, Y. The BRAF–MAPK signaling pathway is essential for cancer-immune evasion in human melanoma cells. *J Exp Med.* **203,** 1651–1656 (2006).

[361] Khalili, J. S., Liu, S., Rodríguez-Cruz, T. G., Whittington, M., Wardell, S., Liu, C., Zhang, M., Cooper, Z. A., Frederick, D. T., Li, Y., Zhang, M., Joseph, R. W., Bernatchez, C., Ekmekcioglu, S., Grimm, E., Radvanyi, L. G., Davis, R. E., Davies, M. A., Wargo, J. A., Hwu, P. & Lizée, G. Oncogenic BRAF(V600E) Promotes Stromal Cell-Mediated Immunosuppression Via Induction of Interleukin-1 in Melanoma. *Clin Cancer Res.* **18,** 5329–5340 (2012).

[362] Ilieva, K. M., Correa, I., Josephs, D. H., Karagiannis, P., Egbuniwe, I. U., Cafferkey, M. J., Spicer, J. F., Harries, M., Nestle, F. O., Lacy, K. E. & Karagiannis, S. N. Effects of

BRAF mutations and BRAF inhibition on immune responses to melanoma. *Mol Cancer Ther.* **13,** 2769–2783 (2014).

[363] Li, W. Q., Kawakami, K., Ruszkiewicz, A., Bennett, G., Moore, J. & Iacopetta, B. BRAF mutations are associated with distinctive clinical, pathological and molecular features of colorectal cancer independently of microsatellite instability status. *Mol Cancer.* **5,** 2 (2006).

[364] Overman, M. J., Lonardi, S., Wong, K. Y. M., Lenz, H. J., Gelsomino, F., Aglietta, M., Morse, M. A., Van Cutsem, E., McDermott, R., Hill, A., Sawyer, M. B., Hendlisz, A., Neyns, B., Svrcek, M., Moss, R. A., Ledeine, J. M., Cao, Z. A., Kamble, S., Kopetz, S. & André, T. Durable Clinical Benefit With Nivolumab Plus Ipilimumab in DNA Mismatch Repair-Deficient/Microsatellite Instability-High Metastatic Colorectal Cancer. *J Clin Oncol.* **36,** 773–779 (2018).

[365] Phipps, A. I., Buchanan, D. D., Makar, K. W., Burnett-Hartman, A. N., Coghill, A. E., Passarelli, M. N., Baron, J. A., Ahnen, D. J., Win, A. K., Potter, J. D. & Newcomb, P. A. BRAF mutation status and survival after colorectal cancer diagnosis according to patient and tumor characteristics. *Cancer Epidemiol Biomarkers Prev.* **21,** 1792–1798 (2012).

[366] Sinicrope, F. A., Foster, N. R., Thibodeau, S. N., Marsoni, S., Monges, G., Labianca, R., Yothers, G., Allegra, C., Moore, M. J., Gallinger, S. & Sargent, D. J. DNA mismatch repair status and colon cancer recurrence and survival in clinical trials of 5-fluorouracil-based adjuvant therapy. *J Natl Cancer Inst.* **103,** 863–875 (2011).

[367] Zaanan, A., Henriques, J., Cohen, R., Sefrioui, D., Evrard, C., De La Fouchardiere, C., Lecomte, T., Aparicio, T., Svrcek, M., Taieb, J., André, T., Vernerey, D. & Tougeron, D. Efficacy of Anti-EGFR in Microsatellite Instability Metastatic Colorectal Cancer Depending on Sporadic or Familial Origin. *J Natl Cancer Inst.* **113,** 496–500 (2021).

[368] Herbst, R. S., Soria, J. C., Kowanetz, M., Fine, G. D., Hamid, O., Gordon, M. S., Sosman, J. A., McDermott, D. F., Powderly, J. D., Gettinger, S. N., Kohrt, H. E., Horn, L., Lawrence, D. P., Rost, S., Leabman, M., Xiao, Y., Mokatrin, A., Koeppen, H., Hegde, P. S., Mellman, I., Chen, D. S. & Hodi, F. S. Predictive correlates of response to the anti-PD-L1 antibody MPDL3280A in cancer patients. *Nature.* **515,** 563–567 (2014).

[369] Tumeh, P. C., Harview, C. L., Yearley, J. H., Shintaku, I. P., Taylor, E. J., Robert, L., Chmielowski, B., Spasic, M., Henry, G., Ciobanu, V., West, A. N., Carmona, M., Kivork, C., Seja, E., Cherry, G., Gutierrez, A. J., Grogan, T. R., Mateus, C., Tomasic, G., Glaspy, J. A., Emerson, R. O., Robins, H., Pierce, R. H., Elashoff, D. A., Robert, C. & Ribas, A. PD-1 blockade induces responses by inhibiting adaptive immune resistance. *Nature.* **515,** 568–571 (2014).

[370] Liao, N. S., Bix, M., Zijlstra, M., Jaenisch, R. & Raulet, D. MHC class I deficiency: susceptibility to natural killer (NK) cells and impaired NK activity. *Science.* **253,** 199–202 (1991).

[371] Jager, M. J., Hurks, H. M., Levitskaya, J. & Kiessling, R. HLA expression in uveal melanoma: there is no rule without some exception. *Hum Immunol.* **63,** 444–451 (2002).

[372] Reimers, M. S., Bastiaannet, E., Langley, R. E., Eijk, R. V., Vlierberghe, R. L. V., Lemmens, V. E., Herk-Sukel, M. P. V., Wezel, T. V., Fodde, R., Kuppen, P. J., Morreau, H., Velde, C. J. V. D. & Liefers, G. J. Expression of HLA Class I Antigen, Aspirin Use, and Survival After a Diagnosis of Colon Cancer. *JAMA Intern Med.* **174,** 732–739 (2014).

[373] Phillips, S. M., Banerjea, A., Feakins, R., Li, S. R., Bustin, S. A. & Dorudi, S. Tumour-infiltrating lymphocytes in colorectal cancer with microsatellite instability are activated and cytotoxic. *Br J Surg.* **91,** 469–475 (2004).

[374] Michael-Robinson, J. M., Radford-Smith, G. L., Biemer-Hüttmann, A. E., Purdie, D. M., Walsh, M. D., Simms, L. A., Biden, K. G., Young, J. P., Leggett, B. A. & Jass, J. R. Tumour infiltrating lymphocytes and apoptosis are independent features in colorectal cancer stratified according to microsatellite instability status. *Gut.* **48,** 360–366 (2001).

[375] Budczies, J., Kirchner, M., Kluck, K., Kazdal, D., Glade, J., Allgäuer, M., Kriegsmann, M., Heußel, C. P., Herth, F. J., Winter, H., Meister, M., Muley, T., Fröhling, S., Peters, S., Seliger, B., Schirmacher, P., Thomas, M., Christopoulos, P. & Stenzinger, A. A gene expression signature associated with B cells predicts benefit from immune checkpoint blockade in lung adenocarcinoma. *Oncoimmunology.* **10,** 1860586 (2021).

[376] Budczies, J., Kirchner, M., Kluck, K., Kazdal, D., Glade, J., Allgäuer, M., Kriegsmann, M., Heußel, C. P., Herth, F. J., Winter, H., Meister, M., Muley, T., Goldmann, T., Fröhling, S., Wermke, M., Waller, C. F., Tufman, A., Reck, M., Peters, S., Schirmacher, P., Thomas, M., Christopoulos, P. & Stenzinger, A. Deciphering the immunosuppressive tumor microenvironment in ALK- and EGFR-positive lung adenocarcinoma. *Cancer Immunol Immunother.* **71,** 251–265 (2022).

[377] Danaher, P., Warren, S., Ong, S., Elliott, N., Cesano, A. & Ferree, S. A gene expression assay for simultaneous measurement of microsatellite instability and anti-tumor immune activity. *J Immunother Cancer.* **7,** 15 (1 2019).

[378] Von Bernstorff, W., Voss, M., Freichel, S., Schmid, A., Vogel, I., Jöhnk, C., Henne-Bruns, D., Kremer, B. & Kalthoff, H. Systemic and local immunosuppression in pancreatic cancer patients. *Clin Cancer Res.* **7,** 925s–932s (2001).

[379] De Visser, K. E., Eichten, A. & Coussens, L. M. Paradoxical roles of the immune system during cancer development. *Nat Rev Cancer.* **6,** 24–37 (2006).

[380] Loskog, A., Ninalga, C., Paul-Wetterberg, G., de la Torre, M., Malmström, P. U. & Tötterman, T. H. Human bladder carcinoma is dominated by T-regulatory cells and Th1 inhibitory cytokines. *J Urol.* **177,** 353–358 (2007).

[381] Piersma, S. J. Immunosuppressive tumor microenvironment in cervical cancer patients. *Cancer Microenviron.* **4,** 361–375 (2011).

[382] Grabowski, M. M., Sankey, E. W., Ryan, K. J., Chongsathidkiet, P., Lorrey, S. J., Wilkinson, D. S. & Fecci, P. E. Immune suppression in gliomas. *J Neurooncol.* **151,** 3–12 (2021).

[383] Yamada, N., Kuranaga, Y., Kumazaki, M., Shinohara, H., Taniguchi, K. & Akao, Y. Colorectal cancer cell-derived extracellular vesicles induce phenotypic alteration of T cells into tumor-growth supporting cells with transforming growth factor-1-mediated suppression. *Oncotarget.* **7,** 27033–27043 (2016).

[384] Powell, D. R. & Huttenlocher, A. Neutrophils in the Tumor Microenvironment. *Trends Immunol.* **37,** 41–52 (2016).

[385] Møller, P., Seppälä, T., Bernstein, I., Holinski-Feder, E., Sala, P., Evans, D. G., Lindblom, A., MacRae, F., Blanco, I., Sijmons, R., Jeffries, J., Vasen, H., Burn, J., Nakken, S., Hovig, E., Rødland, E. A., Tharmaratnam, K., de Vos Tot Nederveen Cappel, W. H., Hill, J., Wijnen, J., Jenkins, M., Green, K., Lalloo, F., Sunde, L., Mints, M., Bertario, L., Pineda, M., Navarro, M., Morak, M., Renkonen-Sinisalo, L., Frayling, I. M., Plazzer, J. P., Pylvanainen, K., Genuardi, M., Mecklin, J. P., Möslein, G., Sampson, J. R., Capella, G. & Mallorca Group (http://mallorca-group.org). Incidence of and survival after subsequent cancers in carriers of pathogenic MMR variants with previous cancer: a report from the prospective Lynch syndrome database. *Gut.* **66,** 1657–1664 (2017).

[386] Silverberg, M. J., Chao, C., Leyden, W. A., Xu, L., Horberg, M. A., Klein, D., Towner, W. J., Dubrow, R., Quesenberry, C. P., Neugebauer, R. S. & Abrams, D. I. HIV infection, immunodeficiency, viral replication, and the risk of cancer. *Cancer Epidemiol Biomarkers Prev.* **20,** 2551–2559 (2011).

[387] Jiang, N., He, J., Weinstein, J. A., Penland, L., Sasaki, S., He, X. S., Dekker, C. L., Zheng, N. Y., Huang, M., Sullivan, M., Wilson, P. C., Greenberg, H. B., Davis, M. M., Fisher, D. S. & Quake, S. R. Lineage Structure of the Human Antibody Repertoire in Response to Influenza Vaccination. *Sci Transl Med.* **5,** 171ra19 (2013).

[388] Goronzy, J. J. & Weyand, C. M. Ageing, autoimmunity and arthritis: T-cell senescence and contraction of T-cell repertoire diversity – catalysts of autoimmunity and chronic inflammation. *Arthritis Res Ther.* **5,** 225–234 (2003).

[389] Brodin, P. & Davis, M. M. Human immune system variation. *Nat Rev Immunol.* **17,** 21–29 (2017).

[390] Ferson, M., Edwards, A., Lind, A., Milton, G. W. & Hersey, P. Low natural killer-cell activity and immunoglobulin levels associated with smoking in human subjects. *Int J Cancer.* **23,** 603–609 (1979).

[391] Sopori, M. Effects of cigarette smoke on the immune system. *Nat Rev Immunol.* **2,** 372–377 (2002).

[392] Kantor, E. D., Udumyan, R., Signorello, L. B., Giovannucci, E. L., Montgomery, S. & Fall, K. Adolescent body mass index and erythrocyte sedimentation rate in relation to colorectal cancer risk. *Gut.* **65,** 1289–1295 (2016).

[393] Rebersek, M. Gut microbiome and its role in colorectal cancer. *BMC Cancer.* **21,** 1325 (2021).

[394] Wild, C. P., Scalbert, A. & Herceg, Z. Measuring the exposome: A powerful basis for evaluating environmental exposures and cancer risk. *Environ Mol Mutagen.* **54,** 480–499 (2013).

[395] Hofseth, L. J., Hebert, J. R., Chanda, A., Chen, H., Love, B. L., Pena, M. M., Murphy, E. A., Sajish, M., Sheth, A., Buckhaults, P. J. & Berger, F. G. Early-onset colorectal cancer: initial clues and current views. *Nat Rev Gastroenterol Hepatol.* **17,** 352–364 (2020).

[396] Mauri, G., Sartore-Bianchi, A., Russo, A. G., Marsoni, S., Bardelli, A. & Siena, S. Early-onset colorectal cancer in young individuals. *Mol Oncol.* **13,** 109–131 (2019).

[397] Tilg, H., Adolph, T. E., Gerner, R. R. & Moschen, A. R. The Intestinal Microbiota in Colorectal Cancer. *Cancer Cell.* **33,** 954–964 (2018).

[398] Brennan, C. A. & Garrett, W. S. Gut Microbiota, Inflammation, and Colorectal Cancer. *Annu Rev Microbiol.* **70,** 395–411 (2016).

[399] Mima, K., Sukawa, Y., Nishihara, R., Qian, Z. R., Yamauchi, M., Inamura, K., Kim, S. A., Masuda, A., Nowak, J. A., Nosho, K., Kostic, A. D., Giannakis, M., Watanabe, H., Bullman, S., Milner, D. A., Harris, C. C., Giovannucci, E., Garraway, L. A., Freeman, G. J., Dranoff, G., Chan, A. T., Garrett, W. S., Huttenhower, C., Fuchs, C. S. & Ogino, S. Fusobacterium nucleatum and T Cells in Colorectal Carcinoma. *JAMA Oncol.* **1,** 653–661 (2015).

[400] Wang, D. & Dubois, R. N. Eicosanoids and cancer. *Nat Rev Cancer.* **10,** 181–193 (2010).

[401] Kalinski, P. Regulation of Immune Responses by Prostaglandin E2. *J Immunol.* **188,** 21–28 (2012).

[402] Reyes-Uribe, L., Wu, W., Gelincik, O., Bommi, P. V., Francisco-Cruz, A., Solis, L. M., Lynch, P. M., Lim, R., Stoffel, E. M., Kanth, P., Samadder, N. J., Mork, M. E., Taggart, M. W., Milne, G. L., Marnett, L. J., Vornik, L., Liu, D. D., Revuelta, M., Chang, K., You, Y. N., Kopelovich, L., Wistuba, I. I., Lee, J. J., Sei, S., Shoemaker, R. H., Szabo, E., Richmond, E., Umar, A., Perloff, M., Brown, P. H., Lipkin, S. M. & Vilar, E. Original

research: Naproxen chemoprevention promotes immune activation in Lynch syndrome colorectal mucosa. *Gut.* **70,** 555–566 (2021).

[403] Mowat, A. M. & Agace, W. W. Regional specialization within the intestinal immune system. *Nat Rev Immunol.* **14,** 667–685 (2014).

[404] Kirby, J. A., Bone, M., Robertson, H., Hudson, M. & Jones, D. E. J. The number of intraepithelial T cells decreases from ascending colon to rectum. *J Clin Pathol.* **56,** 158 (2003).

[405] Bajwa - ten Broeke, S. W., Ballhausen, A., Ahadova, A., Suerink, M., Bohaumilitzky, L., Seidler, F., Morreau, H., van Wezel, T., Krzykalla, J., Benner, A., de Miranda, N. F., von Knebel Doeberitz, M., Nielsen, M. & Kloor, M. The coding microsatellite mutation profile of PMS2-deficient colorectal cancer. *Exp Mol Pathol.* **122,** 104668 (2021).

[406] Binder, H., Hopp, L., Schweiger, M. R., Hoffmann, S., Jühling, F., Kerick, M., Timmermann, B., Siebert, S., Grimm, C., Nersisyan, L., Arakelyan, A., Herberg, M., Buske, P., Loeffler-Wirth, H., Rosolowski, M., Engel, C., Przybilla, J., Peifer, M., Friedrichs, N., Moeslein, G., Odenthal, M., Hussong, M., Peters, S., Holzapfel, S., Nattermann, J., Hueneburg, R., Schmiegel, W., Royer-Pokora, B., Aretz, S., Kloth, M., Kloor, M., Buettner, R., Galle, J. & Loeffler, M. Genomic and transcriptomic heterogeneity of colorectal tumours arising in Lynch syndrome. *J Pathol.* **243,** 242–254 (2017).

[407] Shevach, E. M. Mechanisms of Foxp3+ T Regulatory Cell-Mediated Suppression. *Immunity.* **30,** 636–645 (2009).

[408] Schmidt, A., Oberle, N. & Krammer, P. H. Molecular Mechanisms of Treg-Mediated T Cell Suppression. *Front Immunol.* **3,** 51 (2012).

[409] Cui, G., Yuan, A., Li, Z., Goll, R. & Florholmen, J. ST2 and regulatory T cells in the colorectal adenoma/carcinoma microenvironment: implications for diseases progression and prognosis. *Sci Rep.* **10,** 5892 (2020).

[410] Akeus, P., Langenes, V., Von Mentzer, A., Yrlid, U., Sjöling, Å., Saksena, P., Raghavan, S. & Quiding-Järbrink, M. Altered chemokine production and accumulation of regulatory T cells in intestinal adenomas of APC(Min/+) mice. *Cancer Immunol Immunother.* **63,** 807–819 (2014).

[411] Chang, K., Taggart, M. W., Reyes-Uribe, L., Borras, E., Riquelme, E., Barnett, R. M., Leoni, G., Anthony San Lucas, F., Catanese, M. T., Mori, F., Diodoro, M. G., Nancy You, Y., Hawk, E. T., Roszik, J., Scheet, P., Kopetz, S., Nicosia, A., Scarselli, E., Lynch, P. M., McAllister, F. & Vilar, E. Immune Profiling of Premalignant Lesions in Patients With Lynch Syndrome. *JAMA Oncol.* **4,** 1085–1092 (2018).

[412] Lynch, H. T. & de la Chapelle, A. Hereditary colorectal cancer. *N Engl J Med.* **348,** 919–932 (2003).

[413] Kupfer, S. S. Broadening our Understanding of the Immune Landscape in Lynch Syndrome. *Gastroenterology.* **162,** 1024–1025 (2022).

[414] Welsh, R. M. & Selin, L. K. No one is naive: the significance of heterologous T-cell immunity. *Nat Rev Immunol.* **2,** 417–426 (2002).

[415] Gil, A., Kenney, L. L., Mishra, R., Watkin, L. B., Aslan, N. & Selin, L. K. Vaccination and heterologous immunity: educating the immune system. *Trans R Soc Trop Med Hyg.* **109,** 62–69 (2015).

[416] Leng, Q., Tarbe, M., Long, Q. & Wang, F. Pre-existing heterologous T-cell immunity and neoantigen immunogenicity. *Clin Transl Immunology.* **9,** e01111 (2020).

[417] Snyder, A., Makarov, V., Merghoub, T., Yuan, J., Zaretsky, J. M., Desrichard, A., Walsh, L. A., Postow, M. A., Wong, P., Ho, T. S., Hollmann, T. J., Bruggeman, C., Kannan, K., Li, Y., Elipenahli, C., Liu, C., Harbison, C. T., Wang, L., Ribas, A., Wolchok, J. D. & Chan, T. A. Genetic Basis for Clinical Response to CTLA-4 Blockade in Melanoma. *N Engl J Med.* **371,** 2189–2199 (2014).

[418] Balachandran, V. P. *et al.* Identification of unique neoantigen qualities in long term pancreatic cancer survivors. *Nature.* **551,** 512–516 (2017).

[419] Kouwenhoven, M., Özenci, V., Teleshova, N., Hussein, Y., Huang, Y. M., Eusebio, A. & Link, H. Enzyme-Linked Immunospot Assays Provide a Sensitive Tool for Detection of Cytokine Secretion by Monocytes. *Clin Diagn Lab Immunol.* **8,** 1248–1257 (2001).

[420] Anthony, D. D., Hricik, D. E. & Heeger, P. S. in *Measuring Immunity* 380–395 (2005).

[421] Negri, D., Sestili, P., Borghi, M., Ciccolella, M. & Bracci, L. Enzyme-linked immunospot assay to monitor antigen-specific cellular immune responses in mouse tumor models. *Methods Enzymol.* **632,** 457–477 (2020).

[422] Rosati, E., Dowds, C. M., Liaskou, E., Henriksen, E. K. K., Karlsen, T. H. & Franke, A. Overview of methodologies for T-cell receptor repertoire analysis. *BMC Biotechnol.* **17,** 61 (2017).

[423] Miyasaka, A., Yoshida, Y., Wang, T. & Takikawa, Y. Next-generation sequencing analysis of the human T-cell and B-cell receptor repertoire diversity before and after hepatitis B vaccination. *Hum Vaccin Immunother.* **15,** 2738–2753 (2019).

[424] Hiam-Galvez, K. J., Allen, B. M. & Spitzer, M. H. Systemic immunity in cancer. *Nat Rev Cancer.* **21,** 345–359 (2021).

[425] Gabrilovich, D. I., Ostrand-Rosenberg, S. & Bronte, V. Coordinated regulation of myeloid cells by tumours. *Nat Rev Immunol.* **12,** 253–268 (2012).

[426] Almand, B., Clark, J. I., Nikitina, E., van Beynen, J., English, N. R., Knight, S. C., Carbone, D. P. & Gabrilovich, D. I. Increased production of immature myeloid cells in cancer patients: a mechanism of immunosuppression in cancer. *J Immunol.* **166,** 678–689 (2001).

[427] Wu, W. C., Sun, H. W., Chen, H. T., Liang, J., Yu, X. J., Wu, C., Wang, Z. & Zheng, L. Circulating hematopoietic stem and progenitor cells are myeloid-biased in cancer patients. *Proc Natl Acad Sci U S A.* **111,** 4221–4226 (2014).

[428] Mamessier, E., Sylvain, A., Thibult, M. L., Houvenaeghel, G., Jacquemier, J., Castellano, R., Gonçalves, A., André, P., Romagné, F., Thibault, G., Viens, P., Birnbaum, D., Bertucci, F., Moretta, A. & Olive, D. Human breast cancer cells enhance self tolerance by promoting evasion from NK cell antitumor immunity. *J Clin Invest.* **121,** 3609–3622 (2011).

[429] Ichihara, F., Kono, K., Takahashi, A., Kawaida, H., Sugai, H. & Fuji, H. Increased populations of regulatory T cells in peripheral blood and tumor-infiltrating lymphocytes in patients with gastric and esophageal cancers. *Clin Cancer Res.* **9,** 4404–4408 (2003).

[430] Cui, J. H., Lin, K. R., Yuan, S. H., Jin, Y. B., Chen, X. P., Su, X. K., Jiang, J., Pan, Y. M., Mao, S. L., Mao, X. F. & Luo, W. TCR Repertoire as a Novel Indicator for Immune Monitoring and Prognosis Assessment of Patients With Cervical Cancer. *Front Immunol.* **9,** 2729 (2018).

[431] Manuel, M., Trédan, O., Bachelot, T., Clapisson, G., Courtier, A., Parmentier, G., Rabeony, T., Grives, A., Perez, S., Mouret, J. F., Perol, D., Chabaud, S., Ray-Coquard, I., Labidi-Galy, I., Heudel, P., Pierga, J. Y., Caux, C., Blay, J. Y., Pasqual, N. & Ménétrier-Caux, C. Lymphopenia combined with low TCR diversity (divpenia) predicts poor overall survival in metastatic breast cancer patients. *Oncoimmunology.* **1,** 432–440 (2012).

[432] Liu, Y. Y., Yang, Q. F., Yang, J. S., Cao, R. B., Liang, J. Y., Liu, Y. T., Zeng, Y. L., Chen, S., Xia, X. F., Zhang, K. & Liu, L. Characteristics and prognostic significance of profiling the peripheral blood T-cell receptor repertoire in patients with advanced lung cancer. *Int J Cancer.* **145,** 1423–1431 (2019).

[433] Zitvogel, L., Apetoh, L., Ghiringhelli, F. & Kroemer, G. Immunological aspects of cancer chemotherapy. *Nat Rev Immunol.* **8,** 59–73 (2008).

[434] Shaked, Y. The pro-tumorigenic host response to cancer therapies. *Nat Rev Cancer.* **19,** 667–685 (2019).

[435] Zhang, F., Li, R., Yang, Y., Shi, C., Shen, Y., Lu, C., Chen, Y., Zhou, W., Lin, A., Yu, L., Zhang, W., Xue, Z., Wang, J. & Cai, Z. Specific Decrease in B-Cell-Derived Extracellular Vesicles Enhances Post-Chemotherapeutic CD8 + T Cell Responses. *Immunity.* **50,** 738–750.e7 (2019).

[436] Liu, W. M., Fowler, D. W., Smith, P. & Dalgleish, A. G. Pre-treatment with chemotherapy can enhance the antigenicity and immunogenicity of tumours by promoting adaptive immune responses. *Br J Cancer.* **102,** 115–123 (2010).

[437] Casares, N., Pequignot, M. O., Tesniere, A., Ghiringhelli, F., Roux, S., Chaput, N., Schmitt, E., Hamai, A., Hervas-Stubbs, S., Obeid, M., Coutant, F., Métivier, D., Pichard, E., Aucouturier, P., Pierron, G., Garrido, C., Zitvogel, L. & Kroemer, G. Caspase-dependent immunogenicity of doxorubicin-induced tumor cell death. *J Exp Med.* **202,** 1691–1701 (2005).

[438] Suzuki, E., Kapoor, V., Jassar, A. S., Kaiser, L. R. & Albelda, S. M. Gemcitabine selectively eliminates splenic Gr-1+/CD11b+ myeloid suppressor cells in tumor-bearing animals and enhances antitumor immune activity. *Clin Cancer Res.* **11,** 6713–6721 (2005).

[439] Bracci, L., Schiavoni, G., Sistigu, A. & Belardelli, F. Immune-based mechanisms of cytotoxic chemotherapy: implications for the design of novel and rationale-based combined treatments against cancer. *Cell Death Differ.* **21,** 15–25 (2013).

[440] Krall, J. A., Reinhardt, F., Mercury, O. A., Pattabiraman, D. R., Brooks, M. W., Dougan, M., Lambert, A. W., Bierie, B., Ploegh, H. L., Dougan, S. K. & Weinberg, R. A. The systemic response to surgery triggers the outgrowth of distant immune-controlled tumors in mouse models of dormancy. *Sci Transl Med.* **10,** eaan3464 (2018).

[441] Angka, L., Martel, A. B., Kilgour, M., Jeong, A., Sadiq, M., de Souza, C. T., Baker, L., Kennedy, M. A., Kekre, N. & Auer, R. C. Natural Killer Cell IFNγ Secretion is Profoundly Suppressed Following Colorectal Cancer Surgery. *Ann Surg Oncol.* **25,** 3747–3754 (2018).

[442] Cohen, R., Hain, E., Buhard, O., Guilloux, A., Bardier, A., Kaci, R., Bertheau, P., Renaud, F., Bibeau, F., Fléjou, J. F., André, T., Svrcek, M. & Duval, A. Association of Primary Resistance to Immune Checkpoint Inhibitors in Metastatic Colorectal Cancer With Misdiagnosis of Microsatellite Instability or Mismatch Repair Deficiency Status. *JAMA Oncol.* **5,** 551–555 (2019).

[443] Lemery, S., Keegan, P. & Pazdur, R. First FDA Approval Agnostic of Cancer Site — When a Biomarker Defines the Indication. *N Engl J Med.* **377,** 1409–1412 (2017).

[444] Mantovani, A., Marchesi, F., Malesci, A., Laghi, L. & Allavena, P. Tumor-Associated Macrophages as Treatment Targets in Oncology. *Nat Rev Clin Oncol.* **14,** 399–416 (2017).

[445] Gonzalez, H., Hagerling, C. & Werb, Z. Roles of the immune system in cancer: from tumor initiation to metastatic progression. *Genes Dev.* **32,** 1267–1284 (2018).

[446] Fritsch, E. F., Rajasagi, M., Ott, P. A., Brusic, V., Hacohen, N. & Wu, C. J. HLA-binding properties of tumor neoepitopes in humans. *Cancer Immun Res.* **2,** 522–529 (2014).

[447] Ghorani, E., Rosenthal, R., McGranahan, N., Reading, J. L., Lynch, M., Peggs, K. S., Swanton, C. & Quezada, S. A. Differential binding affinity of mutated peptides for MHC class I is a predictor of survival in advanced lung cancer and melanoma. *Ann Oncol.* **29,** 271–279 (2018).

[448] Maletzki, C., Schmidt, F., Dirks, W. G., Schmitt, M. & Linnebacher, M. Frameshift-derived neoantigens constitute immunotherapeutic targets for patients with microsatellite-instable haematological malignancies: Frameshift peptides for treating MSI+ blood cancers. *Eur J Cancer.* **49,** 2587–2595 (2013).

[449] Bjerregaard, A. M., Nielsen, M., Jurtz, V., Barra, C. M., Hadrup, S. R., Szallasi, Z. & Eklund, A. C. An analysis of natural T cell responses to predicted tumor neoepitopes. *Front Immunol.* **8,** 1566 (2017).

[450] Duan, F., Duitama, J., Al Seesi, S., Ayres, C. M., Corcelli, S. A., Pawashe, A. P., Blanchard, T., McMahon, D., Sidney, J., Sette, A., Baker, B. M., Mandoiu, I. I. & Srivastava, P. K. Genomic and bioinformatic profiling of mutational neoepitopes reveals new rules to predict anticancer immunogenicity. *J Exp Med.* **211,** 2231–2248 (2014).

[451] Engels, B., Engelhard, V. H., Sidney, J., Sette, A., Binder, D. C., Liu, R. B., Kranz, D. M., Meredith, S. C., Rowley, D. A. & Schreiber, H. Relapse or eradication of cancer is predicted by peptide-MHC affinity. *Cancer Cell.* **23,** 516–526 (2013).

[452] Nogueira, C., Kaufmann, J. K., Lam, H. & Flechtner, J. B. Improving Cancer Immunotherapies through Empirical Neoantigen Selection. *Trends Cancer.* **4,** 97–100 (2018).

[453] Bassani-Sternberg, M., Bräunlein, E., Klar, R., Engleitner, T., Sinitcyn, P., Audehm, S., Straub, M., Weber, J., Slotta-Huspenina, J., Specht, K., Martignoni, M. E., Werner, A., Hein, R., Busch, D. H., Peschel, C., Rad, R., Cox, J., Mann, M. & Krackhardt, A. M. Direct identification of clinically relevant neoepitopes presented on native human melanoma tissue by mass spectrometry. *Nat Commun.* **7,** 13404 (2016).

[454] Bonsack, M., Hoppe, S., Winter, J., Tichy, D., Zeller, C., Kupper, M. D., Schitter, E. C., Blatnik, R. & Riemer, A. B. Performance evaluation of MHC class-I binding prediction tools based on an experimentally validated MHC–peptide binding data set. *Cancer Immunol Res.* **7,** 719–736 (2019).

[455] Sidney, B., Peters, A., Sette, S., Paul, D., Weiskopf, M. A. & Angelo, J. Size, Affinity, and Immunogenicity Peptide-Binding Repertoires of Different HLA Class I Alleles Are Associated with. *J Immunol.* **191,** 5831–5839 (2013).

[456] Tian, F., Zhang, S., Liu, C., Han, Z., Liu, Y., Deng, J., Li, Y., Wu, X., Cai, L., Qin, L., Chen, Q., Yuan, Y., Liu, Y., Cong, Y., Ding, B., Jiang, Z. & Sun, J. Protein analysis of extracellular vesicles to monitor and predict therapeutic response in metastatic breast cancer. *Nat Commun.* **12,** 2536 (2021).

[457] Kalluri, R. The biology and function of exosomes in cancer. *J Clin Invest.* **126,** 1208–1215 (2016).

[458] Thakur, B. K., Zhang, H., Becker, A., Matei, I., Huang, Y., Costa-Silva, B., Zheng, Y., Hoshino, A., Brazier, H., Xiang, J., Williams, C., Rodriguez-Barrueco, R., Silva, J. M., Zhang, W., Hearn, S., Elemento, O., Paknejad, N., Manova-Todorova, K., Welte, K., Bromberg, J., Peinado, H. & Lyden, D. Double-stranded DNA in exosomes: a novel biomarker in cancer detection. *Cell Res.* **24,** 766–769 (2014).

[459] Lázaro-Ibáñez, E., Lässer, C., Shelke, G. V., Crescitelli, R., Jang, S. C., Cvjetkovic, A., García-Rodríguez, A. & Lötvall, J. DNA analysis of low- and high-density fractions de-

fines heterogeneous subpopulations of small extracellular vesicles based on their DNA cargo and topology. *J Extracell Vesicles.* **8,** 1656993 (2019).

[460] Malkin, E. Z. & Bratman, S. V. Bioactive DNA from extracellular vesicles and particles. *Cell Death Dis.* **11,** 584 (2020).

[461] Möhrmann, L., Huang, H. J., Hong, D. S., Tsimberidou, A. M., Fu, S., Piha-Paul, S. A., Subbiah, V., Karp, D. D., Naing, A., Krug, A., Enderle, D., Priewasser, T., Noerholm, M., Eitan, E., Coticchia, C., Stoll, G., Jordan, L. M., Eng, C., Kopetz, E. S., Skog, J., Meric-Bernstam, F. & Janku, F. Liquid Biopsies Using Plasma Exosomal Nucleic Acids and Plasma Cell-Free DNA Compared with Clinical Outcomes of Patients with Advanced Cancers. *Clin Cancer Res.* **24,** 181–188 (2018).

[462] Yang, S., Che, S. P., Kurywchak, P., Tavormina, J. L., Gansmo, L. B., Correa de Sampaio, P., Tachezy, M., Bockhorn, M., Gebauer, F., Haltom, A. R., Melo, S. A., LeBleu, V. S. & Kalluri, R. Detection of mutant KRAS and TP53 DNA in circulating exosomes from healthy individuals and patients with pancreatic cancer. *Cancer Biol Ther.* **18,** 158–165 (2017).

[463] Yap, S. A., Münster-Wandowski, A., Nonnenmacher, A., Keilholz, U. & Liebs, S. Analysis of cancer-related mutations in extracellular vesicles RNA by Droplet DigitalTM-PCR. *Biotechniques.* **69,** 99–107 (2020).

[464] Kahlert, C., Melo, S. A., Protopopov, A., Tang, J., Seth, S., Koch, O., Zhang, J., Weitz, J., Chin, L., Futreal, A. & Kalluri, R. Identification of Double-stranded Genomic DNA Spanning All Chromosomes with Mutated KRAS and p53 DNA in the Serum Exosomes of Patients with Pancreatic Cancer. *J Biol Chem.* **289,** 3869–3875 (2014).

[465] García-Silva, S., Benito-Martín, A., Sánchez-Redondo, S., Hernández-Barranco, A., Ximénez-Embún, P., Nogués, L., Mazariegos, M. S., Brinkmann, K., López, A. A., Meyer, L., Rodríguez, C., García-Martín, C., Boskovic, J., Letón, R., Montero, C., Robledo, M., Santambrogio, L., Brady, M. S., Szumera-Ciećkiewicz, A., Kalinowska, I., Skog, J., Noerholm, M., Muñoz, J., Ortiz-Romero, P. L., Ruano, Y., Rodríguez-Peralto, J. L., Rutkowski, P. & Peinado, H. Use of extracellular vesicles from lymphatic drainage as surrogate markers of melanoma progression and BRAFV600E mutation. *J Exp Med.* **216,** 1061–1070 (2019).

[466] Richman, S. D., Chambers, P., Seymour, M. T., Daly, C., Grant, S., Hemmings, G. & Quirke, P. Intra-tumoral Heterogeneity of KRAS and BRAF Mutation Status in Patients with Advanced Colorectal Cancer (aCRC) and Cost-Effectiveness of Multiple Sample Testing. *Anal Cell Pathol (Amst).* **34,** 61–66 (2011).

[467] Tauro, B. J., Greening, D. W., Mathias, R. A., Mathivanan, S., Ji, H. & Simpson, R. J. Two Distinct Populations of Exosomes Are Released from LIM1863 Colon Carcinoma Cell-derived Organoids. *Mol Cell Proteomics.* **12,** 587–598 (2013).

[468] Ludwig, A. K., De Miroschedji, K., Doeppner, T. R., Börger, V., Ruesing, J., Rebmann, V., Durst, S., Jansen, S., Bremer, M., Behrmann, E., Singer, B. B., Jastrow, H., Kuhlmann, J. D., El Magraoui, F., Meyer, H. E., Hermann, D. M., Opalka, B., Raunser, S., Epple, M., Horn, P. A. & Giebel, B. Precipitation with polyethylene glycol followed by washing and pelleting by ultracentrifugation enriches extracellular vesicles from tissue culture supernatants in small and large scales. *J Extracell Vesicles.* **7,** 1528109 (2018).

[469] Simonsen, J. B. What Are We Looking At? Extracellular Vesicles, Lipoproteins, or Both? *Circ Res.* **121,** 920–922 (2017).

[470] Moon, P. G., Lee, J. E., Cho, Y. E., Lee, S. J., Chae, Y. S., Jung, J. H., Kim, I. S., Park, H. Y. & Baek, M. C. Fibronectin on circulating extracellular vesicles as a liquid biopsy to detect breast cancer. *Oncotarget.* **7,** 40189–40199 (2016).

[471] Snook, A. E., Magee, M. S. & Waldman, S. A. GUCY2C-targeted cancer immunotherapy: past, present and future. *Immunol Res.* **51,** 161–169 (2011).

Supplement

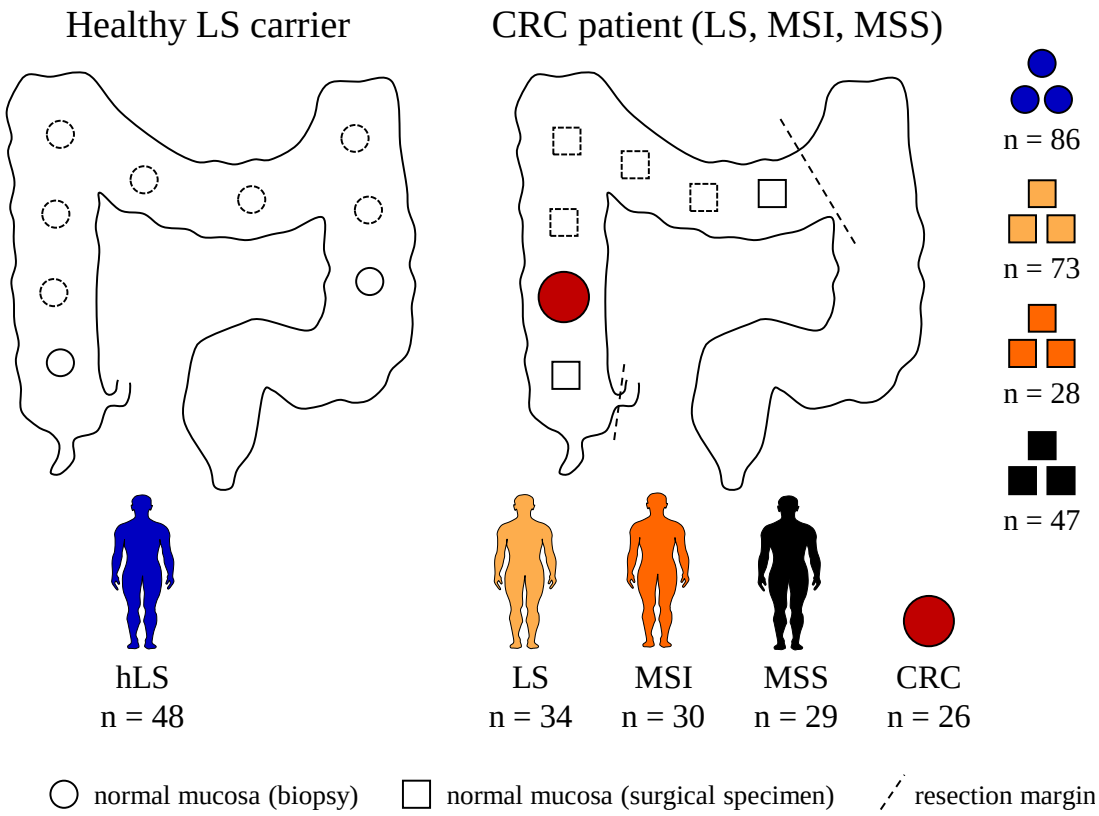

Figure S1: Sampling strategy for normal mucosa from healthy LS carriers and CRC patients. Normal colonic mucosa from healthy LS carriers (hLS) was obtained during surveillance colonoscopy. Tumor-distant, normal mucosa from CRC patients (LS, sporadic MSI and MSS) was obtained from tumor-free margins during tumor resection (here: right hemicolectomy). If several tissue samples (biopsies/surgical specimens) were available (indicated with dashed lines) all analyzable samples were used. Adapted from: [318].

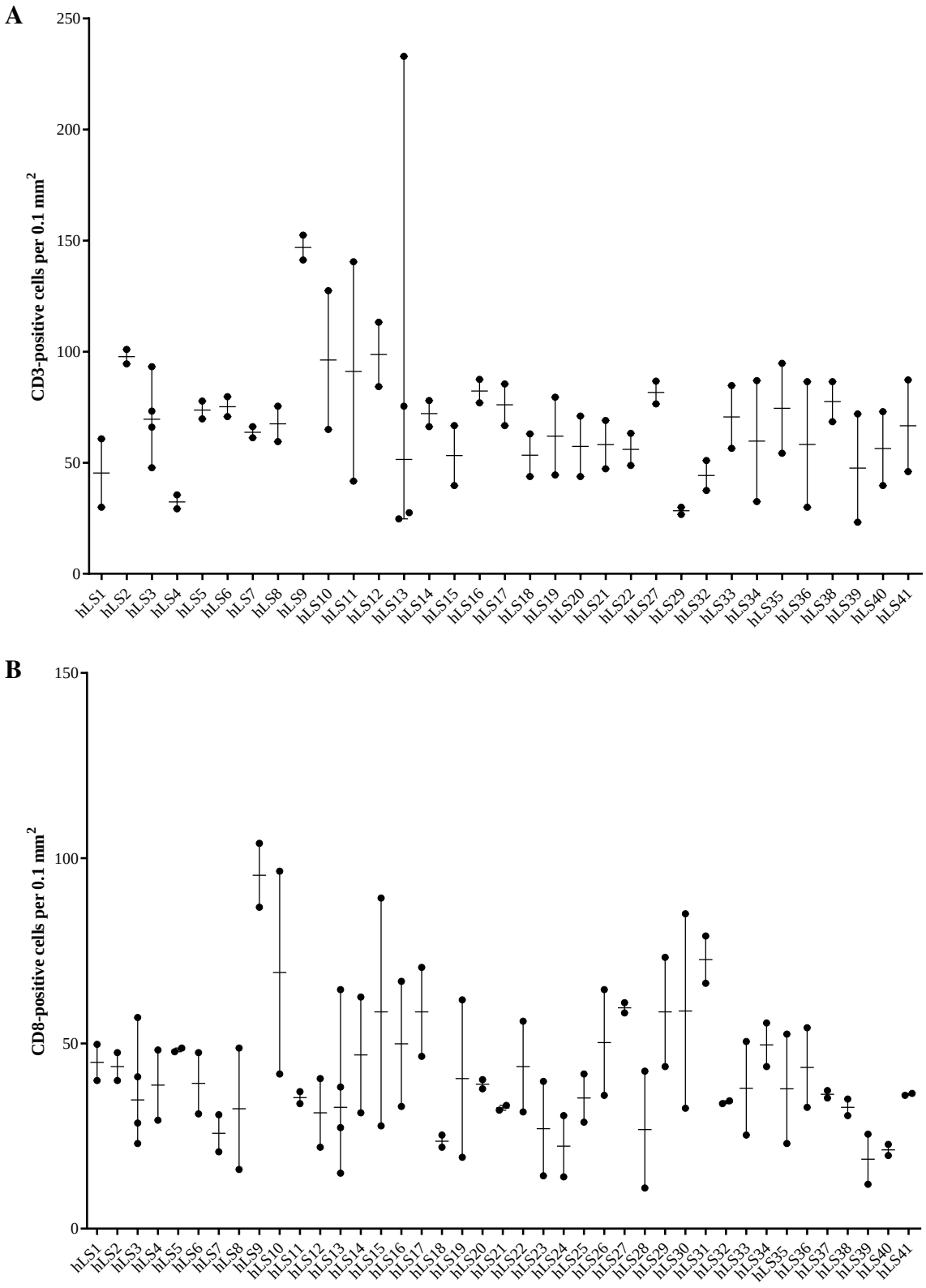

Figure S2: Individual T cell counts for the normal colonic mucosa from healthy LS carriers. Individual counts for CD3- (A) and CD8-positive (B) T cells for all healthy LS carriers (hLS) from which more than one tissue block was analyzed. Each data point represents the mean number of T cells in the defined ROIs of one tissue block. Median and data range are depicted. Adapted from: [318].

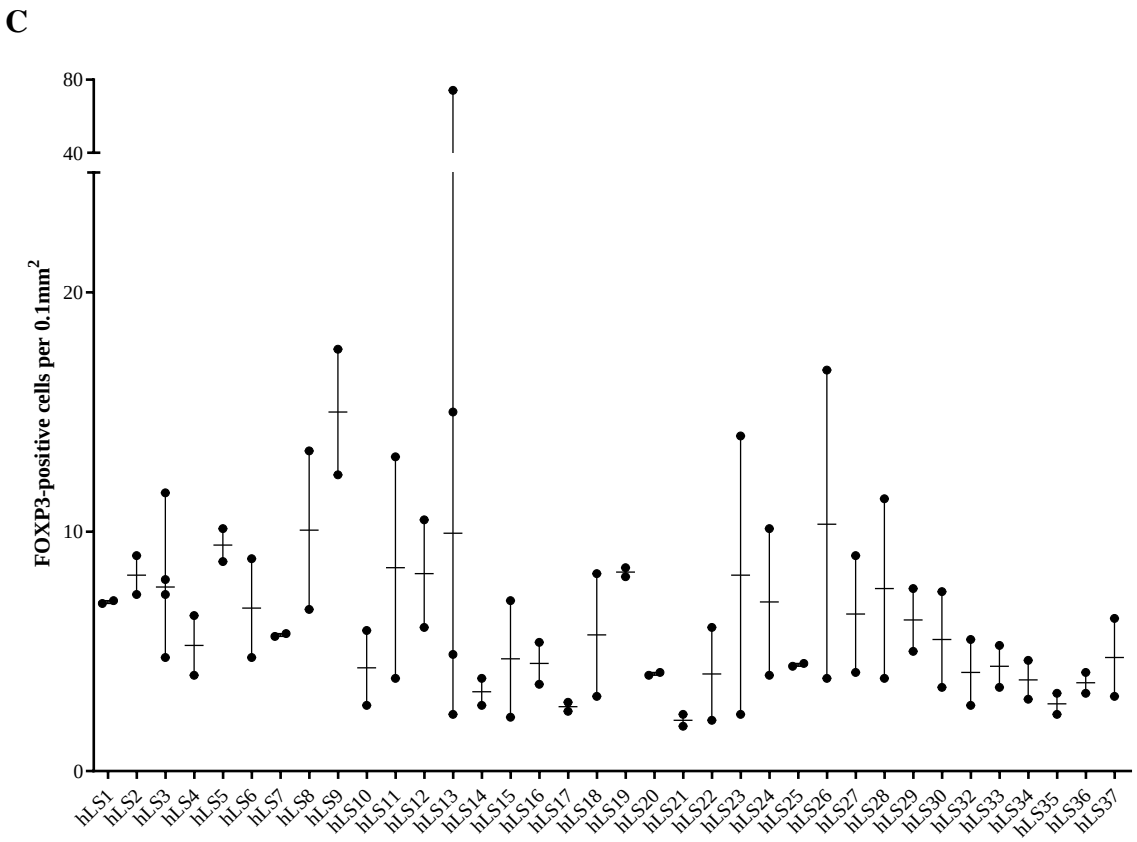

Figure S2: Individual T cell counts for the normal colonic mucosa from healthy LS carriers. Individual counts for FOXP3-positive (C) T cells for all healthy LS carriers (hLS) from which more than one tissue block was analyzed. Each data point represents the mean number of T cells in the defined ROIs of one tissue block. Median and data range are depicted. Adapted from: [318].

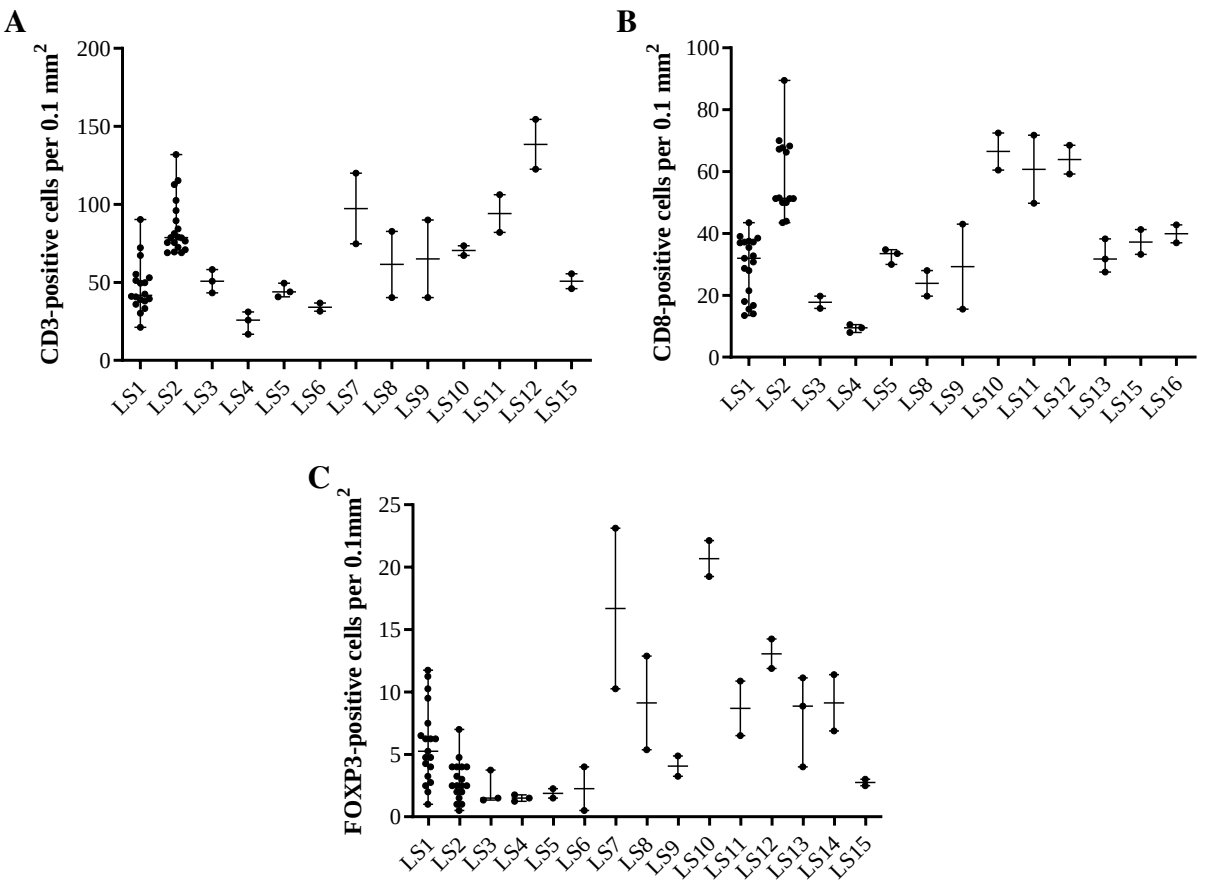

Figure S3: Individual T cell counts for the normal colonic mucosa from LS CRC patients. Individual counts for CD3- (A), CD8- (B) and FOXP3-positive (C) T cells for all LS CRC patients from which more than one tissue block was analyzed. Each data point represents the mean number of T cells in the defined ROIs of one tissue block. Median and data range are depicted. Adapted from: [318].

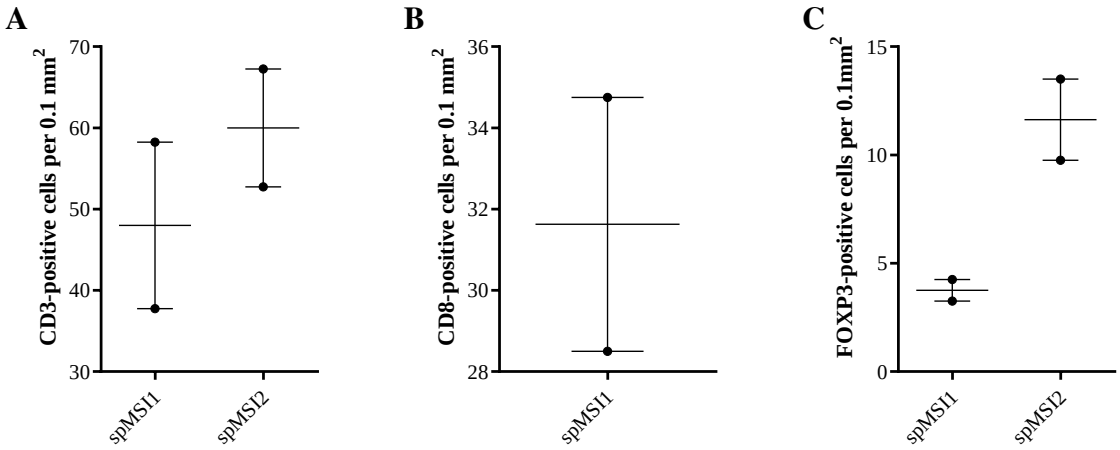

Figure S4: Individual T cell counts for the normal colonic mucosa from sporadic MSI CRC patients. Individual counts for CD3- (A), CD8- (B) and FOXP3-positive (C) T cells for all sporadic MSI CRC patients from which more than one tissue block was analyzed. Each data point represents the mean number of T cells in the defined ROIs of one tissue block. Median and data range are depicted. Adapted from: [318].

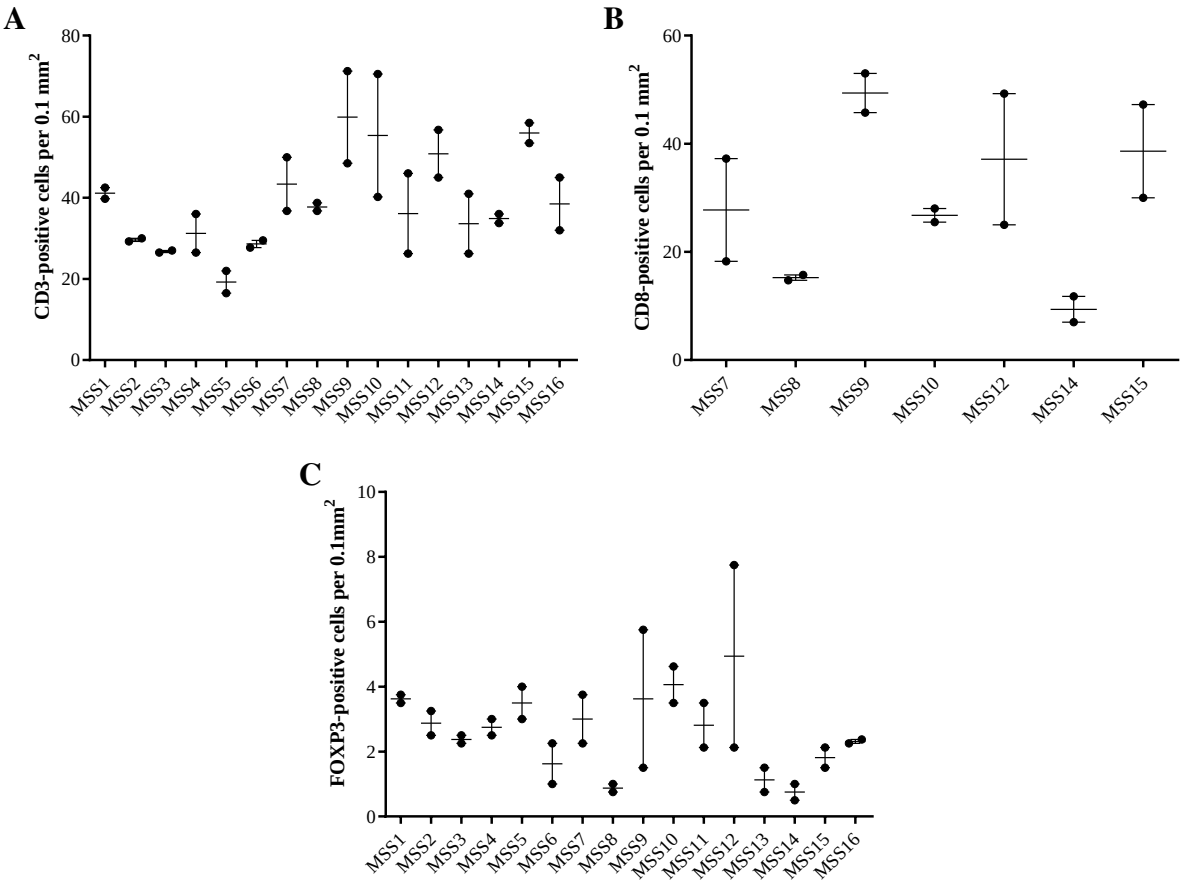

Figure S5: Individual T cell counts for the normal colonic mucosa from MSS CRC patients. Individual counts for CD3- (A), CD8- (B) and FOXP3-positive (C) T cells for all MSS CRC patients from which more than one tissue block was analyzed. Each data point represents the mean number of T cells in the defined ROIs of one tissue block. Median and data range are depicted. Adapted from: [318].

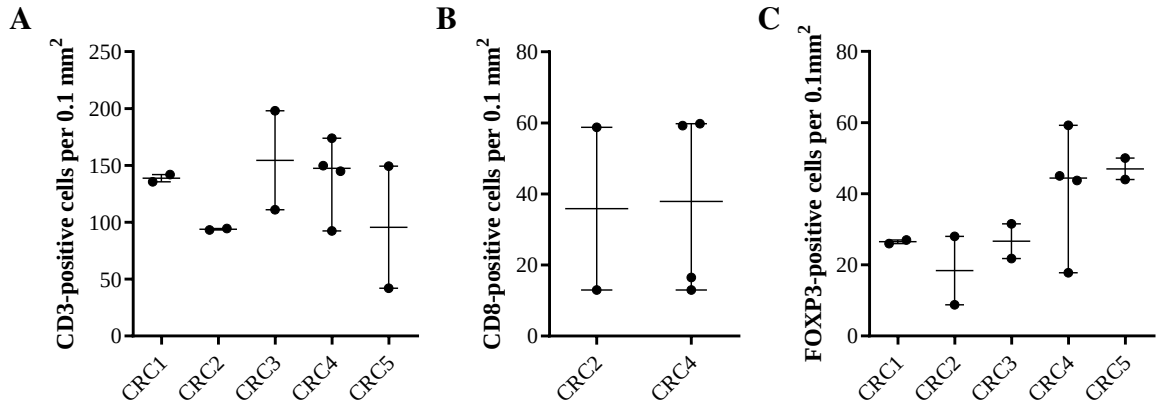

Figure S6: Individual T cell counts for LS CRC tissue. Individual counts for CD3- (A), CD8- (B) and FOXP3-positive (C) T cells for all LS CRCs from which more than one tissue block was analyzed. Each data point represents the mean number of T cells in the defined ROIs of one tissue block. Median and data range are depicted. Adapted from: [318]

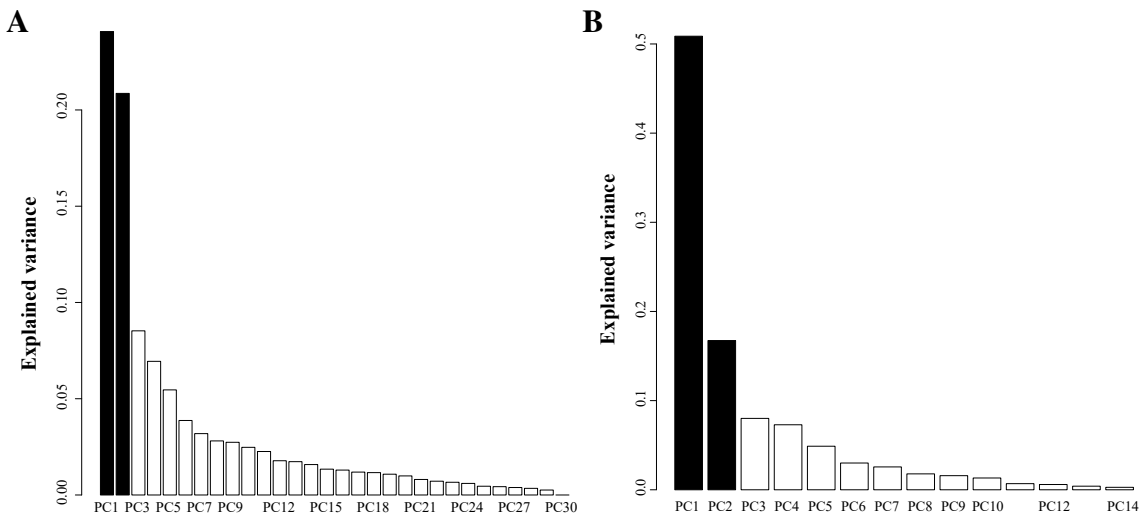

Figure S7: Variance explained by the principal components of the PCA for gene expression and absolute markers. For gene expression (A) 24 % of variance is explained by PC1 and 21 % by PC2. For the absolute markers (B) 51 % of the variance is explained by PC1 and 17 % by PC2. PC1 and PC2 are labeled in black. Adapted from: [318]

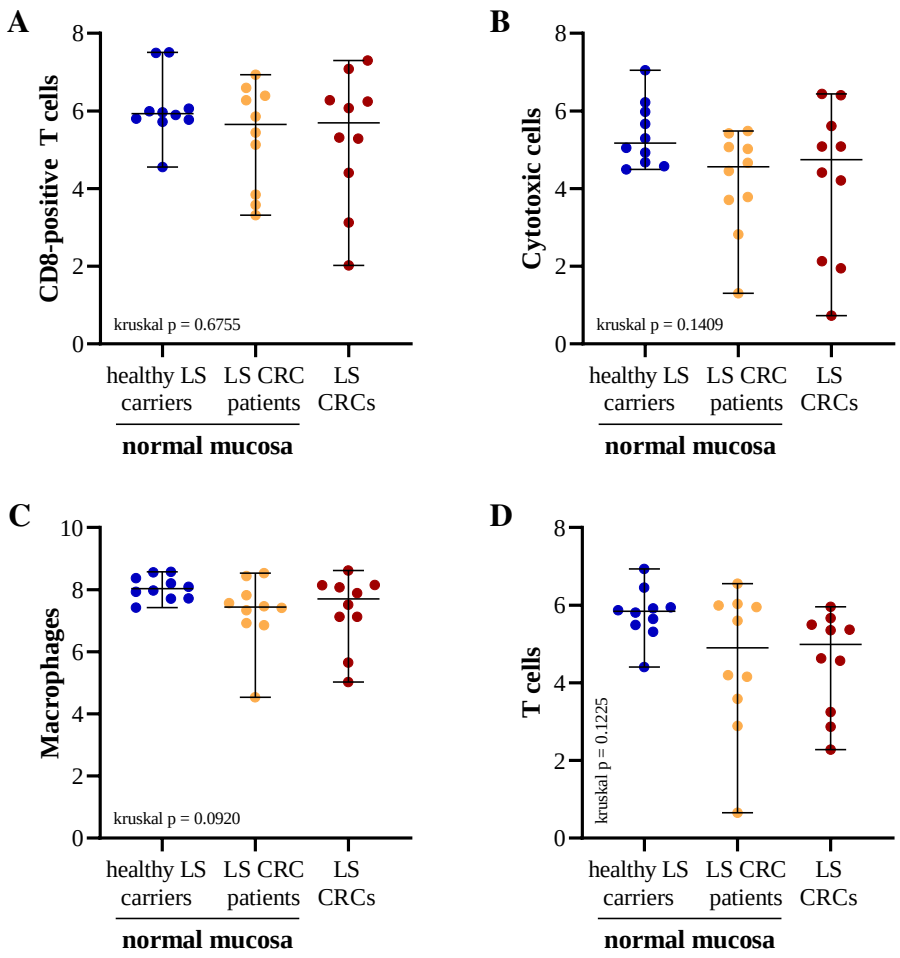

Figure S8: Abundance of immune cell populations which are not significantly changed between the normal mucosa of healthy LS carriers/LS CRC patients and LS CRC tissue. Beeswarm plots present the abundance, estimated by the absolute marker scores, of CD8-positive T cells (A), involved in the recognition of HLA class I-associated antigens; cytotoxic cells (B), including all cells capable of cytotoxic activity, such as T and NK cells; macrophages (C), involved in phagocytosis of abnormal cells and cellular debris; and T cells (D), mediating cell-based immunity by recognizing HLA class I or II antigens. No significant differences between the analyzed groups were observed. The calculated absolute immune cell marker scores for each population are depicted on a log2 scale and p-values for the omnibus Kruskal-Wallis test are indicated. Median and data range are depicted.

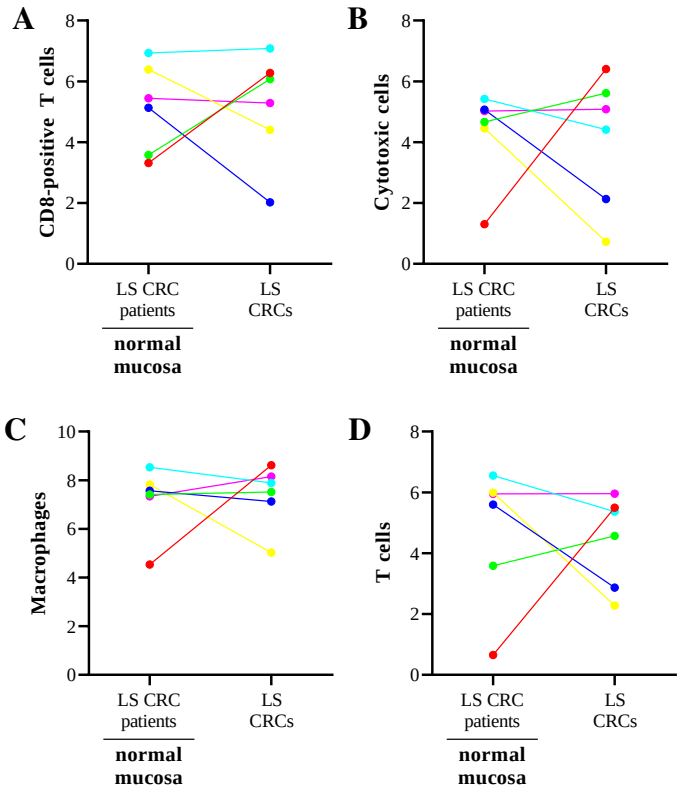

Figure S9: Pairwise comparison of the not significantly changed immune cell population abundance in matched normal mucosa and cancer tissue from LS CRC patients. Spaghetti plots (A-D) depict the estimated abundance of immune cell populations which were not significantly changed in matched tumor-distant, normal mucosa and cancer tissue samples from LS CRC patients (n = 6). Each pair is represented by one color. The log2-transformed y-axis represents the calculated absolute marker scores.

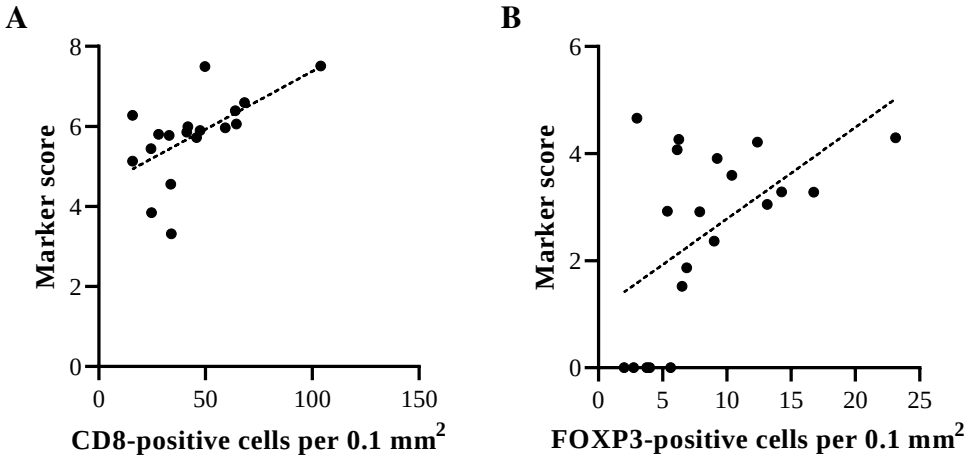

Figure S10: Concordance between T cell counts obtained by IHC and NanoString-based immune cell marker scores. T cells counts, obtained by IHC, and the NanoString-based absolute marker scores for the normal mucosa of healthy LS carriers and LS CRC patients were found to be significantly correlated for CD8- (A) and FOXP3-positive (B) T cells. Spearman correlation for CD8: r = 0.68, p = 0.002 and FOXP3: r = 0.50, p = 0.02. The calculated immune cell marker scores are depicted on a log2 scale. Adapted from: [318].

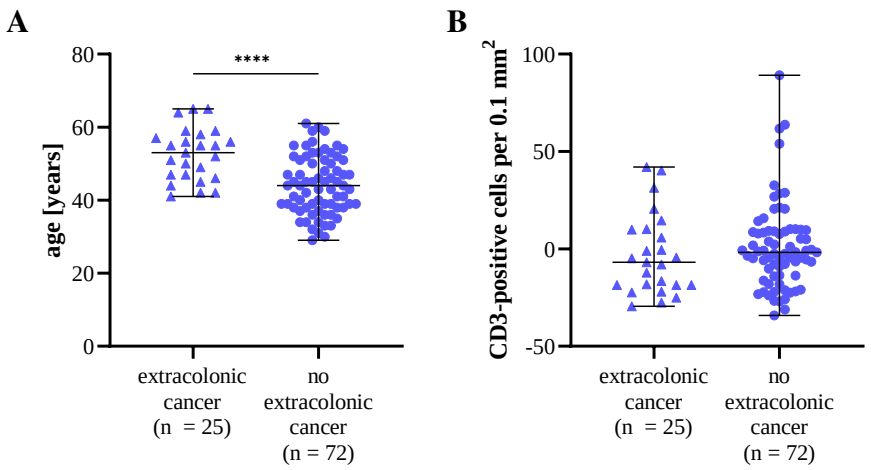

Figure S11: History of extracolonic cancer in CAPP2 participants. (A) Patients with a previous diagnosis of extracolonic cancer displayed a significantly higher age, compared to patients without a history of extracolonic cancer ($p < 0.0001$). Each data point indicates the age of one patient. (B) Age-normalized CD3-positive T cells counts for the normal rectal mucosa of healthy LS carriers did not significantly differ between individuals with and without history of extracolonic cancer ($p = 0.3184$). Each data point indicates the mean T cell count per patient. Median T cell densities and range are illustrated. Adapted from: [318]

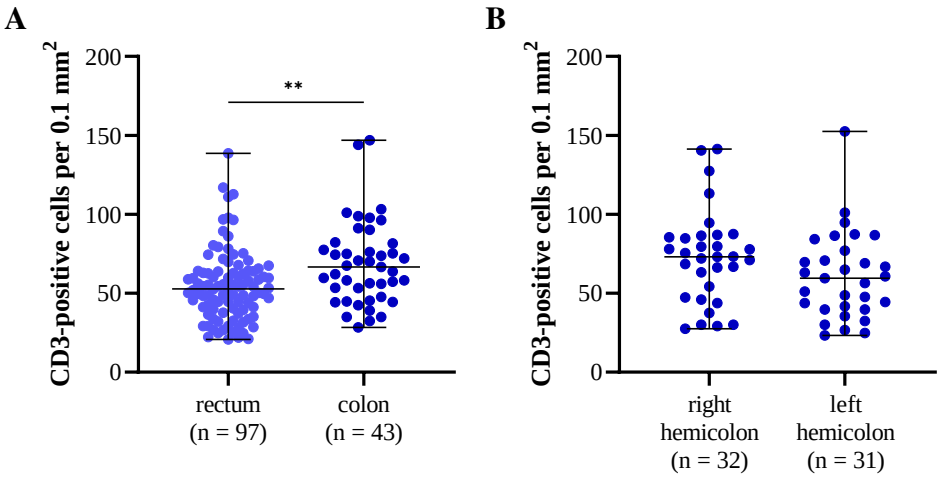

Figure S12: Anatomic localization and CD3-positive T cell infiltration in healthy LS carriers. (A) Significantly higher numbers of CD3-positive T cells were identified in the normal rectal mucosa of LS carriers enrolled in the CAPP2 clinical trial, compared to the colonic mucosa of healthy LS carriers (non-CAPP2) ($p = 0.0013$). (B) The density of CD3-positive T cells was not significantly different between the normal mucosa of the right and left hemicolon ($p = 0.0646$). Adapted from: [318]

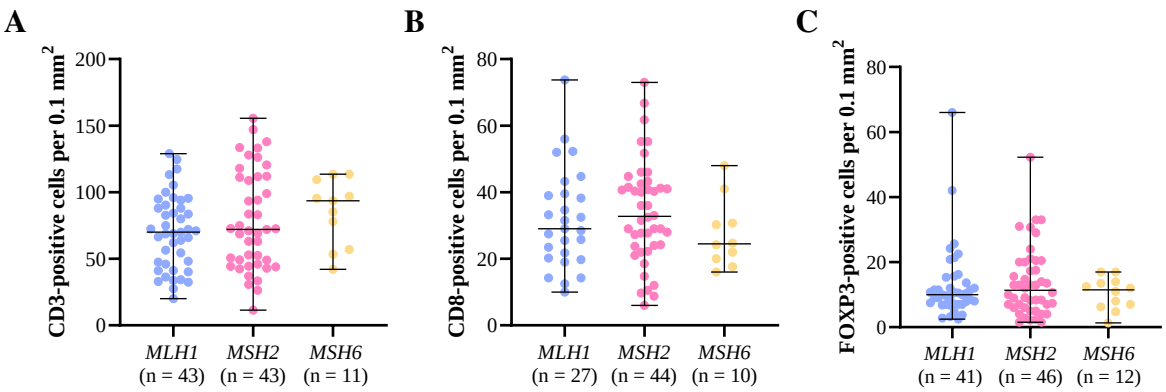

Figure S13: Stratification of T cell densities in LS adenomas according to the underlying MMR gene variant. The infiltration with CD3- (A), CD8- (B) and FOXP3-positive (C) T cells in LS-associated adenomas was not found to be significantly different between *MLH1*, *MSH2* and *MSH6* LS carriers (p = 0.2448/0.3767/0.8807). The median T cell density and data range are depicted.

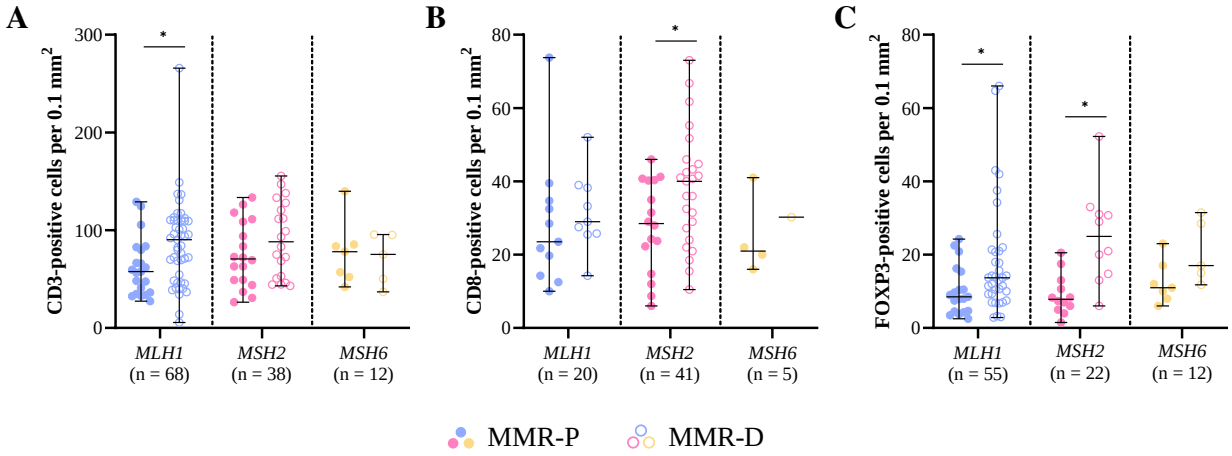

Figure S14: Stratification of T cell densities in MMR-P and MMR-D LS-associated adenomas according to the affected MMR gene. Densities of CD3- (A), CD8- (B) and FOXP3-positive (C) T cells in MMR-P and MMR-D adenomas of *MLH1*, *MSH2* and *MSH6* LS carriers. Regardless of the underlying MMR gene, MMR-D adenomas presented with higher T cell counts, compared to their MMR-P counterparts. Significantly higher CD3-positive T cell counts in MMR-D adenomas were observed for *MLH1* (p = 0.0105). CD8-positive T cells were significantly more prevalent in *MSH2* MMR-D adenomas (p = 0.0463). *MLH1* and *MSH2* MMR-D adenomas presented with significantly higher FOXP3-positive cell counts, compared to MMR-P adenomas (p = 0.0251/0.0014). Median T cell density and its range are depicted.

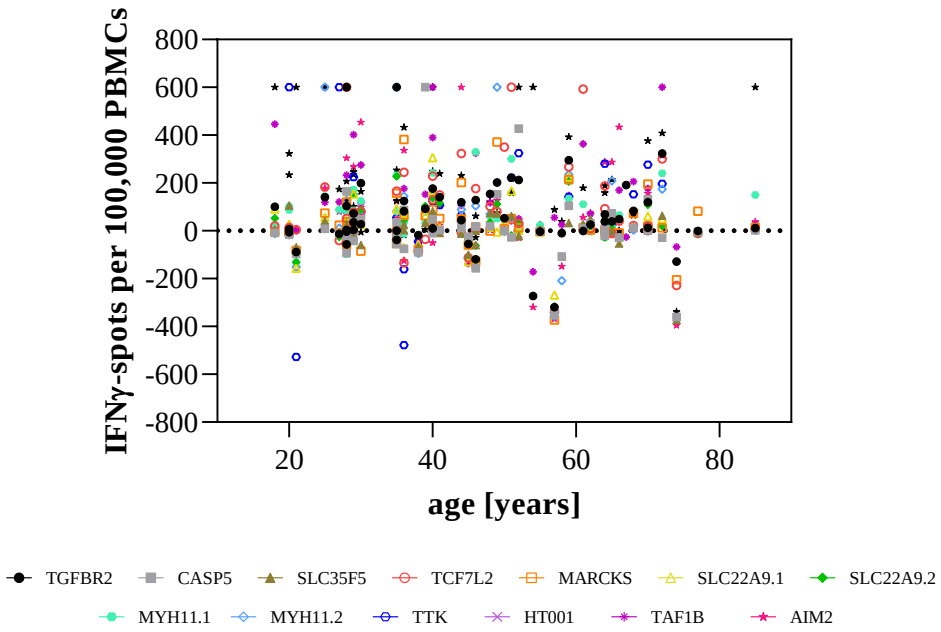

Figure S15: Correlation between age and systemic FSP-specific T cell responses. The correlation between the individual's age and IFNγ-spot counts for the different FSPs was found to be non-significant for all analyzed groups (healthy LS carriers, healthy controls, LS-associated/sporadic MSI and MSS cancer patients). TGFBR2: Spearman r = 0.061, p = 0.6584; CASP5: r = 0.0803, p = 0.5713; SLC35F5: r = 0.0262, p = 0.8585; TCF7L2: r = 0.087, p = 0.5440; MARCKS: r = 0.0652, p = 0.6527; SLC22A9.1: r = 0.0415, p = 0.7820; SLC22A9.2: r = 0.0048, p = 0.9737; MYH11.1: r = -0.0258, p = 0.8633; MYH11.2: r = 0.056, p = 0.6962; TTK: r = 0.1735, p = 0.3967; HT001: r = -0.0294, p = 0.8312; TAF1B: r = -0,1172, p = 0.3987; AIM2: r = -0.0477, p = 0.7318. Each data point represents the normalized spot count mean for one individual. Each FSP is depicted in a different color.

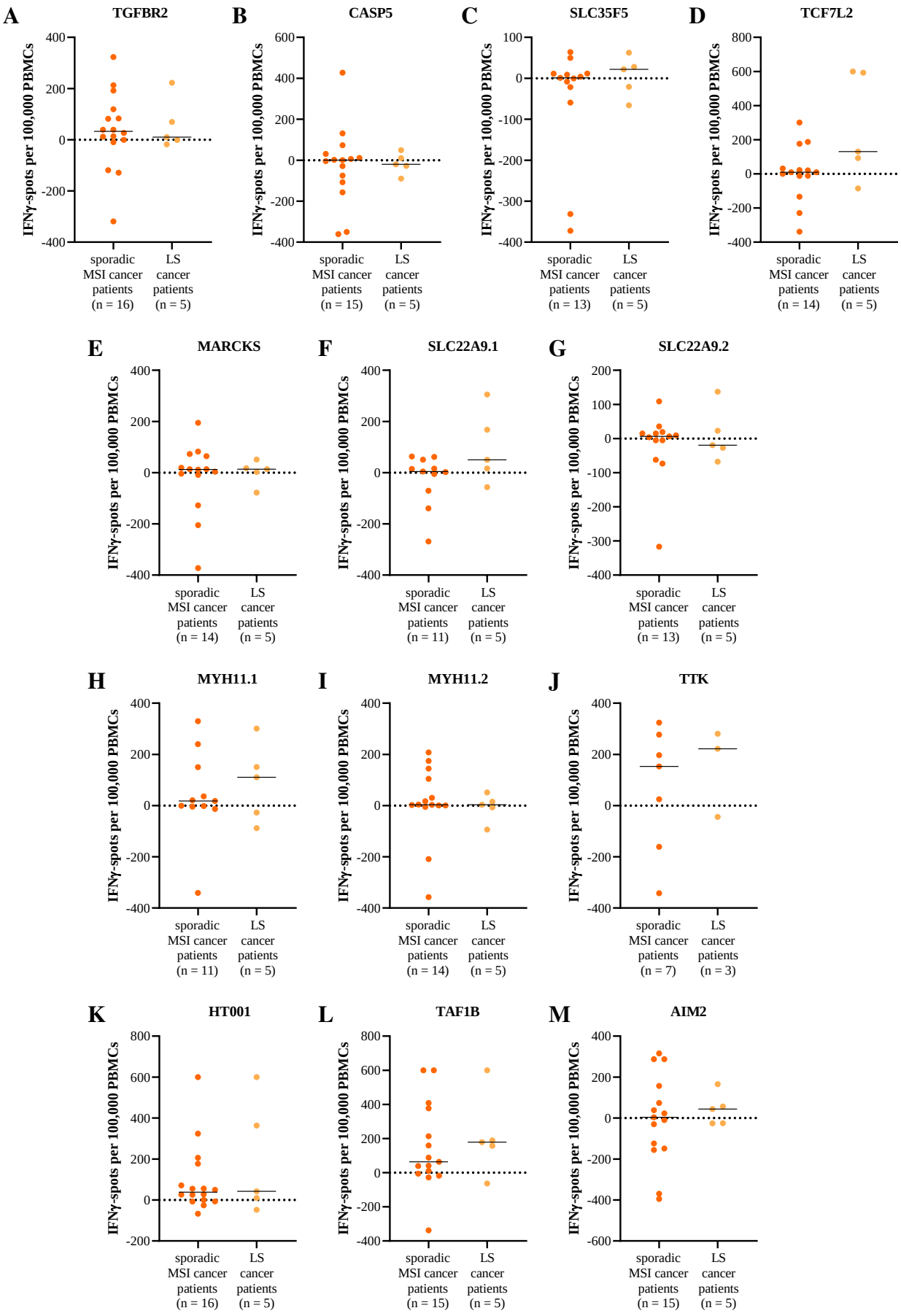
A
TGFBR2
B
CASP5
C
SLC35F5
D
TCF7L2
E
MARCKS
F
SLC22A9.1
G
SLC22A9.2
H
MYH11.1
I
MYH11.2
J
TTK
K
HT001
L
TAF1B
M
AIM2
IFNγ-spots per 100,000 PBMCs
sporadic MSI cancer patients (n = 16)
LS cancer patients (n = 5)
sporadic MSI cancer patients (n = 15)
LS cancer patients (n = 5)
sporadic MSI cancer patients (n = 13)
LS cancer patients (n = 5)
sporadic MSI cancer patients (n = 14)
LS cancer patients (n = 5)
sporadic MSI cancer patients (n = 14)
LS cancer patients (n = 5)
sporadic MSI cancer patients (n = 11)
LS cancer patients (n = 5)
sporadic MSI cancer patients (n = 13)
LS cancer patients (n = 5)
sporadic MSI cancer patients (n = 11)
LS cancer patients (n = 5)
sporadic MSI cancer patients (n = 14)
LS cancer patients (n = 5)
sporadic MSI cancer patients (n = 7)
LS cancer patients (n = 3)
sporadic MSI cancer patients (n = 16)
LS cancer patients (n = 5)
sporadic MSI cancer patients (n = 15)
LS cancer patients (n = 5)
sporadic MSI cancer patients (n = 15)
LS cancer patients (n = 5)

Figure S16: Systemic FSP-specific T cell responses in LS-associated and sporadic MSI cancer patients. The stratification of IFNγ-spot counts according to the hereditary or sporadic origin of the MSI cancer did not reveal significant differences for any FSP. TGFBR2 ($p = 0.7919$, A), CASP5 ($p > 0.9999$, B), SLC35F5 ($p = 0.5028$, C), TCF7L2 ($p = 0.1026$, D), MARCKS ($p = 0.9799$, E), SLC22A9.1 ($p = 0.1451$, F), SLC22A9.2 ($p = 0.9802$, G), MYH11.1 ($p = 0.9130$, H), MYH11.2 ($p = 0.6081$, I), TTK ($p = 0.6667$, J), HT001 ($p = 0.7309$, K), TAF1B ($p = 0.6110$, L) and AIM2 ($p = 0.6116$, M). Each data point represents the normalized spot count mean for one individual. The median is depicted.

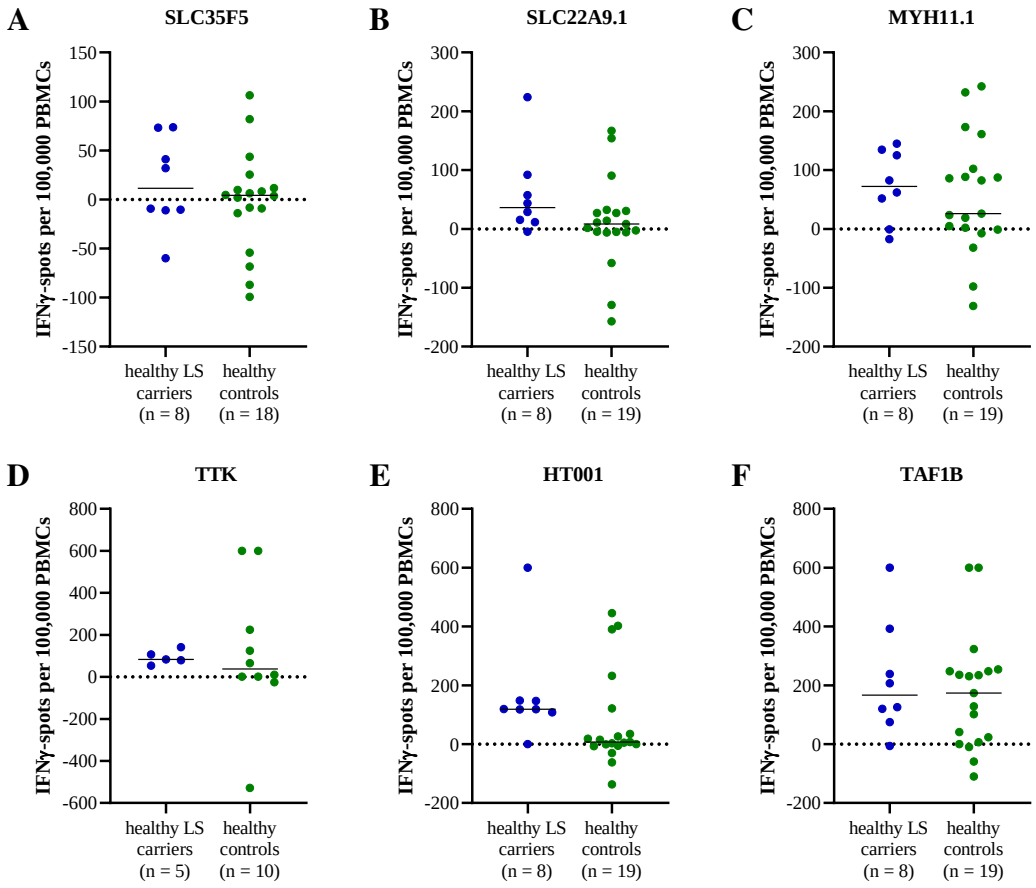

Figure S17: Not significantly different FSP-specific T cell responses in healthy LS carriers and healthy non-LS controls. The direct comparison revealed similar IFNγ-spot counts for healthy LS carriers and non-LS controls: SLC35F5 ($p = 0.6832$, A), TTK ($p = 0.5721$, D) and TAF1B ($p = 0.6962$, F). Elevated counts in healthy LS carriers, without reaching statistical significance, were observed for SLC22A9.1 ($p = 0.0602$, B), MYH11.1 ($p = 0.7049$, C) and HT001 ($p = 0.0662$, E). Each data point represents the normalized spot count mean for one individual. The median is depicted.

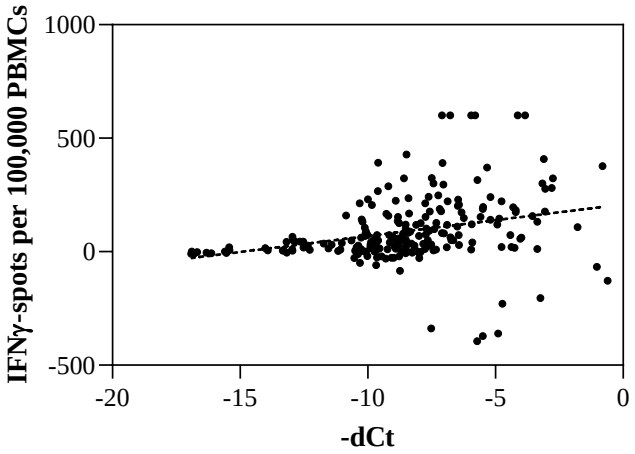

Figure S18: Significant correlation between IFNγ-spot counts and -dC$_t$ values. Spearman $r = 0.4375$, $p < 0.0001$. Each data point represents the analyzed FSP-specific T cell responses of one individual (healthy LS carriers, MSI cancer patients and healthy controls).

Example of the Flow cytometry-based assay:

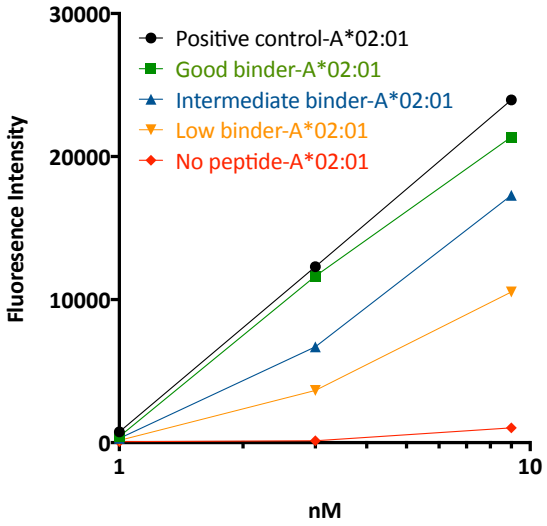

Figure S19: Example of the easYmer®complex formation assay provided by Immun-Aware. Determined binding stability of HLA-A*02:01 complexes and four different peptides (including the CMV peptide pp65) as well as a negative control (no peptide). The known HLA-A*02:01 epitope pp65 presents strong binding affinity to the easYmer®HLA complex. The three remaining peptides were categorized as good, intermediate and low binders.

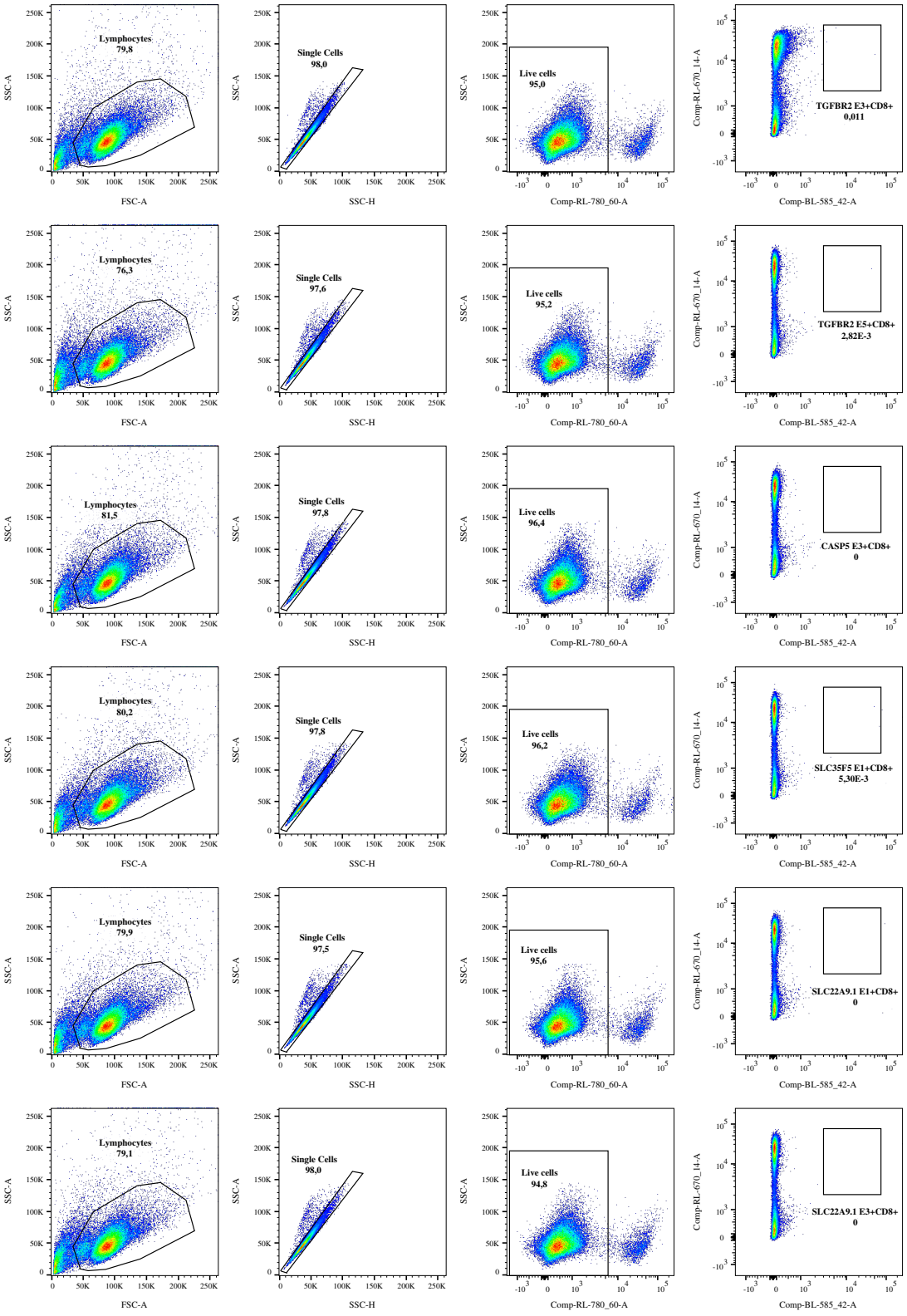

Figure S20: Representative tetramer staining example using expanded PBMCs from a HLA-A*02:01-positive MSI cancer patient. Expanded PBMCs of a MSI cancer patient were stained using an anti-CD8 antibody and the produced FSP-specific tetramers. No specific T cell populations were observed for: TGFBR2 E3/E5, CASP5 E3, SLC35F5 and SLC22A9.1 E1/E3. The percentage of the gated populations is shown next to the respective gate.

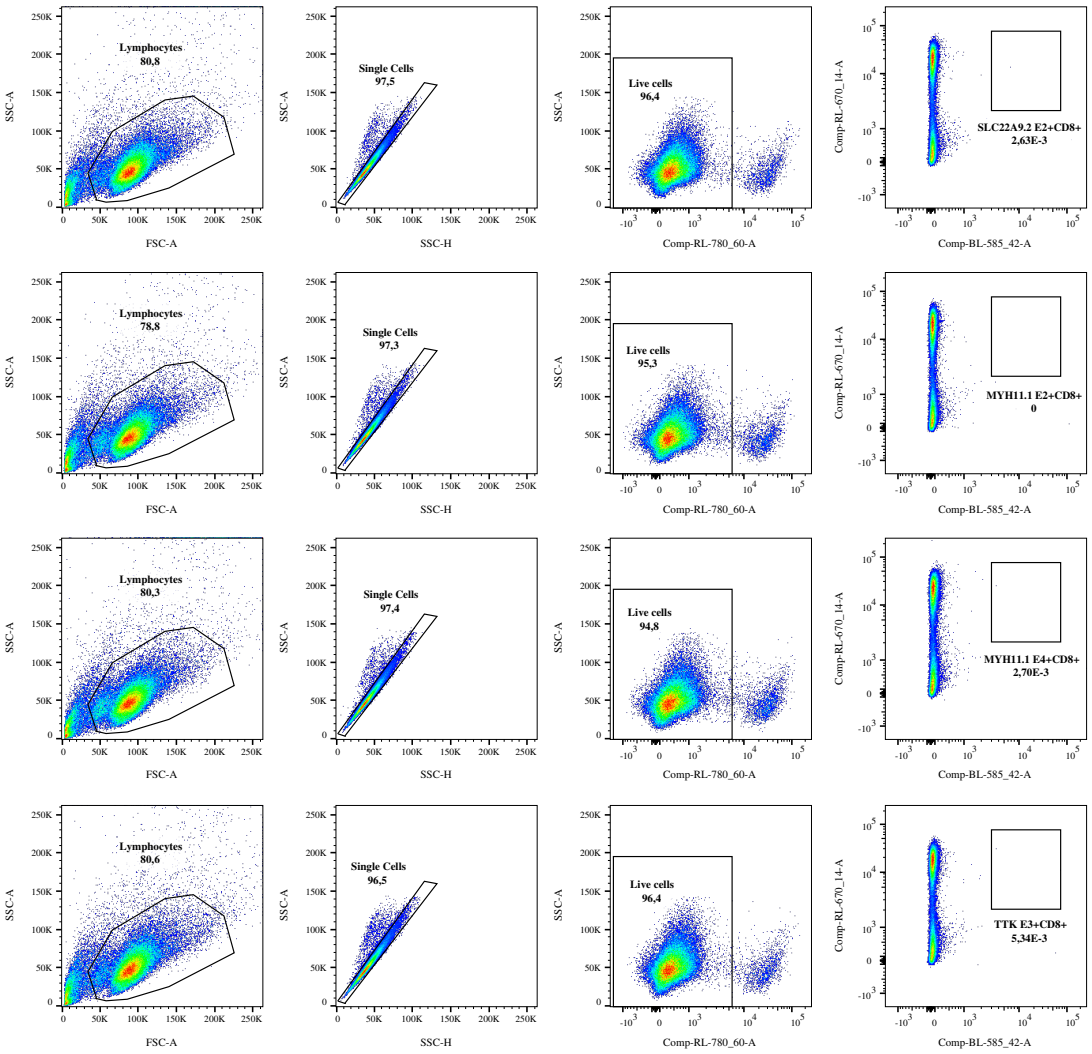

Figure S20: Representative tetramer staining example. Expanded PBMCs of a MSI cancer patient were stained using an anti-CD8 antibody and the produced FSP-specific tetramers. No specific T cell populations were observed for: SLC22A9.2 E2, MYH11.1 E2/E4 and TTK E3. The percentage of the gated populations is shown next to the respective gate.

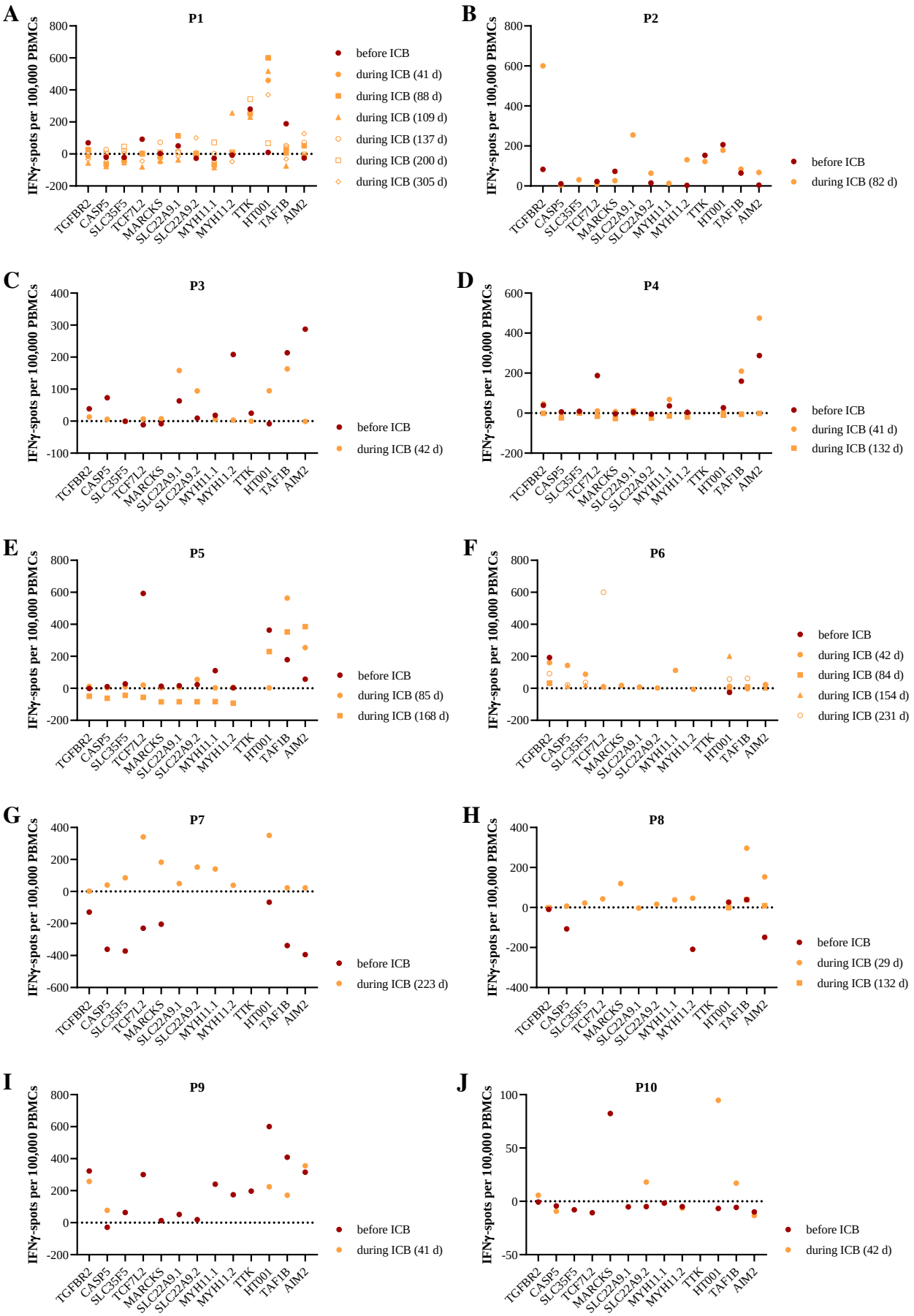
A
P1
IFNγ-spots per 100,000 PBMCs
800
600
400
200
0
-200
TGFBR2
CASP5
SLC35F5
TCF7L2
MARCKS
SLC22A9.1
SLC22A9.2
MYH11.1
MYH11.2
TTK
HT001
TAF1B
AIM2
before ICB
during ICB (41 d)
during ICB (88 d)
during ICB (109 d)
during ICB (137 d)
during ICB (200 d)
during ICB (305 d)
B
P2
IFNγ-spots per 100,000 PBMCs
800
600
400
200
0
TGFBR2
CASP5
SLC35F5
TCF7L2
MARCKS
SLC22A9.1
SLC22A9.2
MYH11.1
MYH11.2
TTK
HT001
TAF1B
AIM2
before ICB
during ICB (82 d)
C
P3
IFNγ-spots per 100,000 PBMCs
400
300
200
100
0
-100
TGFBR2
CASP5
SLC35F5
TCF7L2
MARCKS
SLC22A9.1
SLC22A9.2
MYH11.1
MYH11.2
TTK
HT001
TAF1B
AIM2
before ICB
during ICB (42 d)
D
P4
IFNγ-spots per 100,000 PBMCs
600
400
200
0
-200
TGFBR2
CASP5
SLC35F5
TCF7L2
MARCKS
SLC22A9.1
SLC22A9.2
MYH11.1
MYH11.2
TTK
HT001
TAF1B
AIM2
before ICB
during ICB (41 d)
during ICB (132 d)
E
P5
IFNγ-spots per 100,000 PBMCs
800
600
400
200
0
-200
TGFBR2
CASP5
SLC35F5
TCF7L2
MARCKS
SLC22A9.1
SLC22A9.2
MYH11.1
MYH11.2
TTK
HT001
TAF1B
AIM2
before ICB
during ICB (85 d)
during ICB (168 d)
F
P6
IFNγ-spots per 100,000 PBMCs
800
600
400
200
0
-200
TGFBR2
CASP5
SLC35F5
TCF7L2
MARCKS
SLC22A9.1
SLC22A9.2
MYH11.1
MYH11.2
TTK
HT001
TAF1B
AIM2
before ICB
during ICB (42 d)
during ICB (84 d)
during ICB (154 d)
during ICB (231 d)
G
P7
IFNγ-spots per 100,000 PBMCs
400
200
0
-200
-400
-600
TGFBR2
CASP5
SLC35F5
TCF7L2
MARCKS
SLC22A9.1
SLC22A9.2
MYH11.1
MYH11.2
TTK
HT001
TAF1B
AIM2
before ICB
during ICB (223 d)
H
P8
IFNγ-spots per 100,000 PBMCs
400
200
0
-200
-400
TGFBR2
CASP5
SLC35F5
TCF7L2
MARCKS
SLC22A9.1
SLC22A9.2
MYH11.1
MYH11.2
TTK
HT001
TAF1B
AIM2
before ICB
during ICB (29 d)
during ICB (132 d)
I
P9
IFNγ-spots per 100,000 PBMCs
800
600
400
200
0
-200
TGFBR2
CASP5
SLC35F5
TCF7L2
MARCKS
SLC22A9.1
SLC22A9.2
MYH11.1
MYH11.2
TTK
HT001
TAF1B
AIM2
before ICB
during ICB (41 d)
J
P10
IFNγ-spots per 100,000 PBMCs
100
50
0
-50
TGFBR2
CASP5
SLC35F5
TCF7L2
MARCKS
SLC22A9.1
SLC22A9.2
MYH11.1
MYH11.2
TTK
HT001
TAF1B
AIM2
before ICB
during ICB (42 d)

Figure S21: Individual quantification of systemic FSP-specific T cell responses in MSI cancer patients before and during ICB therapy. Specific T cell responses against 13 FSPs were assessed in ten MSI cancer patients (P1-P10) and at different time points before and during ICB therapy by using IFNγ ELISpot assay. An increase in IFNγ-spot counts in several patients after therapy start might indicate a reactivation of FSP-specific T cells upon ICB treatment. Each data point represents the mean normalized spot count for the respective FSP in one individual at the indicated time point.

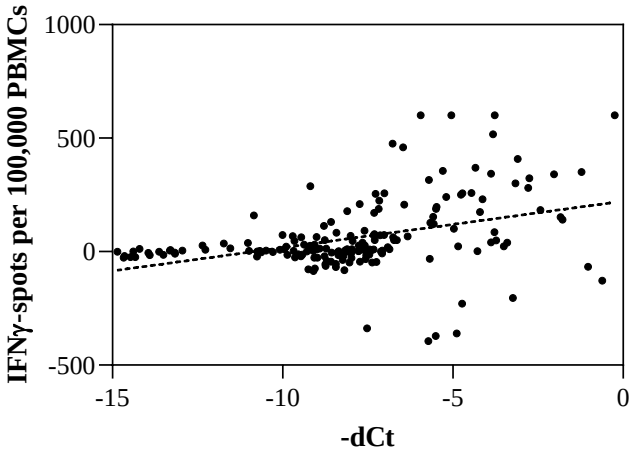

Figure S22: Significant correlation between IFNγ-spot counts and -dC$_t$ values for the analyzed ICB patient cohort. Spearman $r = 0.4375$, $p < 0.0001$. Each data point represents the analyzed FSP-specific T cell responses of one individual.

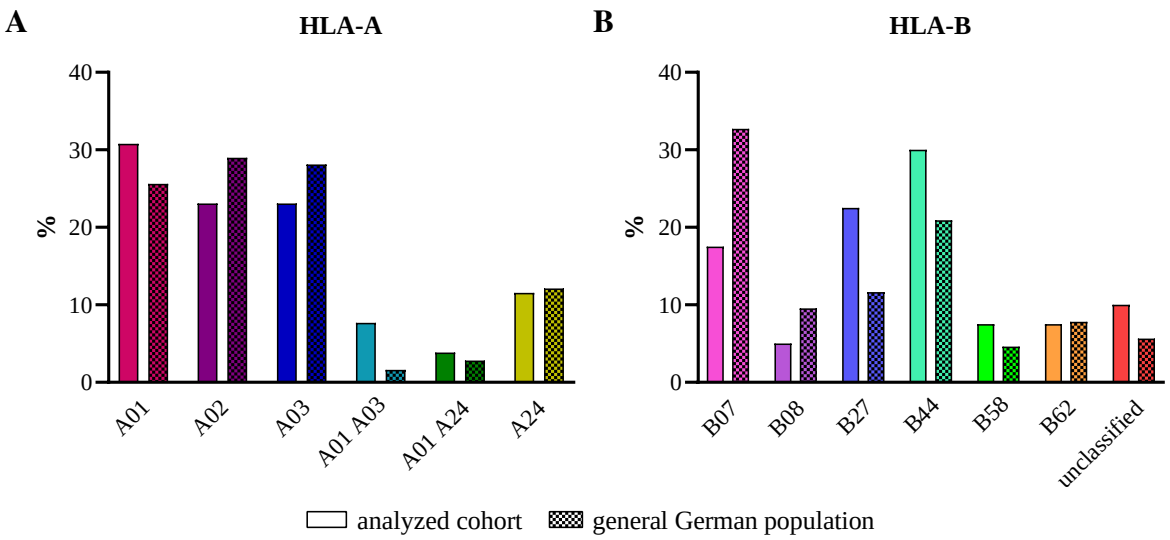

Figure S23: Distribution of HLA class I supertypes in the analyzed cohort comprising healthy LS carriers and MSI cancer patients. (A) The most frequently observed HLA-A supertype was A01. (B) B44 was identified as the most common HLA-B supertype among all analyzed HLA-B alleles. The frequency of the respective HLA-A and -B supertype in the general German population is provided. The classification of HLA class I supertypes by Sidney et al. [312] was applied and the respective percentage of each supertype is indicated on the y-axis.

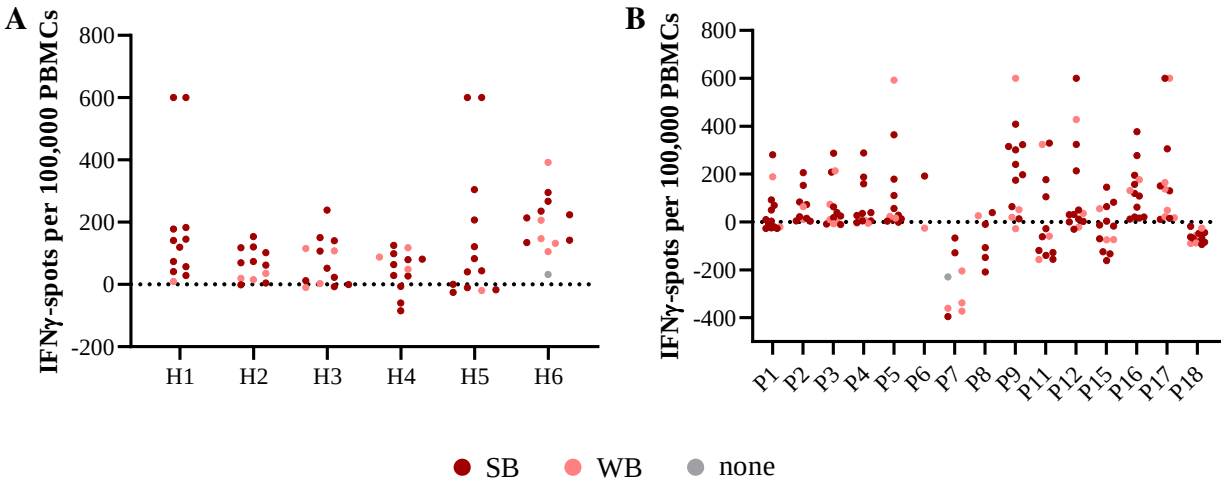

Figure S24: Correlation of FSP-specific T cell responses and epitope binding predictions. The predicted binding (SB, WB, none) of FSP epitopes for an individual's HLA type and the corresponding number of IFNγ-spots were aligned for healthy LS carriers (A) and MSI cancer patients (B). All included individuals presented with predicted binding FSP epitopes. Each data point represents the normalized IFNγ-spot count for one FSP of the given individual (H1-H6; P1-P9, P11-P12, P15-P18). The corresponding epitope binding prediction is indicated by color.

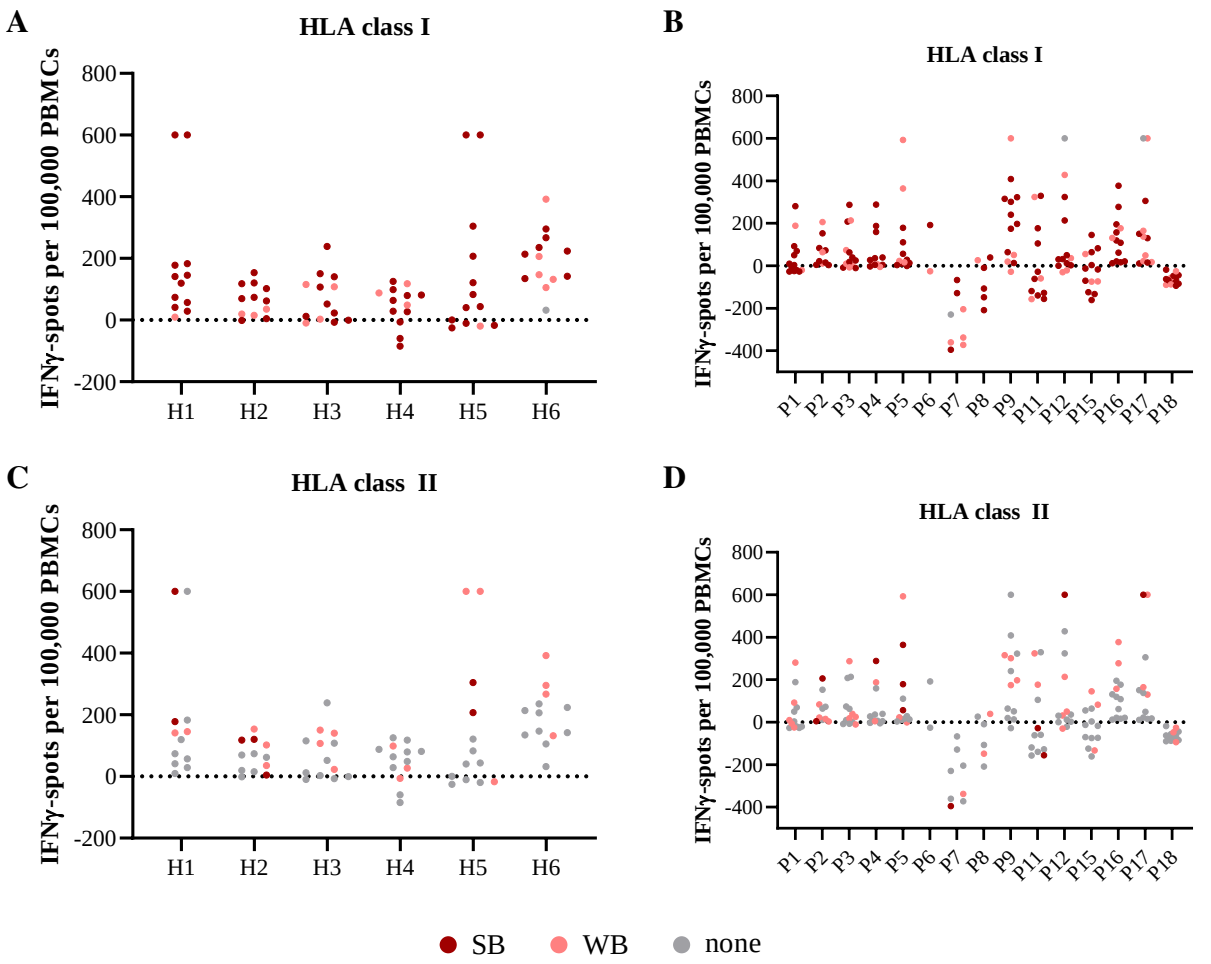

Figure S25: Correlation of FSP-specific T cell responses and epitope binding predictions for HLA class I and II. The predicted binding of FSP epitopes to a given HLA type was assessed separately for HLA class I (covering HLA-A and -B) (A, B) and HLA class II (HLA-DR) (C, D). The predicted binding (SB, WB, none) of FSP epitopes for an individual's HLA type and the corresponding number of IFNγ-spots were aligned for healthy LS carriers (A, C) and MSI cancer patients (B, D). Each data point represents the normalized IFNγ-spot count for one FSP and the given individual. The corresponding epitope binding prediction is indicated by color.

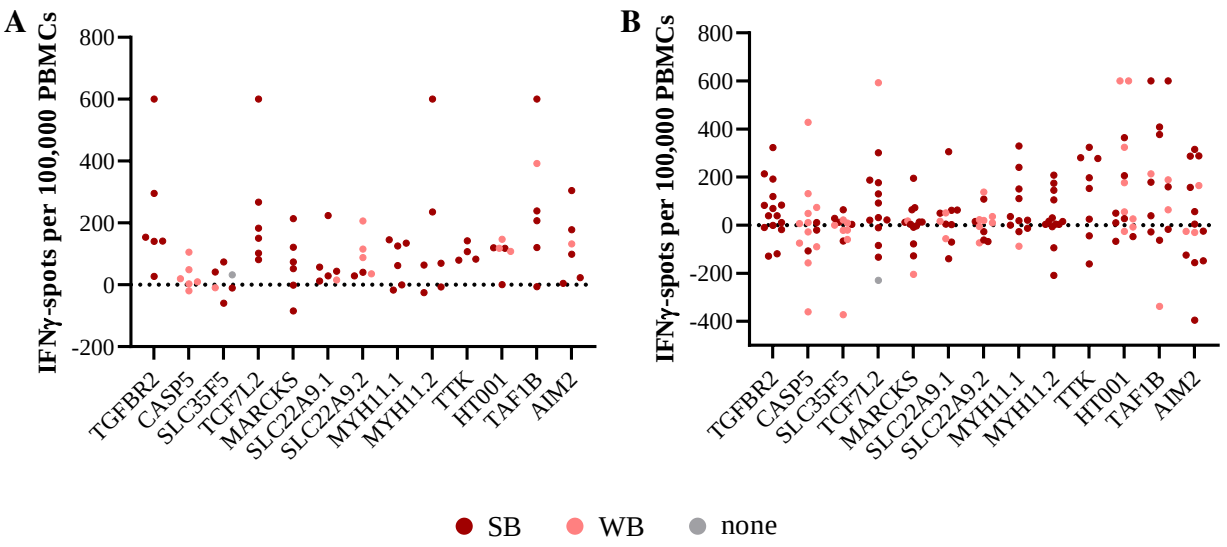

Figure S26: Peptide-wise correlation of FSP-specific T cell responses and epitope binding predictions. The number of IFNγ-spots and the predicted epitope binding (SB, WB and none) for the respective HLA type were aligned individually for each FSP. The correlation analysis was conducted for healthy LS carriers (A) and MSI cancer patients (B). Each FSP harbored multiple predicted WB and SB epitopes for the included HLA types. Each data point represents the normalized number of IFNγ-spots for one individual and the given FSP. The result of the corresponding epitope binding prediction is indicated by color.

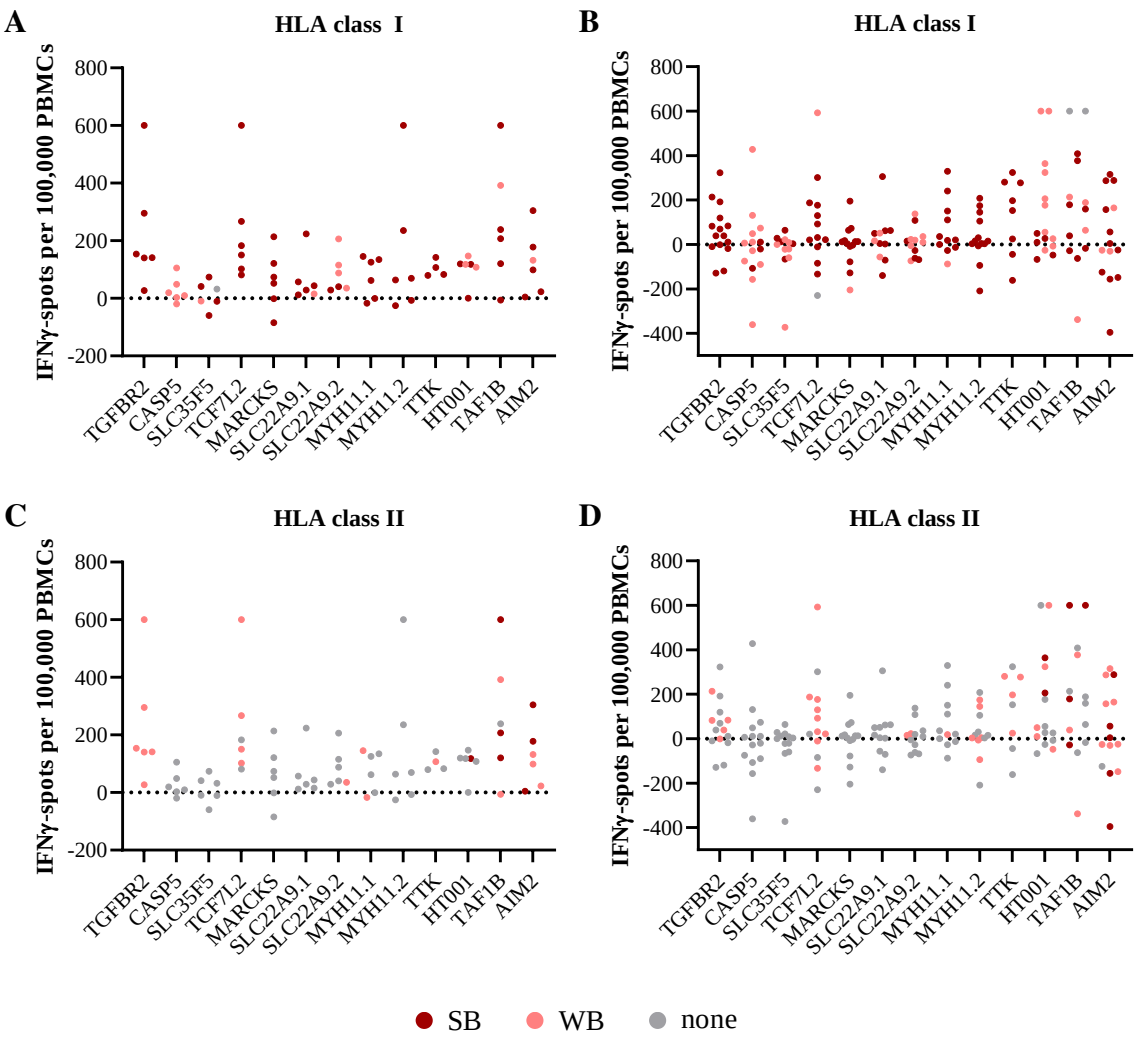

Figure S27: Peptide-wise correlation of FSP-specific T cell responses and HLA class I and II epitope binding predictions. Binding predictions for FSP epitopes were made separately for HLA class I (HLA-A and -B) (A, B) and II (HLA-DR) (C, D). The number of IFNγ-spots and the predicted epitope binding (SB, WB and none) for the respective HLA type were aligned individually for each FSP in two groups: healthy LS carriers (A, C) and MSI cancer patients (B, D). Each data point represents the normalized number of IFNγ-spots for one individual and the indicated FSP. The result of the corresponding epitope binding prediction is indicated by color.

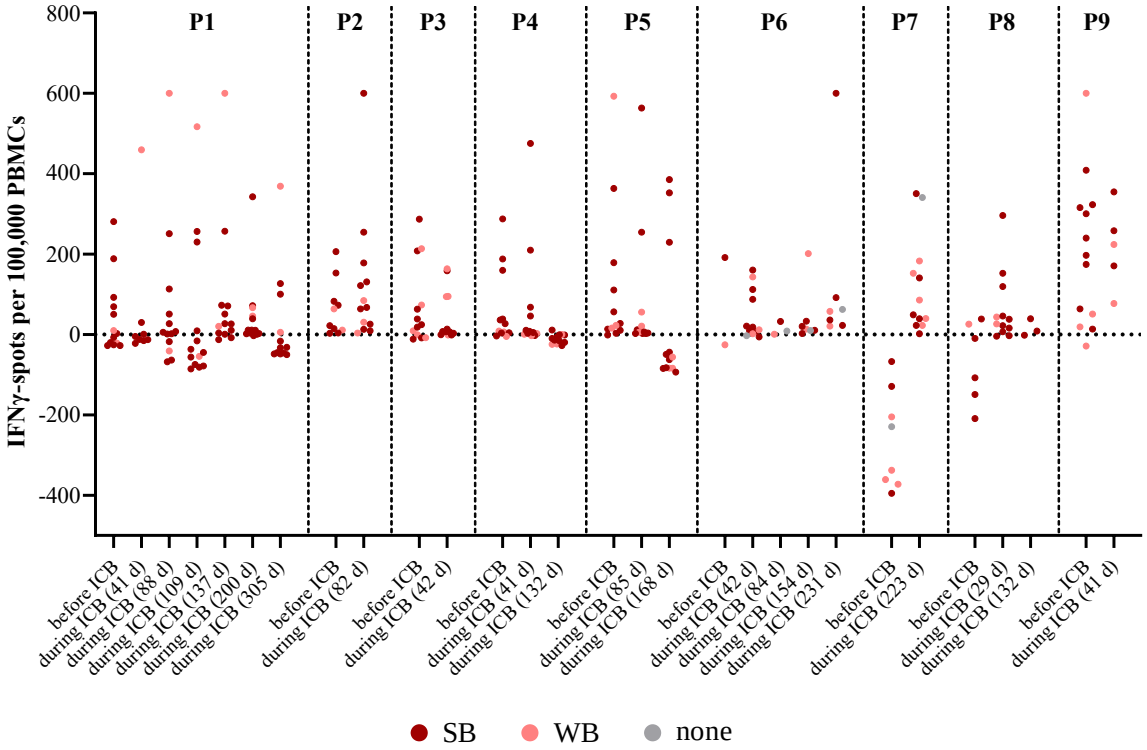

Figure S28: Correlation of FSP-specific T cell responses before and during ICB therapy and corresponding epitope binding predictions. FSP-specific T cell responses were quantified before starting ICB therapy and at several time points during the course of treatment. An increase in FSP-specific T cell responses, potentially due to ICB, was predominantly observed for FSPs comprising predicted SB and WB epitopes. Each data point represents the normalized IFNγ-spot count for one FSP, the given individual and the indicated time point. The corresponding epitope binding prediction is illustrated by color.

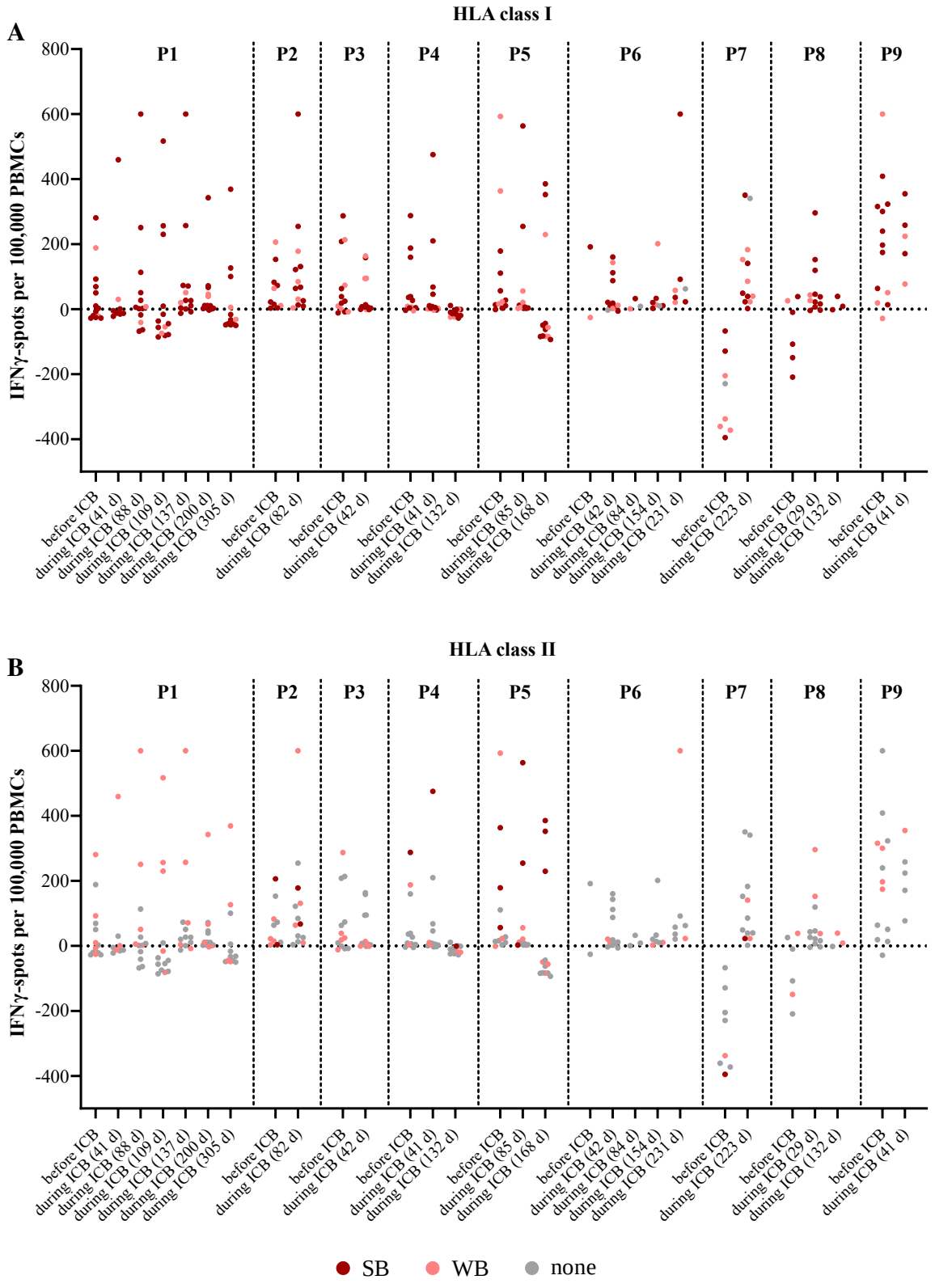

Figure S29: Correlation of FSP-specific T cell responses before and during ICB therapy and corresponding HLA class I and II epitope binding predictions. Epitope binding was predicted for HLA class I (A) and II (B) molecules and combined with the obtained FSP-associated IFNγ-spot counts at different time points before and during ICB therapy. Each data point represents the normalized IFNγ-spot count for one FSP, the given individual and the indicated time point. The corresponding epitope binding prediction is indicated by color.

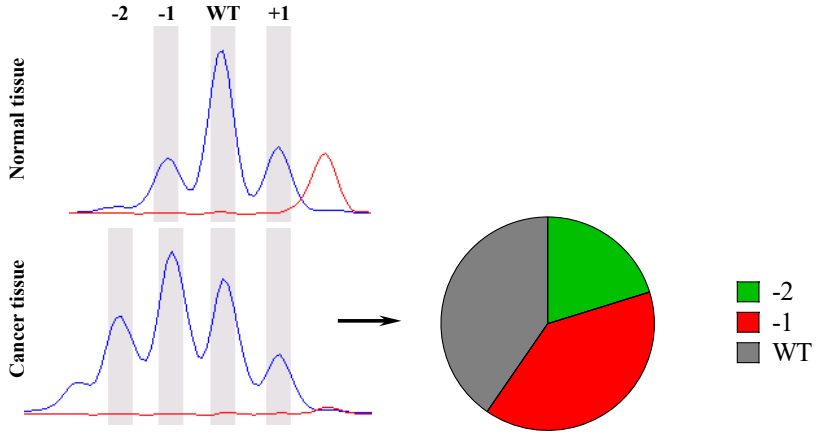

Figure S30: Example of a cMS mutation in MSI cancer. Peak profiles of the *TGFBR2* A10 microsatellite in normal colonic tissue and MSI cancer tissue displaying -1 and -2 mutations. The quantification of the respective indel mutations was carried out by the ReFrame algorithm [79] and the obtained allele ratios are displayed in the pie chart.

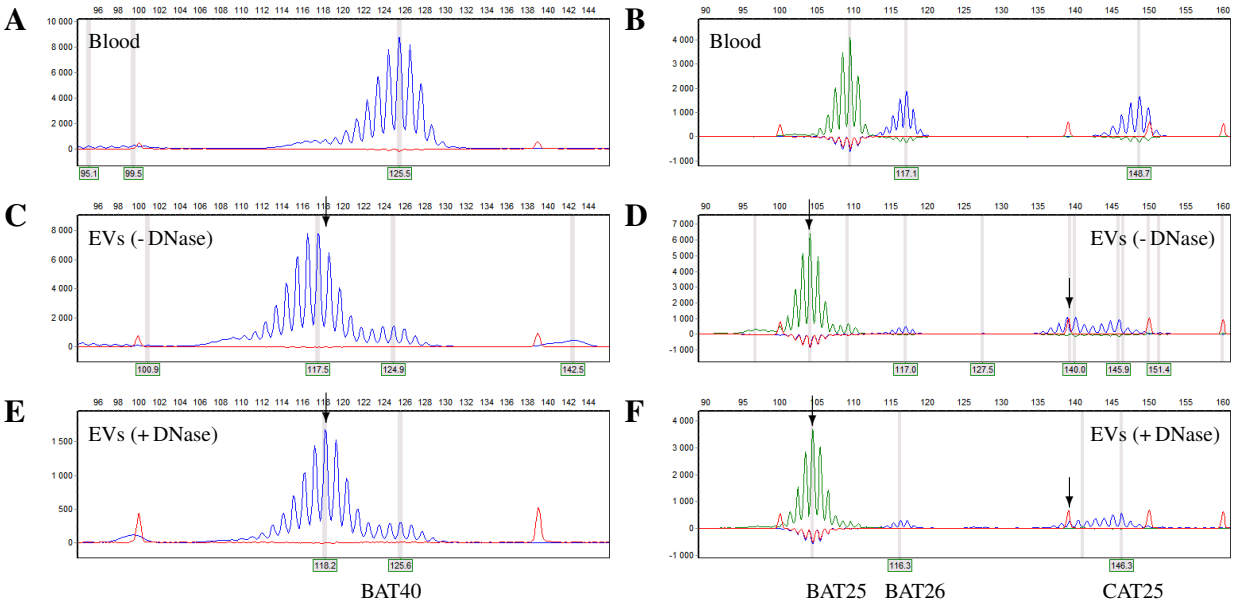

Figure S31: MSI fragment analysis of intravesicular DNA after DNase I digestion of external DNA. EVs from a MSI cancer patient, with known vesicular MSI phenotype, were isolated from 1 ml of plasma using PEG-based precipitation. Isolated EVs were treated with DNase I to remove all external, surface-bound DNA. Intravesicular DNA from digested vesicles still presented the shifted allelic pattern in four MSI markers as observed in untreated EVs. DNA from whole blood, displaying MSS, was used as normal tissue control. The amplicon length in bp is indicated on the top of each figure and the fluorescent signal intensity is provided on the left. The different MSI markers are labeled accordingly.

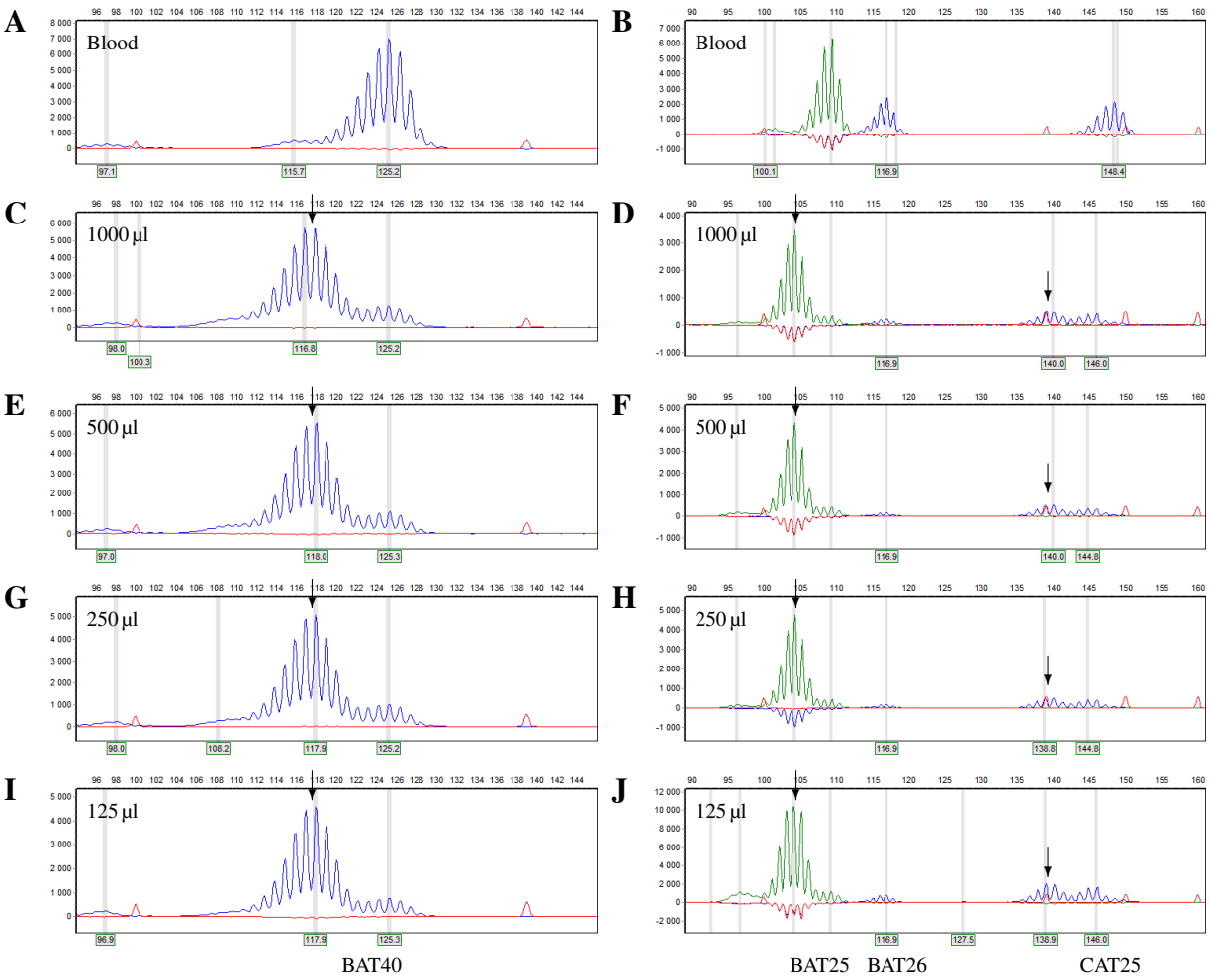

Figure S32: Detection of the MSI phenotype in vesicular DNA using different volumes of plasma. The detectability of the MSI phenotype in plasma-derived EV DNA was tested using four different volumes. Plasma from a MSI cancer patient with known vesicular MSI status was used. Allelic shifts could be observed for all applied volumes down to 125 µl of plasma. DNA from whole blood, displaying MSS, was used as normal tissue control. The amplicon length in bp is indicated on the top of each figure and the fluorescent signal intensity is provided on the left. The different MSI markers are labeled accordingly.

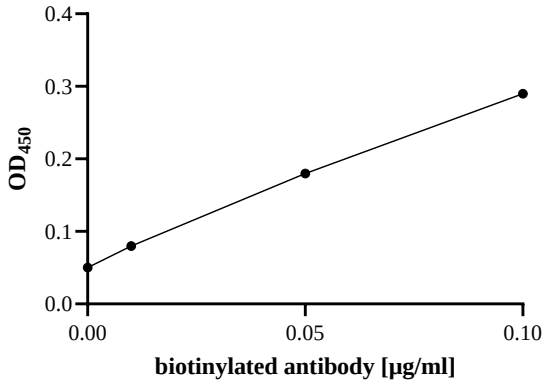

Figure S33: Biotinylation check of the anti-A33 antibody. Three different concentrations of the produced biotinylated antibody were captured in an ELISA plate. The presence of biotin was checked by applying ExtrAvidin®-peroxidase and a chromogenic substrate. The linear increase in OD with increasing concentration of biotinylated antibody confirmed successful biotinylation.

Table S1: Summary of the immune infiltration data identified through the systematic literature search. Included studies all comprised a direct comparison between LS-associated and sporadic MSI tumors. For each study, sample number, LS status, used IHC marker and obtained numbers/results are given. Further, the analyzed tissue area and the applied counting method are specified. Asterisks indicate a statistically significant difference between the hereditary and sporadic group. Modified from: [304].

		sample number		**LS status**			**staining quantification**			
		hereditary	sporadic	proven	suspected	**marker (clone)**	hereditary	sporadic	**analyzed area**	**counting method**
MSI CRC	[113]	n = 18	n = 38	x		CD3 (PS1) PD-1 (NAT105)	143.1* 31*	92.5 2.7	tumor epithelial	median of positive cells per 0.25 mm^2
	[211]	n = 20	n = 26	x	x	CD8 (n.a.)	18.6	23.9	tumor epithelial	mean of positive cells in 10 hpf (400 x magnification)
	[209]	n = 30	n = 35		x	CD3 (n.a.)	65*	19	tumor epithelial	median of positive cells in 10 hpf (= 1.96 mm^2)
	[118]	n = 35	n = 34	n.a.		CD4 (IF6)	53.4	68.9	tumor epithelial	median of positive cells per 0.25 mm^2
						CD4 (IF6)	119.4	141.2	stromal	
	[210]	n = 19	n = 12		x	CD3 (X100) CD4 (X20) CD8 (X20)	165.4 91.2 51.5	153.2 84.7 47.6	stromal	mean/median of positive cells per 250 μm^2
						CD3 (X100) CD4 (X20) CD8 (X20)	no exact counts		tumor epithelial	categories
	[328]	n = 16	n = 79	x		CD3 (n.a.) CD8 (n.a.) FOXP3 (n.a.)	no exact counts		stromal/tumor epithelial	percentages

		sample number		LS status			staining quantification			
		hereditary	sporadic	proven	suspected	**marker (clone)**	hereditary	sporadic	**analyzed area**	**counting method**
MSI CRC	[329]	n = 20	n = 20	x		HE	no exact counts		n.a.	TILs cut-off values and categories
	[327]	n = 79	n = 45	x	x	HE	no exact counts		tumor epithelial	percentages
	[333]	n = 48	n = 94	x		PD-L1 (E1L3N)	no exact counts		tumor center/ invasive front	categories
	[332]	n = 54	n = 132		x	PD-L1 (E1L3N)	no exact counts		tumor center and periphery	categories
	[331]	n = 20	n = 28	n.a.		MECA-79 (SC-19602)	0.094*	0.025	intra- and peritumoral	MECA-79-positive HEV/mm^2
		hereditary	sporadic				hereditary	sporadic		
colorectal adenomas	[211]	n = 50	n = 69	x		CD8 (n.a.)	6.6*	3.9	epithelial	mean of positive cells in 10 hpf (400 x magnification)
	[182]	n = 32	n = 19	x		CD2 (AB75)	no exact counts		epithelial	categories

		sample number		LS status			staining quantification			
		hereditary	sporadic	proven	suspected	marker (clone)	hereditary	sporadic	analyzed area	counting method
MSI EC	[325]	n = 20	n = 38		x	CD3 (SP7)	84.3	84.6	stromal	median of positive cells per 1 mm^2
						CD4 (4B12)	16.3	22.1		
						CD8 (4B11)	82.8*	34.2		
						PD-L1 (E1L3N)	289.3	297.9		
						CD3 (SP7)	18.7	30	tumor epithelial	
						CD4 (4B12)	2.8	8.6		
						CD8 (4B11)	8.2	4.2		
						PD-L1 (E1L3N)	4.8	8.2		
	[326]	n = 25	n = 33	x		CD3 (F7.2.38)	590	617	tumor center	mean of positive cells per 200 μm^2
						CD8 (C8/144B)	291	233		
						CD45RO (UCLH1)	597	653		
						FOXP3 (236A/E7)	72	58		
						PD-1 (NAT105)	156*	108		
						CD3 (F7.2.38)	386	241	invasive margin	
						CD8 (C8/144B)	287*	116		
						CD45RO (UCLH1)	548*	296		
						FOXP3 (236A/E7)	61	28		
						PD-1 (NAT105)	118*	49		

Table S2: Summary of all identified studies analyzing HLA class I and II immune evasion mechanisms in MSI CRCs and colorectal adenomas. For all publications sample number, LS status and mutation frequency of the respective gene are provided. The association between the *B2M* mutation status and the origin of MSI CRCs was calculated by using a Fisher's exact test ($\alpha = 0.05$) and the 95 % CI is provided. Modified from: [304].

HLA I - B2M mutations					
				LS status	
	hereditary MSI CRC	sporadic MSI CRC	colorectal MSI adenomas	proven	suspected
[335]	17.1 % (7/41)	29 % (20/69)	0 % (0/42)	x	x
[334]	20 % (15/75)	3 % (1/33)		x	
[113]	50 % (9/18)	26.3 % (10/38)		x	
[111]	36.4 % (16/44)	15.4 % (4/26)	15.8 % (6/38)	x	
Total	35.9 % (47/131)	26.7 % (35/131)	7.5 % (6/80)		
95 % CI	0.2816 to 0.4440	0.1985 to 0.3491			
p-value	0.1425				

HLA II - *CIITA* and *RFX5* mutations						
	CIITA		***RFX5***		**LS status**	
	hereditary MSI CRC	sporadic MSI CRC	hereditary MSI CRC	sporadic MSI CRC	proven	suspected
[118]	8.9 % (3/35)	0 % (0/34)	14.3 % (5/35)	26.5 % (9/34)	n.a.	

Table S3: Clinical information on the different normal mucosa groups.

		healthy LS carriers	LS CRC patients	sporadic MSI CRC patients	MSS CRC patients
	total	n = 48	n = 34	n = 30	n = 29
age	age range [years]	22–78	25–86	48–91	33–81
	median age [years]	43	51.5	72.5	55
sex	male	n = 22	n = 20	n = 7	n = 18
	female	n = 26	n = 14	n = 23	n = 11
MMR gene	*MLH1*	n = 20	n = 15		
	MSH2	n = 22	n = 16		
	MSH6	n = 6	n = 2		
	PMS2	n = 0	n = 1		

Table S4: Clinical parameters of LS CRC patients included in the analysis of local T cell infiltration.

	total	n = 26
age	age range [years]	30–81
	median age [years]	50
sex	male	n = 17
	female	n = 9
MMR gene	*MLH1*	n = 21
	MSH2	n = 5
	MSH6	n = 0
	PMS2	n = 0

Table S5: Correlation between principle components and covariates. No statistically significant correlation was identified between PC1/PC2 and any covariant. P-values for sex, age and the affected MMR gene are given.

	sex	**age**	**MMR gene**
	gene expression		
PC1	0.0947	0.6185	0.0578
PC2	0.1047	0.2528	0.2082
	absolute markers		
PC1	0.1531	0.6504	0.0701
PC2	0.1397	0.2383	0.2082

Table S6: Clinical characteristics of CAPP2 participants included in the analysis of local T cell infiltration.

sex (0 = male)	**age at trial entry [years]**	**randomization (0 = placebo)**	**follow-up [years]**	**advanced neoplasia (0 = no)**	**time to advanced neoplasia [months]**
1	41	1	10	0	n.a.
1	33	1	10	0	n.a.
1	53	1	10	0	n.a.
1	42	1	7	0	n.a.
1	59	1	6	0	n.a.
1	51	1	4	0	n.a.
1	38	1	7	0	n.a.
1	58	1	10	0	n.a.
0	45	0	4	0	n.a.
1	45	1	4	0	n.a.
1	38	0	5	0	n.a.
0	36	0	3	0	n.a.
1	55	0	3	0	n.a.
1	50	1	10	0	n.a.
1	48	1	10	0	n.a.
0	29	1	3	0	n.a.
0	34	1	10	0	n.a.
0	54	1	9	0	n.a.
1	50	1	10	0	n.a.

sex (0 = male)	age at trial entry [years]	randomization (0 = placebo)	follow-up [years]	advanced neoplasia (0 = no)	time to advanced neoplasia [months]
0	53	1	10	0	n.a.
0	51	0	10	0	n.a.
0	40	0	10	0	n.a.
1	57	1	3	0	n.a.
1	64	0	3	0	n.a.
1	55	1	3	0	n.a.
0	55	1	3	0	n.a.
1	55	0	4	0	n.a.
1	56	0	8	0	n.a.
1	47	1	10	0	n.a.
1	52	1	8	0	n.a.
1	44	0	10	0	n.a.
1	39	1	7	0	n.a.
1	59	0	9	0	n.a.
1	48	0	3	0	n.a.
0	47	1	9	0	n.a.
0	37	0	5	0	n.a.
1	38	0	10	0	n.a.
0	47	1	10	0	n.a.
0	37	1	10	0	n.a.
1	45	0	10	0	n.a.
0	43	1	10	0	n.a.
1	31	0	5	0	n.a.
0	46	1	9	0	n.a.
0	40	1	10	0	n.a.
0	33	1	7	0	n.a.
0	30	0	7	0	n.a.
0	51	0	6	0	n.a.
1	52	1	7	0	n.a.
0	39	0	6	0	n.a.
1	39	1	10	1	132
1	65	1	8	1	99
0	36	0	10	1	86
0	42	0	4	1	0
1	52	0	10	1	69
0	39	1	4	1	82
0	52	1	5	1	37
0	54	0	3	1	36

sex (0 = male)	age at trial entry [years]	randomization (0 = placebo)	follow-up [years]	advanced neoplasia (0 = no)	time to advanced neoplasia [months]
0	45	0	10	1	50
0	35	1	10	1	75
1	39	0	10	1	115
0	41	1	5	1	17
0	45	1	0	1	20
1	49	1	9	1	119
1	56	1	8	1	44
1	41	1	10	1	53
0	34	0	8	1	93
1	43	0	10	1	23
1	45	0	4	1	86
0	51	0	4	1	26
0	34	0	4	1	79
1	53	1	10	1	22
1	47	0	0	1	25
0	44	0	9	1	157
0	32	1	0	1	30
0	61	1	5	1	29
0	42	n.a.	10	1	66
1	55	1	7	1	124
0	60	n.a.	5	1	45
1	39	1	4	1	41
1	44	0	2	1	24
0	50	0	10	1	20
1	38	1	3	1	0
0	53	0	2	1	0
1	55	1	6	1	93
0	47	0	8	1	112
0	46	0	7	1	6
1	59	1	6	1	24
0	36	0	7	1	75
0	46	0	0	1	20
0	43	0	0	1	18
1	65	0	1	1	20
1	41	0	3	1	78
1	56	n.a.	9	1	24
0	47	0	8	1	63
1	44	0	7	1	44

sex (0 = male)	age at trial entry [years]	randomization (0 = placebo)	follow-up [years]	advanced neoplasia (0 = no)	time to advanced neoplasia [months]
1	59	0	10	1	25
0	39	1	7	1	53

Table S7: Clinical parameters of LS adenoma patients included in the analysis of local T cell infiltration.

	total patients	n = 74
age at adenoma resection	age range [years]	19–88
	median age [years]	55
sex	male	n = 44
	female	n = 28
MMR gene	*MLH1*	n = 36
	MSH2	n = 28
	MSH6	n = 10
	PMS2	n = 0
	total adenomas	n = 140
MMR status	proficient	n = 46
	deficient	n = 72
	n.a.	n = 22

Table S8: Clinical features of individuals included in the analysis of systemic FSP-specific immune responses.

		MSI cancer patients	MSS cancer patients	healthy LS carriers	healthy controls
	total	n = 21	n = 7	n = 8	n = 17
age	age range [years]	37–85	30–66	25–59	18–55
	median age [years]	64	45	38	29
sex	male	n = 9	n = 3	n = 3	n = 4
	female	n = 12	n = 4	n = 5	n = 13
LS	total	n = 6		n = 8	
	MLH1	n = 0		n = 3	
	MSH2	n = 1		n = 4	
	MSH6	n = 3		n = 1	
	PMS2	n = 1		n = 0	
	unclassified	n = 1		n = 0	
cancer entity	CRC	n = 12	n = 6		
	gastric	n = 6	n = 0		
	esophagus	n = 1	n = 1		
	endometrium	n = 2	n = 0		
post surgery		n = 8	n = 4		
therapy	ICB	n = 10	n = 0		
	chemotherapy	n = 1	n = 2		
	n.a	n = 4	n = 4		

Table S9: Clinical features of MSI cancer patients receiving ICB therapy and included in the analysis of systemic T cell responses.

	total	n = 10
age	age range [years]	58–78
	median age [years]	66.5
sex	male	n = 3
	female	n = 7
LS	total	n = 2
	MLH1	n = 0
	MSH2	n = 0
	MSH6	n = 1
	PMS2	n = 1
cancer entity	CRC	n = 7
	gastric	n = 2
	endometrium	n = 1
prior therapy line	FLOT	n = 1
	FOLFIRINOX	n = 1
	FOLFIRI	n = 1
	FOLFIRI plus bevacizumab	n = 1
	n.a.	n = 6
ICB	pembrolizumab	n = 6
	nivolumab plus ipilimumab	n = 3
	n.a.	n = 1

Table S10: Clinical characteristics of individuals who underwent HLA typing.

		MSI cancer patients	healthy LS carriers
	total	n = 32	n = 6
age	age range [years]	28–76	25–59
	median age [years]	61	35.5
sex	male	n = 15	n = 3
	female	n = 17	n = 3
LS	total	n = 13	n = 6
	MLH1	n = 2	n = 1
	MSH2	n = 3	n = 4
	MSH6	n = 2	n = 1
	PMS2	n = 3	n = 0
	n.a.	n = 3	n = 0
cancer entity	CRC	n = 25	
	gastric	n = 3	
	esophagus	n = 2	
	endometrium	n = 1	
	n.a.	n = 1	

Table S11: Clinical features of patients included in the correlation analysis of FSP-specific immune responses and epitope binding predictions.

		MSI cancer patients	healthy LS carriers
	total	n = 15	n = 6
age	age range [years]	37–75	25–59
	median age [years]	64	35.5
sex	male	n = 6	n = 3
	female	n = 9	n = 3
LS	total	n = 4	
	MLH1	n = 0	n = 1
	MSH2	n = 1	n = 4
	MSH6	n = 2	n = 1
	PMS2	n = 1	n = 0
cancer entity	CRC	n = 10	
	gastric	n = 3	
	esophagus	n = 1	
	endometrium	n = 1	
post-surgery		n = 5	
therapy	ICB	n = 9	
	chemotherapy	n = 1	
	n.a.	n = 2	

Table S12: Clinical features of MSI cancer patients included in the cMS mutation analysis of cancer tissue.

	total	n = 12
age	age range [years]	37–75
	median age [years]	61
sex	male	n = 7
	female	n = 5
LS	total	n = 4
	MLH1	n = 0
	MSH2	n = 1
	MSH6	n = 2
	PMS2	n = 1
cancer entity	CRC	n = 8
	gastric	n = 3
	esophagus	n = 1
post-surgery		n = 4
therapy	ICB	n = 7
	chemotherapy	n = 1
	n.a.	n = 2

Table S13: Clinical features of individuals whose plasma/serum samples were included in the analysis of humoral immune responses.

		MSI cancer patients	LS with cancer history	healthy LS carriers	healthy controls
	total	n = 15	n = 15	n = 15	n = 15
age	age range [years]	25–77	29–77	24–64	24–65
	median age [years]	65	53	34	45
	n.a.	n = 5	n = 0	n = 0	n = 0
sex	male	n = 2	n = 9	n = 5	n = 11
	female	n = 8	n = 6	n = 10	n = 4
	n.a.	n = 5	n = 0	n = 0	n = 0
LS	*MLH1*		n = 0	n = 2	
	MSH2		n = 0	n = 1	
	MSH6		n = 0	n = 2	
	PMS2		n = 0	n = 1	
	n.a.		n = 15	n = 8	
cancer entity	CRC	n = 4			
	gastric	n = 2			
	stomach	n = 3			
	bile duct	n = 1			
	n.a.	n = 8			

Table S14: Clinical features of individuals whose plasma samples were included in the analysis of the vesicular MSI phenotype.

		MSI cancer patients	healthy controls
	total	n = 15	n = 24
age	age range [years]	41–76	21–55
	median age [years]	67	28.5
sex	male	n = 5	n = 4
	female	n = 10	n = 20
LS	total	n = 3	
	MLH1	n = 1	
	MSH2	n = 0	
	MSH6	n = 1	
	PMS2	n = 1	
cancer entity	CRC	n = 13	
	gastric	n = 2	

Acknowledgements

First and foremost I would like to thank Prof. Dr. med. Magnus von Knebel Doeberitz for the fantastic opportunity of conducting my PhD in the Department of Applied Tumor Biology. As a bastion of calm he provided the stability that was essential for the completion of this thesis.

My gratitude also goes to Prof. Dr. Hans-Reimer Rodewald for being my second referee.

Further, I would like to thank Prof. Dr. Michael Platten and Prof. Dr. med. Michael Thomas for being excellent TAC members and accompanying my PhD journey in the last three years. I am very grateful for your scientific guidance and insightful comments.

I would also like to express my sincere gratitude to Dr. Aysel Ahadova and PD Dr. Matthias Kloor for being my supervisors and supporting me every step of the way. Thank you for your seemingly unswerving confidence in the project and your optimism that I was often lacking.

Special thanks to Dr. Johannes Gebert for introducing me to the world of extracellular vesicles and coming up with new, exciting ideas. Thank you very much for always having an open ear and a realistic view on the scientific process.

Further, I would like to thank Dr. Jürgen Kopitz for his support and helpful ideas in all protein-related matters.

My gratitude also goes to all co-authors of my publication, particularly to Klaus Kluck, Prof. Dr. Jan Budczies and Dr. Martina Kirchner for the extensive Nanostring and biostatistical analyses of my samples.

Further, I would like to express my thankfulness to the PEPperPRINT team for conducting the peptide microarray screening and agreeing to this exciting cooperation.

A big thank you to Dr. med. Mirjam Tariverdian, Dr. med. Elena Busch, Dr. med. Georg Martin Haag and Thomas Walle for collecting the essential blood samples and the overall productive cooperation.

I am also deeply grateful to Dr. Ingrid Hausser and Ulrike Ganserer for the wonderful visualization of extracellular vesicles.

I would also like to thank Andrea Klingmann for always having an open door and her indispensable help in all bureaucratic and organizational matters.

I gratefully acknowledge the financial support of the Helmholtz International Graduate School for Cancer Research.

I consider myself very lucky to be part of ATB and would like to thank all of its people for making my PhD such a special time. In particular I would like to thank Nina Nelius, for cutting countless tissue blocks, diving into archives and her overall constant support. Vera Fuchs, thank you so much for joining my EV journey and being such a joy to work with. Petra Höfler, Ricarda Mehr, Sigrun Himmelsbach, Iris Martin and all the others, thank you!

Special thanks goes to the most wonderful office – Dr. Julia Sieber-Frank, Alex Hernandez Sanchez, Lara Schlegel and Dr. med. Simon Kalteis. On our Chihuahua mood board I would be a very happy and grateful one for having such amazing colleagues. Particularly I would like to thank the office book club: Julia for her irreplaceable moral support and the abundant snack drawer. And Dr. Malwina Michalak, aka Mama Malwina, you are missed and I would like to thank you for all of your scientific and non-scientific advice. A big thank you also goes to the office alumni, Dr. Katharina Urban, Dr. Fabia Fricke and Florian Seidler.

I would also like to thank Victoria Lippert who took on the deed of quantifying CD8-positive T cells in adenomas during her internship and therefore helped to finish my thesis.

To all my friends, thank you for being the crazy bunch you are and for taking my mind off of colorectal cancer when I needed it. Thank you for broadening my natural science horizon and introducing me to topics I did not even know existed.

Lastly, I am deeply grateful for having such an amazing family that always believed in me. Thank you for endless phone calls, Austrian care packages and especially your unwavering support.

And Patrick, I cannot thank you enough for being the most patient, affectionate and supportive partner one could wish for. Thank you for all the cups of coffee, the delicious food, late-night LaTeX support and your unconditional love. Without you, I would have never dreamt of pursuing this PhD and to leave my comfort zone so far behind (also I definitely would have eaten pasta daily). I cannot wait for everything that is to come ♡.